Monitoring of fresh concrete by a combined methodology based on stress waves and optical techniques

Thesis submitted in fulfilment of the requirement for the award of the degree of Doctor of Engineering Sciences (Doctor in de ingenieurswetenschappen) (VUB) and Doctor of Civil Engineering (Doctor in de ingenieurswetenschappen: bouwkunde) (UGent) to

Evin Dildar Dzaye

Advisors: Prof. dr. ir. Dimitrios Aggelis,

Prof. dr. ir. Geert De Schutter

Vrije Universiteit Brussel
Faculty of Engineering
Mechanics of Materials and Constructions (Memc)

Ghent University
Magnel Laboratory for Concrete Research
Department of Structural Engineering

Academic year 2019 - 2020

Supervisors

Prof. dr. ir. Dimitrios Aggelis
Prof. dr. ir. Geert De Schutter

Research Institutes

Vrije Universiteit Brussel
Faculty of Engineering
Department of Mechanics of
Materials and Constructions (MeMC)

Ghent University
Magnel Laboratory for Concrete Research
Department of Structural Engineering
Faculty of Engineering and Architecture

Examination Committee

Prof. dr. ir. Dimitrios Aggelis (supervisor)

Prof. dr. ir. Geert De Schutter (supervisor)

Prof. dr. ir. Thomas Geernaert (chair VUB)

Prof. dr. ir. Luc Taerwe (chair UGent)

Prof. dr. ir. Pintelon Rik (vice-chair VUB)

Prof. dr. ir. Tine Tysmans (secretary VUB)

Prof. dr. ir. Patricia Verleysen (secretary UGent)

Prof. dr. ir. Volker Slowik (external Jury member)

Dr. ir. Mohammed Sonebi (external Jury member)

II

Acknowledgements

In the last four years, I worked with great pleasure on my PhD project. I enjoyed every moment and I gained great experiences. The present research work can never be done without the help that I received from all the friends. I would like to express my gratitude to all the people who supported me during the last four years.

Firstly, I would like to express my sincere gratitude to my supervisor professor Dimitrios Aggelis for the continuous support during my PhD study and related research, for his patience, motivation, and immense knowledge. Your guidance helped me in all these four years of research. Your office door was always open for any question at any time. Our discussions have always been fruitful and at the end of any of them, I have always felt like I have learnt something new. You are an excellent supervisor and I am very lucky to have the opportunity to work with you. You are omniscient in the field of non-destructive techniques. It was a pleasure to work under your supervision. Many thanks also for the trust and the confidence given to me to present our work at international conferences around the world. I could not have imagined having a better supervisor for my PhD. My sincere appreciations go also to my supervisor professor Geert De Schutter from Ghent University for the recommendations, the support, the revisions, the advices and the meetings. It has been a pleasure to work with you.

I am deeply thankful to professor Slowik for the interesting discussions and advices regarding my experimental setup. You have presented me the world of fresh concrete and supported me during my Bachelor, Master and PhD research. Thank you for visiting MeMc and giving the fruitful presentation that increased so much my confidence.

A special mention goes also to the amazing members of the MeMC department. Without the valuable help and support of Frans in the laboratory, I would have not been able to carry out my experimental setup successfully. I would like to express my gratitude to professor Danny for delivering the material and the cement bags.

"Gratitude is not only the greatest of virtues, but the parent of all others."

Cicero

IV

Table of Contents

VI

List of abbreviations

A	Amplitude
ACC	Accelerator
AE	Acoustic Emission
AF	Average Frequency
AFm	Monosulphate
AFt	Ettringite
C-S-H	Calcium-Silicate-Hydrate
C_2S	Dicalcium silicate
C_3A	Tricalcium aluminate
C_3S	Tricalcium silicate
C_4AF	Tetracalcium aluminoferrite
CEM	Cement paste
DIC	Digital Image Correlation
DUR	Duration
FA	Fly ash
LVDT	Linear variable displacement transformer
NDE	Nondestructive Evaluation
NDT	Nondestructive Testing
OPC	Ordinary Portland Cement
RA	Rise Angle
REF	Reference
RET	Retarder
RH	Relative humidity
RT	Rise Time
SEM	Scanning electron microscope
SRA	Shrinkage-reducing admixture
UPV	Ultrasonic Pulse Velocity
UT	Ultrasonic Testing
w/b	Water to binder ratio
w/c	Water to cement ratio

x

Abstract

The present PhD thesis deals with a combination of experimental techniques to monitor fresh concrete in view of acquiring relevant information concerning the quality of the concrete. The early age hydration of concrete is important for concrete durability and quality. Concrete properties are affected by different phenomena occurring during the fresh state, potentially impacting the long-term concrete performance. Characterizing the origin of different processes occurring in fresh concrete at the very early hydration process is challenging. Studies in the field have proposed several techniques with good potential as well as limitations in the accuracy regarding the characterization of concrete that could be obtained. Several researchers have applied different techniques to monitor the early hydration process, such as ultrasonic wave spectroscopy, to determine the microstructure evolution and associated connectivity of the solid phase, scanning electron microscopy, to investigate the degree of hydration, X-ray tomography, to estimate the early stage hydration. Further, isothermal calorimetry and thermal analysis can deliver relevant information on the different chemical processes occurring during early hydration. In addition, a sensitive and precise technique is substantial to characterize the influence of early-age processes like hydration formation, settlement evolution which are related to the mechanical properties and durability at a later stage. The implementation of non-destructive evaluation of fresh concrete by stress waves has attracted increasing attention.

Acoustic emission (AE) is a technique recently applied in fresh concrete which enables recording elastic waves from cementitious material processes from casting up to the hardened state, thus allowing the monitoring of the cement hydration and hardening. The passive and non-destructive technique of AE is capable of recording waves caused by several processes (settlement, capillary pressure evolution, formation of hydrates and shrinkage). Furthermore, the technique of AE has proven

its reliability to illustrate changes due to damage growth in many types of materials. Considering the progress in electronics and signal acquisition, AE is a good alternative technique as it can continuously monitor the material changes. Although AE monitoring is very promising because of its non-invasive, global and passive nature, it is however, challenging to explain the numerous AE activities that are recorded as their possible source is not unique. Despite the number of signals acquired during the early stage, a clear correlation between the actual processes and the AE signals has not been established in the hydration state. Understanding the several mechanisms, such as particle settlement, hydrates formation, microstructure evolution and thermomechanical changes of early hydration is substantial as the long-term performance of concrete is closely connected to its early age properties.

Apart from AE, digital image correlation (DIC) has been applied to study the deformation process of cementitious material at very early age. After mixing of cement-based materials, the cement hydration process begins, resulting in a 3D deformation process (shrinkage). Monitoring fresh concrete deformation is essential to follow the drying process and hydration while concrete shrinks. The application of DIC on fresh cement-based materials implies a challenging speckle pattern application since the speckles might move due to the fresh material as well as due to the bleed water on the specimen surface. In this research, the fresh sample surface was covered by a black and white speckle to allow DIC monitoring. The technique of DIC is highly sensitive and allows an accurate and non-contact optical monitoring of the settlement and shrinkage of fresh cementitious material. 3D-DIC realizes monitoring the global surface displacement measurement as well as records non-uniform displacement distributions of the fresh concrete. The DIC system provides a full-field 3D surface observation that allows a deeper characterization and understanding of fresh concrete deformation process. It should be highlighted that DIC, compared to traditional contact sensors, measures the settlement in contactless mode, therefore the sensor cannot affect the measurement process, due to self-weight of the sensor. Based on the observed 3D full-field DIC maps, it is evident that a point measurement of settlement is not sufficient to describe settlement. For the first time in literature, contactless settlement and shrinkage monitoring on the fresh concrete begins 15 to 20 min after

II

casting. The surface displacement determined by DIC is compared to the displacement measured by linear variable differential transformer (LVDT) sensors for calibration purposes. The DIC method showed a good concordance with the classical LVDT sensors.

Furthermore, ultrasonic pulse velocity (UPV) monitoring has been applied to study the very early process of hydration mechanism. The UPV exhibited an increase during hydration that is related to the connectivity of the solid phase due to the material stiffening and allowing the estimation of the setting time. Moreover, the capillary pressure development of fresh cement-based material has been monitored to study the drying process as well as to indicate the risk of early age cracking. In fresh cement-based materials, water evaporation from the specimen surface drives to a capillary pressure increase in the liquid phase.

Thus, a combined approach of several monitoring techniques such as acoustic emission (AE), ultrasound, capillary pressure measurement, shrinkage and settlement measurement was applied to study the impact of very early process due to physical phenomena and hydration heat on the AE characteristics. Experimental AE parameters related to frequency content, amplitude, energy, risetime, waveform shape, and cumulative activity are determined. The experimental observations showed the high sensitivity of AE to the early activities occurring within the early hydration stage which dominates the settlement process. Focused experiments of isolated sources enlighten the mechanisms behind the acquired population of AE signals. By using AE and DIC this study intends to build a full-field experimental setup that simultaneously and continuously monitors the different ongoing processes of fresh concrete. This research emphasizes the possibility of implementing quantitative AE and DIC in fresh concrete and aims to assess the quality of the fresh concrete from an early age.

IV

Samenvatting

Deze thesis beschrijft het onderzoek inzake de aanwending van een combinatie van experimentele technieken voor de opvolging van beton op jonge leeftijd, met het oog op het verkrijgen van relevante informatie over de betonkwaliteit. De vroegtijdige hydratatie van beton wordt beheerst door verschillende fenomenen die zich voordoen tijdens de verse toestand en die verder een invloed hebben op de duurzaamheid en kwaliteit van het beton. De vroegtijdige hydratatie is de dominante factor voor het voorspellen van de kwaliteit van het beton. Verschillende fenomenen die zich voordoen tijdens de verse toestand beïnvloeden de prestaties op lange termijn.

 Het karakteriseren van de oorsprong van de verschillende processen in het verse beton tijdens het zeer vroege hydratatieproces is een uitdaging. Studies in het onderzoeksveld hebben verschillende technieken voorgesteld met potentieel alsook beperkingen in de nauwkeurigheid met betrekking tot de karakterisering van beton. Zo werd onder andere gebruik gemaakt van ultrasone golfspectroscopie om de evolutie van de microstructuur en de bijbehorende connectiviteit van de vaste fase te bepalen, scanning elektronenmicroscopie om de mate van hydratatie te bepalen, en röntgentomografie om de vroege hydratatie in te schatten. Verder kunnen isotherme calorimetrie en thermische analyse relevante informatie opleveren over de verschillende chemische processen die zich voordoen tijdens de vroege hydratatie. Een gevoelige en nauwkeurige techniek is essentieel om de invloed van vroege ouderdomsprocessen te karakteriseren, zoals de hydratatievorming en zettingsevolutie die gerelateerd zijn aan de mechanische eigenschappen en duurzaamheid in een later stadium. Er is een toenemende interesse naar de implementatie van niet-destructieve evaluatie van vers beton door akoestische emissie.

Akoestische emissie (AE) is een techniek die recent toepast wordt op vers beton. Deze techniek maakt het mogelijk om elastische golven in cementachtige materialen te registreren, vanaf het storten tot aan de

V

verharde toestand. Hierdoor kan de cementhydratatie en de verharding worden opgevolgd. De passieve en niet-destructieve techniek van AE is in staat om golven te registreren die veroorzaakt worden door verschillende processen (zettingen, capillaire drukevolutie, vorming van hydraten en krimp). Bovendien heeft AE zijn betrouwbaarheid om veranderingen te illustreren ten gevolge van schade al bewezen voor vele andere materialen. Gezien de vooruitgang op het gebied van elektronica en signaalacquisitie, is AE een goed alternatief omdat het continu de materiaalveranderingen kan monitoren. Hoewel AE-monitoring veelbelovend is vanwege het niet-invasieve, wereldwijde en passieve karakter, is het echter niet eenvoudig om de vele AE-activiteiten die zijn geregistreerd te verklaren, aangezien de mogelijke bron niet uniek is. Ondanks al de signalen die in het beginstadium zijn verkregen, is er in de hydratatietoestand geen duidelijke correlatie tussen de werkelijke processen en de vastgestelde AE-signalen. Inzicht in de verschillende mechanismen, zoals de afzetting van deeltjes, de vorming van hydraten, de evolutie van de microstructuur en de thermomechanische veranderingen tijdens de vroege hydratatie, is noodzakelijk, aangezien de prestaties van het beton op lange termijn nauw verbonden zijn met de eigenschappen van het beton op jonge leeftijd. Naast AE is ook digitale beeldcorrelatie (DIC) toegepast om het vervormingsproces van cementachtig materiaal op zeer jonge leeftijd te bestuderen. Na het mengen van het cementmateriaal begint het cementhydratatieproces, wat een 3D vervormingsproces veroorzaakt (krimp). Het monitoren van de vervorming van vers beton is essentieel om het droogproces en de hydratatie te volgen terwijl het beton krimpt. De toepassing van DIC op vers cementmateriaal is een uitdaging met betrekking tot het spikkelpatroon, aangezien de spikkels kunnen verschuiven door het verse materiaal en door het oppervlaktewater van het preparaat. In dit onderzoek werd het verse preparaatoppervlak bedekt met een zwart-wit spikkelpatroon om DIC-monitoring mogelijk te maken. DIC maakt het mogelijk om een nauwkeurige en contactloze optische monitoring van de zetting en krimp van vers cementachtig materiaal te doen. 3D-DIC realiseert de monitoring van de globale oppervlakteverplaatsingsmeting en registreert niet-uniforme verplaatsingsverdelingen van het verse beton. Het DIC systeem biedt een full-field 3D oppervlakte-observatie die een diepere karakterisering en begrip van het vervormingsproces in vers beton toelaat. Er dient benadrukt te worden dat DIC, in vergelijking met traditionele contactsensoren, de zetting contactloos meet, waardoor het

eigengewicht van de sensor het meetproces niet kan beïnvloeden. Op basis van de waargenomen 3D full-field DIC metingen is het duidelijk dat een puntmeting van de zetting niet voldoende is om de zetting te beschrijven.

Voor het eerst in de literatuur zijn op contactloze wijze de zetting en krimp op vers beton vanaf 15 tot 20 minuten na het gieten gemeten. De oppervlakteverplaatsing bepaald door DIC wordt vergeleken met de verplaatsing gemeten door lineaire variabele differentiaaltransformers (LVDT sensoren) voor kalibratiedoeleinden. DIC toonde een goede overeenstemming met de klassieke LVDT sensoren.

Verder is ultrasone pulssnelheidsmonitoring (UPV) toegepast om het zeer vroege proces van hydratatiemechanisme te bestuderen. De UPV vertoonde een toename tijdens de hydratatie die gerelateerd is aan de connectiviteit van de vaste fase als gevolg van de verstijving van het materiaal en zo een schatting van de uithardingstijd mogelijk maakt. Bovendien werd de capillaire drukontwikkeling van vers materiaal op basis van cement gemonitord om het droogproces te bestuderen en om het risico op vroegtijdige scheurvorming aan te tonen. In verse materialen op basis van cement leidt de verdamping van water van het preparaatoppervlak tot een capillaire drukopbouw in de vloeibare fase.

Er werd een gecombineerde aanpak van verschillende monitoringstechnieken zoals akoestische emissie (AE), ultrasoon, capillaire druk, krimp en zettingsmetingen toegepast om de impact van zeer vroege processen als gevolg van fysische fenomenen en hydratatiewarmte op de AE-kenmerken te bestuderen. Experimentele AE-parameters met betrekking tot frequentie-inhoud, amplitude, energie-evolutie, golfvorm en cumulatieve activiteit worden bepaald. De experimentele observaties toonden de hoge gevoeligheid van AE voor de activiteiten die zich voordoen tijdens de vroege hydratatiefase die het zettingsproces domineert. Experimenten met geïsoleerde bronnen verduidelijken de mechanismen achter de verworven populatie van AE-signalen. Door gebruik te maken van AE en DIC wil deze studie een volledige experimentele opstelling bouwen die simultaan en continu de verschillende lopende processen van vers beton monitort. Dit onderzoek benadrukt de mogelijkheid om kwantitatieve AE en DIC te implementeren in vers beton met als doel de kwaliteit van het verse beton vanaf jonge leeftijd te beoordele

Chapter 1: **Introduction**

This chapter introduces the general background of the doctoral thesis. First, the motivations and background of the doctoral thesis are presented, followed by the objectives and the original contributions. Also, the experimental techniques applied in this thesis are presented in this chapter. Finally, the chapter closes with a brief outline of the doctoral thesis. Parts of this chapter were taken from the following papers:

Dzaye, E., De Schutter G., and Aggelis D.G. 2017. "Study on Mechanical Acoustic Emission Sources in Fresh Concrete." *Archives of Civil and Mechanical Engineering* 18(3):742–54.

Dzaye, E., Tsangouri E., Spiessens K., De Schutter G., and Aggelis D.G. 2019. "Digital Image Correlation (DIC) on Fresh Cement Mortar to Quantify Settlement and Shrinkage." Archives of Civil and Mechanical Engineering 19(1):205–14.

Dzaye, E. D., Tsangouri E., De Schutter G., and Aggelis D.G. 2019. "Full-Field Settlement Measurement at Fresh Cementitious Material by Digital Image Correlation." Journal of Advanced Concrete Technology 17(April):168–76.

Dzaye, E., De Schutter G., and Aggelis D.G. 2018. "Application of Digital Image Correlation to Cement Paste." Pp. 2–7 in 18th International Conference on Experimental Mechanics (ICEM 2018). Brussel, Belgium.

1.1 Motivation and background

Ensuring the quality of fresh concrete and implementing suitable curing conditions substantially reduces the possibility of premature failure to perform as designed. Assessing the fresh concrete is of supreme importance to increase the durability of concrete structures. In past decades, insufficient focus on the durability of concrete structures has sometimes led to catastrophic consequences, see Fig. 1.1. Therefore, the maintenance of the quality of concrete is crucial to increase structures' durability, appearance and performance. The main causes affecting the quality of concrete are low quality of raw material (cement, aggregate, water), inadequate compaction, environmental condition during casting, overloading of concrete, crack formation, sulphate and chloride attack, misuse of admixtures, steel corrosion in reinforced concrete (McGinley and Choo 1990).

Fig. 1.1 The collapse of Morandi road bridge in Genoa.

Further, concrete microstructure is very complex. Concrete is a heterogeneous material with different constituents, mainly cement, sand, water and aggregates. The quality of concrete depends not only on the constituents but also on the interaction between those constituents.

Indication of high concrete quality depends primarily on the strength, durability, impermeability and volume stability. The quality of hardened concrete is evaluated by the compressive strength as the structural design codes are based on it. To evaluate the concrete suitability or quality, several conventional tests can be performed on fresh concrete (slump test, compacting factor test) and on hardened concrete (compression test, tensile test and flexural test). The aforementioned techniques are not highly sensitive to accurately interpret the behaviour of both fresh and hardened concrete. Thus, the conventional techniques provide only qualitative information. A continuous monitoring of the fresh concrete properties is substantial to follow the different ongoing processes especially at the early age.

Several researchers studied the fresh state of concrete (Aggelis and Philippidis 2004; Safiuddin et al. 2018; Wierig 1990). Furthermore, numerous techniques have been applied to monitor the early hydration, such as ultrasonic wave spectroscopy to determine the connectivity of the solid phase due to material stiffening (Ye et al. 2004), scanning electron microscope to obtain the degree of hydration (Feng et al. 2004), X-ray computed tomography to determine density changes and to follow early hydration (Chotard et al. 2003), nonlinear and linear ultrasonic measurement to investigate the setting and corresponding stiffening behaviour (Chung et al. 2017) electrical impedance measurement to study the stages of early hydration and the hydrate formation (Suryanto et al. 2018). Lu et al. (Lu et al. 2013) investigated the hydration process of early age concrete applying an embedded active acoustic method along with non-contact complex resistivity. In this study, more detailed literature review of different techniques that have been applied, will be supplied in the following sections.

At early age, fresh concrete may develop cracks since its tensile strength is low. These cracks might negatively influence the concrete durability. Hence, eliminating the early age cracking in concrete structures is crucial in order to increase its service life. Cracking in concrete may occur even within a few hours after casting, before the concrete has achieved a significant strength (Slowik et al. 2008). After casting and up to setting time, concrete is in plastic state (Sant et al. 2009). In this state, concrete is a semi-fluid or fluid mixture of cement and aggregate particles with water, and does not attain any strength gain (Sant et al. 2009). A typical

crack pattern in concrete slabs can consist of parallel or meshed cracks. Fig. 1.2(a) presents early age cracks of a concrete slab 4 h after casting. It is possible that early age cracks reflect the geometrical pattern of the reinforcement as shown in Fig. 1.2(b) (Combrinck et al. 2018a).

(a)   (b)
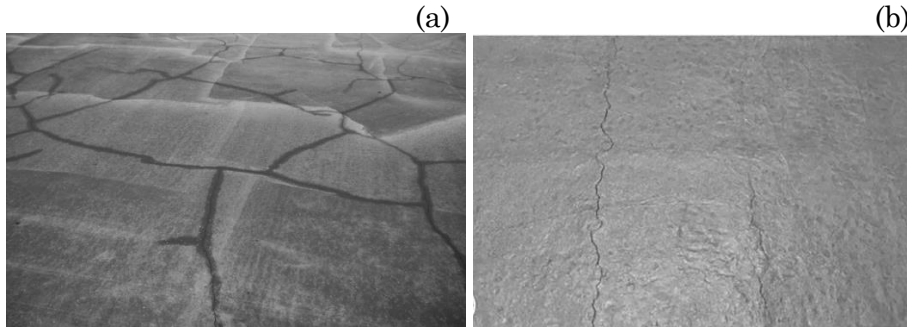
Fig. 1.2 Pattern of plastic shrinkage cracking of concrete slab;(a) crazed crack evolution (Slowik et al. 2008); (b) crack pattern attributed to the reinforcement (Combrinck et al. 2018a).

The early age concrete properties are predominantly attributed to the evaporation rate that is influenced by the concrete temperature, air temperature and relative humidity as well as wind speed (Kosmatka et al. 2002). In addition, the fresh properties of concrete are also affected by the concrete composition, the casting conditions, the specimen geometry, the reinforcement and the mechanical boundary conditions.

An effective way to improve the concrete quality is to reduce the plastic shrinkage cracking. The application of shrinkage reducing admixtures on high strength concretes reduces the surface tension of the mixing water leading to the reduction of the plastic cracking, lower evaporation rate, lower settlement and delayed capillary pressure peak (Mora-Ruacho et al. 2009). In another approach, Lura et al. investigated the fresh state of concrete and the evolution of the plastic cracks that form between the casting time and the setting time of mortars containing shrinkage reducing admixture (Lura et al. 2007).

An effective and sensitive technique to monitor the early stage of concrete is important as this stage defines the final properties of the hardened concrete. Up to now, the most reliable examination for concrete is mechanical testing after hardening. The demand for a more reliable,

sensitive, nondestructive and trustworthy assessment of concrete quality, attracted several researchers.

The technique of acoustic emission (AE) can be applied as an indicator for estimating the transition from the plastic to the hardened state of concrete. The AE sources as well as the propagation of the elastic waves change from the fresh state to the hardened state of concrete.

This study intends to discuss the effect of the fresh and the hardened cementitious materials on the AE parameters through experimental measurements. To obtain better control on the process from very early age, a combination of different techniques has been applied to verify the source of the AE signals. Different parameters like frequency content and energy of the waves seem to be sensitive to the transformation of the material from a viscous suspension to a solid. In the next paragraphs, some important phenomena, processes and techniques are introduced, which will be referred to the volume changes of cementitious material that has an impact on concrete quality.

1.2 Objectives of the thesis

The specific objectives of the research work are the following:

- The development of a methodology that can evaluate significant AE parameters of the concrete starting from the moment after casting, when it is still possible to adjust the fresh concrete before it hardens and becomes a permanent part of the structure (curing treatment).

- Monitoring the mechanisms affecting the very early age hydration (settlement, capillary pressure, shrinkage, temperature evolution) by the non-destructive technique of AE.

- A clear correlation and analysis of the early age hydration and the AE signals of concrete.

- To check whether the composition of the cementitious media alters the AE behaviour in order to allow evaluation on the specific mixes.

- The development of an innovative method that provides a global view of the early age deformations by the optical non-contact DIC technique.

1.3 Original contributions

This PhD thesis summarizes the work obtained during the four-year PhD program. The results have been communicated to the scientific community by publishing several papers in internationally peer-reviewed journals and high-impact international conferences. The original contributions of this study are presented below:

- For the first time in literature, DIC technique has been applied on fresh cementitious material 15 to 20 min after casting. An innovative method of the speckle pattern on fresh concrete is developed. A spray speckle pattern is applied on the specimen surface immediately after casting concrete into the mould and DIC monitoring begins a few minutes after mixing. 3-D DIC measurement of non-uniform surface displacement of concrete, mortar and cement paste was applied which cannot be detected by traditional LVDTs.

- For the first time, the AE, DIC, capillary pressure, temperature development, settlement and shrinkage measurement were simultaneously applied on fresh cementitious material and the monitoring started 15 min after casting.

- Different mechanisms occurring during the hydration process have been isolated and their AE measurements have been investigated.

- Experimental AE parameters related to frequency content, energy, waveform shape, and cumulative activity are determined. These are correlated to shrinkage evolution, capillary pressure development, temperature rise, and settlement progression.

- The application of concrete admixtures (accelerators and retarders) allowed studying the impact of hydration process on the AE characteristics and the early age hydration processes.

- The passive monitoring of AE measurements was combined with the numerical simulations of wave propagation for the classification of fresh cementitious materials. It was found that sources taking place near the mould are more likely to be recorded by the sensors.

- The development of an experimental setup that allows monitoring of sources even during the settlement stage, that is not common in the literature.

1.4 Outline of the thesis

This thesis consists of 7 chapters. More specifically:

Chapter 1 presents a general introduction of the doctoral thesis. Herein, the motivations and background are disclosed, followed by the objectives and the original contributions. Furthermore, the basic phenomena occurring in fresh concrete are presented and the non-destructive testing techniques used in this research are introduced.

Chapter 2 provides the description of the exact sources of acoustic emission in fresh cement. The effect of wave propagation between the source and the receiver is investigated during very early age of cement. The mechanical impact by aggregate and air bubble formation and movements are demonstrated. In addition, experimental results are complemented with numerical simulations to enhance the understanding due to the complexity of the wave propagation problem.

Chapter 3 focuses on experimental observations performed on cement paste and fly ash to characterize the origin of different processes occurring in cement paste during hydration. As a result, mechanical sources like settlement and shrinkage are isolated from the chemical ones (e.g. hydration reaction).

Chapter 4 describes a 3D DIC monitoring on cement paste, mortar and concrete at very early age. The optical technique of DIC enables a full-field 3D continuous monitoring of the surface displacement and strain distribution. Additionally, an innovative technique of speckle pattern creation allows the monitoring of the surface displacement few minutes after casting.

Chapter 5 provides the impact of different admixtures on the hydration process of concrete. Admixtures (accelerator and retarder) have been added to concrete to investigate their impact on AE parameters.

Chapter 6 presents the analysis of AE parameters at three different scales of cement based-materials (cement paste, cement mortar and concrete), indicating the effect of hydration on AE evolution.

Chapter 7 is the final chapter summarizing the findings of this investigation. At the end of the chapter, suggestions for future work are provided and all the conclusions are explained.

1.5 State of knowledge

1.5.1 Volume changes of concrete

The properties of concrete are affected by the volume changes (shrinkage) which can appear soon after concrete casting. Volume change (deformation) in concrete is defined as a decrease or increase in volume that deals with contraction or expansion. There are various reasons for the volume changes in concrete.

The volume change of concrete is influenced by the volume change of cement paste (Kurdowski 2014a). The presence of aggregate in concrete is able to restrain to an extent the concrete global deformation. Concrete presents lower volume change compared to paste, by having similar w/c ratio. The coarse aggregates provide the concrete volumetric stability by restraining the shrinkage of the hydrated cement paste. By increasing the coarse aggregate content and decreasing the fine aggregate content, the concrete deformation and corresponding final shrinkage will be reduced (Aïtcin 2008). However, it has to be mentioned that the coarse aggregate content does not affect the unhindered paste volume change. The latter one is attributed to the w/c ratio.

When concrete is exposed to wind and dry air, a decrease of its mass and loss of water content occurs. Thereafter, a decrease of concrete moisture content occurs caused by its drying. In the surface the menisci are formed leading to the increase of tensile stresses. This effect leads to a reduction of concrete volume and loss of concrete mass which is known as drying shrinkage. Higher w/c ratio can lead to a delayed shrinkage evolution and capillary pressure build-up, since increased bleed water needs longer time to evaporate. Furthermore, the drying shrinkage depends on the porosity of concrete as well as the atmospheric relative humidity.

Shortly after casting, the volume change of concrete begins. At early ages, within 24 hours the volume changes can influence the crack formation in hardened concrete. There are different types of shrinkage, namely, chemical shrinkage, autogenous shrinkage, drying shrinkage, plastic shrinkage (Holt 2001; Kurdowski 2014a; Lourenco et al. 2011). In the following paragraphs, the formation of water menisci leading to capillary pressure development are discussed.

1.5.2 Capillary pressure build-up

Loose particles in moist and granular shaped materials are held together due to the capillary forces that act at the interparticle contacts. Water capillarity controls part of the interparticle bonding forces in moist granular materials. The capillary force depends on the surface tension as well as the radius of menisci curvature. Thus, the bonding forces between the particles are depending on the water menisci located at the contact surfaces. These water menisci depend on the surface tension, curvature and contact angle of the menisci. The water menisci are concave with negative water pressure. The capillarity depends mainly on two physical actions of water menisci on solid grains, namely, the exerted water pressure and the surface tension that acts inside air/ water interface. The water pressure is negative (tensile) if the water menisci is concave. The curvature of water menisci could differ from one point to another in moist granular materials with variable particle shapes, size and nature. Predominantly, the menisci have a concave shape that is corresponding to the tensile capillary water pressure (Lourenco et al. 2011). Schematic representations of concave menisci between two solid grains is presented in Fig. 1.3(a). The forces applied by water pressure and surface tension for a concave water meniscus are illustrated in Fig. 1.3(b).
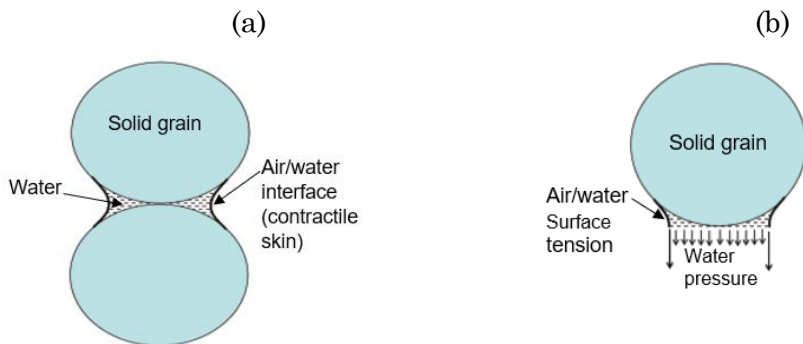
Fig. 1.3 Representation of (a) concave meniscus between two solid grains; (b) tensile force by the surface tension and water pressure for concave meniscus (Lourenco et al. 2011).

In a concave meniscus the tensile water pressure pulls the two solid grains together, as the surface tension acts inside the contractile skin. Furthermore, the contact angle between the solid grains and the

10

contractile skin affects the geometry arrangement of the menisci at the particle contacts.

The formation of menisci in cementitious material leads to the capillary pressure development. After casting concrete, a plane water film is formed at the material surface, known in literature as bleed water. As hydration begins, the bleed water diminishes as water evaporation proceeds. Consequently, the solid particles on material surface are no longer covered by bleed water and a pressure difference is built up between water and the surrounding air. Curved water surfaces (menisci) are now formed at the liquid phase between solid particles (Slowik et al. 2008). As hydration evolves, both capillary pressure and surface curvature progressively increase leading finally to contracting tensile forces between the particles since the water can no longer bridge the pores and possibly air penetrates the saturated pore system (Slowik et al. 2014). In the following paragraphs, the evolution of capillary pressure is discussed in detail.

The capillary pressure development indicates concrete drying process as well as the risk of plastic cracking. In drying suspensions and in fresh cementitious materials, water evaporation from the surface leads to a capillary pressure development in the liquid phase. Monitoring the capillary pressure is crucial to determine the risk of early age cracking (Slowik et al. 2008). Plastic concrete in the fresh state experiences evaporation of the bleed water at the surface resulting in a capillary pressure rise (Ghourchian et al. 2018, 2016; Olivier et al. 2018). The capillary pressure has been detected by means of pressure transducer, see Fig. 1.4(a). The pressure transducer was connected to a brass tube as shown in Fig. 1.4(b).

(a)   (b)
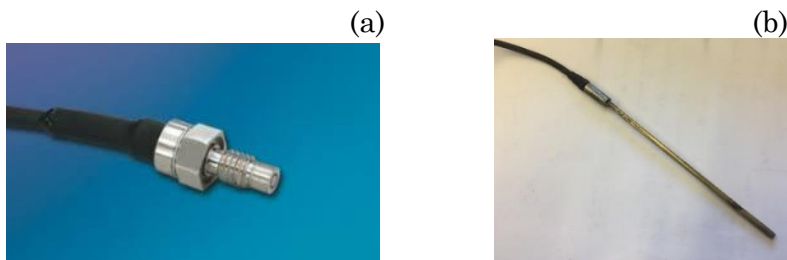
Fig. 1.4(a) pressure transducer for capillary pressure measurement; (b) pressure transducer connected to the brass tube.

Fig. 1.5 shows the capillary pressure development in a drying suspension. The solid particles in the material may be either inert or cementitious as the physical process occurs in both types of materials. The liquid phase contains mostly water. After casting the material, the solid particles settle caused by the gravitational force and on the surface a water layer is formed that is called bleeding, see Fig. 1.5A.
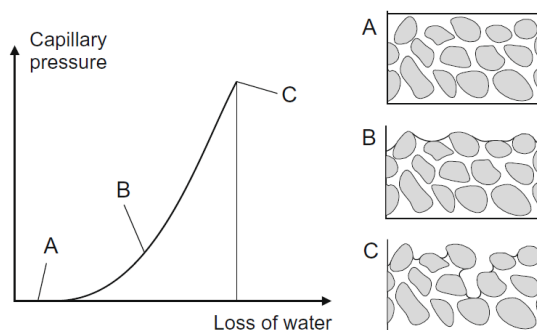
Fig. 1.5 Capillary pressure development in a drying suspension (Slowik et al. 2009).

Firstly, a layer of bleed water accumulates on the specimen surface. Later, the continuous evaporation of the bleed water reduces the water layer at the surface depending of the bleeding rate versus the evaporation rate. Thus, the bleed water near the surface vanishes as shown in Fig. 1.5B. The surface tension leads to a curved shape of the water surface. The water curvature is 'R' at the surface with maximum radii R_1 and minimum radii R_2. Beside the water curvature, the negative pressure build-up is influenced by the water surface tension γ, see Gauss-Laplace equation Eq. 1.1. The surface tension of a liquid is attributed to the attraction of the particles in the surface by the bulk of the liquids.

$$p = \gamma \left(\frac{1}{R_1} + \frac{1}{R_2} \right) \quad \text{Eq. 1.1}$$

In cement-based materials , the hydration process may be a further cause for the water loss that leads to capillary pressure evolution (Holt and Leivo 2004). The capillary pressure affects the particle faces and causes the specimen volume reduction. Initially, settlement or vertical shrinkage strain takes place, and later transfers in a horizontal

shrinkage strain. Furthermore, the capillary pressure increase is affected by the water to cement ratio, see Fig. 1.6. The capillary pressure build-up is delayed for higher water to cement ratio since more water is available for evaporation. Additionally, the effect of hydration on internal desiccation also influences the capillary pressure development.
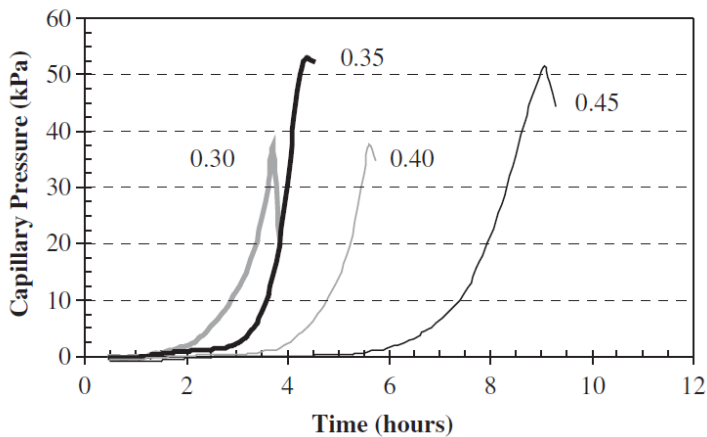
Fig. 1.6 Influence of water to cement ratio on capillary pressure build-up in a mortar specimen (Holt and Leivo 2004).

During the capillary pressure increase, the interparticle distances reduce, leading to a reduction of the specimen volume. At a certain pressure, the radii between the particles can no longer be bridged at the surface. Therefore, the capillary pressure breaks down locally since air enters the pore system. Firstly, air enters the largest gaps, see Fig. 1.5C. At this point, the air penetration is not uniform since the particles are not regularly arranged. Consequently, the highest absolute capillary pressure value is different at different locations, see Fig. 1.7. In the following sections, the heat evolution is presented to follow the heat of hydration.
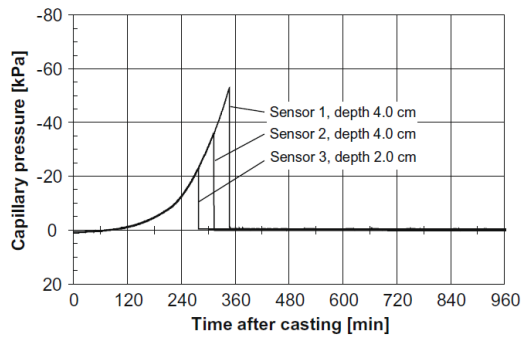
Fig. 1.7 Capillary pressure sensors at different locations in a concrete specimen (Slowik et al. 2009).

1.5.3 Heat of Hydration

By mixing cement with water the cement hydration process begins, also generating heat of hydration. The generated heat depends on the cement mineralogical composition that produce primarily high amount of heat evolution. Besides the effect of the mineralogical composition, the water-cement ratio, the curing temperature and the cement fineness are affecting the generated heat of hydration (Zongjin 2011). An increase in the cement content, cement fineness and curing temperature leads to an increase in the heat of hydration. At early ages, the rate of heat hydration is the greatest. Within the first three days, a large amount of hydration heat evolves with the greatest rate occurring during the first 24 hours (Copeland et al. 1960). Therefore, monitoring the early hydration is essential which affects the stages of hydration. In the present study, the hydration heat is determined in accordance with ASTM C186 or by means of conduction calorimetry and is discussed in the following paragraph.

1.5.3.1 Isothermal calorimetry

Cement hydration is an exothermal chemical process. Isothermal calorimetry allows continuous monitoring of the heat of hydration (ASTM C1679 2014) and testing the early hydration process of cement (Kosmatka et al. 2002; Taylor 1997). The hydration heat flow was monitored using TAM Air isothermal calorimeter (TA instrument) at a

14

constant temperature of 20 °C in this study, see Fig. 1.8(a). Immediately after mixing, the fresh cement paste was placed within the calorimeter channels and were tested for a period of 7 days.

(a)   (b)
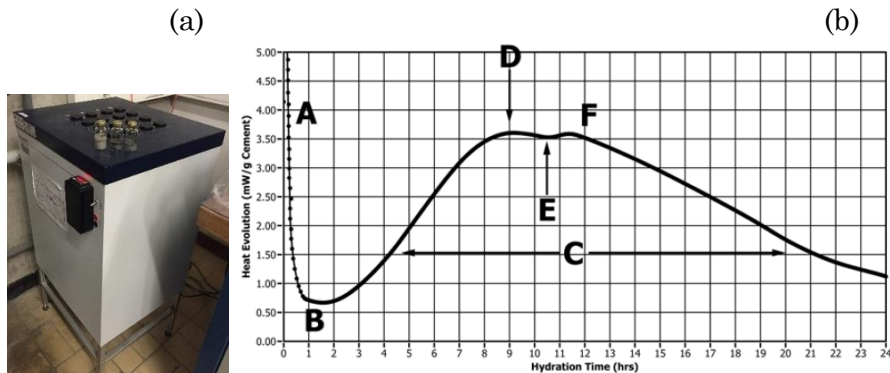
Fig. 1.8(a) representation of calorimetry set-up; (b) the rate of heat development in function of time (ASTM C1679 2014).

At early ages, cement produces a high heat production rate and isothermal calorimetry allows monitoring the stages of hydration. Ordinary Portland cement experiences five stages of heat hydration during the hydration process, as mentioned by several researchers (Frølich et al. 2016; Mostafa and Brown 2005; Taylor 1997). (1) the initial reaction; (2) the induction period; (3) the acceleration period; (4) the deceleration period and (5) the period of slow continued reaction (Mostafa and Brown 2005). Fig. 1.8(b) presents an example of heat evolution for isothermal hydration of Portland cement according to ASTM 1679-14. (A) initial reaction by dissolution of alkali sulfates and aluminates. Initial cement hydration and the hydration of free lime. Sometimes called heat of wetting and is due to the heat emitted by the initial hydration reaction such as C_3A; (B) dormant period or induction period related to very low thermal power representing slow hydration and a slow activity period; (C) main hydration peak or the accelerated period related mainly to the hydration reaction leading to setting and early strength development, with maximum at (D). The second peak occurs between 6 and 12 hours due to the C_3S hydration indicating the start of the hardening process;

15

(E) sulfate depletion point and lastly (F) accelerated calcium aluminate activity (ASTM C1679 2014). The third peak is attributed to the renewed activity of C_3A and is obtained between 12 and 90 hours. This stage is an accelerated reaction that determine the rate of hardening and final set. Finally, after (F) this period presents a slow activity hydration that is attributed to the formation of the hydration products and the rate of later strength evolution.

1.5.3.2 Temperature measurement

One thermocouple was inserted in the specimen to measure the temperature development (Fig. 1.9). The temperature evolution is directly linked to the heat of hydration, thereby allowing the monitoring of the hydration process. Several researchers applied thermocouples to measure the hydration temperature of concrete (Slowik et al. 2008; Wu and D. 2017). Beside the effect of the heat of hydration on the specimens, the effect of the hydration process on the non- destructive techniques is investigated, as will be seen in the following chapters.

Fig. 1.9 Thermocouple type K.

1.5.4 Non-destructive techniques applied on fresh and hardened concrete

1.5.4.1 Acoustic emission

Several processes occur in concrete within the fresh and hardened state. In the fresh state, the cement particles are in close contact with one another due to the attraction force. The particles can move throughout the liquid, settle at the bottom and they may hit other particles. This effect can lead to release of energy and generate elastic waves. In the

hardened state, there are several sources of the energy release, e.g., thermal effect, shrinkage processes, crack formations, gas bubble creation. The elastic waves propagate inside a material can be perceived by the AE sensors (Chotard et al. 2001, 2002). AE concerns the transient elastic waves that propagate in a medium by a rapid release of energy (Grosse and Ohtsu 2008). In this way, AE detects signals due to stress waves caused by mechanical deformation or movement by means of piezoelectric transducers, see Fig. 1.10(a-b), allowing the detection of even low-intensity activities. Consequently, the non-invasive and passive monitoring technique of AE detect stress waves emitted by processes within a material and can characterize the failure process (Shiotani 2008). These processes may be usually related to damage propagation of any form, as well as other specific processes, like leakage from a pipe or the processes occurring in fresh concrete. The transducers convert the elastic waves into electrical signal that is displayed by a software and allows data interpretation.
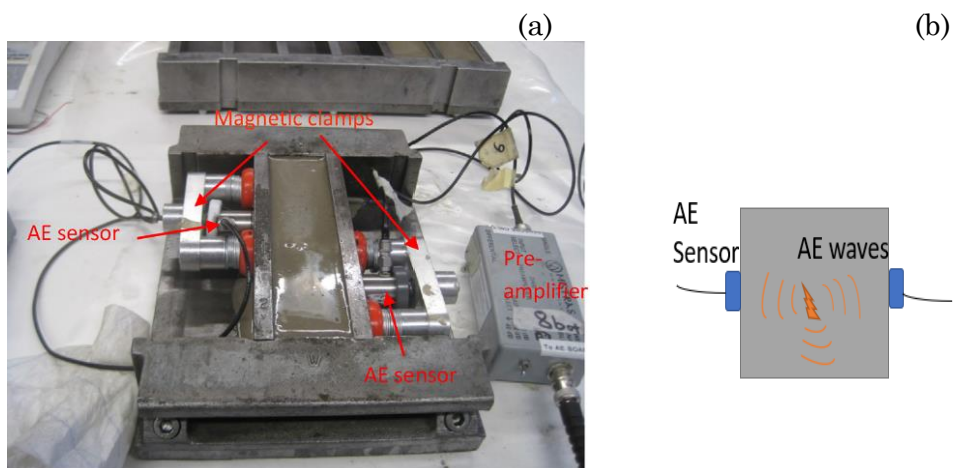
Fig. 1.10 (a) AE monitoring of fresh paste in standard mould (Dzaye et al. 2017); (b) Acoustic emission wave propagation.

In a general case, piezoelectric transducers are applied on the surface of the material to transform pressure changes on their surface in electric waveforms (Grosse and Ohtsu 2008). These signals are amplified and driven to the acquisition board where they are stored in a digital form (Mix 2003). A representation of an AE setup is given in Fig. 1.11.
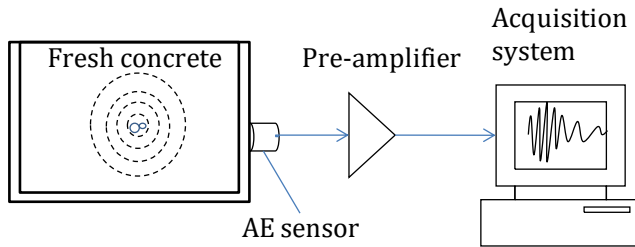
Fig. 1.11 Representation of AE setup.

An AE waveform is depicted in Fig. 1.12. The full waveform can be retained for further analysis or discarded after storing certain parameters that are considered indicative of the source and the wave propagation condition (Grosse et al. 2016). Sensor characteristics (frequency sensitivity) exercise additional influence on the waveform (Ohtsu 2010).
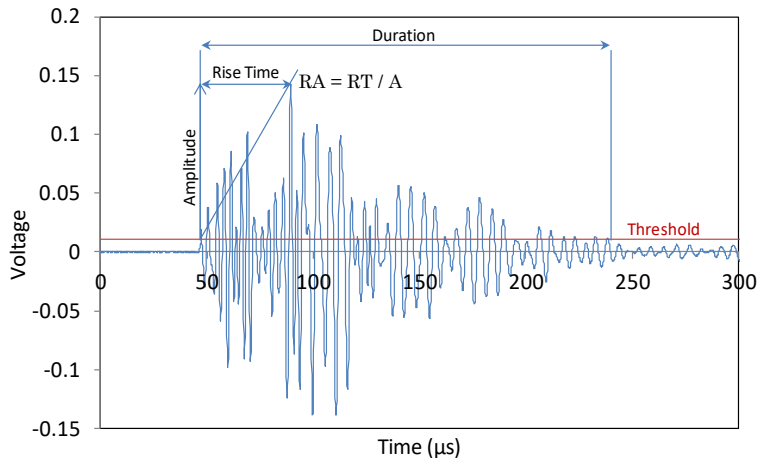
Fig. 1.12 Typical AE parameters.

The waveform starts with a "threshold crossing". The threshold is a predefined voltage set by the user to define the onset of the wave. When background noise allows the setting of a low threshold, then the measured onset is close to the real one. The time between the first threshold crossing (count) of the signal and the time of the maximum

peak is called Rise time (RT). Similarly, duration (Dur) is defined as the time between the first and last threshold crossings. Intensity related parameters include Amplitude (A) which is the highest voltage of the waveform. Additionally, energy (MARSE, measured area under the rectified signal envelope) considers the content of the waveform between the 1st and last threshold crossings. These parameters can be indicative of the mechanical energy released by the source. Based on the shape of the first part of the signal, the RA value (RT/A) or the inverse of the rising angle has been introduced. The frequency content is also important, and several parameters are used to exploit the frequency information. One of them is the "average frequency" (AF) which is calculated in time domain as the ratio of the total number of threshold crossings over the duration of the waveform in kHz. The early part of the waveform is characterized by the "initiation frequency" (IF) which is the number of threshold crossings during the RT over the RT. Additionally, the peak frequency (PF) is defined as the frequency with the highest magnitude in the FFT domain, while central frequency (CF) is the centroid of the spectrum. In addition, AE is able to detect the location of the sources (Verbruggen et al. 2016). Further, the technique of AE concerns the number of active sources and also classifies the fracture mode (Goszczyńska et al. 2012). The number of AE signals relative to the load may be important in health monitoring scheme (Suzuki and M. 2004). An important feature of AE is the cumulative activity (or the number of recorded signals during a process) and the parameters related to the waveform shape and frequency content. Additional information about the AE source can be supplied by analysis of waveform parameters. High frequency content of the waveforms is indicative of the tensile failure mechanism, while signals with long duration and rise time (RT) (see Fig. 1.11) indicate shearing as has been seen in composites, concrete and granite (McCrory et al. 2015; Mpalaskas et al. 2014, 2016; Vidya Sagar and B. K. 2012). In the following sections, the stress wave technique of AE in cementitious material is presented, as it shows sensitivity to different mechanisms occurring in fresh and hardened concrete.

Acoustic emission in cementitious materials

The application of AE that allows the detection of stress waves, have become the focus of attention. AE is traditionally applied to hardened concrete to assess the damage formation during loading (Arrington and Evans 1977). Other researchers studied AE signal recorded by concrete frost damage due to freeze-thaw cycles (Kaufmann 2004) or by early-age cracking in restrained fiber-reinforced mortar (Kim and Weiss 2003). The non-destructive technique of AE has been also applied to concrete structures to determine the shrinkage development (Shiotani et al. 2003), to assess the damage level after loading (Ohtsu et al. 2007) and to classify the mode of cracks (Ohtsu and Watanabe 2001). Furthermore, the passive monitoring of AE has been applied to identify the crack location (Ohtsu et al. 2005), to investigate the corrosion of steel bars in reinforced concrete (Van Steen et al. 2019) and to determine the degradation (Nguyen-Tat et al. 2018). The non-destructive technique of AE has been used in the field of bridge inspection to monitor bridge health (Nair and Cai 2010), to determine different failure mechanisms in steel-fiber reinforced concrete (Wu et al. 2000) and to predict concrete residual life (Ohtsu 2018) among others.

AE has been increasingly used in fresh concrete as it shows sensitivity to wave signals during the setting of concrete. Information of the different AE parameters clarifies the understanding of the several activities in fresh concrete, as well as during hydration of concrete at an early age. Van Den Abeele et al. (Van den Abeele et al. 2006) studied the effect of water to cement ratios on AE activity and determined the highest AE number for the specimen with the lowest water to cement ratio. The AE signal started some hours after casting since the fresh concrete has a damping effect on the waveforms. In another approach, Van Den Abeele et al. applied AE to monitor the processes occurring at different hydration stages. (Van den Abeele et al. 2009) used two sensors of 375 kHz resonance placed on top of waveguides to collect signals from the microstructural activity of fresh cement mortar. The main AE activity started prior to the main temperature change and it is expected that the mobility of bubbles and aggregates were restrained. According to the authors intensive AE activity indicated strong hydration phenomena and therefore, was combined with higher temperature development and strength. Fig. 1.13(a) illustrates an increase of cumulative AE events

starting prior to the main temperature increase. The observation can be related to several changes in the hydration process. At this point, the pulse velocity (P-wave velocity and S-wave velocity) continues to rise as shown in Fig. 1.13(b) due to intense hydration activity. It is expected that a network of solid compounds has been formed in the volume of the material. After achieving the temperature peak, the cumulative AE events increases further. This reflects shrinkage evolution of concrete during the hardening process.
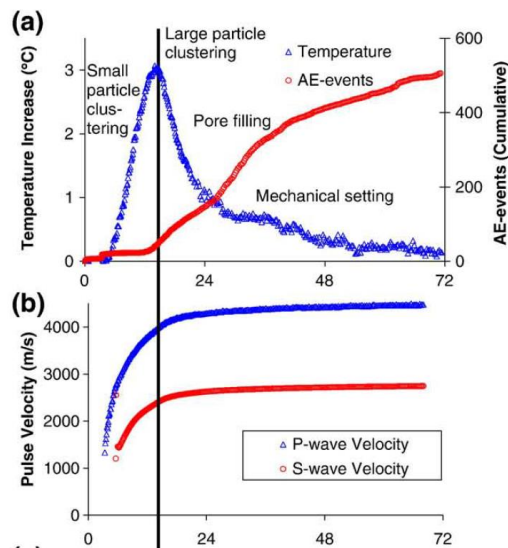
Fig. 1.13 Temperature evolution, cumulative AE events and pulse velocity increase during the first three days (Van Den Abeele et al. 2009).

Several researchers have used AE to monitor cement hydration at the early age. Chotard et al. considered AE to study internal changes of the cement paste and observed 3 different stages of hydration during the first 24 h. AE count and internal temperature evolution increased during the second stage from 3 h to 6 h due to the exothermic peak of the accelerated hydration process and setting due to the formation of hydrates and creation of porosity (Chotard et al. 2001). Chotard et al. (Chotard et al. 2003) measured the setting of calcium aluminate cement and observed a shift of the frequency range from viscoelastic state with 0-100 kHz to an elastic state with 300-400 kHz due to the hardening of the material. The

AE events were associated to the creation of hydrates, emptying of the capillary pores and the consumption of the water (Chotard et al. 2003). Fig. 1.14 presents the internal temperature development and AE cumulative hits increase of calcium aluminate cements during the first 24 hours. In their further work, they presented that during cement hydration AE can qualitatively predict the mechanical behaviour of cement paste (Chotard et al. 2005). Similarly, in (Bardakov and Sagaidak 2016) AE sensors with a frequency range of 30-300 kHz mounted on a waveguide has been used to predict the mechanical behaviour of fresh concrete of size (200x200x200) mm from its early age properties since the number of recorded signals was attributed to the amount of hydration products.

During cement hydration, AE parameters of amplitude, signal strength and duration presented a correlation with internal temperature gradient (Assi et al. 2018). Assi et al. employed AE technique to study the correlation between recorded AE activity and potential cement hydration mechanisms during the first 72 h of curing. They investigated 3 distinct stages of early hydration process depend on the temperature evolution curves, and AE signals were divided into signal subsets. AE signals recorded the highest duration, amplitude and signal strength in the acceleration stage near the temperature peak. Possible causes for AE signals are the formation of CSH, emptying capillary pores, crystallization of ettringite, delayed C_3A hydration (McLaskey et al. 2007).
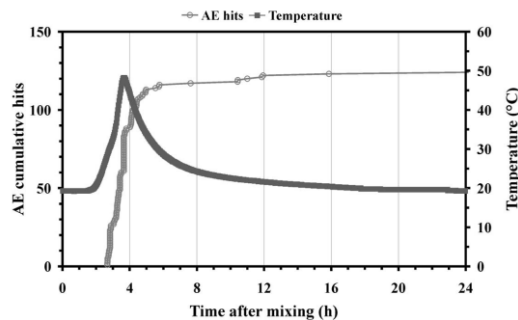
Fig. 1.14 Cumulative AE hits and internal temperature versus time after mixing (Chotard et al. 2003).

In (Qin et al. 2014) embedded piezocomposites with sensitivity up to 600 kHz were applied for AE monitoring along with a commercial transducer fixed on a waveguide. Based on the cumulative hits curve, three stages were discriminated, starting with low activity, followed by high AE rate escorted by strong temperature increase and shrinkage cracking, while later low AE was again recorded. AE was considered sensitive to crystal evolution and grain sizes. More AE was recorded for higher grain size (Chotard et al. 2002). The dissolution of grain and the formation of new phases produce AE events.

In another approach, AE was attributed to the cavitation in cementitious materials. Cavitation involves bubbles that influence each other, grow and coalesce (Leighton 1995). Similar observations for AE activity were presented by Lura et al. (Lura et al. 2009), demonstrating the formation of gas filled bubbles in the pore system and associated cavitation due to self-desiccation, as the main cause for AE activity. In this study, sensors of 375 kHz were used and carbonized refreshments were also tested showing quite high activity during the first minutes after opening the bottle and pouring into the mould. Cavitation of air bubbles was considered the most dominant source in the AE activity recorded from fresh concrete in this study approximately 8-10 h after mixing. Low water to cement ratio presented significant AE activity around the setting time. The main period of AE signals started around the final setting time for cement paste as shown in Fig. 1.15.
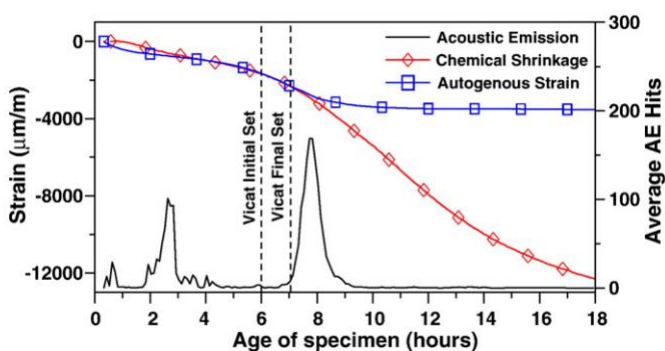
Fig. 1.15 AE activity, chemical shrinkage, autogenous shrinkage and vicat setting time (Lura et al. 2009).

Another approach AE activity was connected to the development of the crystal structure and when it was mostly completed (i.e. up to 6 h) AE noticeably decreased. This technique was based on waveguide concerned the frequency band 100-500 kHz (Skal's'kyi et al. 2004). The specimen was cubic of 100 mm side and AE was recorded earlier, approximately 20 min after material preparation.

Recently, another approach was published (Bardakov and Sagaidak 2016), where after mixing, the AE recording rate in the range of 30-300 kHz started at a maximum and gradually decreased later on. The authors attributed this activity to the mobility, or the mechanical deformation of the mixture that occurs during the early hours. The rate of AE at specific periods of the experiment (when microstructure was being developed) was positively correlated to the final compressive strength.

The onset of AE activity may indicate the transition from fluid-solid state because of hydration. In this way, the consistency of fresh concrete during mixing as well as the degree of compaction can be determined by AE (Grosse and Ohtsu 2008). Higher numbers of microcracks during the hardening and setting of concrete caused higher numbers of AE events (Pazdera et al. 2015).

Furthermore, the evolution of shrinkage contributes to an increase of AE events caused by an increase of the internal stresses (Topolár et al. 2017). Topolár et al. focused on the monitoring of the early-age cracking of mortars with different w/c ratio using two AE sensors of frequency range 100-800 kHz attached to steel waveguides. Here, the AE activity started at approximately 1 h after mixing. The initial hits were attributed to "plastic setting" and early hydration products formation, while the peak of AE rate came at 4 hours. The activity continued with some silent stages up to 72 h when the experiments were terminated. They studied acoustic emission activity during hardening of cement-based composites and observed that the higher the AE signal amplitude values, or the AE signal energy, the more significant structural changes arise in the form of newly formed hydrates. Additionally, at the time of early age cracking AE exhibited higher amplitude with longer duration signals in restrained cement mortars (Kim and Weiss 2003). Slightly different approaches are reported by (Ohtsu 2018) where concrete was monitored by an AE sensor

on the outer surface of the container during vibration in order to check the degree of compaction.

In another recent effort AE was monitored by sensors of 150 kHz resonance placed on the external side of the mould of concrete, with varying water to cement ratio and aggregate to cement ratio. Large recording rate was shown initially, being gradually decreased after the first hours. Good correlations were noticed between the AE parameters during setting like the total number of hits, and RA value with the final 28 days strength, without however, specific identification of the different sources (Iliopoulos et al. 2016). AE activity was greater for lower aggregate to cement ratio within the first 24 hours.

Moreover, AE has been used for characterizing the deformation of granular media due to jamming of grains and frictional slip of particles which release strain energy (Michlmayr and Or 2014). Different features in the evolution of the AE parameters can be connected to the changes in the hydrates production caused by chemical reactions, including the progressive mechanical setting of the specimen.

To better understand the relationship between the cement hydration and the microstructure development of cement systems at discrete hydration stages, the elastic-wave method of AE has been applied in this study. Many activities can be monitored as there are thousands of AE signals, and many times the AE rate seems to increase with the temperature development. The AE signals increase at distinct stages of hydration indicating several sources (e.g., settlement, temperature increase, formation of hydrates). However, the exact sources have not been identified, while in most cases, AE is scarce at the first hours providing limited information about the settlement stage. Therefore, a joint measurement of AE technique, capillary pressure measurement, DIC, temperature and displacement measurement have been performed to determine the several parameters of AE during discrete monitoring stages. This integrated approach helps to assess fresh concrete processes and allows to investigate the hydration heat evolution with the elastic wave propagation.

1.5.4.2 Digital image correlation

DIC is a well-established optical, full-field surface measurement technique (Lionello et al. 2014) in the field of engineering materials. 3D-DIC considers a pair of high-resolution cameras that builds a stereoscopic vision system as shown in Fig. 1.16. The cameras are synchronized to capture simultaneous images of the sample under investigation, at a constant time interval (Pan et al. 2016). Two charge couple device (CCD) are provided to determine strain distribution and displacement fields of a specimen. The cameras record digital images and store it on a data acquisition system. The applied software is Vic-snap to analyze the digital images. Prior to testing, the software of DIC (Vic-snap) is calibrated by means of a target-table having a uniformly spaced marker.

Fig. 1.16 DIC set-up.

The sample surface is covered with randomly distributed black/white speckles. The technique of DIC is able to track speckle patterns before and after a deformation and provides a 3D, full-field image analysis on an object surface (Sutton et al. 2009). DIC method can be applied to investigate the movement of a target in a series of digital images relative to the undeformed initial state. The high resolution of the digital cameras and high computing performance provide an accurate and precise tool to assess the surface structural deformations. Digital images are recorded

during an experiment and are post-processed to determine information that includes global displacements, relative displacements and changes in strain evolution.

The DIC software recognizes the speckles distribution and measures the grey intensity of local zones. Displacement in space translated to movement of the speckle pattern is detected as a change on the grey intensity level compared to a reference stage (Lecompte et al. 2006). In other words, the correlation between a reference and a 'deformed' image is based on the degree of grey level similarity (Sutton et al. 2009). The plane strain field is calculated as the derivative of the deformation field. Normal, shear and principal strains can be obtained (Omondi et al. 2016; Rouchier et al. 2013). The analysis techniques is based on images of the surface displacement. The analysis is determined by comparing a reference image with a series of deformed images, that is divided into subsets Fig. 1.17.

In order to optimize the calculation time and the data volume, pixels are grouped and analyzed in subset areas (Gencturk et al. 2014). The subsets are identified by their pixel intensity variation. The difference in pixels between the reference image and the target image is the displacement vector. The subset must be unique from the surrounding zone to obtain an accurate displacement measurement.

A good quality pattern should carry small subsets to have an analysis sensitive enough to detect the surface movement. From another perspective, subset should be optimally chosen to keep measuring even in the case of great movements.
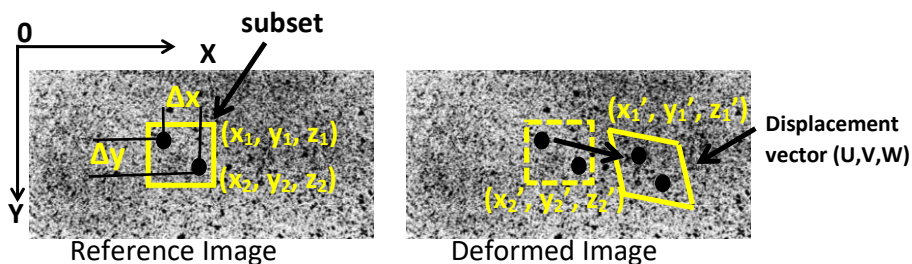

Fig. 1.17 Stochastic pattern distribution on a fresh concrete surface.

The speckle pattern quality significantly affects the DIC measurement accuracy (Lecompte et al. 2006). There are different techniques with various accuracy levels depending on the application, to create black-white speckle patterns, in which some of them are time-consuming. Beside the speckle pattern quality, DIC measurement is controlled by black-white contrast, sharpness and speckles size and distribution. There is no standardized and optimized method to apply the speckles, therefore there is a variety of different application procedures in literature, such as marked pen (Sutton et al. 2009), spray paint, screen printing and airbrush guns (Barranger et al. 2010; Lionello and Cristofolini 2014; Serra et al. 2017). The pattern should be prepared to have a clear contrast between black and white color. In the following section, the non-contact optical strain measurement technique of DIC is applied on cementitious materials to monitor the surface strain distribution.

Digital image correlation in cementitious materials

DIC can provide accurate information of the surface deformation and strain distribution due to its fully non-destructive and non-contact manner. Several researchers have used DIC to examine surface strain and surface displacement distribution. Yamaguchi is amongst the first who introduced the method of DIC (Yamaguchi 1981). This technique was extended later to measure surface profile of specimens (McNeill et al. 1997) and 3-D displacement measurements (Luo et al. 1993). The technique of DIC can capture large deformations as long as the specimen remains in the field view of the cameras (Pan et al. 2009; Schmidt et al. 2003). In several research fields, DIC has been applied to investigate textile deformability (Lomov et al. 2008), fatigue performance of polymer materials (Tao and Xia 2005), crack variation of masonry walls (Tung et al. 2008), strengthening of reinforced concrete specimens with composite plates (Muller et al. 2004), multiple growing cracks in reinforced concrete slabs (Helm 2008).

Digital image correlation (DIC) has been applied due to its optical and non-contact measurement, high precision as well as its efficiency (Banthia and Gupta 2009; Chen et al. 2018; Qi et al. 2003). DIC has been widely applied to monitor the cracking propagation in concrete structures (Choi and Shah 1997; Corr et al. 2007; Omondi et al. 2016).

Several studies have applied DIC to monitor concrete displacement, as DIC can monitor full-field and has the sensitivity to record non-uniform displacement distributions. Mauroux et al. (Mauroux et al. 2012) examined cracking of a coating mortar caused by restraint of drying shrinkage. 2D-DIC was applied to capture the mapping of shrinkage strain and to study the evolution of micro-cracking pattern on mortar surface during several days. DIC measurement was compared with classical LVDT sensors and a good concordance between both methods was obtained. In another study, surface cracking due to water transfer process and stress distribution during concrete drying was evaluated using DIC (Maruyama and Sasano 2013). Lagier et al. (Lagier et al. 2011) applied 2D-DIC to determine cracking due to drying process. They quantified the incompatibility effects between cement paste and aggregates related to drying shrinkage. Yang et al. (Chen et al. 2018) determined the effect of aggregate size and volume on drying shrinkage of concrete and mortar by 3D-DIC. The non-uniform strain distribution increased with drying time. The application of DIC in fresh cementitious materials will be discussed in detail in Chapter 4.

Up to date, there is no literature study at which DIC is applied on fresh concrete 15 to 20 minutes after casting, since the application of the speckles on a wet surface is challenging: speckles move or get absorbed on wet surface. In this work, an innovative method of the speckle pattern on fresh concrete is analyzed that allows enlightening the fresh concrete behaviour for the first time. A spray speckle pattern is applied on the specimen surface immediately after casting concrete into the mould and DIC monitoring begins a few minutes after mixing. In this way, the surface strain distribution of fresh cementitious material is investigated in a contactless mode by DIC, providing 3D full-field maps and allowing a global view of the early age deformations and strain distributions. Therefore, the measurement is not affected by the sensors due to self-weight of the sensor. The optical technique of DIC would be an improvement over the conventional methods with LVDT point measurement for settlement and shrinkage measurement. The observation has shown that DIC can deliver a series of strain contour maps to better understand the processes in fresh concrete.

1.5.4.3 Ultrasonic pulse velocity

The non-destructive method of ultrasonic pulse velocity (UPV) is an active monitoring technique that is widely used for quality control (Naik et al. 2004; Saint-Pierre et al. 2016) and damage detection of concrete structures (Petro and J. 2012). This wave-based technique proved the efficiency for monitoring the cracks and defects in concrete (Ben-Zeitun 1986; Pal Kaur et al. 2019), estimate the modulus of elasticity and the Poisson's ratio of concrete (Carrillo et al. 2019), evaluation of concrete degradation (Hwang et al. 2018), concrete deteriorations and the evaluation of concrete strength (Ashrafian et al. 2018; Kaplan and Akroyd 1959; Komlos et al. 1996; Naik et al. 2004). Furthermore, several researchers applied ultrasound pulse velocity measurements to monitor cement hydration and to detect the transition from plastic to solid state (Bhalla et al. 2018; Carlson et al. 2003; D'Angelo et al. 1995; Robeyst et al. 2009; Trtnik and Gams 2014).

The technique of ultrasonic is based on the propagation speed of the wave through a material. The ultrasonic test is applied allowing the estimation of the setting time. The wave is caused by an electric wave generator that feeds an electric pulse to the sensor acting as pulser. The pulser transforms the electric signal into mechanical wave through its piezoelectric element and this is transmitted through the material and received by a receiving transducer, which is usually of the same type as the pulser. The received pulse is transferred into an electric signal that is amplified and stored, see Fig. 1.18.
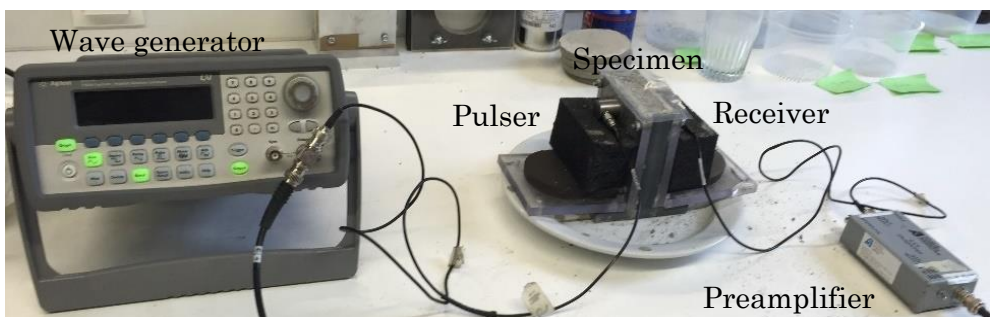
Fig. 1.18 Ultrasonic pulse velocity set-up.

The ultrasonic pulse velocity (V) is the ratio of the propagation distance (L) to the propagation time (δt).

$$V = \frac{L}{\delta t} \qquad \text{Eq. 1. 2}$$

The fresh state of concrete presents a low ultrasonic measurement due to the negligible stiffness and the high attenuation of the material. With increasing age, concrete micro-structure stiffens due to the drying process and the CSH gel formation that causes an increase in the pulse velocity. The specific details of the application of UPV in fresh cementitious materials in this study will be discussed in Chapter 3.

Chapter 2: **Acoustic emission of isolated sources**

This chapter presents two main mechanisms of mechanical origin: the aggregate and bubble movement through cement paste are isolated and their characteristics on AE are studied. In addition, experimental results are complemented with numerical simulations to enhance the understanding due to the complexity of the wave propagation problem. Recently, several studies have emerged related to fresh concrete monitoring, as AE has the sensitivity to record waves from many different processes, even though no external load is applied to the specimens. Due to the complexity of the activity including among others formation of hydrates, settlement, water migration, early age cracking, the accumulated AE cannot be easily explained. Therefore, these mechanical sources, which are active in the fresh state of the material, are isolated in an effort to study the conditions under which they produce recordable acoustic emission. This chapter is based on the following paper:

Dzaye, E., De Schutter G., and Aggelis D.G. 2017. "Study on Mechanical Acoustic Emission Sources in Fresh Concrete." *Archives of Civil and Mechanical Engineering* 18(3):742–54.

2.1 Introduction

The physical and chemical processes taking place during setting and hardening of concrete is complex. Even though concrete technology has made great advancements, the exact interpretation of phenomena and interaction between different physical and chemical parameters are yet to be precisely determined. Monitoring of the early stage of the material is important as this stage defines in a great degree the final properties of the hardened concrete.

As will be discussed below, many processes occur like settlement, formation of bubbles and hydrates, mobility of bubbles and water and shrinkage cracking, among others. Since all of them may overlap in time, it is in general a very difficult task to explain the origin of AE populations. This chapter wishes to contribute to the field by isolating and examining two physical mechanisms, namely impact of aggregates due to settlement, segregation and bubble release. These are processes that occur while the cement-based material is still fresh and viscous before the matrix hardens and restrains any mobility. Experiments are conducted by impacting aggregates in paste in a controlled way as well as creating bubbles by inducing air pressure in cement paste through a hose. Results are compared with reference conditions like bubbles in water matrix and aggregate impact on empty moulds. In addition, numerical simulations of wave propagation are conducted to enlighten the propagation path and help to understand the conditions under which the different signals are received.

This chapter will focus on cases where the monitoring starts from the liquid stage, meaning just minutes after mixing. However, there are also studies on hardening cement when the material is not yet fully hardened and is prone to shrinkage cracking, but it can still be considered "fresh", like (Chotard et al. 2001; McLaskey et al. 2007; Pazdera et al. 2014; Shiotani et al. 2003). An overview of the AE in fresh and hardening concrete was given and discussed in the previous chapter and will not be repeated here.

The different studies do not utilize the same experimental setup including type of AE sensors, coupling conditions with or without waveguide, specimen size and material composition. However, their contribution is important in that different mechanisms are targeted; mechanisms that are dominant at different ages after mixing. A general conclusion is that, if the setup allows, numerous AEs are monitored even from the moment of mixture, before hydration reaction essentially starts.

2.2 Objectives

Still many questions are open. A basic one concerns the exact sources of AE in fresh cement and concrete. In addition, the effect of wave propagation between the source and the receiver is also of great importance. This study aims at making a contribution to the field by studying in isolated fashion two mechanisms that are active during the very early age of cement; this is mechanical impact by aggregates and air bubble formation and movement. Air bubbles are in any case included in the matrix in a percentage between 1% and 10% depending on the compaction. Due to gravitational forces, heavy aggregates tend to move downwards, and cement particles settle down forcing water and air bubbles to rise (bleeding). Aggregates are heavier than fresh cement paste having a common density of approx. 2600 kg/m^3 compared to paste of 1800–2000 kg/m^3. Therefore, it is reasonable that they move downwards in the mixture. To examine this issue, the mechanisms are physically isolated. A long vertical steel mould is used in this case. Glass spheres of specific diameters are used as aggregates and they are let to drop from the surface of the paste. Due to gravity, they impact the bottom and create waves that are received by AE sensors. The results are analyzed relatively to the medium (reference air, water and cement paste) and the diameter of the spheres. Similarly, the contribution of air bubbles is explored based on controlled air pressure introduction in the cement paste filled mould. It is shown that both individual mechanisms are certainly capable of producing noticeable AE and conclusions are drawn about improvement of the setup in order to receive this activity.

2.3 Experimental setup

The applied AE system used in this study is a Micro-II express of Mistras Group that allows recording of the AE parameters and the full waveform. AE monitoring was applied by means of three piezoelectric sensors (R15, Mistras). Specifically, the AE sensors of 150 kHz were attached on the outer side of the steel mould which has the shape of 40x40x200 mm (internal dimensions) and thickness of 10 mm. To improve the coupling between the mould surface and the sensors, a viscous silicon grease was applied on the surface of the sensors. The low ambient noise allowed applying a low and sensitive threshold of 35 dB and the signals were amplified by 40 dB. During the test, magnetic clamps were used to hold the sensors on the outer sides of the metallic mould.

Fig. 2.1(a) presents a photograph of the experimental setup. The distance between the sensors on the steel mould is 50 mm. The positioning of the sensors is shown in Fig. 2.1(b). For the experiment with aggregate emissions, different sizes of glass spheres were used, namely 3, 5 and 8 mm to study the impact in air, water and fresh cement paste. The glass spheres were let to drop to the bottom of the mould to monitor the impact on AE by the three sensors. Three different cases of filling were investigated, namely the empty mould, water-filled mould and mould with cement paste.

Furthermore, concerning the air bubble investigation a nozzle was arranged vertically at different heights in the same steel mould. The nozzle allowed air into the mould, containing either water or fresh cement paste, see Fig. 2.1(c). The pressure was set to the minimum as the intention was to have a slightest possible bubble creation (the indication was essentially 0 bar in the meter device).

The materials used in the experiment to prepare the cement paste (cement CEM I 52.5 N and water) were mixed for 3 min in a mortar mixer at moderate speed. Cement paste was made using Portland CEM I 52.5 N with a density of 3090 kg/m³. Cement and water were mixed in a mortar mixer. After that, the paste was poured into the mould in a single layer. The measurement started immediately after casting the cement paste into the mould. The duration of the AE experiments was between 5 and 8 min in order not to allow any change of the texture due to possible

36

hydration. Four different specimens were cast to check the repeatability of the glass sphere drops. It was seen that for low w/c (0.5) the paste was too viscous and therefore, the w/c was adjusted to 0.7 while a small quantity of plasticizer was added to the paste (Sikaplast Techno 80, 0.15% by weight of cement) to ensure the desired fluidity in order to achieve penetration of the glass sphere to the bottom of the mould.
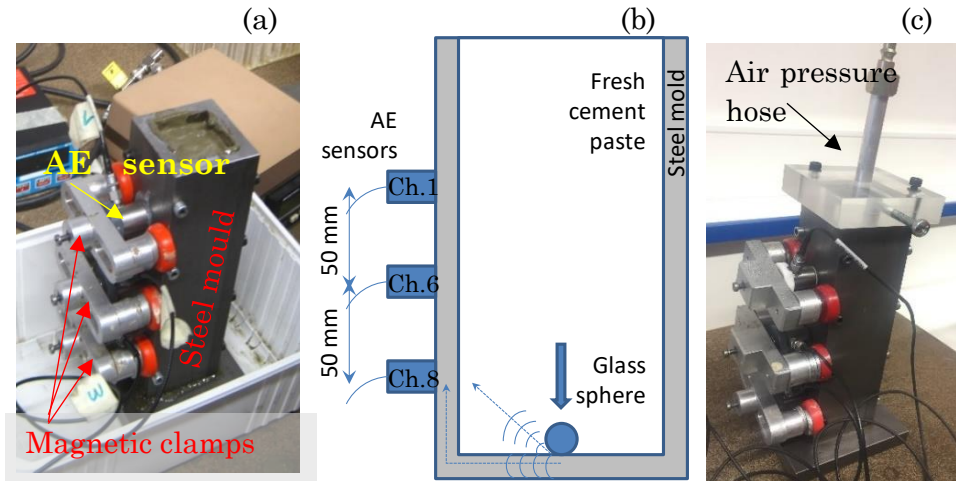
Fig. 2.1 (a) Photograph of the experimental setup; (b) representation of the experiment in cross section including the sphere impact, steel mould, sensors (channels 1, 6, 8) and possible propagation paths; (c) photograph of the experimental setup for air pressure.

In the following sections, the impacts of aggregate in empty mould, water-filled mould and paste-filled mould are discussed. After that, the effect of bubble release in different media and the corresponding AE waveform during bubble creation are discussed.

2.4 Results

2.4.1 Aggregate impacts

Each time a sphere was let to drop in an empty mould (reference), it had several bounces, which could be easily measured by the corresponding AE signals. Specifically, each drop was accompanied by three hits (one received by each sensor). The sensor at the bottom (ch.8), which was

closer to the impact point, registered each time the highest amount of energy. After the sphere bounced on the bottom surface another sequence of three hits was recorded by all sensors and with the same order in energies and delay times related to the position of the sensors. In Fig. 2.2 one can see the energy of the successive signals and even measure how many times the sphere bounced on the bottom (in this case 11 times). As reasonable, the energies of the successive bounces decrease until no more bounces are noticed. The whole action lasted more than 1 s. For each impact, the delay between acquisition at the bottom (ch. 8) and top (ch. 1) sensor was between 16-18 µs. Considering their distance of 100 mm, it corresponds to pulse velocity of approximately 5900 m/s that is characteristic of the steel material of the mould. The three hits indicated in the circle of Fig. 2.2(a) come from the reflection of the initial wave from the top of the mould as is indicated by the opposite order of time arrival (first ch.1 top, last ch.8 bottom). There was usually no reflection noticed for the 2nd or later bounces, as it was more likely below the acquisition threshold.

The corresponding results from a similar test in a water-filled mould are shown in Fig. 2.2(b). In this case, the energy of the first hits is one order of magnitude lower (10^7 attoJ), the delay between successive bounces is much longer and only three bounces are evident. This difference can be attributed to the effect of friction and water viscosity that does not allow transformation of the whole dynamic energy to kinetic during the drop of the sphere, essentially slowing down the sphere.
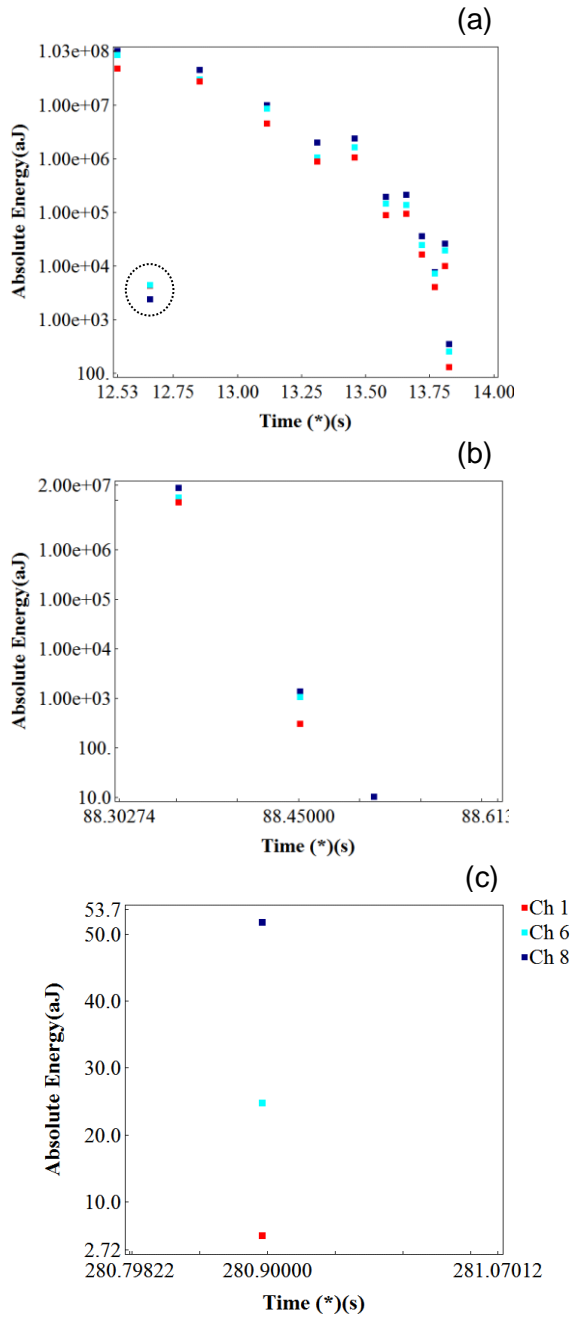
Fig. 2.2 absolute AE energy for impact of glass sphere in (a) empty mould; (b) water-filled mould; (c) paste-filled mould.

Finally, Fig. 2.2(c) presents the AE energy registered by the three sensors in the presence of fresh cement paste. In this case the viscosity and density of the cementitious matrix is much higher than water and this does not allow any bounce after the initial impact while the energy level is much lower.

These results come from individual representative drops of a sphere of 3 mm. Numerous drops have been conducted and averaging results are discussed later in this chapter.

Fig. 2.3 shows actual waveforms as received by the three AE sensors in all types of experiments (a) empty mould, (b) filled with water, and (c) filled with cement paste for all three sensors). The waveforms come from the first impact of the sphere with the highest energy (and not possible subsequent bounces). The amplitude in the water-filled matrix (b) is slightly lower and the waveforms seem to contain some higher frequency components than the ones in empty mould (a). The propagation conditions are very complicated, but is seen that, especially in the third top sensor (Ch.1, further away from the impact) some initial weak arrivals precede the higher amplitude burst coming some tens of µs later. This is typical for plate wave dispersion and it is the possible reason for this observation, as considering the frequency of the waves (approximately 150 kHz), the wavelength is calculated at around 30 mm, much longer than the thickness of the mould wall of 10 mm. For the case of cement matrix, as seen in Fig. 2.3(c), the waves are of much smaller amplitude, less than 1% of the water and air waveforms.

As aforementioned the waveforms in an empty mould present lower frequency (Fig. 2.3(a)), than the water or paste filled mould (b) and (c). Indeed, as seen in Table 2.1 the initiation frequency for the first case is 120 kHz, while for water filled and paste filled mould the frequencies average on 162 kHz and 778 kHz respectively. This difference is quite important bearing in mind that the same sensors of 150 kHz resonance are used in all cases.
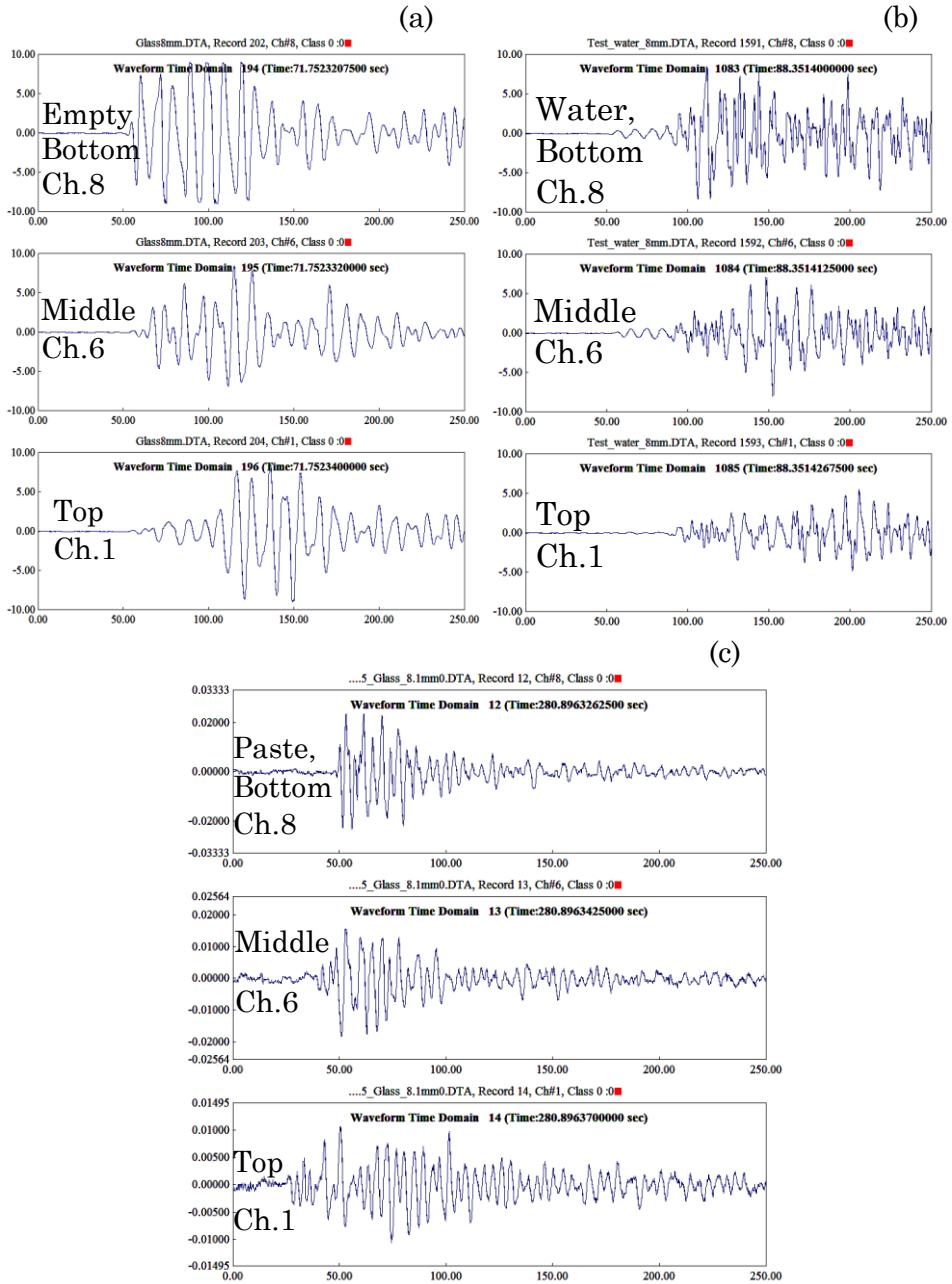
Fig. 2.3 AE Waveforms of the three sensors after a single impact in (a) empty mould, (b) water-filled mould, (c) paste-filled mould.

It should also be mentioned that the resonance behaviour of the sensors would not allow reliable spectral analysis; still the initiation frequency is a parameter considering how many cycles occur in the initial part of the time domain signal (during "rise time"). Therefore, it certainly indicates much higher frequency for the paste than the empty mould even though the value may not be exact. This would seem contradictive with the trend of increasing viscosity, but it should be considered that (nearly the whole amount of) acoustic energy propagates through the metal wall and not the liquid medium. This will be further demonstrated in the numerical simulation part.

The duration and rise time indicators are reasonably in the inverse order than frequency, with impacts in empty mould exhibiting 30 times longer waveforms than paste-filled. A reasonable explanation is the contact time between the sphere and the bottom surface of the mould. This time is inversely proportional to the excited frequencies after impact, something utilized in the technique of Impact-Echo (Ohtsu et al. 2013). The contact time is expected much shorter in the case of paste-filled mould since the speed of the sphere at the moment of impact is low. It is mentioned that the waveform durations of the successive impacts due to bouncing in an empty mould, decrease gradually from approximately 10 ms to below 1 ms at the 10th successive impact, a trend that supports the above argument, as each consecutive impact has lower velocity than the previous and the contact time of the impact that is the source of the AE hits is therefore shorter.

Table 2.1 Average values of AE parameters for 3 mm glass sphere impacts.

Filling of mould	Duration (µs)	Risetime (µs)	Amplitude (dB)	AF (kHz)	Initiation Frequency (kHz)
Empty (air)	10500	178	98.2	95.7	120
Water	3680	140	97.7	251	162
Paste	33.7	1.67	44.7	117	778

In addition, the existence of the hydrostatic pressure from the inside in case of water and even more of paste which has nearly double density, could also contribute in imposing a "stiffer" boundary condition increasing the resonant frequency of the mould.

The general conclusion from the above results is that particle impacts (due to settlement or segregation) are a mechanism that can certainly be monitored by AE sensors attached on the mould. Going a step further, the tests were repeated to check if more quantitative measurements can be conducted. Different sizes of aggregates (glass spheres) were used, namely 3 mm, 5 mm and 8 mm for impact in water and paste.

Different AE parameters (energy, duration) as recorded for the different diameters of spheres are shown in Fig. 2.4. These points come from averaging of all the relevant impacts and therefore, they do not necessarily correspond to the exact value of energies shown in the previous figures which come from individual drops. As the diameter increases from 3 mm, to 5 mm and finally to 8 mm, the absolute energy received by the sensors moves three orders of magnitude from 10^4 attoJ to 10^7 attoJ for water matrix (Fig. 2.4(a)). The results in cement paste have a similar trend but they lay a couple of orders of magnitude lower. An impact of glass sphere of 3 mm through paste on the bottom of the mould produces an average energy of 134 attoJ while a larger sphere of 5 mm has 345 attoJ and finally a sphere of 8 mm results in hits of average energy 391 attoJ.

For AE waveform duration, the situation is similar as there is again a monotonic relation with the glass sphere size. Durations in water are much longer than in paste, as seen in Fig. 2.4(b). As aforementioned, the lower values of energy and duration in paste can be attributed to two main factors. One is the viscous nature of paste that does not allow fast drop of the sphere and therefore, the kinetic energy at impact is much less than in water. Another reason could be the damping of the fresh paste compared to water that could lower the amplitude of the waveform travelling directly to the sensor through the paste. However, as will be seen later in the simulation section, this part of energy is nearly negligible, and most of the energy propagates through the metal mould.

In any case, the energy and duration of the AE hits in paste are lower than in water but they are well measurable, while there is a certain

increasing tendency with the diameter of the sphere. This is reasonable as the larger the diameter, the heavier is the weight and the energy released at impact resulting in a signal with longer duration.
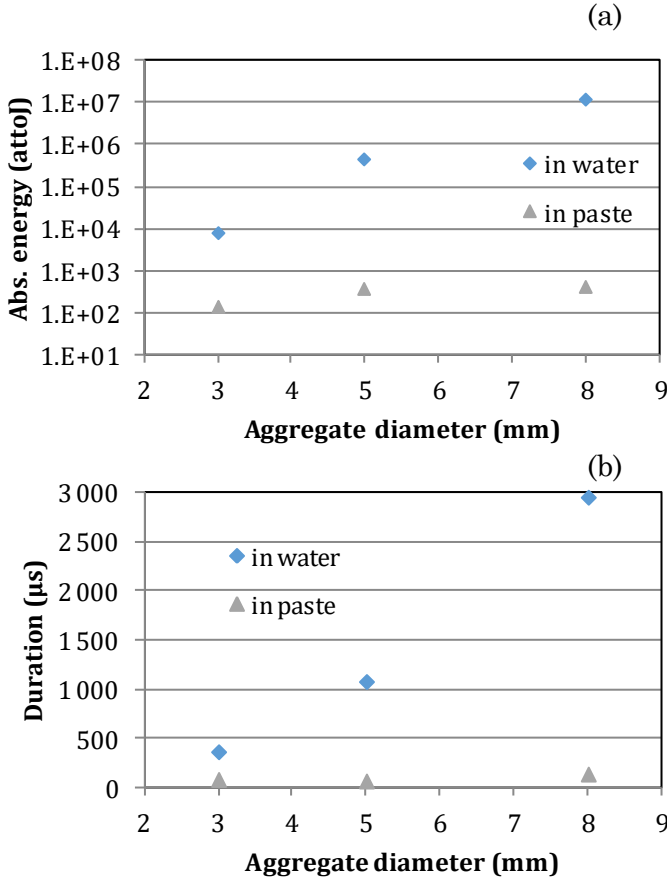
(a)

(b)

Fig. 2.4 AE parameters vs. aggregate diameter for different matrix (a) Absolute energy; (b) Duration.

The terminal settling velocity v for the glass spheres is obtained from the Stokes law (Colbeck and Lazaridis 2014; Nichols 2009; Selly 2000):

$$v = \frac{g\, d^2\, (\rho_s - \rho_f)}{18\, \eta} \qquad \text{Eq. 2.1}$$

Where g is the acceleration caused by gravity with 9.81 m/s², η presents the fluid viscosity, $(\rho_s - \rho_f)$ stands for the density difference between the particle with 2600 kg/m³ and the paste with 2000 kg/m³, and d represents the diameter of the sphere. The settling velocity increases rapidly with larger particle size. The viscosity of water was 0.001 Pa s and the viscosity of the paste was assumed to be 0.1 Pa s, being in accordance with the order of values measured in the literature for similar cases of cement paste (Bentz et al. 2012; Konsta-Gdoutos et al. 2010; Papo and Piani 2004; Struble and Guo Kuang 1995). The settling velocity in different liquids is presented in Table 2.2.

The theoretical terminal velocity for the 3 mm sphere in paste is 0.029 m/s which is lower than in water with 2.943 m/s due to the higher viscosity and density of the paste. As the diameter increases from 3 mm, to 5 mm and finally to 8 mm, the settling velocity of the sphere in water as well as in paste increases. It is proven that the velocity in water is higher than in paste and thus it is justified that due to higher speed at impact, the duration, amplitude and energy in water are higher and the frequency lower.

Table 2.2 Settling velocity in different liquids.

Particle diameter [mm]	3	5	8
Settling velocity in paste [m/s]	0.029	0.081	0.209
Settling velocity in water [m/s]	2.943	8.175	20.928
Time to fall 200 mm in paste [s]	6.795	2.446	0.955
Time to fall 200 mm in water [s]	0.067	0.024	0.009

2.4.2 Effect of bubble release in water

In this type of experiment, after establishing a certain minimum pressure in the pipe, a steady state was accomplished; regular AEs were recorded, and visible bubbles were seen on the surface of water, when the nozzle was placed close to the bottom of the mould. For cement paste the same pressure did not result in visible bubbles when the nozzle was placed close to the bottom of the mould. This is reasonably connected to the hydrostatic pressure which seems too high to allow air out of the nozzle at the bottom of the mould filled with cement paste. However, when the

nozzle was placed 70 mm from the top or approximately at the middle of the mould at 120 mm from the top, air bubbles were again visible. Therefore, the results presented for paste, are taken with the nozzle at the middle of the height.

Fig. 2.5(a) and (b) show the energy of AE according to the different channels for bubble creation in water and in cement paste, while Fig. 2.5(c) and (d) show the corresponding amplitudes. Though the range of values of energy and amplitude do not seem to differ much, a certain observation is that bubbles in paste create a much higher number of AEs. While for water the AE rate is about 1 hit/s, for paste it is nearly 30 times higher. The duration graph however, shows a difference even visually, with emissions in paste (f) being more densely located at the bottom of the duration axis than in water (e).

Table 2.3 shows the basic parameters of AE for bubbles released in water and paste. AE waveforms in paste have much shorter duration in average. Correspondingly they also have shorter rise time. One reasonable explanation is the damping of paste which would quickly attenuate the later cycles of the signal. In this case, the bubble is created within the paste matrix and not necessarily in contact with the mould. Therefore, the viscosity of the matrix plays a more important role as there is no other way for wave energy but to propagate through paste. This is somehow consistent with the fact the waveforms through paste exhibit lower amplitudes at the receiver, but considering the viscous nature of paste, this difference would be expected larger than just 1 dB. Even though the experiment was done with resonant sensors, the average frequency (AF) and initiation frequency (IF) again present consistent differences. The AE through paste again shows higher frequency measures (AF and IF).
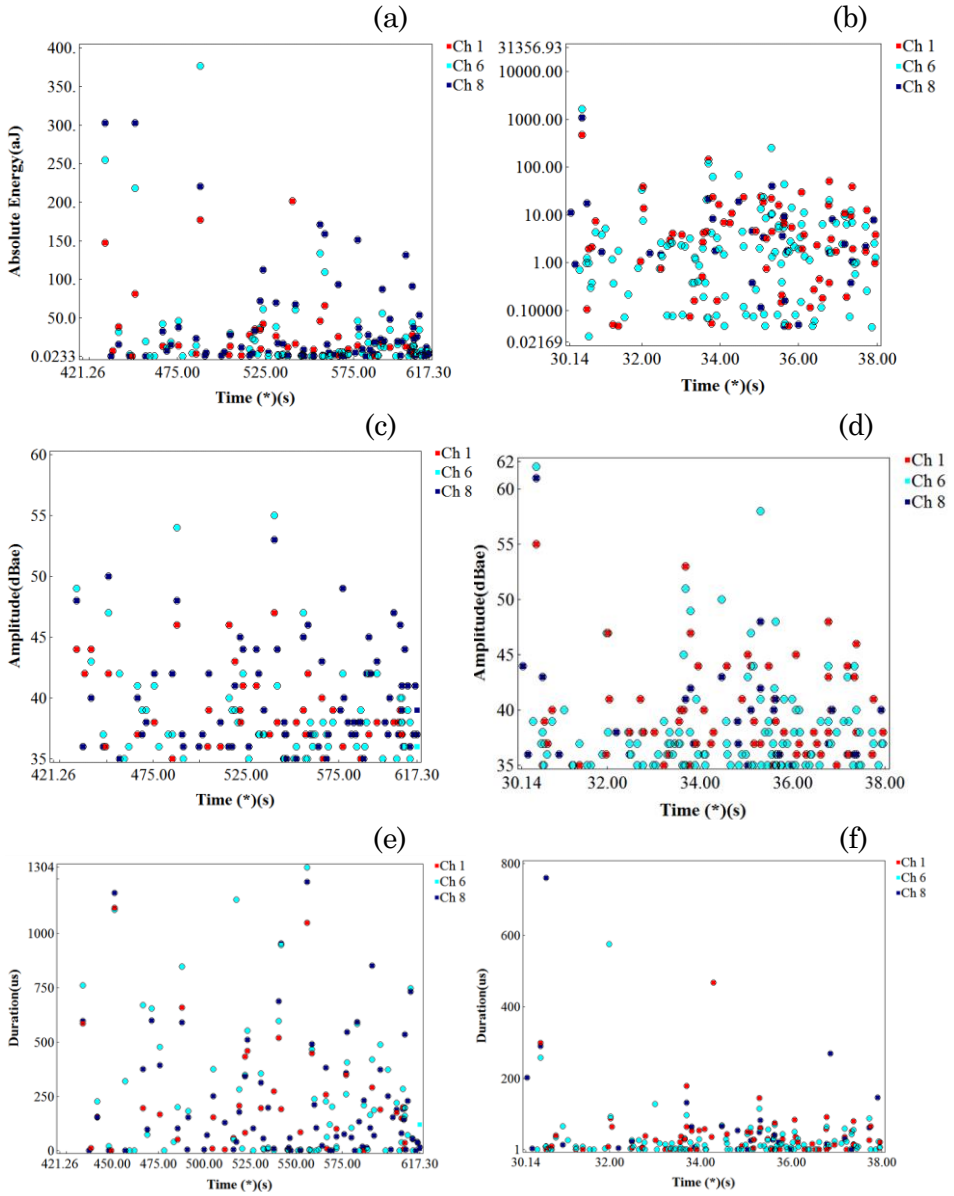
Fig. 2.5 AE parameters for bubbles release in different media: (a) energy in water, (b) energy in cement paste, (c) amplitude in water, (d) amplitude in paste, (e) duration in water, (f) duration in paste.

Table 2.3 Average values of AE parameters for bubbles in different liquid matrices.

Filling of mould	Duration (µs)	Risetime (µs)	Amplitude (dB)	AF (kHz)	Initiation Frequency (kHz)
Water	236.5	48.2	39.3	138.9	359.8
Paste	42.1	8.1	38.6	222.5	565.8

As was seen in the Table 2.3 above, the indicative waveforms of Fig. 2.6 confirm that AE waveforms through water exhibit longer duration characteristics. The waves in this case come from the creation of the bubble and the local displacement of the liquid as the bubble forms outside the nozzle. However, it is possible that one bubble creates more AE signals while it rises to the surface, e.g. by "friction" with the mould or the air pressure pipe.

In the experimental results, it is evident that both mechanisms of aggregate impact, as well as bubble creation and movement produce recordable AE within a fresh cement specimen. The aggregate impact seems much more intensive mainly because of the direct contact to the mould. In the next section, numerical simulations are discussed in order to enlighten the wave propagation conditions.
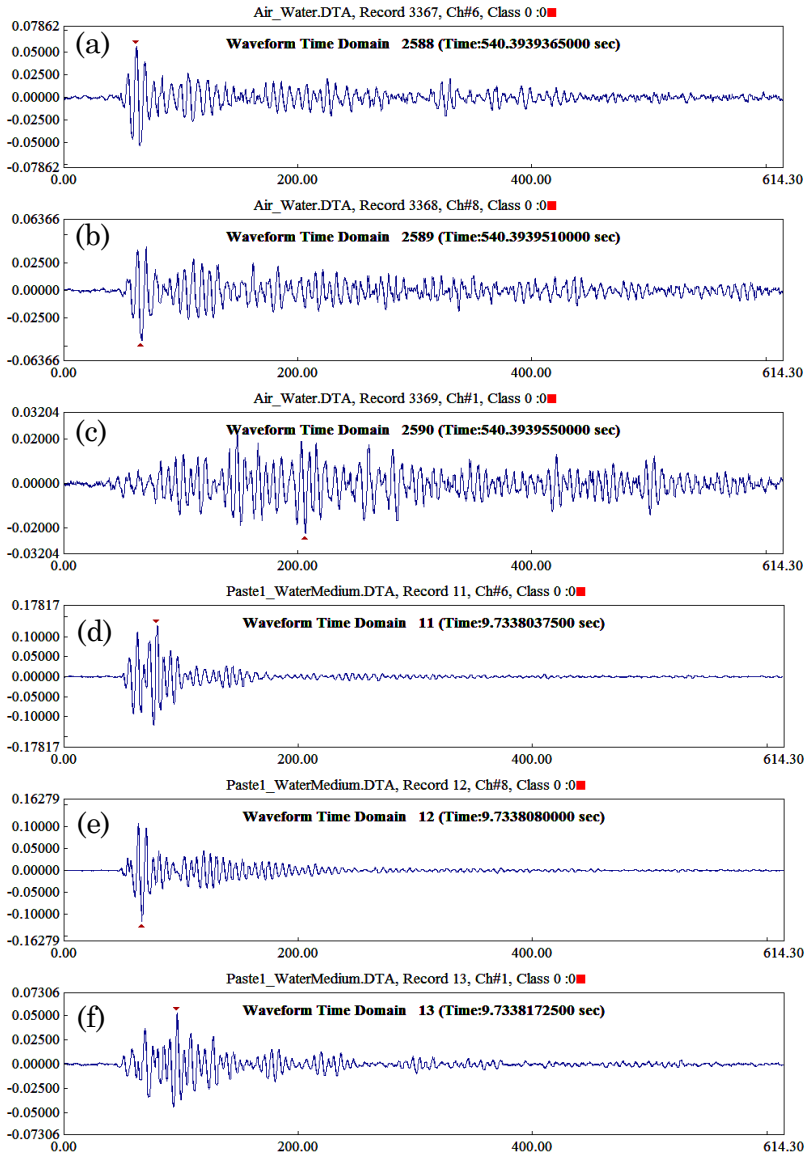
Fig. 2.6 Successive typical AE waveforms during bubble creation, (a to c) water-filled mould, (d to f) paste-filled mould.

Following are discussions on numerical simulation of AE propagation and corresponding excitation at the bottom of the mould. Initially, the simulation of impact is discussed. Later, the simulation of bubble effect is discussed in detail.

2.5 Numerical simulation

2.5.1 Simulation of impact

Numerical simulations are conducted to enlighten the conditions of propagation. Using AE sensors at the predefined locations gives information on the energy that arrives on the sensor surface, but it provides less information on the followed path. In the specific case, it is important to know if most of the energy propagates through the metal or through the liquid. Herein simulations are conducted with the commercially available software WAVE2000. It solves the 2D elastic wave equations using a method of finite differences. The specific acoustic equation that is simulated is:

$$\rho \frac{\partial^2 u}{\partial^2 t} = \left[\mu + h\frac{\partial}{\partial t}\right]\nabla^2 u + \left[\lambda + \mu + \varphi\frac{\partial}{\partial t} + \frac{h}{3}\frac{\partial}{\partial t}\right]\nabla(\nabla \cdot u) \quad \text{Eq. 2.2}$$

where: u is the displacement vector (consisting of two vertical u_x and u_y components), ρ is the density (kg/m^3), λ and μ are the first and second Lamè constants (Pa), h and φ are the "shear" and "bulk" viscosity (Pa s) and t is time (s) (CyberLogoc 2017).

The first case concerns the experiment of aggregate impact at the bottom of the mould. The geometry is shown in Fig. 2.7 and it follows the dimensions of the experimental mould and the sensor placement. The excitation is one cycle of 150 kHz exactly on the interface between the inner bottom side of the mould and the liquid and the direction is vertical. The material properties are seen in Table 2.4.

Table 2.4 Material properties for simulation.

Property	Cement paste	Steel mould
Density, ρ (kg/m3)	2000	7800
Bulk modulus, λ (GPa)	1	121
Shear modulus (GPa)	1e-6	80
Resulted damping attenuation (dB/cm)	1.41	3.05x 10-5
Longitudinal wave velocity (m/s)	707	6002
Shear wave velocity (m/s)	34	3200
Acoustic impedance, Z (MRayl)	1.41	46.8

The longitudinal wave velocity in paste was adjusted to a value lower than 1000 m/s as is common from literature (Aggelis and Philippidis 2004). The shear wave velocity was adjusted to a much lower value through the shear modulus to simulate the nature of a liquid that cannot carry shear waves. For the steel material, negligible damping was included while damping was much higher for the paste material. The equivalent damping properties where indicatively tuned in order to result in large discrepancies between the fresh paste (strong damping) and steel mould (negligible damping). The important issue is to depict the great difference between the two materials, while attenuation is again mentioned in the "Discussion" section.

The convergence of the method was checked by decreasing the element size until no serious change in transit time to the top sensor was noticed. The finally applied space resolution was 0.1 mm while the time resolution was 0.01396 µs (or sampling rate 72 MHz). The excitation was three cycles of 150 kHz resulting in a corresponding wavelength was 33 mm for the metal and 5 mm for the paste. Therefore, these specifications are certainly sufficient as in any case there are at least 50 measuring points within a single wavelength and each cycle (period) of the waveform in time domain is represented by several hundred of points. Some successive snapshots of the displacement field are placed in Fig. 2.7.
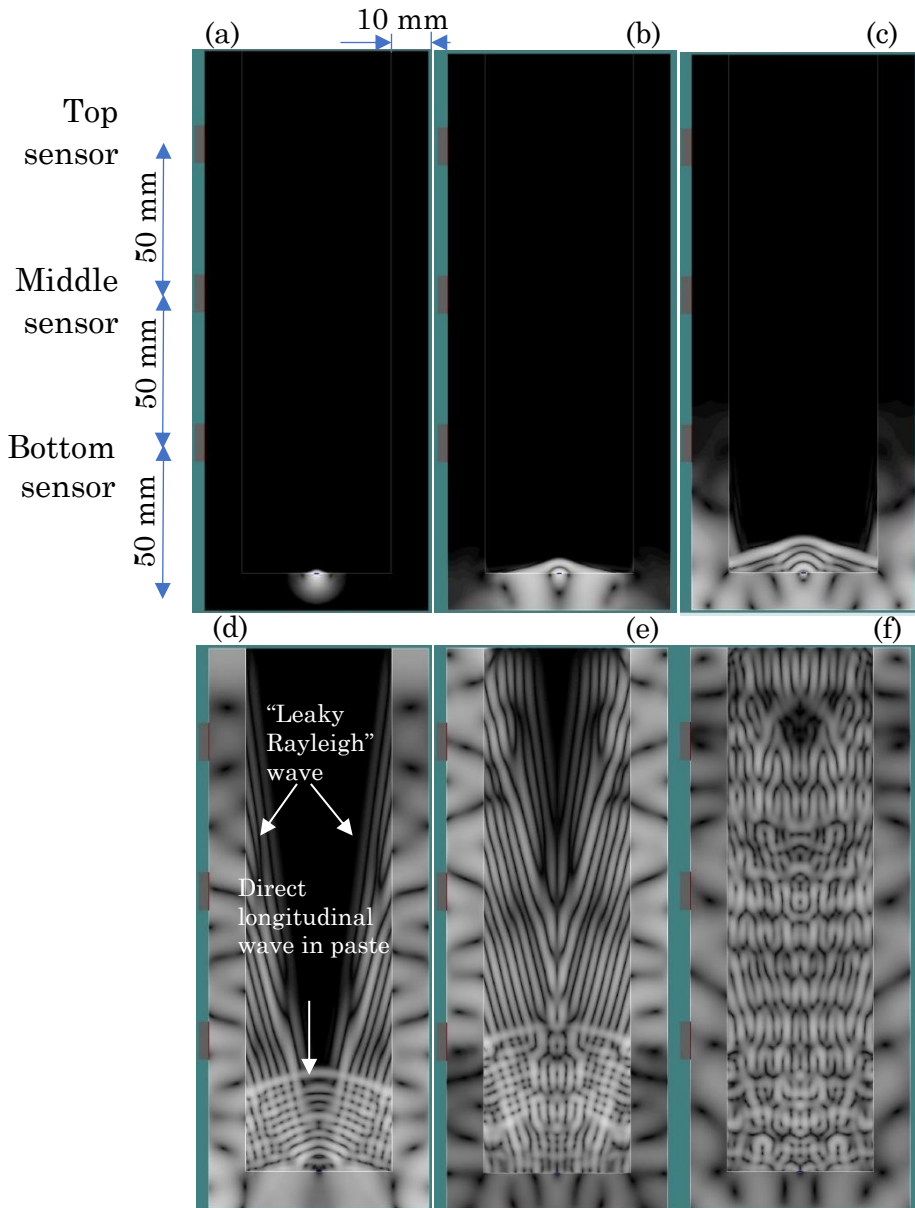
Fig. 2.7 Snapshots of the displacement field in the case of excitation at the bottom of the mould at times (a) 1.7 µs; (b) 5.8 µs; (c) 14.2 µs; (d) 39.6; (e) 57.8 µs and (f) 143.4 µs.

It is obvious that the wave energy moves much faster and reaches the receivers by the propagation through the stiff wall even though it has to

follow the geometry (right angle at the bottom left), rather than the straight diagonal path through paste. Indeed, it is seen that the contribution on the bottom receiver through the steel is expected at approximately 14 µs Fig. 2.7(c), while the wave propagating through paste seems to reach the level of the bottom sensor at 57.8 µs Fig. 2.7(e). However, as will be seen in the next paragraph, this contribution is not visible in the waveforms, as it is masked by the energy still running through the metal due to reflections. It is also worth to mention the existence of the "leaky Rayleigh wave" in the paste (see for example Fig. 2.7(d). This wave is created much earlier in paste as it is triggered on the paste-steel interface by the motion of the fast-primary wave in steel.
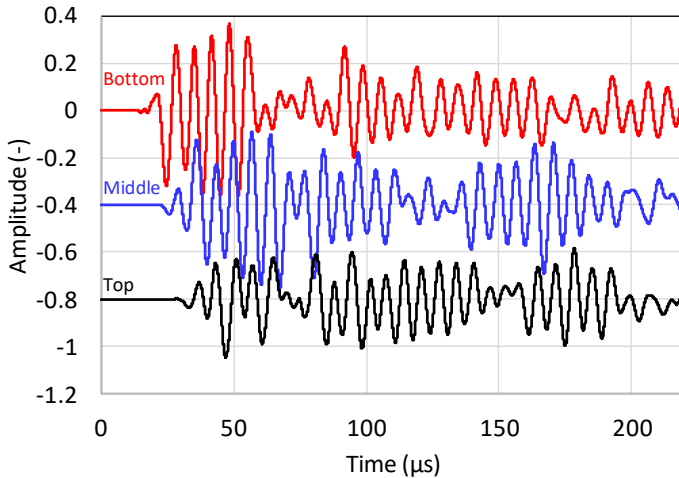
Fig. 2.8 Numerical AE waveforms of the three sensors after sphere impact at the bottom of the mould.

The exact simulated waveforms as "measured" on the sensors (displacement on the horizontal direction) are seen in Fig. 2.8. Practically at the time that the wave through paste reaches the level of the bottom sensor (e.g. after 57 µs) there is no obvious contribution to the obtained waveform. This is approximately the point when the initial burst stops and then lower energy components start arriving. This contribution is not noticeable in the numerical waveform, as it was also not noticeable in the experimental waveforms (see Fig. 2.3). This leads to the strong conclusion

that the wave energy through paste is negligible compared to the amount propagating through the metal setup. The above simulations show that positioning the sensors on the mould allows to directly get a large part of the energy of the impacts.

2.5.2 Simulation of bubble effect

In this case, the settings are the same, so they are not repeated. The only difference is the position of the excitation. Now it was indicatively placed within the paste matrix a few cm from the bottom. In addition, the excitation has both horizontal and vertical component. This was accomplished by adding two sources, one horizontal (practically executing its excitation cycle up and down) and one vertical (motion left and right). The important characteristic is that now in order for the wave to reach the sensor, it will propagate solely through the paste before reaching the metal mould and the sensor. Successive snapshots of the displacement field are seen in Fig. 2.9. A major observation is that the displacement field seems more simplified than the previous case, as most of the energy is damped within paste, without propagating into the steel. After the wave impacts the mould walls at 32 µs (Fig. 2.9(b)) a reflection is clearly visible back into the paste (see Fig. 2.9(c)). The acoustic impedance mismatch does not allow strong transmission into the steel mould, as will be discussed later.
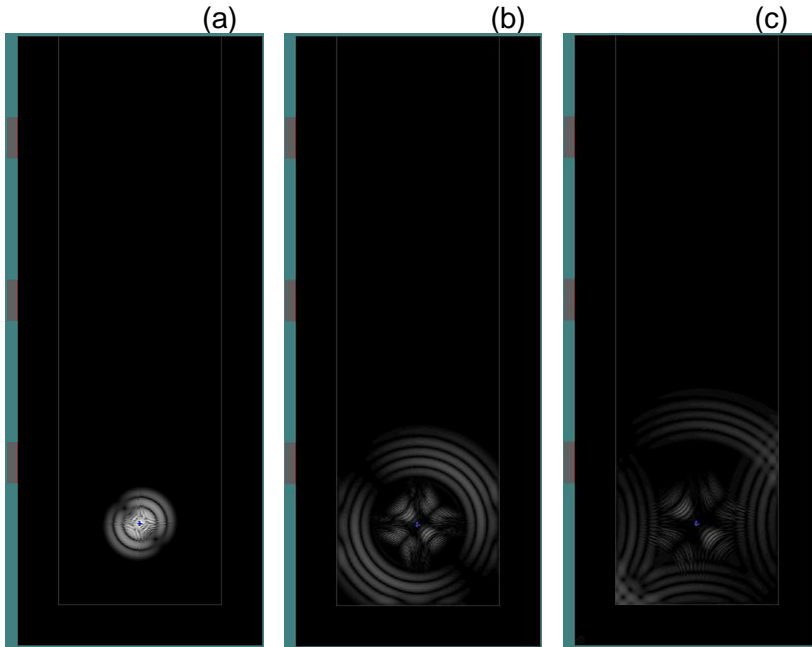
Fig. 2.9 Snapshots of the displacement field in the case of excitation at the bottom of the mould at times (a)12 µs; (b) 32 µs; (c) 45 µs.

Fig. 2.10 shows the waveforms recorded by the three sensors after the above explained excitation. They again concern the horizontal motion on each of the sensors' surfaces, in analog with the sensitivity of the experimental sensor to the same direction.

The waveforms are very weak as their amplitude is two orders of magnitude lower than the corresponding waveforms from aggregate impact, presented earlier in Fig. 2.8. As expected, due to the location of the source, the bottom sensor receives the wave first and with higher amplitude.

Fig. 2.10 Numerical AE waveforms of the three sensors after bubble excitation inside the mould.

2.6 Discussion

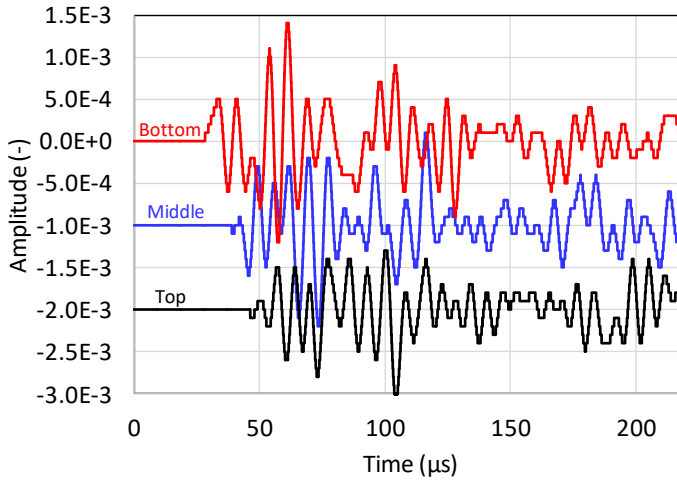Simulation results show that sources in contact to the mould are much more likely to produce a noticeable acoustic wave. Using the same amplitude of excitation directly on the mould (case of Fig. 2.7), the received signals are hundreds of times stronger than the case of Fig. 2.9 where the excitation is within the paste. This can be very well understood in terms of the acoustic impedance mismatch between the fresh liquid cement and the stiff metal mould. Taking into account the properties supplied in Table 2.4, a wave propagating from paste to steel, would exhibit a reflection of 0.94, allowing minimal amount of energy to penetrate into the mould. Most energy remains into the viscous material and it is attenuated due to its highly damping properties.

The experimental results confirm this trend as the impact of the small glass sphere of 3 mm in fresh paste, is received with an average amplitude of 44.7 dB (Table 2.1) while the bubbles created by the controlled pressure result in a considerably lower amplitude of 38.6 dB (Table 2.3). The difference in water filled mould is more impressive as the

aggregate impacts are recorded with almost 98 dB while the bubble creation is much lower at 39.3 dB.

The basic conclusion is that although several mechanical sources may be present in fresh paste, only those located close to the mould would create a strong elastic wave. This way it is indicated that a good strategy to increase the AE capability is to attach the sensors on the mould itself. If, even a small amount of energy is transmitted into the mould, this will propagate easily through the steel material and sensors located on the steel would receive it. The sensitivity of AE is such that it can record processes of the energy level of aJ (10^{-18}J). By placing AE sensors on the mould essentially the monitored volume is increased, as any source that happens close to the interface between paste-mould will be recorded.

2.7 Conclusions

Two physical processes occurring in fresh cement-based materials are targeted as to their potential to create AE as well as the possibility to be characterized through it. The basic conclusions can be summarized as follows:

- Movement of aggregates due to settlement and segregation as well as creation and movement of bubbles through the liquid matrix constitute detectable AE sources.
- Processes that occur close to the container mould wall are received by the sensors with higher amplitude indicating that placing sensors on the mould is a suitable experimental strategy.
- Numerical simulations show that most of the acoustic energy propagates through the container wall, acting thus as a "waveguide".
- Although the liquid matrix supports only a small amount of the acoustic energy, it exercises a certain effect on the received wave indirectly as it controls the mobility (e.g. physical speed) of the constituents (e.g. aggregates and bubbles).

This study is the preliminary investigation of the effect of physical mechanisms occurring in fresh concrete. The study goes on with continuous monitoring to check how the mechanisms behave with time

and to include other mechanisms that can be of physical (cement grain settlement, early age cracking) or chemical character (formation of hydrates) as will be analyzed in the next chapters.

Chapter 3: **Acoustic emission monitoring of cement paste and fly ash suspension**

In this chapter, a combined approach of several monitoring techniques was applied to allow correlations between the AE activity and related processes such as shrinkage and settlement evolution, capillary pressure and temperature development in fresh cementitious media. Characterization of the origin of different processes occurring in cement paste during hydration is complex. Therefore, in an effort to further isolate sources, just like in the previous chapter with aggregates impact and bubble movement, in this chapter, cement paste is compared to fly ash. AE is used to study the activity of cement paste and not activated fly ash (FA) leading to isolation of the mechanical sources like settlement and shrinkage from the chemical ones (e.g. hydration reaction). The results showed the sensitivity of AE to the early activities occurring in the two-reference media as well as the particle size distribution which dominates the settlement process. The content of this chapter is based on the following paper:

Dzaye, E., De Schutter G., and Aggelis D.G. 2020. "Monitoring early-age acoustic emission of cement paste and fly ash." Cement and concrete Research 129(105964).

3.1 Introduction

The early age hydration and the associated microstructural formation of concrete are the dominant factors that determine concrete durability and service life. Isolating the different mechanisms such as hydrates production, microstructure evolution and other thermomechanical changes taking place during setting and hardening, appears to be a challenging task. The risk of early age cracking arising from the development of stress concentrations is high at the initial stages of hydration (Pane and Hansen 2008). Therefore, understanding and isolating the different mechanisms of early hydration is significant as the long-term behaviour of concrete is closely related to its early age properties. As already discussed in Chapter 1, during this period, an exothermic reaction between cement particles and water takes place leading to the formation of hydration products with a complex microstructure (Taylor 1997). Isothermal calorimetry (De Schutter 1995) and thermal analysis (Pane and Hansen 2005) can provide relevant information on the different chemical processes occurring during hydration. In addition, a sensitive and precise technique is essential to characterize the influence of early-age processes like settlement and hydration which are associated with microstructural transformation and the mechanical properties and durability at a later stage. As already discussed in Chapter 1, AE has been used for monitoring of cementitious media. The results imply that it is capable of recording waves due to several processes (settlement, capillary pressure rise, formation of hydrates and shrinkage).

The present chapter aims to investigate the connection between the early age processes in cement paste and the AE signals. This is attempted by comparing measurements made on cement paste specimens with a purely FA suspension to separately study the chemical reaction (only in cement paste) and the physical phenomena occurring to both cement and FA suspension. In addition, the pulse velocity for all types of materials was monitored at the early stage. The processes occurring in freshly cast cement paste as well as during the curing period were studied and significant correlations to AE parameters, such as average frequency, rise time, absolute energy, and cumulative hits were found. These parameters are explained in the next paragraph.

3.2 Materials and methods

Three types of specimens were prepared. One type was pure cement paste while another was fly ash (FA) suspension. The reason for selecting FA was that FA in water without any further activation will not react and therefore, it was studied to eliminate the possible influence by early cement hydration on AE parameters. In addition, a third type of specimen which was a combination of cement paste and FA was also examined where mild hydration was expected. The combination of cement paste and fly ash which is an intermediate case was investigated for completeness. In literature, the mineral additive FA is applied in concrete to control the early age hydration (Ismail et al. 2007; Sakai et al. 2005), thereby improving its properties, such as autogenous deformation, Young's modulus, relaxation, thermal dilation, creep, etc. (Pane and Hansen 2008). Fly ash concrete develops lower strength at an early age since the pozzolanic reaction is activated at a mature age (Pazdera et al. 2014). However, as aforementioned, it is just used herein as reference FA suspension to study the AE produced by settlement and shrinkage without having the possibility of chemical reaction activity (that occurs in the cement paste).

Specimens of cement paste were prepared with ordinary Portland cement (CEM I 52.5N and water). The cement paste mix design had a water to binder ratio of 0.4, see Table 3.1. In addition to cement paste, the material FA class F was studied. Suspensions of FA and water with a water-solid ratio of 0.27 were prepared as shown in Table 3.1. The mixed specimens included a 50% cement -50% fly ash composition by mass (50/50 CEM-FA) with a water-solid ratio of 0.33 as seen in Table 3.1. The flow test has been applied for all the specimens according to ASTM C1437-07, see Table 3.1. All specimens were mixed for 3 min at a moderate speed in the laboratory concrete mixer. Afterwards, the material was cast into the metallic mould of size 150 x 150 x150 mm (internal dimensions) in a single layer. Throughout the study, 9 specimens were monitored, and this chapter presents firstly three specimens, while in discussion section all the specimens of FA suspension and cement paste are presented. The mixing and casting of the materials were completed in approximately 15

minutes, thereby monitoring started within approximately 15 minutes after casting.

Table 3.1 Composition of different specimens.

	Cement Paste	Cement & Oil*	FA Suspension	FA & Oil*	50% Cement & FA
Cement [kg/m³]	1481	1481	-	-	888
Fly ash [kg/m³]	-	-	1777	1777	888
Water/solid ratio	0.4	-	0.27	-	0.33
Oil/ solid ratio	-	0.44	-	0.35	-
Flow test [mm]	220	220	190	190	220

* The use of oil is explained later in Section 3.5.

The particle size distribution of the two materials is presented in Fig. 3.1. The particle size distribution of cement has one local peak in the range 0.2-0.4 µm and a second maximum peak at about 10-20 µm. The FA's particle size distribution extends to at least 300–400 µm while the cement's stops at about 80–90 µm. The particle size distribution of the ordinary portland cement (OPC) and FA were obtained by applying a laser diffractometry using a Malvern Mastersizer 2000 E particle analyser with wet unit Hydro 2000SM.
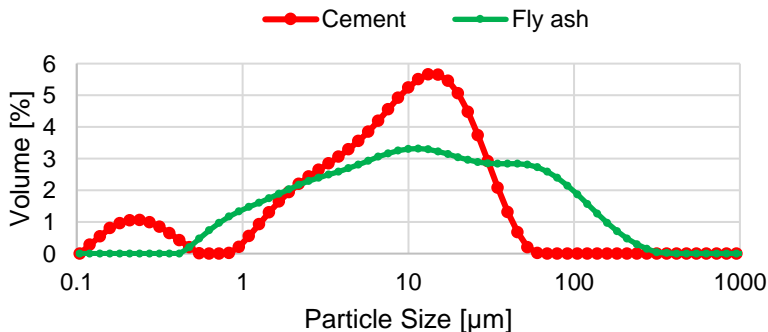

Fig. 3.1 Particle size distribution of cement CEM I 52.5N and fly ash.

3.2.1   Experimental program

The experiments were performed in a metallic cubic mould, see Fig. 3.2(a). On each side of the mould, AE was monitored by applying four piezoelectric sensors (R15, Mistras). The sensors of 150 kHz resonance frequency were placed on the outer side of the mould and a viscous silicone grease was applied on the sensor surface to improve the coupling between the sensor surface and the mould. A low and sensitive threshold of 35 dB was selected and the AE signals were amplified with a preamplifier 1220A of 40 dB. In order to hold the AE sensors on the outer sides of the mould, magnetic clamps were used during the test. The sensors were positioned at a height of 100 mm from the mould bottom. The AE system used for acquisition in this study is a Micro-II express of Mistras Group.

Displacement transformers were applied to measure the displacement caused by concrete shrinkage (Olivier et al. 2018; Slowik et al. 2008). In the metallic mould shown in Fig. 3.2(b), two linear variable differential transformers LVDTs were mounted and were used to measure the horizontal displacement between the mould and the markers installed in the specimen at opposite sides. The LVDTs were placed 50 mm from the bottom of the mould. Both LVDTs, unguided D6/02500URS, ± 2.5mm with a sensitivity of 155.68mV/V/mm, were arranged horizontally and placed 50 mm from the bottom of the mould. The LVDTs have an uncertainty of calibration of 1.6 µm. The metallic mould has a quadratic base form, thereby identical displacement was expected in both horizontal directions, e.g. x and y, which are perpendicular with each other. The horizontal displacement $\varepsilon_{horizontal}$ has been determined according to the following equation. Negative $\varepsilon_{horizontal}$ describe shrinkage, while positive $\varepsilon_{horizontal}$ expresses expansion of the specimen.

$$\varepsilon_{horizontal} = \frac{\delta_{LVDT1} + \delta_{LVDT2}}{L_{mould}} \qquad \text{Eq. 3. 1}$$

One further LVDT, captive guided ACT500-L10S/N, ±12.5mm with a sensitivity of 53.04mV/V/mm, was placed vertically at the specimen's free surface to measure the settlement. The vertical LVDT has an uncertainty of calibration of 6.2 µm. The sensor tip was applied on a 20 x 20 mm2 wide metallic wire lattice which was placed on the specimen surface,

thereby preventing the penetration of the sensor tip and the floating of the sensor target.

(a)

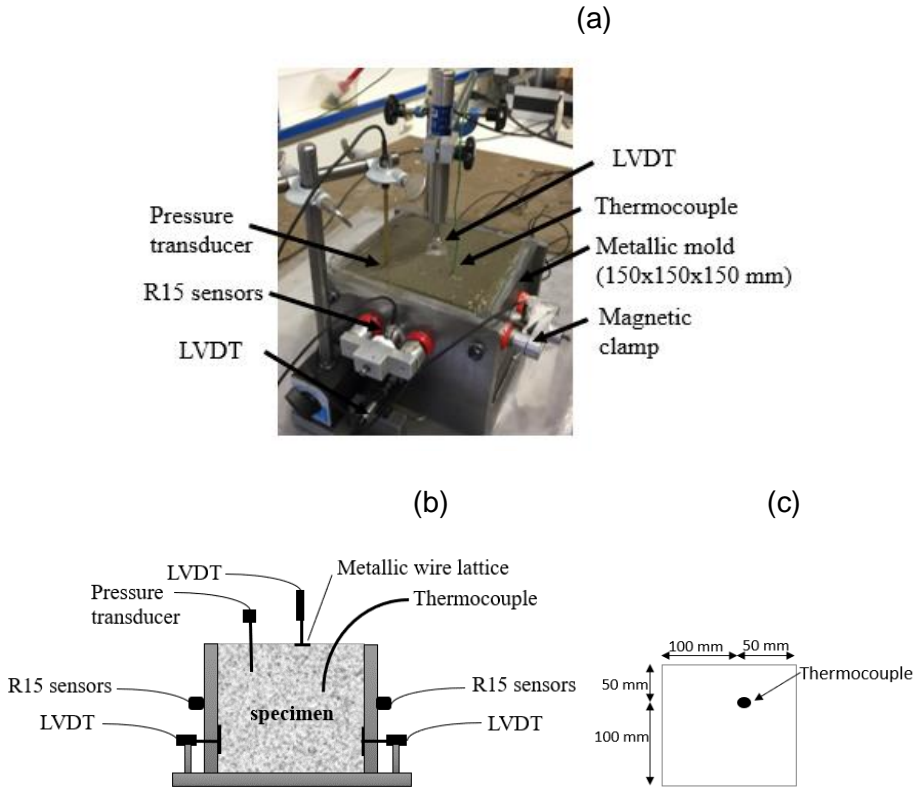(b)   (c)

Fig. 3.2 Experimental setup (a) overview of the experimental setup; (b) metallic mould including LVDT, pressure transducer, thermocouple and AE sensors; (c) Thermocouple position in top view.

In addition, the capillary pressure and specimen temperature were monitored. The capillary pressure has been detected by means of Kulite Semiconductor XTL-123-190M-1.7BARA with a sensitivity of 58.9mV/barA. The pressure transducer to measure the capillary pressure development was connected to the pore system of the fresh specimen by a 150 mm long brass tube with an inside diameter of 4 mm. A piece of water saturated sponge was inserted into the tip of the brass tube to prevent the outflow of the water. The brass tube was filled with de-ionized water and was arranged vertically 30 mm deep into the material from the top surface. The pressure sensor converts pressure into an

electrical signal. These signals are transferred to the acquisition board where they are stored in a digital form.

Moreover, one thermocouple, type K with an accuracy of ± 0.8°C was inserted in the specimen at a depth of 40 mm, prior to the start of the test to measure the temperature development, thereby monitoring the hydration process as shown in Fig. 3.2(c). The thermocouple sensor contains two wire legs of different metals that are welded together at one end to build a junction. In this way, the thermocouple produces voltage that is temperature dependent due to the thermoelectric effect and can be interpreted for temperature measurement.

All the measurements were simultaneously recorded in the same mould, ensuring the precise correlation between all the parameters. All inside surfaces of the metallic mould were lubricated with a release agent to minimize any frictional forces. Curing of the specimens occurred in a temperature-controlled laboratory room and the duration of the monitoring experiments was approximately 2 days. The room temperature was set at 20 ±1 °C and relative air humidity at 50%.

To provide an estimation of the setting time (Trtnik and Gams 2014) of the specimens, the ultrasonic measurements were conducted on a separate U-shaped plexiglass container, using two AE sensors of 150 kHz, one as pulser and one as receiver. The pulser was connected to a waveform generator Wave Gen 1410, that sent a pulse of 150 kHz and duration 5 cycles every 3 min. The electric signal was transformed to elastic wave through the piezoelectric transducer (PZT) of the sensor and propagated through the plexiglass wall into the examined specimen and the 2nd container wall. Then it was recorded by the receiver and transformed back into an electric waveform. The transit time was calculated by comparing the time of the electric excitation (also directly recorded in one acquisition channel) and the response of the receiver after eliminating the propagation time through the walls and sensors (delay time of the system equal in this case to 6.9 µs) measured in a face to face configuration (walls touching each other, without cement in between). The thickness of the sample was nominally 19 mm but measured each time with a sliding calliper and the sampling rate of the acquisition was 10 MHz (time step 0.1 µs). For hardened material, transit times of approximately 7 µs were recorded (through cement paste) resulting in a

typical error of 0.1/7=1.4%. The velocity was calculated by dividing the aforementioned thickness over the transit time, which was detected by the first threshold crossing. The threshold was kept as low as possible to increase the sensitivity and it was determined as 20% higher than the maximum noise level which was recorded in the "pre-trigger" time of the waveform (first 500 points or 50 µs). Slight changes in the threshold did not result in meaningful changes in the velocity values and certainly not in the (increasing) trend of ultrasonic pulse velocity (UPV).

3.3 Results

To show the direct effect that produces the heat of hydration, the heat of evolution is presented in the following. The degree of hydration $\alpha(t)$ presents the stage of the hardening process and is defined as the hydrated cement fraction $C(t)$ to the initial cement amount C_0 ,as shown in Eq. 3.2 (De Schutter et al. 2014).

$$\alpha(t) = \frac{C(t)}{C_0} \qquad \text{Eq. 3.2}$$

The approximated degree of hydration can estimate the released fraction of heat of hydration, as presented in Eq. 3.3 (De Schutter 1995). Where Q(t) stands for the cumulated heat of hydration after time t, Q_{tot} stands for the cumulated heat of hydration at complete hydration and q(t) stands for the heat production rate at time t.

$$\alpha(t) = \frac{Q(t)}{Q_{tot}} = \frac{1}{Q_{tot}} \int_0^t q(t)dt \qquad \text{Eq. 3.3}$$

The total heat of hydration Q_{tot} at completion of hydration depends on the cement composition. In the case of Portland cement, Q_{tot} can be estimated from the chemical composition by Bogue's formulas for A/F $\geq$ 0.64 (Eq. 3.4). The mineralogical composition of ordinary Portland cement was determined with the Bogue's formulas as aforementioned and is shown in Table 3.2. Ordinary Portland cement (OPC) CEM I 52.5N was used for all the specimens. The total heat production for complete hydration of

different cement minerals can be seen in Table 3.3. Subsequently, the total theoretical hydration heat Q_{tot} is determined and is 474.7 J/g.

Table 3.2 The mineralogical and chemical composition for different cement types according to Bogue calculations (Gruyaert 2011).

		OPC(I)	OPC(II)	OPC(III)	OPC(IV)	OPC/HSR(I)[*]	OPC/HSR (II)
CaO	C	62.21	63.12	63.37	63.48	61.56	63.36
SiO$_2$	S	18.84	18.73	18.90	19.61	19.94	21.65
Al$_2$O$_3$	A	5.39	4.94	5.74	5.96	3.13	3.62
Fe$_2$O$_3$	F	3.79	3.99	4.31	4.13	4.76	4.13
MgO	M	0.86	1.02	0.89	0.92	/	2.02
K$_2$O		/	/	0.73	0.64	0.66	0.51
Na$_2$O		/	/	0.47	0.49	0.24	0.19
SO$_3$		3.06	3.07	3.34	2.72	2.54	2.26
CO$_2$		0.72	0.65	0.50	0.83	/	0.43
Insoluble residue		0.25	0.21	0.41	0.36	/	0.36
LOI		1.65	2.12	1.51	1.78	5.45	1.28
C$_3$S		59.67	66.92	60.05	55.64	63.93	56.68
C$_2$S		9.00	3.22	8.89	14.25	9.03	19.32
C$_3$A		7.87	6.34	7.92	8.81	0.25	2.61
C$_4$AF		11.53	12.14	13.12	12.57	14.47	12.57
Blaine fineness		390	359	353	/	310	447
Density		/	3062	3122	3107	/	3137

(/) value not determined
(*) values obtained from Baert (2009)

$$C_3S = 4.07C - (7.6S + 6.72A + 1.43F + 2.85.SO_3)$$
$$C_2S = 2.87S - 0.754C_3S \hspace{2cm} \text{Eq. 3.4}$$
$$C_3A = 2.65A - 1.69F$$
$$C_4AF = 3.04F$$

Table 3.3 Total heat production for complete hydration of the cement minerals (Gruyaert 2011).

mineral	Hydration heat (Taerwe, 1997)	Hydration heat (Meinhard and Lackner, 2008)	Hydration heat (Bentz, 1995)	Hydration heat (Taylor, 1997)
C$_3$S	502	500	517	517
C$_2$S	260	250	262	262
C$_3$A	867	1340	1144	1144[*] / 1672[**]
C$_4$AF	419	420	725	418[***]

[*] Reaction with gypsum, producing C$_4$A$\overline{S}$H$_{12}$
[**] Reaction with gypsum, producing ettringite
[***] Reaction in presence of excess CH to give hydrogarnet

The heat evolution of cement paste, FA suspension and 50/50 CEM-FA mixture are presented in Fig. 3.3(a-b). Fig. 3.3(b) demonstrates a zoomed-in heat evolution for all mixtures up to 3000 min. Within the first 20 min, an exothermic reaction between cement and water occurs due to wetting of cement, dissolution of cement, initial cement hydration and hydration of free lime. The greatest heat emission occurs during the first 24 hours for cement paste and 50/50 CEM-FA mixture, while FA suspension does not present hydration process, see Fig. 3.3(a). Between 170 min and 320 min the induction period of cement paste occurs with slow chemical reactivity as shown in Fig. 3.3(b). The mixture of 50/50 CEM-FA presents an induction period between 120 min and 300 min. Afterwards, the heat evolution increases reaching a peak at around 830 min for cement paste and at around 800 min for 50/50 CEM-FA mixture presenting an accelerated heat evolution and indicating the onset of the hardening process. In addition, the formation of hydration products takes place. The 50/50 CEM-FA mixture presents a second peak or a shoulder that could be ascribed to the conversion reaction of ettringite to monosulphate as a consequence of a lower C_3A (Gruyaert 2011; Poppe and De Schutter 2005). The curve of heat evolution presents a steady state after 6 days and it continues due to a slow activity hydration. The formation of hydration products proceeds as well as the strength evolution.

In Fig. 3.3(c) the cumulative heat of cement paste, FA suspension and 50/50 CEM-FA mixture are illustrated. The heat production rate is strongly temperature dependent. After 6 days, cement paste illustrated the greatest cumulative heat with 313 J/g solid followed by the 50/50 CEM-FA mixture with 193 J/g solid, whereas the FA suspension does not demonstrate any hydration and presents low cumulative heat curve.
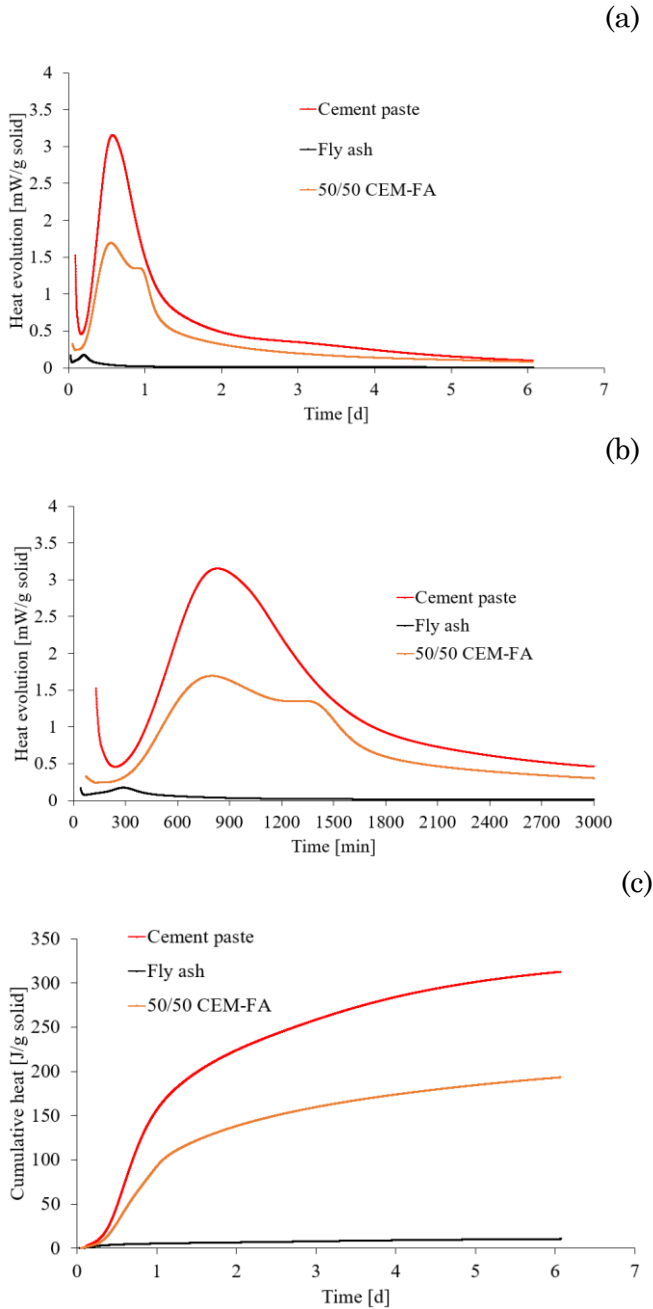
(a)

(b)

(c)

Fig. 3.3(a) Heat evolution for cement paste, FA suspension and 50/50 CEM-FA mixture; (b) zoomed-in heat evolution up to 3000 min; (c) cumulative heat as a function of time.

The heat evolution peak appears later compared to the temperature peak for cement paste as shown in Fig. 3.4(a). Presumably, this could be attributed to the effect of temperature on rate of reaction. The rate of reaction increases with temperature increase. In the isothermal hydration test, the temperature is kept at 20°C. In the larger specimen, the test starts at higher temperature, and due to the heat production, even further increase the temperature of the specimen (as the specimen is not cooled, contrary to the situation of the isothermal test).

Fig. 3.4 presents the temperature and the AE rise time (RT) results for all mixes. In this figure, as well in (Fig. 3.8 and Fig. 3.9) the plotted AE of each bar corresponds to the average of 24 minutes. The temperature of the cement paste was observed to decline slightly during the first 200 min of curing, followed by a rapid rise as the exothermic chemical reactions occurred, achieving a peak of 44 °C, see Fig. 3.4(a). After the temperature peak at approximately 750 min, the sample temperature dropped to 21°C. At early stages and before the temperature peak, the observed average RT was essentially low, approximately 10 µs, indicating that relatively short signals were received. At later times, when the temperature increased, the average rise time also increased. RT values possibly are sensitive to the point at which the cement particles become interconnected. From the obtained results, it can be seen that the average RT could be affected by the evolution of temperature.

Compared with the cement paste, the suspension of FA presented a constant temperature as well as an average rise time history as shown in Fig. 3.4(b). The average value is approximately at 50 µs, being much higher than cement paste while the bars do not exhibit as strong fluctuation. The RT curves for the 50/50 CEM-FA were very similar to those obtained for the cement paste. During the first 250 min, the temperature dropped to 24 °C, with a low average RT of approximately 20 µs. Later, the temperature increased, achieving a peak of 30 °C after 1100 min of curing, indicating an increase of the average rise time up to 145 µs. The absolute temperature of FA was lower compared to the cement paste, see Fig. 3.4(c).

It is interesting to note that for the first 3 hours, the cement paste exhibited the lowest RT with an average of 11 µs, the FA the highest with approximately 51 µs while the 50/50 CEM-FA mixture was in between at

around 25 µs. In addition, the RT history in the FA showed much less fluctuation than the other mixes. Therefore, the increase in the duration of the AE signals seems well related to the average size of the particles (for cement 10.5 µm, for FA 57.3 µm) and it will be further discussed later along with the energy and frequency results.
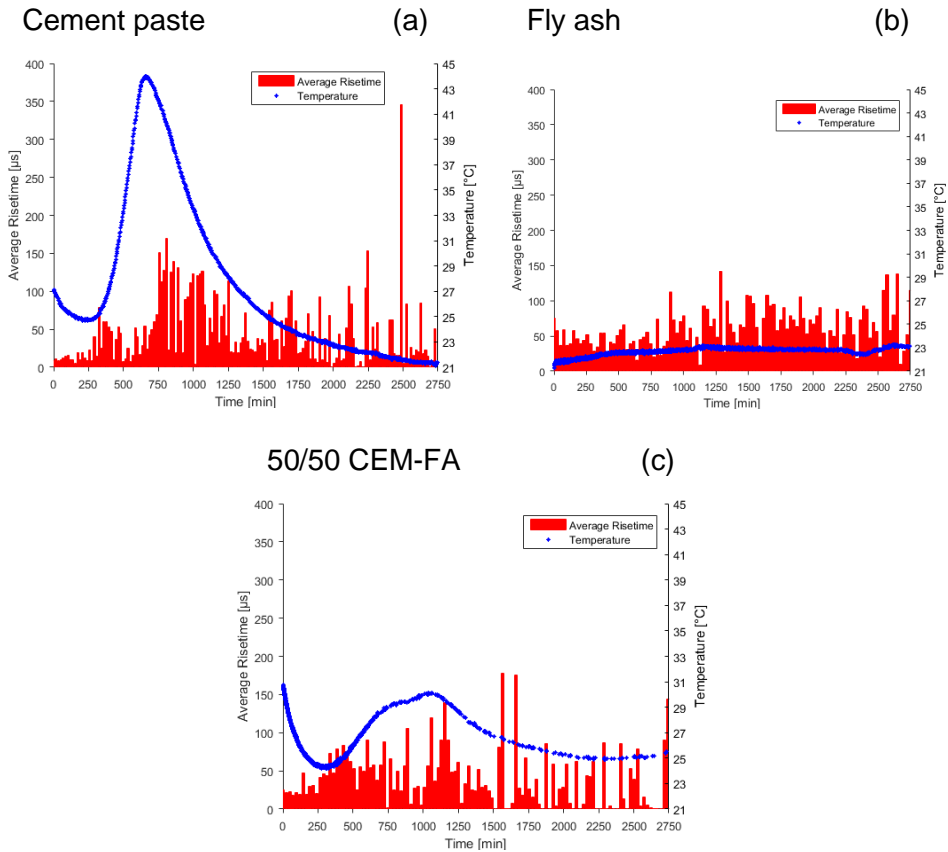

Fig. 3.4 Average rise time and sample temperature for (a) cement paste; (b) fly ash suspension; (c) 50/50 CEM-FA mixture.

Following, the results of the cumulative activity are demonstrated. AE hits recorded for the cement paste are compared with those of FA. The cumulative hits of cement paste rapidly increased during the first few hours after mixing and were accompanied by a rapid rise of the settlement due to the gravitational force, since the cement paste was in

the plastic state, see Fig. 3.5(a). After approximately 4 hours, the settlement behaviour stabilized, and this resulted in a change in the characteristics of the observed cumulative hits. This way, the settlement rate and the cumulative hits rate of the cement paste presented a significant decrease after 250 min of curing with 11 mm/m and approximately 7000 AE hits. At the early stages, the detected AE involved signals of the fluid paste while at the later stages it involved signals of the solid paste. This point of transition is significant since the connectivity of the solid paste is responsible for the strength development leading to the final mechanical strength. In addition, this point is signified by the bending on the settlement curve as after the setting the mobility is restrained and the settlement is essentially completed.

It was also found that in the case of FA the measured cumulative hits were followed by the settlement at early times as the material is in the fluid state, see Fig. 3.5(b). Compared with the cement paste, the suspension of the FA demonstrated a substantially decreased settlement with a maximum value of 4.5 mm/m and cumulative hits of approximately 1100 hits after 250 min of mixing. Hence, the application of FA suspension led to lower settlement and AE activity. Based on the obtained results, a high number of acoustic hits may be associated with settlement progression in both specimens at least for the first three hours. However, it is obvious that the correlation between the cumulative AE and the settlement was stronger for the cement paste, as the AE curve exhibited a bending point at the same period when the settlement rate was reduced. For the FA, the rate of the AE was continuously decreasing but there was no evident characteristic point in this decrease.

In addition, the AE cumulative curve is compared with the horizontal shrinkage for the cement paste and the FA in Fig. 3.5(c) and (d) respectively. The solid state may be characterized by an increase in shrinkage caused by the horizontal deformation of the cement paste. This horizontal deformation was induced by the several processes, e.g. drying process as shown in Fig. 3.5(c).
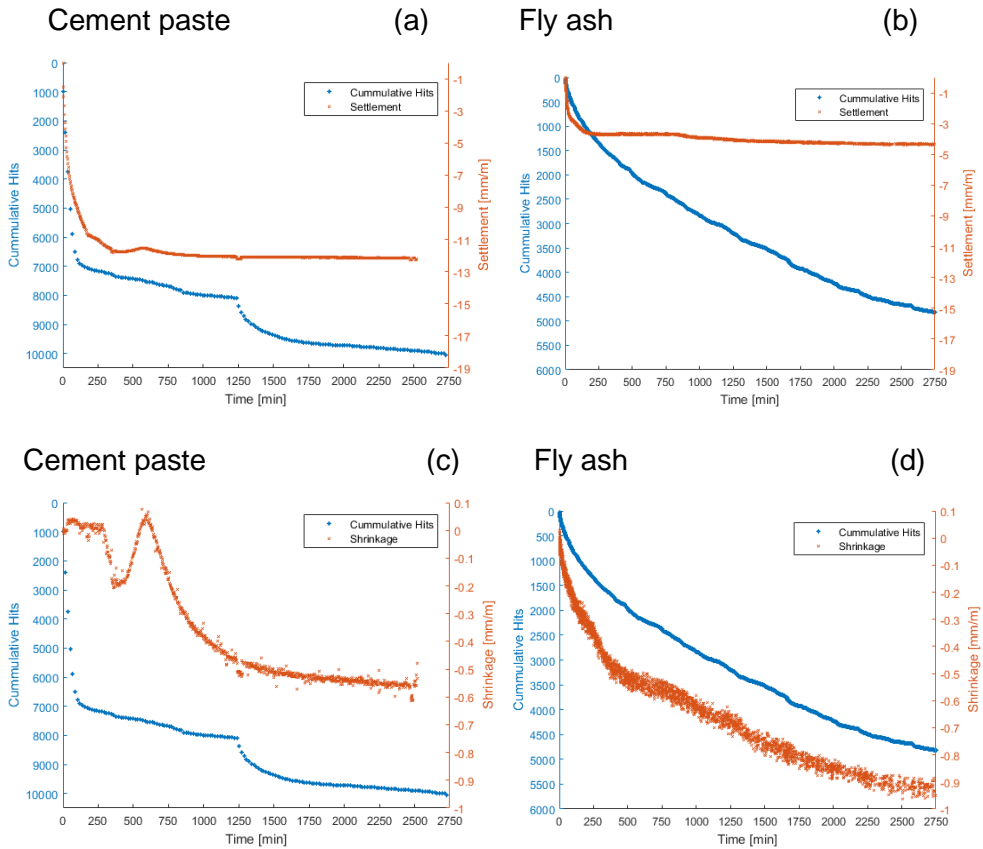
Fig. 3.5 Cumulative hits and settlement for (a) cement paste; (b) fly ash suspension; cumulative hits and shrinkage evolution for (c) cement paste; (d) fly ash suspension.

Cement paste did not present any increase in shrinkage during the first few hours after casting. Throughout the onset of the setting, a slight increase of shrinkage occurred, followed by a decrease, as the cement paste experienced thermal expansion due to hydration process, see Fig. 3.5(c). It is shown that this expansion behaviour is also present in the settlement curve in the same period, see Fig. 3.5(a), just after 500 min. After the expansion, the cement paste presented a continuous increase of shrinkage as the drying was proceeding. In contrast to cement paste, the FA suspension exhibited a tendency of monotonic increase of shrinkage from the beginning with a continuously decreasing rate, see Fig. 3.5(d).

Considering the settlement and the shrinkage curves of the paste, it can be concluded that the significant cumulative hits increase is attributed to the settlement evolution at an early age since the shrinkage progress started at a later age. However, the inverse trend was shown for the FA, where the AE curve showed to be much more compatible to the shrinkage curve, thus implying that the AE activity of the FA may be attributed to the shrinkage evolution, see Fig. 3.5(d).

The behaviour of the mixed specimen 50/50 CEM-FA is shown in Fig. 3.6(a). It is clear that there was a delay in the saturation of the settlement curve, as in this case, it stabilized after 500 min. The bending point in the AE curve was at approximately 500 min, while for the paste it came earlier at approximately 200 min and for the FA a bending point was not noticed.
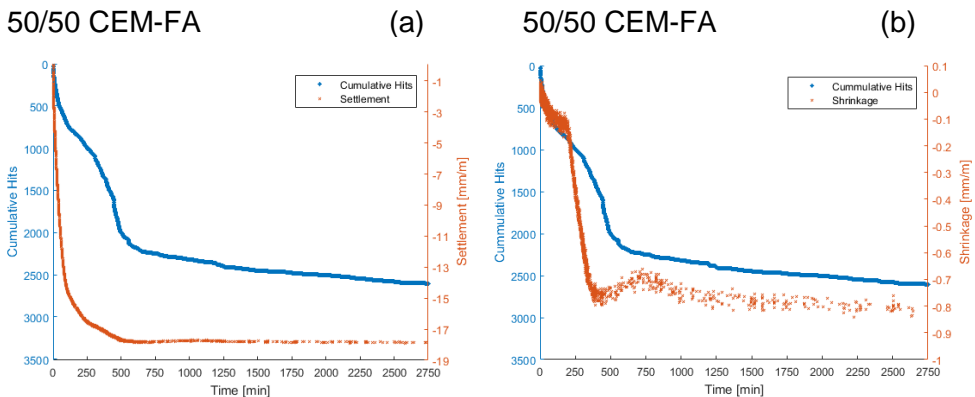

Fig. 3.6 (a) Cumulative hits and settlement during curing for 50/50 CEM-FA, (b) cumulative hits and shrinkage during curing for 50/50 CEM-FA.

The mixture of 50/50 CEM-FA demonstrated an increase of shrinkage at early stages followed by a slight decrease during the expansion period between 500 min and 750 min as shown in Fig. 3.6(b). At this point, the delayed expansion period is associated with the replacement of cement by FA since the heat of hydration is reduced. Under these observations, it can be concluded that the 50/50 CEM-FA mixture behaviour is in between the other two extreme cases. The shrinkage behaviour (see Fig. 3.6b) is again in between as it starts immediately, as in the case of FA, but progresses with a lower rate. A weak temporary reversing trend

74

leading to a local maximum in the curve at 750 min is attributed to thermal expansion, something much more evident in the paste (see Fig. 3.4c), where the expansion noticed between 500 and 750 min coincides with the temperature peak .
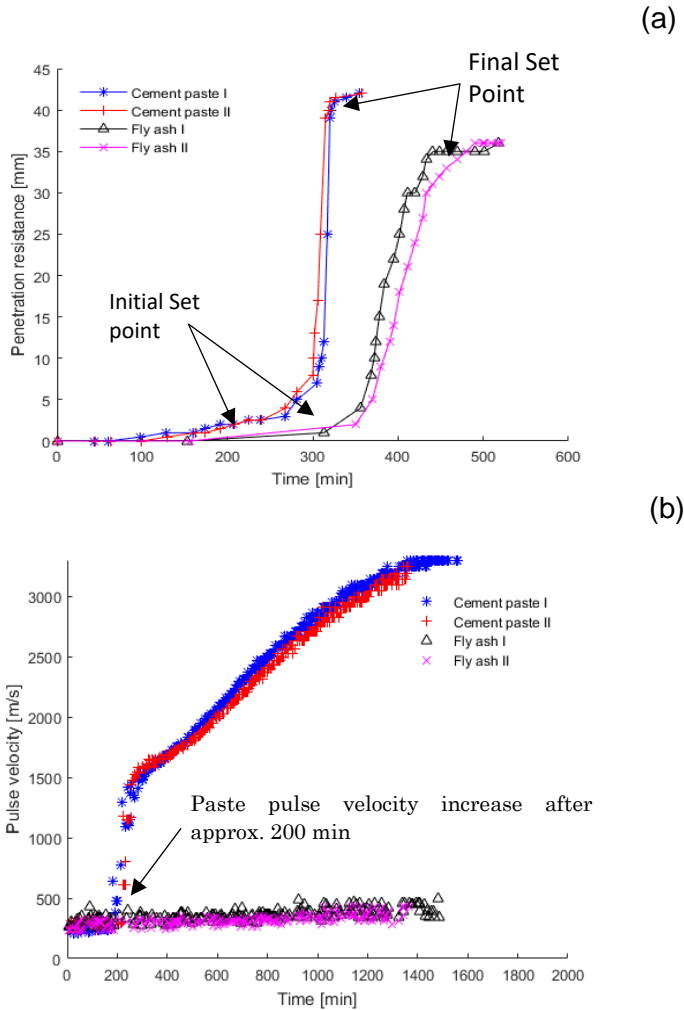
(a)

(b)

Fig. 3.7 (a) Time of setting by Vicat Needle test; (b) time of setting by ultrasonic pulse velocity.

The setting times of the cement paste and the FA suspension have been determined by means of Vicat apparatus as well as an ultrasonic pulse

velocity (UPV), as shown in Fig. 3.7. The Vicat measurements for cement paste and FA suspension have been performed according to EN 196-3. The UPV indicated an initial setting time at about 200 min for cement paste while the Vicat needle test indicated an initial setting time of about 280 min after casting. The FA suspension exhibited a "setting time" at approximately 320 min, see Fig. 3.7(a), but this is rather linked to the drying of the sample and not to real hydration processes.

The pulse velocity of the FA remained at approximately 300 m/s while the cement paste demonstrated an increase at approximately 200 min as shown in Fig. 3.7(b). It can be seen that the pulse velocity of FA remained constant, as FA in water without any further activation will not react. The increase of the RT follows the aforementioned increase in UPV of cement paste and comes a little after the bending point of the cumulative AE curve, indicating the interconnection between these parameters.

Fig. 3.8 shows the results of the average absolute energy and capillary pressure development. Cement paste exhibited a capillary pressure increase in the pore system at approximately 100 min. At this point, the evaporation of the bleed water from the surface led to the formation of menisci between the solid surfaces (Leemann et al. 2014). Consequently, the negative capillary pressure increased due to the continuous drying process (Slowik et al. 2008). The capillary pressure peak that occurs around 270 min may signify what in literature is called "air entry point" (Slowik et al. 2009). This point also implies the onset of possible shrinkage cracking either immediately or a little later. This is confirmed by AE as the collapse of capillary pressure coincided with strong peaks of the absolute AE energy. Moreover, around the capillary pressure peak, the settlement curve of cement paste achieves its maximum as well. However, due to the non-uniform pore structure distribution at the surface of the material, air penetration occurs locally. The air entry into the capillary tube of the pressure sensor is variable between different sensors within one sample at similar depths (Ghourchian et al. 2018). From the obtained measurements, it can be shown that the absolute energy increase during capillary pressure progression and collapse is valid for all mixes and with increasing energy from cement paste, to 50/50 CEM-FA and finally to pure FA suspension. Specifically, close to or at the moment of pressure drop, AE energy in paste reached 1440 aJ, while for FA the readings were between 8000 aJ and 14000 aJ, while the 50/50

CEM-FA sample was again in between. Similar trends were also shown for the very early behaviour a few minutes after mixing. The average absolute energy for cement paste during the first 24 min was 13 aJ followed by the sample of 50/50 CEM-FA with 132 aJ and lastly by FA with 528 aJ. This is related to the impact of the particle size distribution on the absolute energy signals as cement paste presented the smallest average particle size of 10.5 µm and FA presented the largest average particle size of 57.3 µm. It is reasonable that as the particle size becomes larger any movement or impact leading to the production of elastic waves will obtain higher energy as well as longer duration of the source impact, something that was confirmed in the scale of mm, by releasing glass spheres of different diameters in cement paste, as presented by the Stokes law in Chapter 2. Further, impact velocity, particle surface and plasticity could also affect the stress wave evolution and the corresponding average absolute energy (McLaskey and Glaser 2010; Troccaz et al. 2000). The elastic energy could be smaller when the particle surface roughness increases due to smaller contact radius and on smooth surfaces, the viscoelastic dissipation leads to great energy loss (Farin et al. 2015).
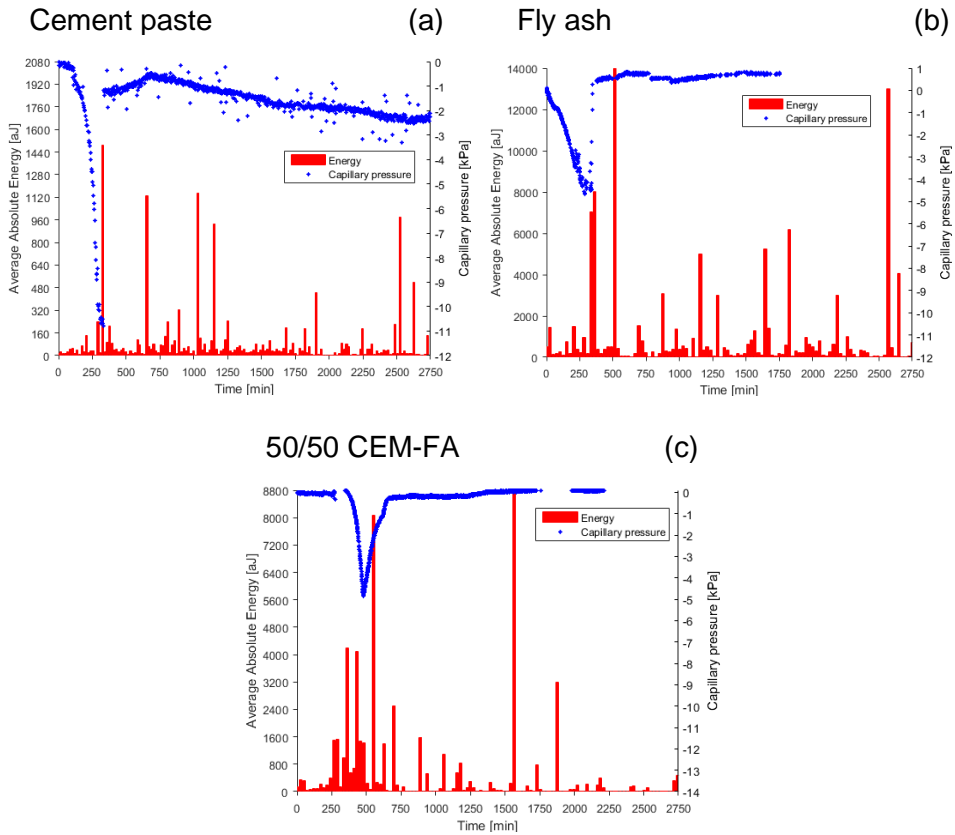
Fig. 3.8 Average absolute energy and capillary pressure development (a) cement paste; (b) fly ash suspension; (c) 50/50 CEM-FA mixture.

The absolute energy illustrated a significant increase for all three specimens at around 300 min. In this period, the risk of plastic shrinkage cracking achieves its maximum since the air-filled pores on the specimen surface are weak points.
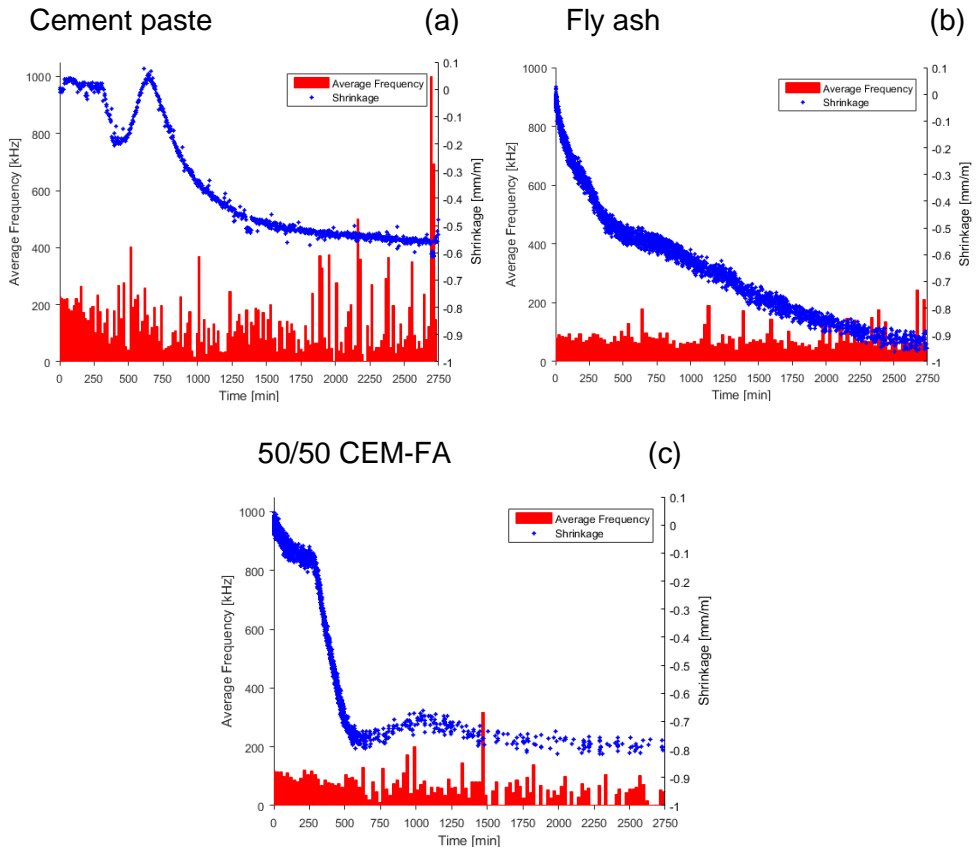
Fig. 3.9 Average frequency and shrinkage development for (a) cement paste; (b) fly ash suspension; (c) 50/50 CEM-FA mixture.

After the capillary pressure drop, the average absolute energy curve presents several peaks as the material solidifies at a later stage. The fluctuation or the several peaks of the average absolute energy may be caused by the air entry into the material since the air entry into the material does not occur simultaneously everywhere at the same pressure. It is reasonable to have similar or even higher amount of energy later than the capillary pressure drop moment as the material becomes stiffer and can transmit more energy even with a similar level of excitation source. In addition, potential mechanisms associated to AE increase may be creation of gas-filled bubbles in the pores that occurs during the formation of hydrating cement paste (Lura et al. 2009).

Concerning another important AE feature, Fig. 3.9(a) shows the development of average frequency (AF) along with the shrinkage curves.

Results from the start of the monitoring, where most of the activity is attributed to the settlement were consistent with the previous observations, related to AE energy and RT. The frequency content of the cement paste started at an average of 229 kHz, followed by the 50/50 CEM-FA mixture with approximately 118 kHz and the FA with approximately 80 kHz. This is again in relation with the average particle size. The larger the diameter of the grain, the lower the frequency content inversely to the duration and the energy. This is the equivalent to a macroscopic impact source, as described by the Hertz theory and utilized in the impact-echo test, where the frequency introduced is inversely proportional to the diameter of the particle (Ohtsu and Watanabe 2002; Sansalone and Streett 1997). As shown recently, smaller aggregate particles moving in liquid produce AE with higher frequency, lower RT and lower energy [22], something that seems to hold true for the cement and FA particles as well. For the whole duration (Sansalone and Streett 1997)of the test, cement paste exhibited higher maximum values of AF as well as higher fluctuations.

3.4 Discussion

In the chapter so far, trends from typical specimens of each mix are presented. This section contains data from all the available specimens from the two edge cases (pure cement and pure FA in water suspension) to discuss the representativity of the results. In addition, the results are presented in the form of "moving average" trend line (sliding window of 200 successive points) to show a different perspective than the bar plots which were averaged in 24 min intervals. Interpretation is not always straightforward and comes mainly through the comparison between the behaviour of CP and FA. However, in any case, the experimental observations are highlighted and discussed.

The rise time evolution of cement paste and FA suspension are presented in Fig. 3.10. In this figure, as well in (Fig. 3.11 and Fig. 3.12) the curves of 3 different specimens are illustrated by the moving average. It is noteworthy that all CP specimens exhibit a low start in their curve at the level of 20 μs, much lower than the FA ones which lie at approximately 60 μs. This can be reasonably connected to the particle size difference, as

already discussed, which plays an important role in the settlement period. After setting, the rise time illustrated a significant increase for all three cement paste specimens at around 300 min, see Fig. 3.10(a). Later, the curves seem to deviate while one specimen presented a sudden drop in RT, which can be connected to possible shrinkage cracking in that specimen or detachment from one side of the mould. On the contrary, FA specimens presented a much smoother rise time evolution in the first 500 min after mixing, as shown in Fig. 3.10(b) exhibiting fluctuations after 750 min.
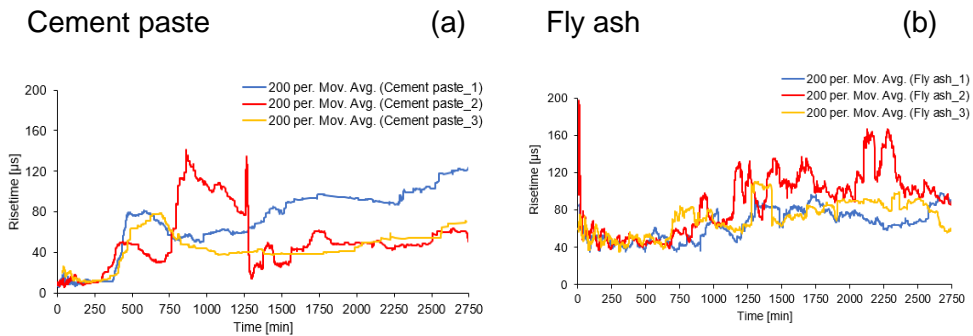

Fig. 3.10 Rise time evolution for (a) cement paste; (b) fly ash suspension.

Fig. 3.11 shows the absolute energy of the AE signals. The experimental results confirm that for the whole duration of the test, FA suspensions exhibited higher values of absolute energy as well as higher fluctuations as revealed in Fig. 3.11. The curves of cement paste demonstrated absolute energy values below 700 aJ, throughout the experiment, while the FA suspensions presented higher peaks with more than 10000 aJ as presented in Fig. 3.11(a) and (b). This is again associated with the impact of the particle size distribution since FA particles are 5 times larger on average than the cement particles.
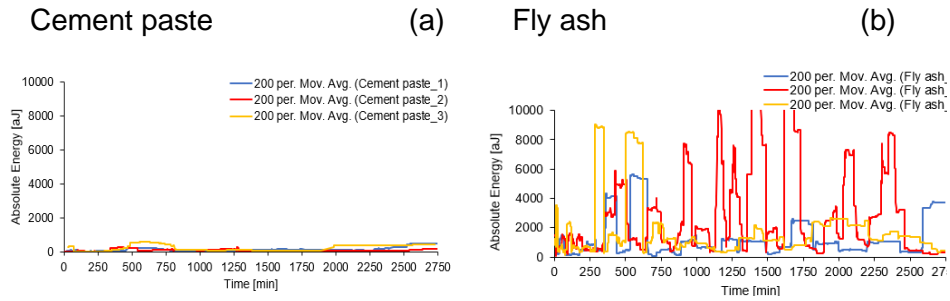
Fig. 3.11 Absolute energy development for (a) cement paste; (b) fly ash suspension.

In addition, based on the obtained results, cement paste curves illustrated higher values of AF as well as higher fluctuations compared to the FA suspensions, see Fig. 3.12. Specifically, in the fresh state, the AF content of the cement paste started at an average of about 250 kHz, while the FA suspensions illustrated a lower value with approximately 80 kHz as shown in Fig. 3.12(a) and (b). Furthermore, the AF curves of all FA suspensions are steady with smaller fluctuations compared to the cement pastes, since FA suspension does not undergo hydration.
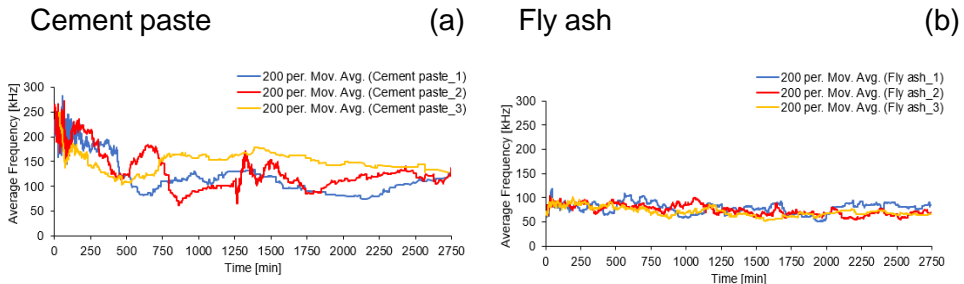

Fig. 3.12 Average frequency development for (a) cement paste; (b) fly ash suspension.

Another point of interest is related to the selection of acquisition parameters and its influence on the final result. AE is a threshold-related technique. The threshold is established as low as possible depending on the noise level of the laboratory environment. In this case it was 35 dB, a

quite low threshold, offering high sensitivity as it allowed recording of events in the absolute energy range of attoJoule (10^{-18} J). The importance is that the threshold (and all layout parameters) are constant for all specimens, thus resulting in the same sensitivity level. Therefore, the comparison between the values of different specimens can be done without fear of masking by the choice of layout. It is stressed that the importance is primarily in the comparison and not the absolute value of the AE parameters. The reason is that they are not mathematically related to a physical process and thus the absolute value is not used to directly derive another property. This contrasts with (e.g.) UPV where its value can be used for calculation of dynamic modulus of elasticity. In that case, a change in the settings may influence the UPV value and this influence would be transferred to the modulus calculation. However, for AE, there is no direct established relation (at least so far) between a parameter (e.g. cumulative AE activity or frequency) and a certain property or process of fresh concrete. Therefore, the importance lies in the studying different mixes which is valid since the exact settings are maintained.

Concerning the analysis and presentation, initially the data are represented by bars corresponding to 24 min activity each. This choice was done in the sense that the window is not too long to become insensitive to the transient evolution of properties, but at the same time it works as a sort of averaging to avoid scatter that may happen in AE monitoring tests. The selection of the time window (24 min) for the analysis is the same for all the specimens, something that allows for comparisons. Obviously, the values would be different if the window was shorter (less absolute AE hits) or longer (more AE hits), but a "reasonable" choice had to be made to proceed to the analysis. Furthermore, if one examines all different aspects, there are many parameters that would influence the absolute values and not only the choice of the time window. For example, the sensors themselves would make a great difference. For different sensor sensitivity responses, AE activity, frequencies etc. would be different in absolute values. Therefore, the key element in the study is that experimental and analysis settings remain constant in order to be able to make comparisons and attribute the different trends directly to the behaviour of the different mixes and their activity.

3.5 Settlement and cumulative hits

In this section, an effort to clarify the source of AE is conducted. As was seen, AE in CP correlates well with the settlement for the first 2 to 3 hours. However, the phenomenon of settlement consists of different processes like downward movement of particles due to gravity, upward movement of water due to the same effect and therefore, relative movement between water and cement particles with the relevant friction. In an effort to enlighten the AE source, mixes with complete replacement of water by oil were tested, as it is believed that oil smoothen any friction action. Reference cement paste is compared to FA suspensions, cement and oil mixture and FA and oil mixture to determine the AE during particle settlement in different liquids. The composition of different specimens is shown in Table 3.1. All specimens were mixed for 3 min at a moderate speed in the concrete mixer. After that, the material was cast into the metallic mould of size 40 x 40 x 200 mm (internal dimensions) in a single layer with 3 AE sensors installed on the side of the metallic mould, as discussed in Chapter 2. An overview of the experimental setup is illustrated in Fig. 2.1.

Fig. 3.13(a-b) illustrates the cumulative hits evolution and settlement evolution for cement paste and cement and oil mixture. Cement paste demonstrated a settlement evolution of -9 mm/m with approximately 750 hits after 350 min, while cement and oil mixture presented a settlement of -19 mm/m with 440 hits at approximately 350 min. The obtained results demonstrate greater settlement for cement in oil suspension compared to cement paste but at the same time less AE activity. Considering that oil is expected to smoothen any friction between particles, this result implies that actually the friction involved in the settlement movement is responsible for a large amount of AE recorded in normal cement paste.

Cement paste (a)

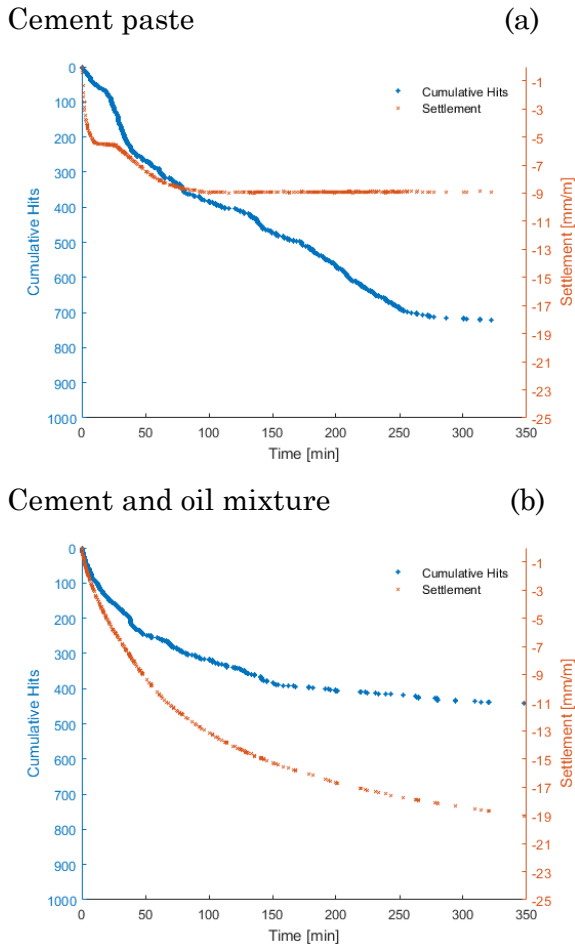
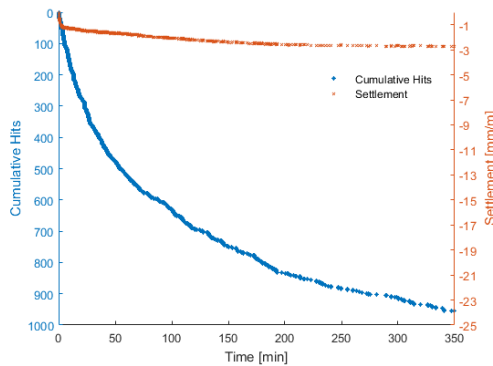Cement and oil mixture (b)

Fig. 3.13 Cumulative hits and settlement for cement paste in different liquids.

Similar pattern has been demonstrated for FA. FA in water suspension illustrated a settlement evolution of -3 mm/m with 950 hits, while FA in oil suspension presented a settlement of -21 mm/m with essentially the same amount of hits (940) after 350 min, as shown in Fig. 3.14(a-b). Therefore, for the mixture in water, the production of AE was approximately seven times higher than the oil mixture, showing how strong the influence of the liquid matrix is. This can again be due to the

reduced friction between the particles due to the oil nature. It could be attributed to the damping effect, however ultrasonic tests in these two matrices exhibited higher transmission for oil compared to water. Further, the mixtures with oil presented greater settlement progression compared to the mixtures with water. Thereafter, there is no hydration process for cement and oil mixture as well as FA and oil mixture and the specimen does not gain stiffness to resist the settlement.

Fly ash in water suspension   (a)
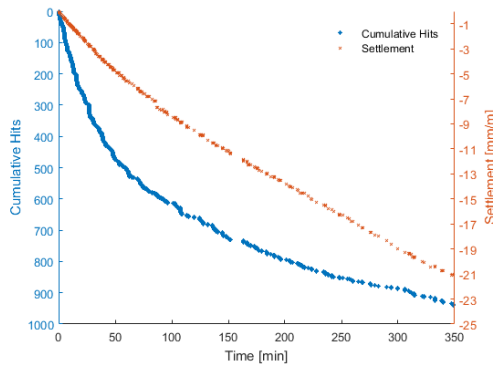

Fly ash and oil mixture   (b)

Fig. 3.14 Cumulative hits and settlement for fly ash in different liquids.

3.6 Conclusions

This chapter focuses on the evolution of the acoustic emission sources in cement paste during early-age hydration. Specimens of FA were compared to cement paste as FA without any further activation does not hydrate and thus enables the study of physical phenomena occurring during drying without the interference of hydration. A combined approach of several monitoring techniques is applied to monitor the settlement, shrinkage, capillary pressure and temperature appearing in specific time intervals due to the drying process. Hence, the combination of different techniques provides additional insight into the mechanisms during the hydration process.

Conclusions drawn from this chapter include the following:

- The significant acoustic activity of cement paste for the first hours is attributed to the settlement process.
- FA suspension led to a lower rate of AE activity during the early hydration process.
- The average absolute energy of AE demonstrated an increase close to capillary pressure drop.
- In the hardened state, the moving average curves of rise time, presented higher values compared to the fresh state for cement paste, attributed to the stiffening of the medium.
- The settlement achieves its maximum around the peak of the capillary pressure for cement paste, which is close to the setting point as measured by Vicat needle.
- Early age AE seems very sensitive to the particle size distribution since the fresh cement paste with smaller particles emits much higher frequency but lower energy and shorter signals than FA, the particles of which are 5 times larger in average.

The sensitivity of the techniques enables monitoring of hydration in a way that complements the traditional approach. This monitoring methodology obtains further value considering the modern developments in cementitious media (inclusion of SAPs, nano-reinforcement etc.) that complicate even more the nature of the material. It could be important, not only for the academic community in terms of basic material studies,

but at the same time also for the industry, given the recent advancements and accessibility of acoustic emission in particular, and non-destructive monitoring technology in general.

Chapter 4: **Digital image correlation on fresh cementitious material**

Monitoring concrete properties at a very fresh state is essential to understand the different ongoing processes. Concrete undergoes strong displacements due to different processes such as, evaporation, water migration, settlement, formation of hydrates, shrinkage, early age cracking. This early state of concrete affects the long-term concrete performance, as discussed previously in Chapter 1. In the present chapter the displacement distribution of fresh cementitious material from plastic state up to hardened state is studied by means of the optical and contactless method of DIC. The principle of DIC enables a full-field 3D continuous monitoring of the surface displacement. An innovative technique of speckle pattern creation allows monitoring the surface displacement few minutes after casting of cement paste and mortar. The experimental results confirmed the effectiveness and correctness of the new technique giving a global overview much more representative than point measurements with traditional displacement meters. The content of this chapter is based on the following papers:

Dzaye,E., Tsangouri, E., Spiessens, K., De Schutter,G., and Aggelis D.G, "Digital image correlation (DIC) on fresh cement mortar to quantify settlement and shrinkage," *Archives of Civil and Mechanical Engineering*, vol. 19, no. 1, pp. 205–214, 2019.

Dzaye,E., Tsangouri, E., De Schutter,G., and Aggelis D.G., "Full-Field Settlement Measurement at Fresh Cementitious Material by Digital Image Correlation," *Journal of Advanced Concrete Technology*, vol. 17, no. April, pp. 168–176, 2019.

4.1 Introduction

Cement-based materials exhibit volume changes and internal particle movements immediately after mixing and throughout curing that may have a detrimental effect on the strength development, durability as well as the long-term mechanical performance. The time-dependent volume reduction phenomenon in concrete is known as shrinkage. In this chapter, firstly the settlement measurement and afterwards the shrinkage measurement will be presented. Concrete stiffens and hardens with age and typically shows a volume reduction (Kurdowski 2014a; Mette Geike and Knudsen 1982; Sant et al. 2009; Wierig 1990). Throughout the hardening process the material shrinks into its casting mould and settles at the free open surface possibly leading to cracks formation (Yamakawa et al. 2003).

There are several important factors that contribute to concrete early-age shrinkage, among them: chemical volumetric changes due to hydration process (Kurdowski 2014b), drying process after casting, and thermal deformations due to hydration heat release.

The vertical deformation (settlement) in the plastic state may also cause plastic settlement cracks and is connected to "bleed water" pushed to the surface. These early-age cracks affect the long-term performance of mortar by giving easy access to water and aggressive species.

Concrete deformation has been extensively studied in the literature using different monitoring methods invoked to identify shrinkage onset and evolution. Stiff fiber optic sensors perform low-coherence interferometry measurements to track the evolution and quantify early-age concrete shrinkage (Glisic and Simon 2000). In another approach, Azenha et al. monitored concrete thermal deformations after casting and predicted early cracking risk by using strain gauges (Azenha et al. 2009). Chen et al. applied a two-dimensional cure reference method (CRM) and Moiré interferometry to study time-dependent surface shrinkage of cementitious materials (Chen et al. 2010). The observed non-uniform deformation can be associated with cracking. Sadowski et al. used a 3D Laser scanning metrology technique to identify the morphological progression from viscous suspension to solidification, and the transition from fluid to the solid state of a lightweight concrete surface (Sadowski

et al. 2017). Plethora of monitoring techniques have been used to track early-age plastic deformation including volume change (Barcelo et al. 2011), electrical conductivity (Topu et al. 2012), rheological measurement (Kozikowski al. 2006) and hydraulic pressure variation (Amziane 2006), shrinkage cone (Kwasny et al. 2009).

It is essential to provide a full-field settlement measurement. Digital Image Correlation (DIC) appears an effective alternative to those methods. This optical method outperforms other methods since it is continuous, contactless and provides accurate and full-field monitoring of surface strain and cracking. Indicatively, (Maruyama et al. 2013) applied DIC to study the crack pattern and crack width due to drying in coating mortar and concrete respectively. In another approach, Sonebi and Bartos (2002) measured the plastic fresh settlement of self-compacting concrete in a column (Sonebi and Bartos 2002).

Maurouc et al. applied 2D Digital Image Correlation (DIC) and examined shrinkage progress on a coating mortar (Mauroux et al. 2012). DIC recorded and illustrated the non-uniform displacement distribution and full-field strain mapping highlighted micro-cracking patterns evolution in time. DIC output was compared with classical point LVDT measurement and a good concordance between both methods was obtained. In another study, the water transfer process and consequent stress distribution effects on the concrete surface were evaluated using DIC (Maruyama and Sasano 2013). It was shown that two crack patterns were detected due to shrinkage, aggregate interconnecting radial cracks and mortar-aggregate interfacial cracks. Lagier et al. used 2D-DIC to track drying shrinkage cracks originated by incompatibility effects between cement paste and aggregates (Lagier et al. 2011). Gajewski et al. presented an integrated methodology to determine concrete model parameters based on full-field DIC measurements treated with inverse problem analyses (Gajewski and Garbowski 2014). Chen et al. studied the effect of aggregate size and volume on drying shrinkage of concrete and mortar by 3D-DIC (Chen et al. 2018). The non-uniform strain concentrations became more remarkable by drying time. Additionally, with the increase in aggregate size, the displacement fields of concrete became more heterogeneous. In all above-mentioned studies, monitoring started at 24 hours after casting at the earliest while the significant mobility of concrete is exhibited from the moment of casting. Further, it

is important to monitor the non-uniform displacement distribution with time at different locations at the surface which is affected by the surrounding area and the bleed water.

At early age and as the media is in plastic state, the potential for settlement cracking is high and is attributed to different driving forces: differential settlement (Weyers et al. 1982); water evaporation that causes high tensile stress and menisci in the capillary water at the surface (Wittmann 1976 and Cohen et al. 1990), differential thermal increase due to temperature progress within the fresh concrete (Bertil et al. 2002) as well as plastic shrinkage that appears during the concrete plastic state (Pease et al. 2004). Understanding and controlling the plastic state settlement is challenging. Kwak et al. (2010) analysed the plastic settlement of mortar based on strain consolidation theory that considers the self-weight and consolidation and compared it with experimental data by means of a non-contact laser measurement device. The distribution of settlement due to self-weight decreases dramatically at approximately 90 min. Combrinck et al. (2018) identified the combined effect of plastic settlement and plastic shrinkage cracking of concrete. Plastic settlement cracking presented multiple tensile surface cracks and shear cracks while plastic shrinkage cracking exhibited a single crack pattern throughout the entire depth of the concrete. Lura et al. (2006) measured the settlement of mortar containing shrinkage-reducing admixture (SRA) using non-contact laser system. The addition of SRA reduces the settlement resulting in a reduction of plastic shrinkage cracks due to differential settlement.

These methods mentioned above cannot deliver a full-field settlement measurement. DIC is an effective alternative to those methods and provides a full-field settlement measurement. DIC enables displacement measurement at any position on the surface in contrast to LVDT that considers only a single point measurement. The following section focuses on the vertical deformation (settlement) of cement paste and cement mortar in plastic state (few minutes after casting) by 3D DIC to study concrete hydration process and drying process as well as the risk of crack formation. The experimental results of DIC will be compared to classical point measurement methods of LVDT. DIC mapping allows evaluating the settlement distribution on the surface that affects the final material properties.

92

This chapter presents 3D-DIC displacement/strain measurements on cementitious media in fresh stage (few minutes after casting) in order to fundamentally understand material's mobility during the drying, hydration and the hardening process. The settlement and strain patterns built due to shrinkage will be visualized and quantified. The DIC outcome will be compared to classic point measurement methods.

It is highlighted that this is the first effort to measure non-contact and in high accuracy the settlement and shrinkage of fresh concrete a few minutes after mixing, when the viscous nature is still present. This poses additional difficulties to the use compared to hardened state since application on fresh mortars requires additional surface treatment as is explained below.

Online accurate shrinkage and settlement measurements provide an additional tool to qualify the curing process on concrete. DIC mapping can highlight in time the presence of extended vertical deformation associated with bleeding and segregation effects that degrade the final material properties. DIC strain maps can indicate the state at which strain limits are exceeded. This way, casting and curing processes can be adjusted to eliminate shrinkage cracking formation (Slowik et al. 2008).

4.2 Materials

Standard cement paste was studied with a water-cement ratio of 0.4 (by mass). The cement used was type I ordinary Portland CEM I 52.5 N with a Blaine specific surface area of 433 m^2/kg, a density of 3090 kg/m^3 and a chemical composition of CaO 63.9%, SiO_2 20%, Al_2O_3 5.1%, Fe_2O_3 3.4%, MgO 0.8%, Na_2O 0.34%, K_2O 0.75%, SO_3 3.1%, CI^- 0.05% (by mass). The cement paste was mixed in a laboratory concrete mixer for 3 min at low speed. Following the casting, external vibration was applied by a standard vibration table. Afterwards, the material was poured into a metallic mould of size 150x150x150 mm (internal dimensions) and the room was kept at a constant temperature of 20 ± 1 °C for 65 h. Besides the cement paste, specimens of cement mortar were similarly prepared using the same cement content, a water -to- cement ratio of 0.45 (by mass) and sand with proportions reported in Table 4.1. Furthermore, concrete

specimens were prepared similarly to the cement mortar with the composition illustrated in Table 4.1. The flow test has been applied for cement paste and cement mortar according to ASTM C1437-07, see Table 4.1. Additionally, slump test according to BS EN 12350-2 has been applied for concrete, as shown in Table 4.1. Anti-washout admixture (MasterMatrix UW 440) 0.2% by cement mass was added to concrete. Throughout the study, 18 specimens per series were investigated to optimize the speckle pattern as well as its effectiveness.

Table 4.1 Ratios of specimens mix design (cement: sand: aggregate).

	Cement paste	Cement mortar	Concrete
Cement	1	1	1
Sand (0/2)	-	2	1.2
Coarse aggregate (2/4)	-	-	1.2
Coarse aggregate (4/16)	-	-	2.3
Anti-washout admixture (%) by cement mass	-	-	0.2
w/c ratio	0.4	0.45	0.5
Fresh density (kg/m^3)	1968	2160	2425
Air content (%)	1.05	5.6	3.4
Flow test [mm]	220	170	-
Slump test [mm]			57

4.3 Traditional measurement tools

Two linear variable differential transformer (LVDT) sensors were embedded into the mould horizontally at a height of 50 mm from the bottom to measure the horizontal displacement between opposite sides in order to determine horizontal shrinkage. It is assumed that identical horizontal displacements were developed in the other horizontal direction due to the quadratic shape of the form. Furthermore, one LVDT was applied to measure the settlement at the specimen surface. The vertically arranged LVDT tip touched a 20x20 mm metallic wire lattice that was applied on the specimen top surface (Fig. 4.1(b)). Consequently, the sensor tip was prevented from penetration as well as floating on the

surface. In addition to the settlement and horizontal displacement, the capillary pressure was used simultaneously to measure the capillary pressure development of the specimen. A pressure sensor was connected to the pore system by a 150 mm long brass tube having an inside diameter of 4 mm. This brass tube was placed in the specimen and was filled with de-ionized and out-gassed water. The capillary pressure transducer was attached vertically 30 mm deep into the material from the top surface.

4.4 DIC measurement

A pair of digital cameras (AVT Stingray) was placed above the specimen surface as shown in Fig. 4.1(a). Both cameras have a resolution of 2504 by 2056 pixels. The lens type was CNG 1.4/12-0902 with a focal length of 12 mm. The cameras were set at 200 mm from the specimen surface. White light was installed above the sample surface to provide lighting to the monitoring area during the measurement. On the specimen surface white-black speckle pattern was created as shown in Fig. 4.1(b).

Besides the DIC, capillary pressure development of the specimen was monitored by a pressure sensor, see Fig. 4.2. A pressure sensor was connected to a 150 mm long brass tube with an inside diameter of 4 mm. The brass tube was filled with de-ionized and outgassed water to allow monitoring the pressure development. The capillary pressure sensor was placed vertically 30 mm deep into the material from the top surface permitting the connection to the pore system.

In addition to the surface settlement and the capillary pressure, thermocouple was used simultaneously to measure the temperature development of the specimen indicating the progression of the hydration process as shown in Fig. 4.2. Throughout the study different speckle pattern by applying different materials have been investigated. In the following section, the 3D-DIC measurement for cement paste and cement mortar by applying the powder speckle pattern is investigated.
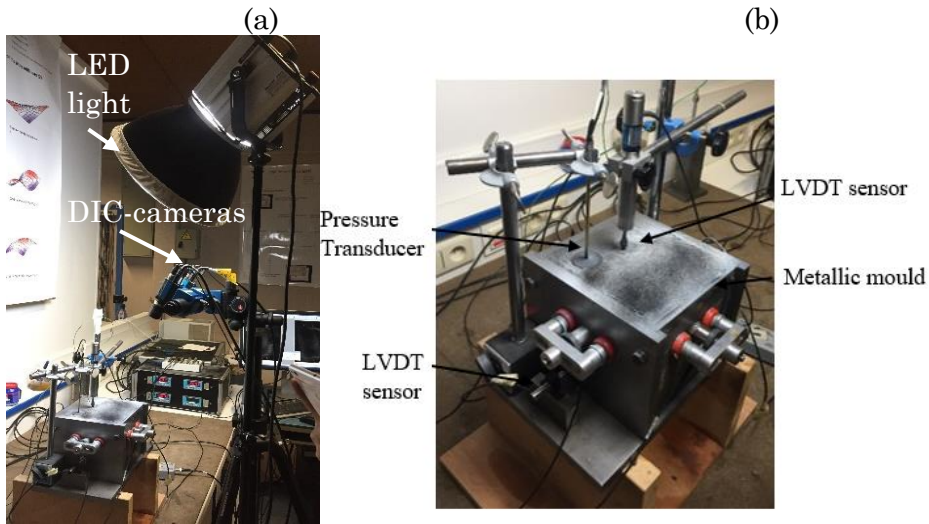
Fig. 4.1 DIC monitoring (a) DIC system setup with metallic mould; (b) metallic mould including LVDT sensors and pressure transducer.
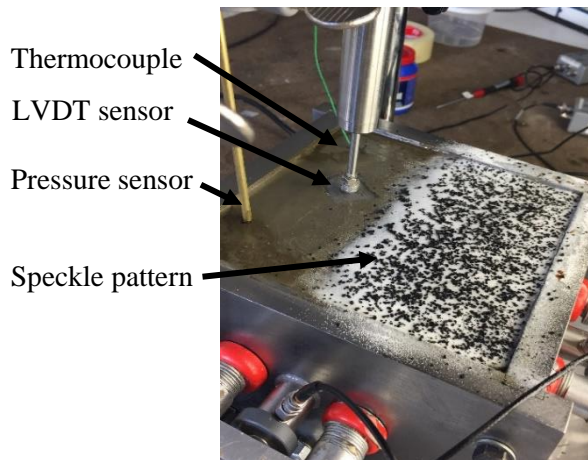

Fig. 4.2 Specimen surface covered with powder speckle pattern including thermocouple, LVDT and pressure sensors.

The cameras are synchronized and triggered to simultaneously capture images at a constant time interval. DIC images are analysed in post-processing stage to detect differences at the surface between reference

(undeformed) and deformed surface state. Any variation at the image intensity can be associated to deformation at the surface. Hence, the sample surface is covered with randomly distributed white and black speckles. The DIC post-processing software measures the grey intensity of local zones (subsets) (Sutton et al. 2009). Displacement in space translated to movement of the speckle pattern is perceived as change on the subset grey intensity degree compared to a reference stage (Lecompte et al. 2006). The measurement and the post-processing analysis were conducted using VIC-Snap software from Correlated Solutions, Inc. and 3D-digital image correlation tool (VIC-3D) provided by Correlated Solutions, Inc.

The accuracy of DIC analysis depends on several parameters, namely, DIC setup, sample geometry, software features, surface morphology, DIC resolution and speckle pattern, the distance from the specimen as well as the cameras angle. DIC speckle pattern quality is controlled by black-white contrast, sharpness and speckles size and distribution. There is no standardized and optimized method to apply the speckles, therefore, there is a variety of different application procedures in literature, such as marked pen, spray paint, screen printing and airbrush gun (Barranger et al. 2010).

Application of DIC on fresh cement-based materials implies a challenging speckle pattern application since the speckles might move due to bleed water or get absorbed on the wet surface. In this study, the development and effectiveness of new speckle methods is investigated considering white-black speckle pattern on the material surface.

DIC monitoring started up to 20 min after casting. Reference starting point (Time 0) is considered the time of casting and the duration of the experiment was approximately 65 h. A powder speckle pattern was applied on the surface of cement paste and mortar to allow monitoring the settlement. Steel fine mesh is used to distribute the white aluminium oxide powder and black carbon powder on the specimen surface. Firstly, a layer of white aluminium oxide powder was applied through a sieve. Afterwards, in the same way well-distributed black dots of carbon powder are applied through a sieve on the surface to create a white/black speckle pattern. This means that the top layer is painted with randomly distributed black/white pattern through a sieve to perform DIC

measurements. Furthermore, during the measurement, a smooth white light was placed above the specimen surface to provide homogeneous lighting at the whole monitoring area, as discussed in Section 5.4.

Only the half of the sample surface is covered with speckle pattern since in the other half the vertical LVDT is placed. Therefore, DIC can visualize an area at which the left, right and bottom sides as shown in Fig. 4.2 are attached to the metallic mould and the top side stands in the middle area of the sample. The boundary conditions are not identical for all four sides of the analysis area. The total DIC field of view is 130 x 64 mm for cement paste and 150 x 75 mm for cement mortar. The spray speckle pattern allowed creating a bigger speckle pattern from a distance because a direct access to the specimen surface was not necessarily needed. DIC analyses were performed with 61x61 subsets with a step size of 10 between subset centres (Gaussian subset weights, optimized 8-tap interpolation with normalized square differences). The measured sensitivity is up to 16 pixels/mm. Images are captured every 120 s. The measurement and the post-processing analysis were conducted by means of VIC-Snap and VIC-3D software respectively.

4.4.1 DIC settlement monitoring with powder speckle pattern

Fig. 4.3 and Fig. 4.4 illustrate the DIC value of vertical displacement as measured considering the full-field surface for cement paste and cement mortar after casting, as average value for the whole monitored area (roughly accounting for half the specimen surface, as mentioned above). Settlement describes the volume reduction caused by gravitational settlement of the solid particles in the fresh concrete (Combrinck et al. 2018). A large amount of surface settlement (vertical displacement) was recorded at very early age since the plastic material settles. Cement mortar achieves its maximum settlement with 1.3 mm/m after 150 min and beyond this moment mortar demonstrates a decrease of the settlement rate. The settlement increases at early stage for the cement paste while the curve presents fluctuations reaching its maximum value of 7.1 mm/m 1600 min after casting, see Fig. 4.3. It is evident that the settlement development follows similar trends in both cases due to common cement material nature. However, the quantitative difference in settlement can be attributed to the materials composition, the addition of

sand in the case of cement mortar and the different w/c ratios. Fig. 4.4 illustrates the DIC 3D surface settlement (vertical displacement) progression at different curing stages. It is noted that the settlement is non-uniformly distributed at the surface.
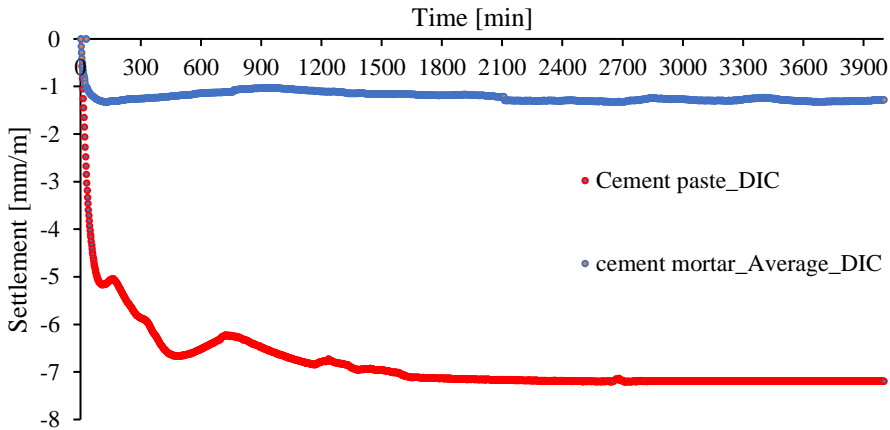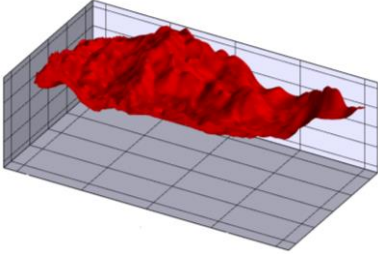

Fig. 4.3 DIC vertical displacement (settlement) versus time for cement paste and cement mortar.

The level of settlement can be related to the existence of the sand grains that offer volume stability in cement mortar. Fig. 4.5 illustrates the temperature progress after casting for cement paste and mortar indicating the evolution of the hydration process. The temperature progress is monitored by applying thermocouples into the specimens close to the top edge of the mould.
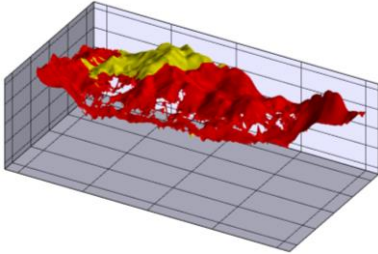
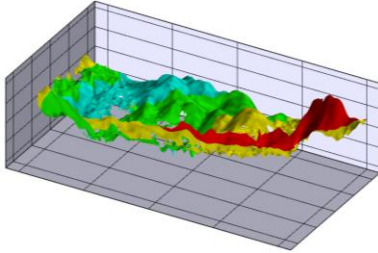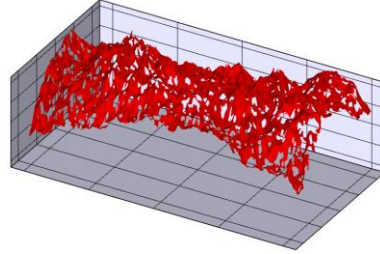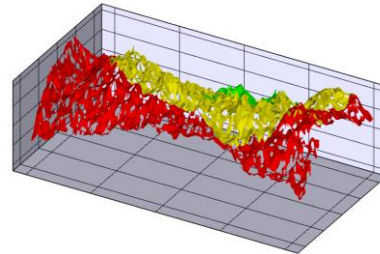Cement paste
3D DIC Settlement (vertical displacement) [mm]
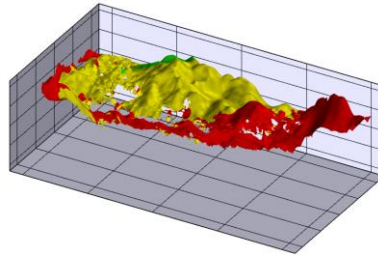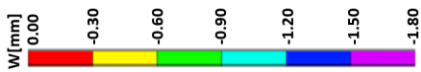
Cement mortar
3D DIC Settlement (vertical displacement) [mm]
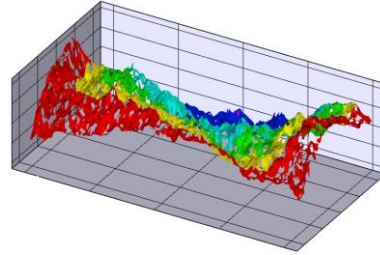
Fig. 4.4 3D DIC Settlement (vertical displacement) representatively shown for cement paste and cement mortar.

During the first hours of drying and hydration process, the specimen temperature drops due to the initial temperature differences between the fresh material and the mould/environment in the plastic state. It is interesting to note that the initial cement mortar tempera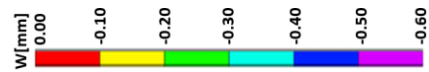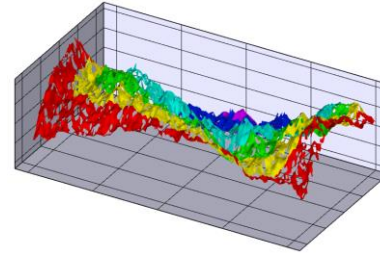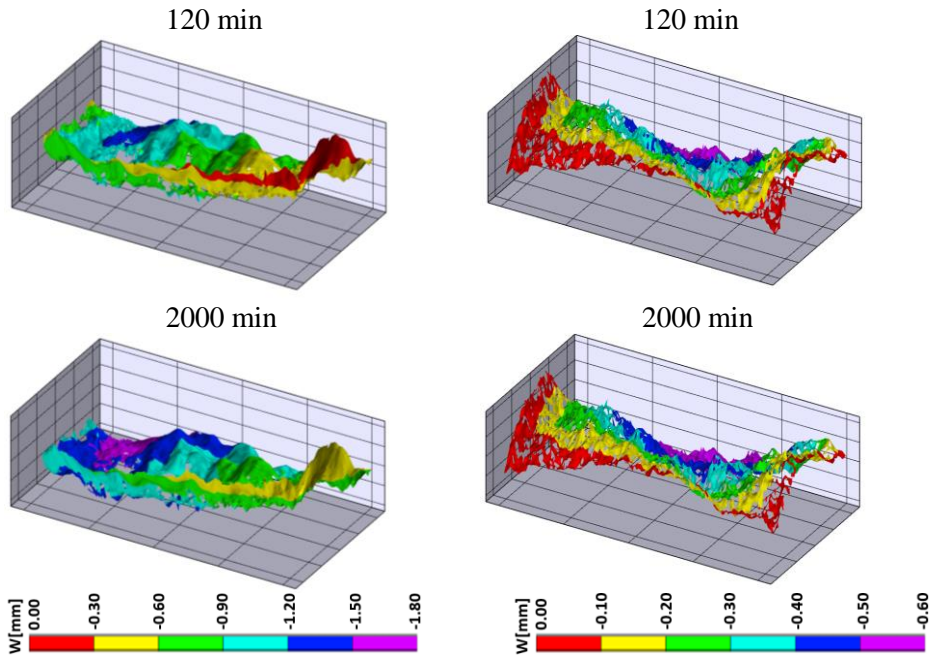ture is 23°C while cement paste presents an initial temperature of 27°C. The temperature considerably increased after approximately 300 min from casting reaching 26°C for cement mortar and 44°C for cement paste representing the accelerated and dominant hydration process. It is demonstrated that the cement paste that carries higher cement content than the mortar reaches higher temperatures as hydration occurs. Since the hydration reaction occurs uniquely between the cement and the water, the addition of sand in the case of the mortar does not enhance the hydration process but does control the settlement evolution.
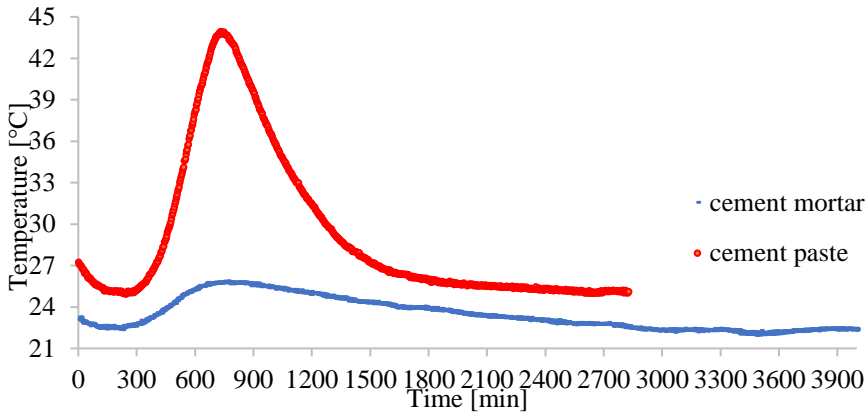
Fig. 4.5 Temperature evolution for cement paste and cement mortar.

Both materials reach their peak approximately 740 min after casting. Beyond the temperature peak, both temperature curves drop progressively demonstrating the hardening progress and afterwards the temperature remains constant at low levels. It is interesting to note that the temperature peak coincides with a local peak of the settlement curves. This is partially attributed to the hydration process which results in the larger amount of heat release and reverses temporarily the settlement trend. This is more pronounced in the curve of paste, when between 600 and 900 min a relatively sharp peak is exhibited before the settlement curve becomes stable.

The free thermal deformation Δl for cement paste and cement mortar is obtained from the thermal expansion equation:

$$\Delta l = \alpha l_0 \, \Delta T \qquad \text{Eq. 4.1}$$

where Δl is the change in length caused by thermal effect, α presents the coefficient of thermal expansion, l_0 stands for the original length, ΔT represents the change in temperature. The coefficient of thermal expansion was assumed to be 10.44 x 10^{-6} / °C for cement paste and 11 x 10^{-6}/ °C for cement mortar, being in accordance with the order of values measured in the literature for similar cases (Nilsen et al. 2019; Zhou et al. 2014). The estimated thermal deformation is of the same order of magnitude compared to the experimentally obtained values, see

Table 4.2. There are differences in the absolute values, that could be attributed to the non-uniform temperature distribution in the specimen and the (internal) restraint of the thermal deformation. Moreover, a settlement peak followed by expansion is also observed for fly ash. However, the expansion is not as pronounced as in the case of cement paste due to the non-existing hydration effect. The expansion of fly ash suspension results from the beginning of the horizontal shrinkage after crack formation or separation from the mould side-walls. This beginning horizontal shrinkage leads to a strain relief in the vertical direction.

Table 4.2 Free thermal deformation.

Δl experimental obtained for cement paste [mm]	0.0646
Δl theoretical obtained for cement paste [mm]	0.0329
Δl experimental obtained for cement mortar [mm]	0.0463
Δl theoretical obtained for cement mortar [mm]	0.0104
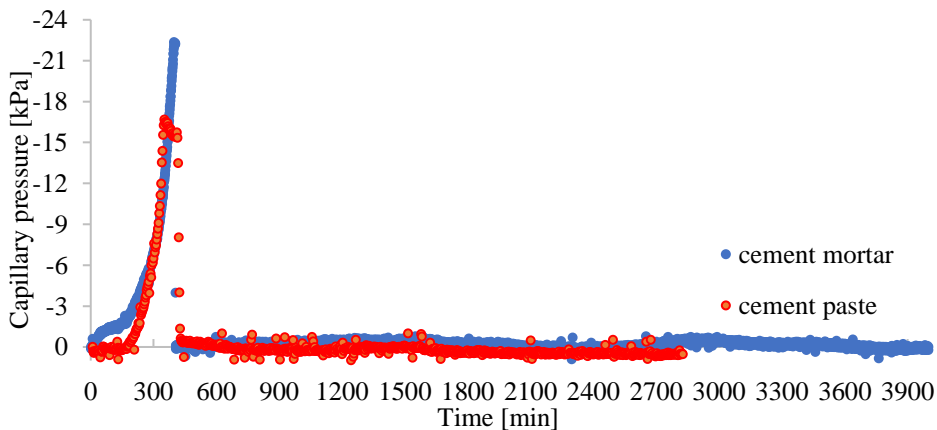
Fig. 4.6 Capillary pressure development in time for cement paste and cement mortar.

The capillary pressure is additionally measured in an attempt to comprehensively track the curing process on cement-based media. The capillary pressure development and later drop is associated to drying process and can be indicative of plastic shrinkage, therefore tracking of it appears essential. In this study, pressure sensors were applied into the

media and the pressure evolution is illustrated in Fig. 4.6 for both cement mortar and cement paste. As hydration begins, the bleed water diminishes as water evaporation accumulates. Consequently, curved water surfaces (menisci) are now formed at the material phase between solid particles (Slowik et al. 2008). The capillary pressure of cement paste increases after 150 min while cement mortar shows an increase immediately after casting. Cement paste presented a delayed increase of the capillary pressure indicating the increased bleed water at the surface. Indeed, the mass of water in the cement paste mixture was greater than the mortar one. This strong development of capillary pressure occurs simultaneously with the settlement progress in the plastic state as shown in Fig. 4.3. After 370 min the capillary pressure of cement paste drops with a negative peak value of -17 kPa. Cement mortar shows a negative peak value of -23 kPa and drops after 400 min. It is evident that cement paste characterised by higher water content is associated to delayed capillary pressure built up comparing to mortar. It was observed, that after the capillary pressure break-through the hydration process is accelerated as shown in temperature curves and the potential for plastic cracking achieves its maximum.

4.4.2 Full-field settlement assessment using DIC compared to conventional method

A fundamental difference between traditional sensing methods (i.e. LVDT point sensor) and DIC that should be highlighted is the fact that DIC measures the settlement in contactless mode, thereby the sensor cannot affect the measurement process, e.g., by increased settlement measured value due to self-weight of the sensor.

Apart from that, it is observed that LVDT point measurement of vertical displacement of a cementitious medium cannot be considered to fully assess settlement from the whole surface. The above statement is justified using DIC 3D full-field displacement maps illustrated in Fig. 4.7(a-b) for both cement mortar and paste samples. Settlement (in mm/m) is calculated as displacement W (in mm) divided by the nominal specimen depth (0.15 m) at points with the highest (P1), the lowest (P2) settlement and as an average considering the average value of the total surface area.

The DIC measurement are compared to classical LVDT point measurement. Points P1 and P2 highlight the extreme cases of point measurement and LVDT and DIC average values stand in between. The P1-P2 settlement difference is measured at 8.1 mm/m and 3.3 mm/m for cement paste and mortar respectively. Additionally, the difference between the point LVDT and average DIC value is around 2 mm/m in both cases. The analysis demonstrates the limitation of unique point measurement of settlement, especially in the case of cement paste where the settlement range significantly varies.

(a)   (b)
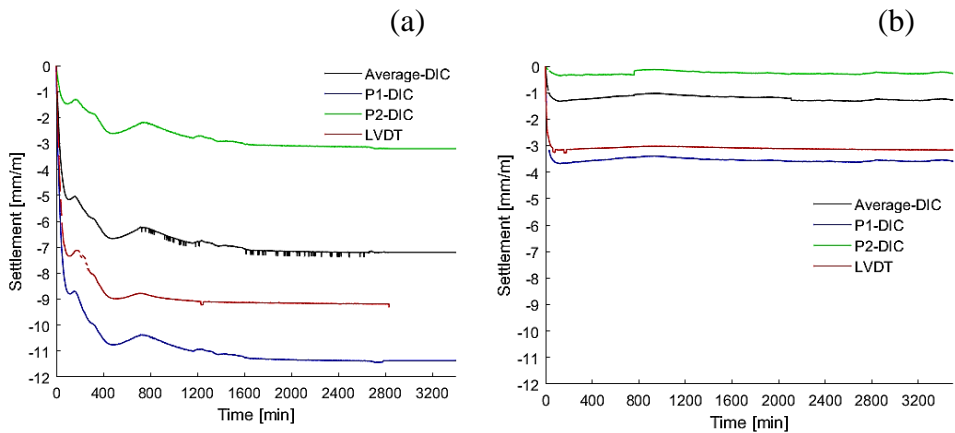
Fig. 4.7 Surface settlement of DIC (representatively P1, P2 and average total area) and LVDT for (a) cement paste and (b) cement mortar sample.

The difference in settlement between LVDT and DIC measurement in the absolute value is attributed to the fact that DIC considers the total surface area and LVDT monitors the settlement at a point of the surface. It is evident that no robust conclusion can be obtained when considering only point analysis. This is an evidence for the significant enhancement offered by the global analysis. Using DIC the variation in settlement in different points is readily available while the average value on the surface can be regarded as a global measurement.

4.4.3   The effect of bleed water distribution on settlement

The settlement along a line that crosses the sample is illustrated in Fig. 4.8(a-b) for cement paste and mortar in discrete monitoring stages in order to track the effect of bleed water and sample geometry on settlement distribution. In both cases, the settlement has a non-uniform distribution along the sample with lower values obtained at the areas attached to mould walls. The settlement peak is detected at different locations: slightly to the left for the cement paste and in the middle zone in the case of mortar. The latter observation presents a randomness that may be related to the initial surface elevation map and the bleed water movement that influences the settlement progression. Slight differences of the settlement peak were observed at different times. Apparently, the bleed water built up on material surface at the first minutes after casting fully controls the settlement distribution, phenomenon observed regardless the material composition (w/c, use of sand, etc.).
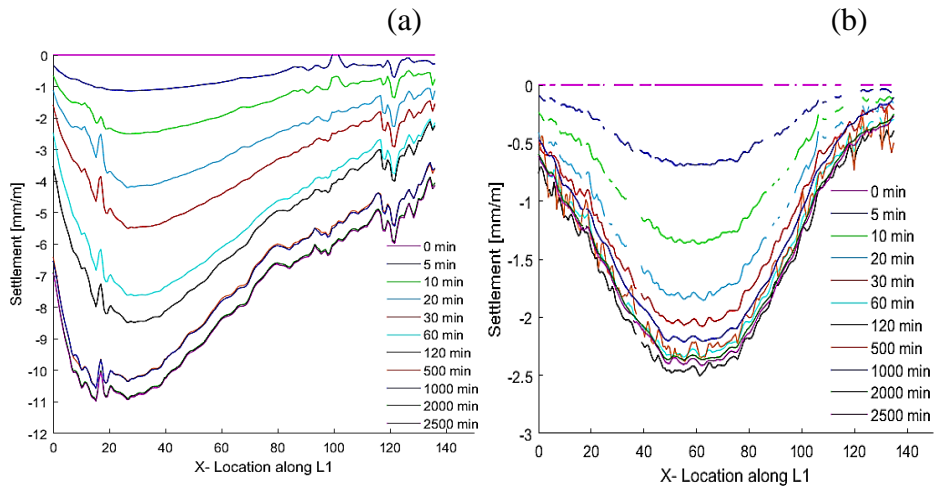

Fig. 4.8 DIC surface settlement along line L1 at discrete monitoring stages (a) cement paste and; (b) cement mortar.

The effect of boundaries on settlement distribution is illustrated in Fig. 4.9 where the settlement of cement mortar obtained 2320 min after casting is measured for three lines crossing the sample: L0 stands at the

middle of the sample, L1 further to the edges and L2 stands the closest to the edge.
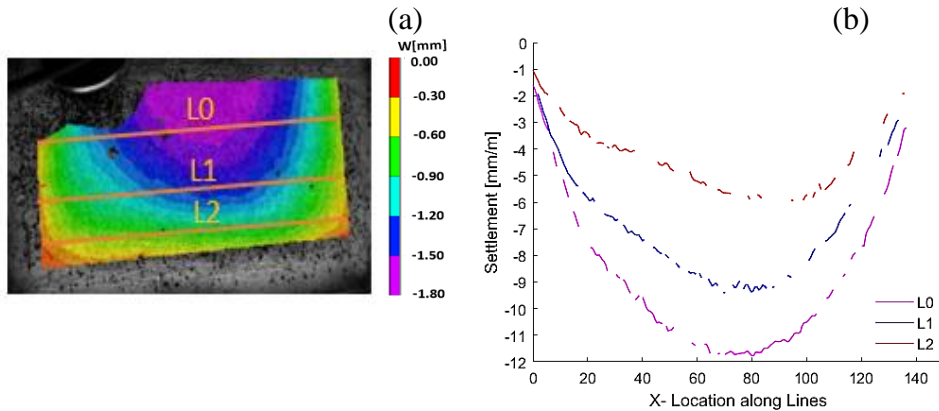

Fig. 4.9 DIC line analyses at different locations for cement mortar; (b) DIC surface settlement along lines (L0, L1 and L2).

All three lines (L0, L1 and L2) illustrate similar trends but with different absolute values, thereby indicating the impact of the surface elevation close to the edge as well as the bleed water movement on the settlement progression. Line L0 is closer to the specimen centre and indicates the highest settlement while L2 is close to the edges indicating the lowest settlement. These results are consistently indicating the maximum settlement near the specimen centre for cement mortar.

4.4.4 The conclusions of the full-field settlement measurement by powder speckle pattern method

3D DIC confirms an effective and innovative technique to evaluate the settlement distribution of cement paste and cement mortar in fresh state (few minutes after casting) in a contactless mode. DIC allows monitoring the non-uniform settlement distribution at different locations on specimen surface by creating a powder speckle pattern. This approach enables a deeper understanding of concrete consolidating process and expands the measurement data to the whole surface.

The results of DIC as well as LVDT clearly show the higher settlement of the cement paste compared to mortar, while they are sensitive enough to the hydration temperature peak that causes a transient expansion. In addition, the 3D full-field character of the measurement confirms the differential settlement on the surface, something not possible with the classical LVDT point measurement. The laser method could be used as an absolute reference method to investigate the displacement on the sample surface. Further study should be done regarding the accuracy of the speckle pattern that is affected by the bleed water in the first hours after casting and the possible influence of aluminium oxide/carbon powder speckle pattern on the hydration process. Thereafter, an improved method of speckle pattern creation by spraying the specimen surface is presented in the following section that allows monitoring not only the settlement evolution but also the horizontal deformations (shrinkage) of cement mortar.

4.4.5 DIC settlement and strain monitoring with spray speckle pattern

In the previous section DIC measurement was performed by applying the powder speckle pattern. In this section, a spray speckle pattern is presented that allows monitoring fresh cement mortar volume changes and strain distributions. Thus, a deeper and more detailed measurement on fresh cement mortar is introduced in the following section.

Specimens of cement mortar were prepared using the same mix design as presented in Section 5.2. A white-black speckle pattern was created on the specimen surface by spraying a white and black paint, see Fig. 4.10(a-b). At first, a layer of white paint covered the material surface. Later, thin well-distributed black dots are prepared by spraying black ink from a distance.

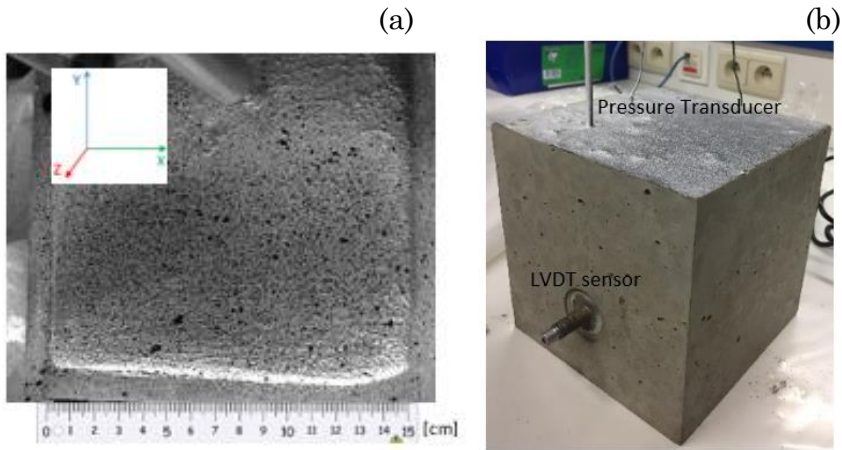(a)   (b)

Fig. 4.10 (a) top view of the surface covered with spray speckle pattern and the DIC coordinate system (X and Y in plane and Z out of the top surface plane) and (b) side view of the specimen after demolding with the speckle pattern on its top surface including LVDT and pressure sensors.

The total area observed by DIC is equal to 144x84 mm². DIC analysis considers subset and step size set at 29 and 7 pixels respectively. The measured (scale factor) sensitivity is up to 17 pixels/mm, which considering the deformation sensitivity of 1/100 pixels, corresponds to 0.000588 mm (Correlated solutions n.d.). The analysis is done considering the axis system shown in Fig. 4.10(a). The displacement vectors U, V, W in mm are calculated at X, Y, Z directions respectively. Normal (Exx, Eyy), plane shear (Exy) and principal (E1, E2) strains in mm/m along the X and Y axis are calculated as well. Displacement W stands for the settlement of the top surface and normal strains Exx/Eyy are selected to assess the shrinkage phenomenon evolution in time.

Reference starting point (Time 0) is considered the time of mixing and the duration of the experiment was approximately 3 days. The mixing and casting of the specimens were completed in approximately 10 min (time=10min). At a next step, the mould was placed at the experimental setup and the surface was covered in black-white speckle pattern. The preparation of the surface for the DIC measurements lasted approximately 10 to 15 min. As a result, DIC monitoring started 15 min after casting.

4.4.6 DIC displacement to detect shrinkage and settlement of cement mortar

In order to detect shrinkage, DIC displacement and strain fields are obtained and presented in Fig. 4.11 and Fig. 4.12, captured at different curing stages. The images are representatively selected to visualize the evolution of shrinkage in the plane (displacements U and V, corresponding to strains Exx and Eyy) and settlement (W) at different monitoring stages.

In the period until approximately 130 min, concrete is in the plastic state as indicated by the isothermal hydration heat curve. Water bleed movement is responsible for the U and V deformations observed in Fig. 4.11 and Fig. 4.12. At the transition from plastic to setting state (indicatively see 130 min) displacement at top surface increases in all 3 directions, a phenomenon attributed to cement-water physical properties changes. Beyond this point, concrete progressively hardens (hardening state) and the deformations are smoother. The curing process is monitored for approximately 3 days.

It should be highlighted that speckle pattern was efficiently and fast applied after casting, therefore DIC for the first time in literature can provide information as soon as 15 min after casting.

(a)

Time [min]	U Displacement [mm]	V Displacement [mm]	W Displacement [mm]

-0.20 -0.15 -0.10 -0.05 0.00 0.05

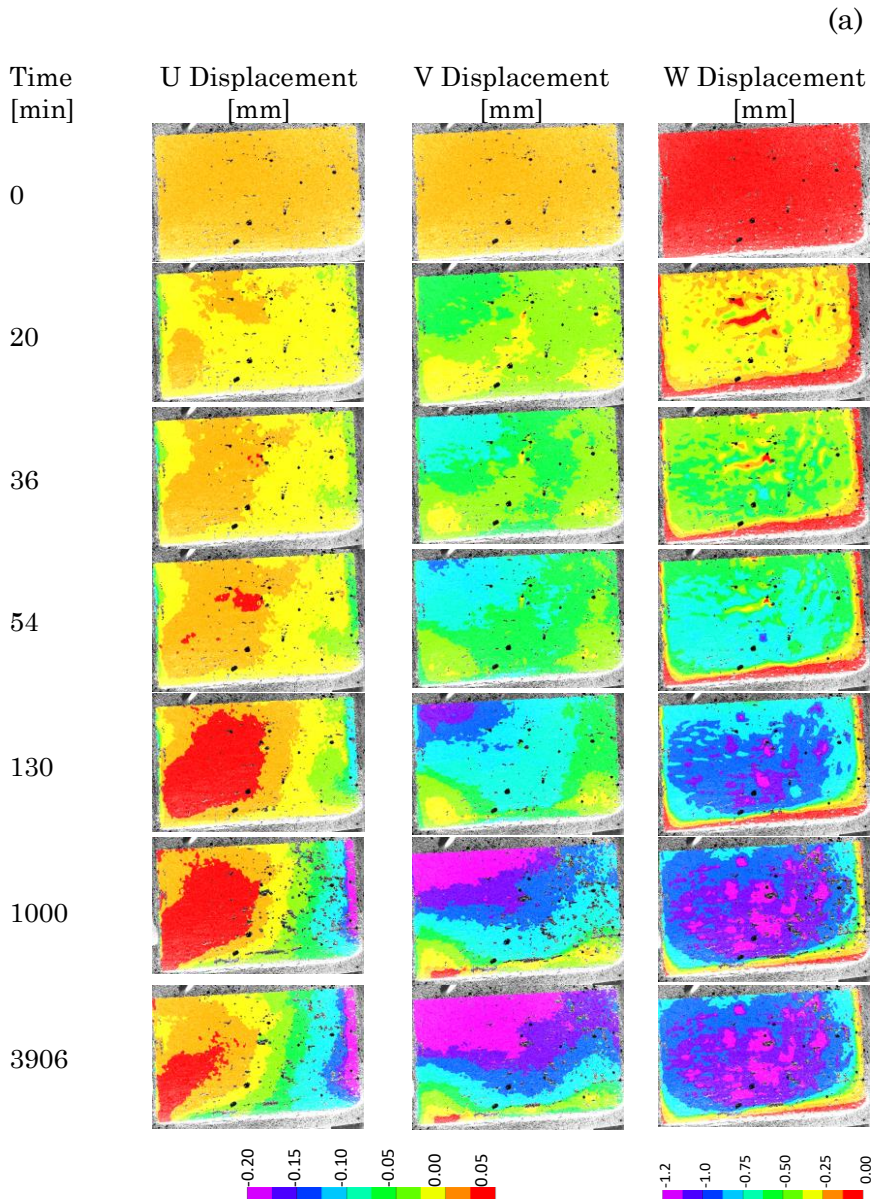-1.2 -1.0 -0.75 -0.50 -0.25 0.00

Fig. 4.11 Displacement field of mortar in three directions in different time stages.

W displacement (perpendicular to the top plane) standing for surface settlement exhibits its highest value in the specimen center. The W displacement aside to the metallic mould remains negligible. In parallel, it is observed that there is significant U displacement only at the right

111

side of the sample corresponding to the detachment from the sides. In parallel, high V displacement values are measured at the top side of the graph standing in the middle of the sample, see Fig. 4.11. It is concluded that three-dimensional displacement is not uniformly distributed, therefore shrinkage cannot be a homogeneous spatial phenomenon, as also shown in Fig. 4.12.

As expected, the horizontal U and vertical V plane displacements and respective strains are not uniformly distributed, and potential shrinkage patterns are not easily identified. During the plastic stage (36 min and later, see Fig. 4.12), strains Exx and Eyy concentration are built up locally at the center and the right side of the sample indicating local movement. Globally, shrinkage (negative) strain is observed with drying time, but in some regions locally the mortar specimen presented expansive (positive) strain. The latter observation comes in agreement with relevant studies documenting that expansive strain develops at the zone surrounding the crack tip (Caduff and Van Mier 2010; Chen et al. 2018; Maruyama and Sasano 2013).

At hardening state (representatively in 1000 and 3906 min), shrinkage effect extends. Settlement reaches its peak value and saturates beyond 1000 min. The purple regions aside to the mould at Exx and Eyy maps illustrate the highest shrinkage as shown in Fig. 4.12. W displacement maps show that the hardened material symmetrically moves from the specimen outer sides to the central zone.

In Fig. 4.13, the Exx and Eyy strain evolution in the top surface are quantified considering the average values of strains measured at the whole gauge surface. Up to 130 min after casting, both Exx and Eyy strains stand in an expansion. The expansive strain may be attributed to bleed water which is treated later with the addition of anti-washout admixture (MasterMatrix UW 440). Beyond 130 min, strain values drop as shrinkage extends reaching a local minimum 200 min after casting. As the exothermal hydration reaction is underway, a local maximum is obtained at approximately 10 hours (600 min). But later, the strain continuously drops to lower values with a lower rate. It is noted that shrinkage strain is not necessarily identical in both X and Y directions, but a similar trend is followed.
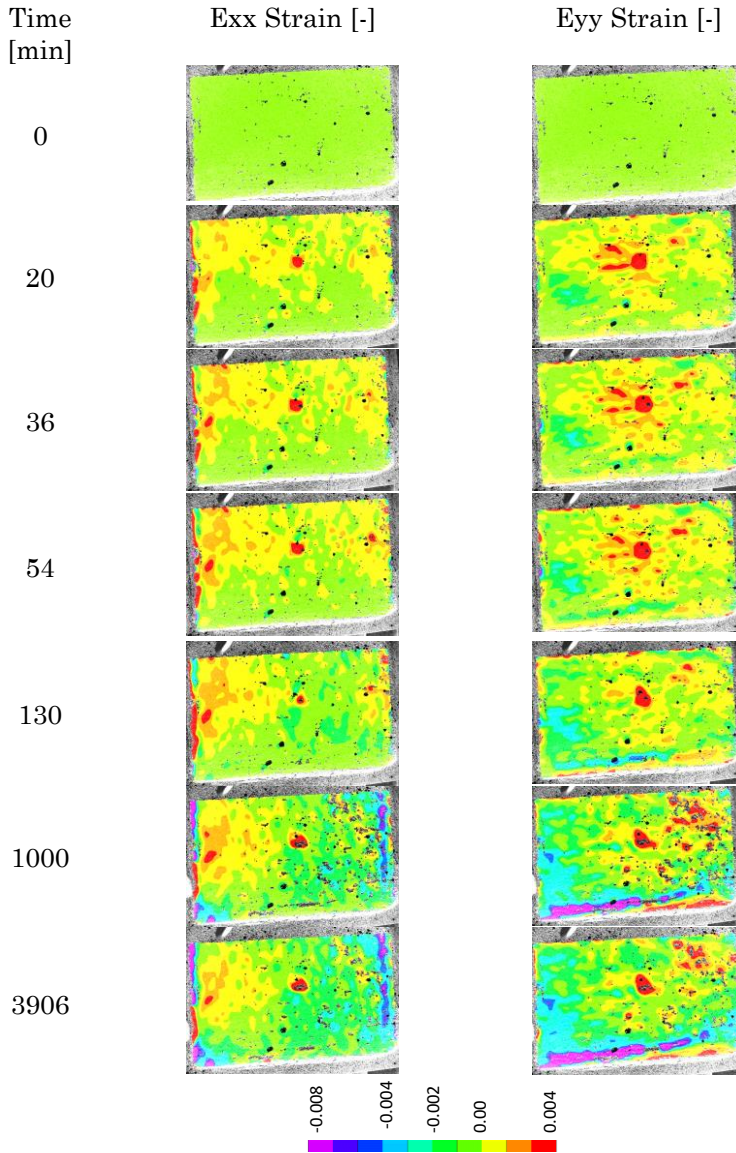
Fig. 4.12 Strain field of mortar in three directions in different time stages.
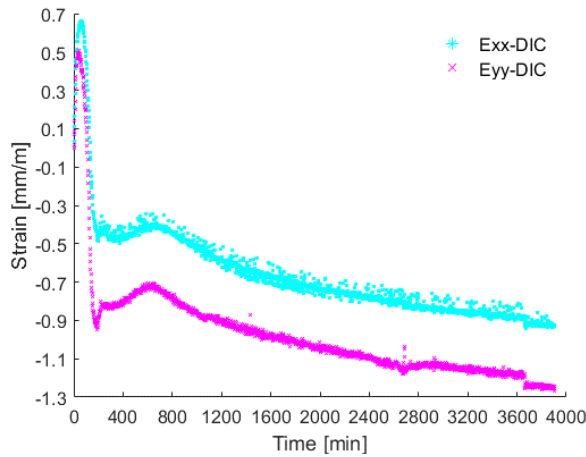
Fig. 4.13 Average strain measurement of the total surface area for mortar in Exx and Eyy directions by DIC.

The 3D projection of W displacement is mapped in order to understand the mechanisms behind this inhomogeneous shrinkage distribution. In Fig. 4.14(a), 3D W displacement maps present the settlement at previously discussed discrete curing stages. In these maps, one can see figuratively the settlement highest values standing at the middle zone of the sample and the edges to have almost negligible settlement till the end of the hardening process. 3D W maps highlight that inhomogeneous settlement occurs, see Fig. 4.14(b). The sample is attached to the mould sides. Therefore, the edges cannot freely move during curing showing limited displacement.

Fig. 4.14 (a) 3D W displacement maps at discrete stages of curing; (b) x-z view of displacement map.

Certainly, the surface morphology of the tested samples is rough due to material's heterogeneous nature (Sadowski and Mathia 2016). Furt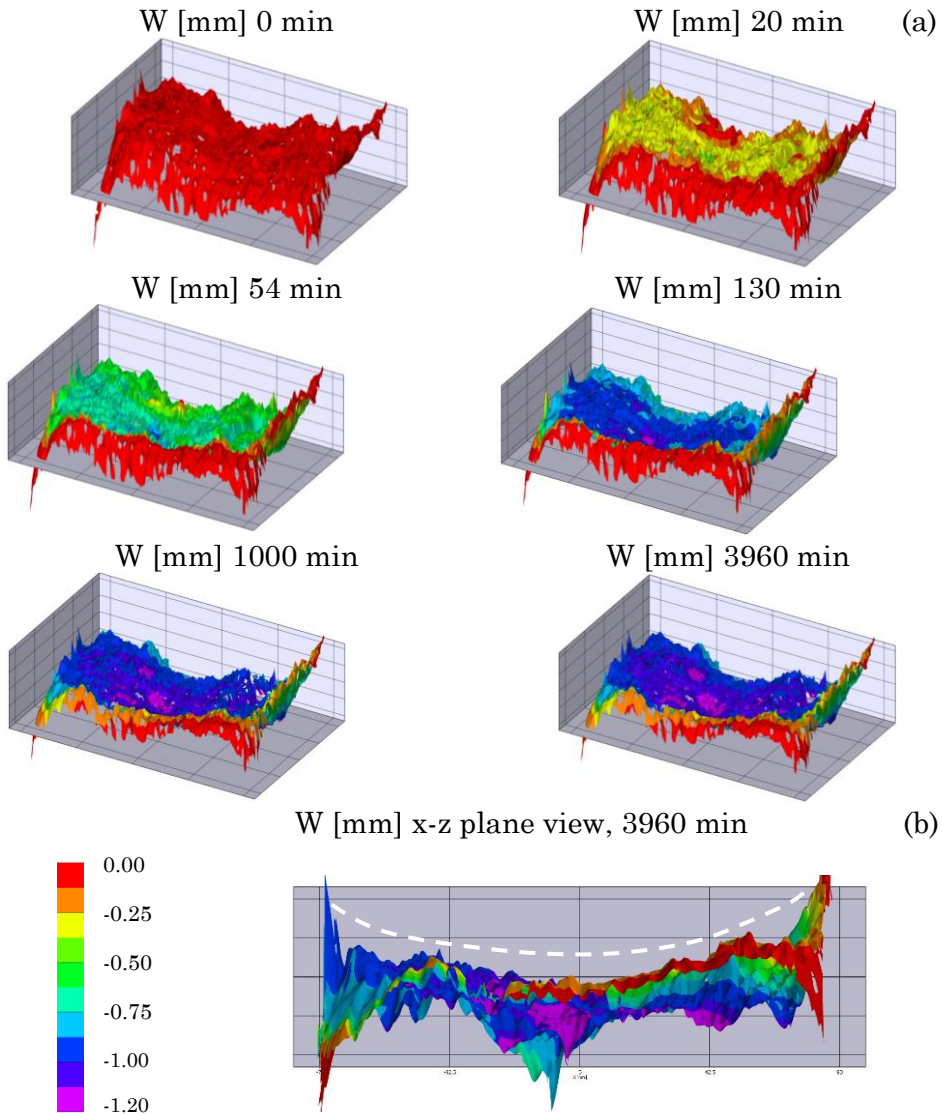hermore, early-age particles movement, settlement, and shrinkage cracks introduce additional complexity. However, the use of DIC technique permits three-dimensional tracking of surface deformations

and strains during testing. The pair of cameras build up a stereovision system able to effectively and in high accuracy track changes in and out of the surface plane.

The fact that settlement of a point at the surface is influenced by its elevation compared to the surrounding areas, as visually presented in Fig. 4.14(a) 3D W maps, is investigated further. The x-z plane view of the settlement is presented in Fig. 4.14(b).
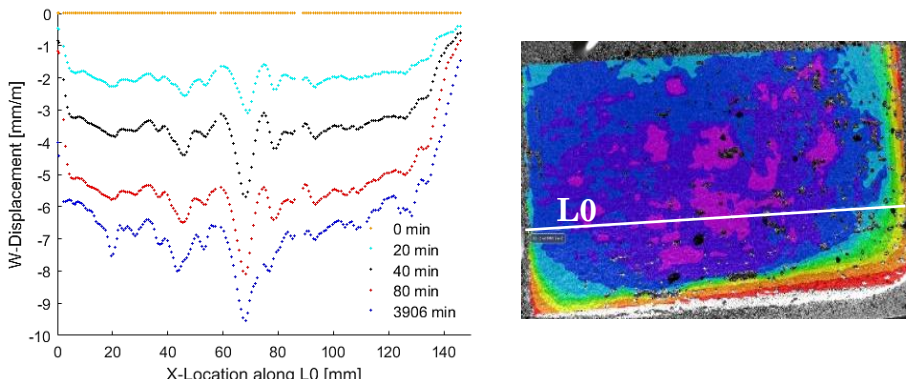
Fig. 4.15 Non-uniform settlement distribution for mortar at Line L0.

In Fig. 4.15, the W distribution of points standing along a line (L0) crossing the sample is presented at discrete stages of curing. In other words, the clear settlement is depicted after subtracting the initial displacement profile. It is shown that as soon as 20 min after casting, the settlement evolves differently at different positions exhibiting the highest value of settlement close to the center of the specimen (discussed in detail above). The x-z view exhibits the relatively "axisymmetric" profile, see Fig. 4.14(b), where a U-shape surface geometry is exhibited. It is evident that the bleed water movement controls the settlement evolution. The consolidation process of the particle structure and the evolution of the mortar microstructure decreases the settlement rate at later stages.

4.4.7 Settlement: DIC analysis of spray speckles compared to point LVDT measurement

The settlement growth in time is quantified by W. The DIC deformation shown in Fig. 4.16 is highlighting the inhomogeneous deformation measured at different locations on the top surface. In Fig. 4.16(a), the settlement obtained as the average of the values measured in the total area is compared to the points with the highest (P0) and the lowest (P1) settlement value, see Fig. 4.16(c), as was previously done for the powder speckle case. In all three lines, the settlement reaches a stable value at 130 min indicating the end of the plastic stage and the start of the hardening process. The vertical shrinkage can continue after the plastic stage due to further drying and hydration process. The cement particles and sand settle to the bottom of the mould due to the gravity force. In this period, heavier sand and cement particles are settled downwards to the specimen bottom and free water is moved upwards and accumulates at the surface due to settlement. Beyond this time, the range is significantly wide between point P0 (9 mm/m) and P1 (1.8 mm/m).

The settlement rate defined as the rate of W displacement in time is shown for point P0, P1 and the average of the total area in Fig. 4.16(b). In this figure, serious changes between the settlement rate at different locations are observed. Point P0 indicates the highest settlement rate, whereas the point P1 indicates the lowest settlement rate. The surface average curve, that is located between P0 and P1, represents the average of the total area. The displacement rate progressively decreases to values close to zero after 130 min.
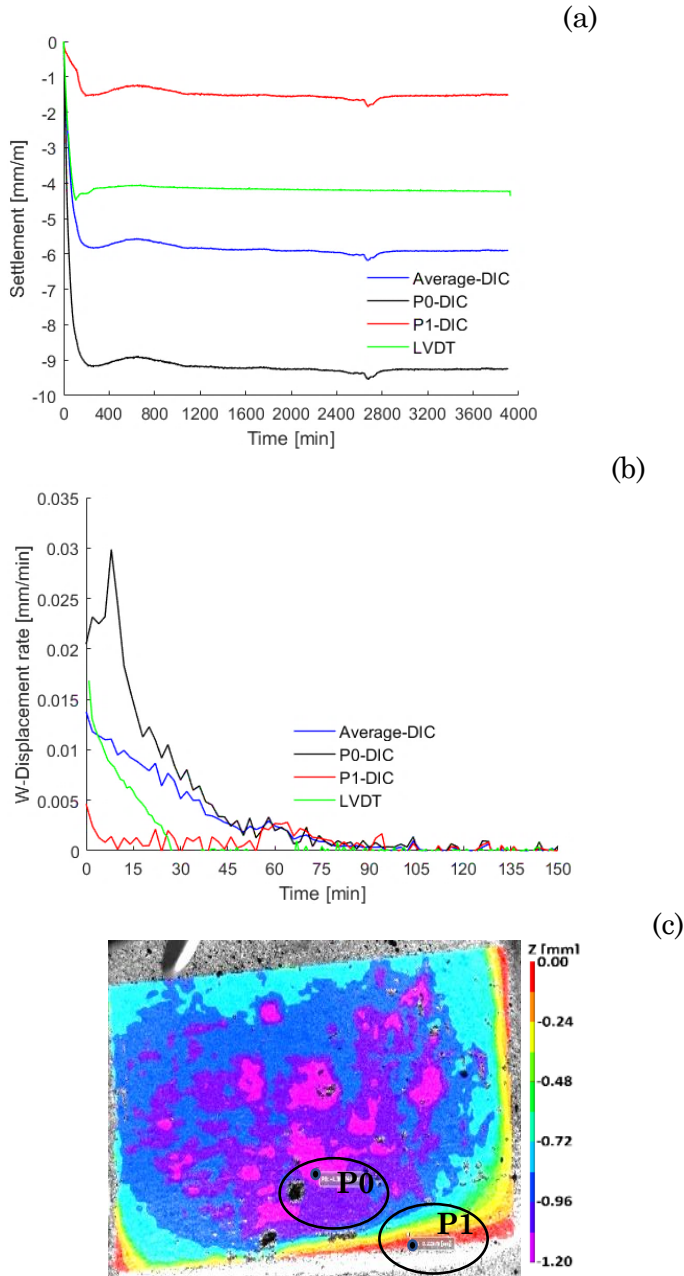
(a)

(b)

(c)

Fig. 4.16 (a) DIC Settlement in average and at discrete surface points (P0, P1) compared to settlement measured by LVDT; (b) W displacement rate versus time; (c) points of extreme values of settlement (highest and lowest).

Classical LVDT result is compared to the one of DIC. The point measurement of LVDT indicates a settlement of 4.3 mm/m and the average DIC measurement presents a settlement of 6 mm/m after 3906 min, as shown in Fig. 4.16(a). The settlement curves of both methods present a displacement increase between 250 min and 650 min indicating an expansive strain due to the thermal effect of the cement hydration process. The difference in the settlement between LVDT and DIC measurement in the absolute value is attributed to the fact that DIC considers the total surface area. However, the LVDT monitors the settlement at a point of the surface. It is evident that no robust conclusion can be obtained when only the point analysis is done. This is a significant drawback of the point analysis. Using DIC, the variation in the settlement at different points is readily available while the average value on the surface can be regarded as a global measurement. In Chapter 5, a point measurement of DIC as close as possible to LVDT point is being investigated.

4.4.8 Shrinkage: DIC analysis compared to point LVDT measurement

In this study, for the first time in literature, a speckle pattern is applied to effectively monitor the material movement a few minutes after casting up to several days. The application of the speckle pattern should be discussed since applying a quality pattern on the fresh cementitious material is challenging. The speckles should be applied without affecting the material composition. Also, due to the presence of bleed water, speckles that are not attached to the cementitious material can float, leading to the loss of the speckle consistency at early monitoring stage.

The DIC accuracy and resolution is affected by the quality of the speckle pattern (Sutton et al. 2009). For that reason, the quality of the patterns must be steady to assure the stability and reliability of the measured deformation (Triconnet et al. 2009). The experimental results validated that the speckle pattern at the surface deforms together with the specimen during the hardening process are allowing a 3D-DIC monitoring of the strain distribution. However, the bleed water could affect the speckle pattern position at plastic state (up to 130 min). Increased bleed water in some regions modifies the speckle pattern by

affecting the white-black contrast and sharpness in plastic state interfering with the analyses. Further, the increased bleed water might cause a reflection of the light, that is not identical on both images. Particularly, the horizontal displacement measurements are affected by the presence of bleed water on the top surface. For this reason, we consider the onset of capillary pressure build-up as the reference to eliminate any "noise" due to bleed water, see Fig. 4.17. At the moment when the capillary pressure increases, no bleed water is expected to be available at the specimen surface that could affect the speckle pattern. Thereafter, any noise due to the bleed water is eliminated by selecting the reference image at the capillary pressure increase. The strains Exx, Eyy, and capillary pressure evolution during curing are presented in Fig. 4.17(a). Capillary pressure is built up after 130 min in the pore system (see vertical red dash line) when menisci form between the solid particles at the surface (Slowik et al. 2008). Capillary pressure is induced by the pore structure and by water loss due to evaporation. These measurements are affected by the presence of bleed water on the top surface. Considering the capillary pressure build-up (130 min) as the reference for the DIC analysis, Exx and Eyy distributions seem almost identical, as seen in Fig. 4.17(a). The analysis highlights the effect of bleed water on the DIC reference and consequent DIC measurements.

DIC strain analysis at the top surface is presented along with LVDT measurements obtained by the pair of LVDT attached to the bottom of the sample. In Fig. 4.17(b) the respective curves are plotted highlighting a significant quantitative difference. At the hardening stage, LVDT measures shrinkage (compressive strain) up to -0.1 mm/m. At that moment, the average DIC measurement shows a shrinkage strain of -0.6 mm/m. Nevertheless, both methods exhibit the same trend, regardless of the difference in the absolute value. It should be highlighted that shrinkage has inhomogeneous distribution along the height of the cement paste sample attributed to a series of phenomena: evaporation, bleed water transportation, segregation, self-weight impact, etc. Consequently, it is expected to measure greater shrinkage near the specimen surface, where the DIC is measuring, since especially the water evaporation is promoted at the surface. The smaller horizontal shrinkage at the bottom of the sample observed in the plastic state is mainly due to the hindered horizontal displacement resulting from the friction at the bottom of the

mould. Further reason could be related to the horizontal extension associated with the increasing self-weight induced vertical stress.
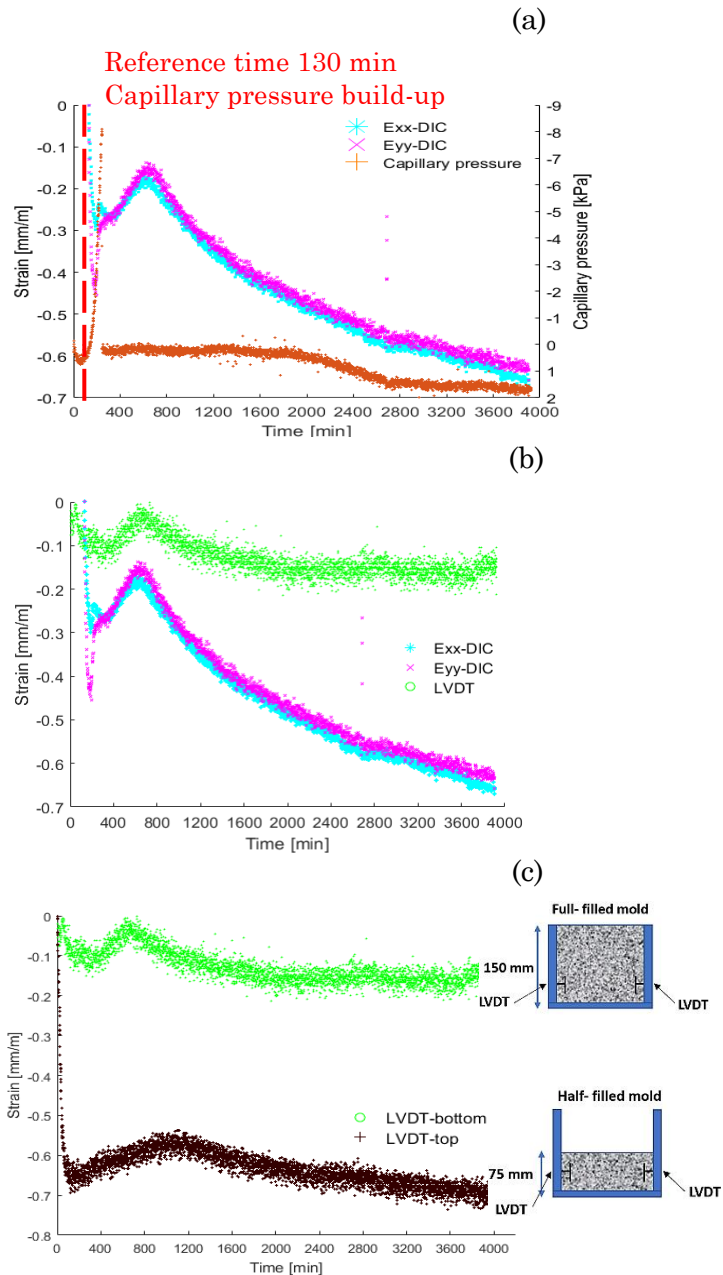
(a)

(b)

(c)

Fig. 4.17 (a) DIC Exx and Eyy strain and capillary pressure distribution in time (DIC reference set at 130 min after casting); (b) DIC Exx and Eyy

strain and LVDT measurement (reference time 130 min); (c) Strain by LVDTs for half-filled mould (LVDT-bottom, specimen height 75 mm) and full-filled mould (LVDT-bottom, specimen height 150 mm).
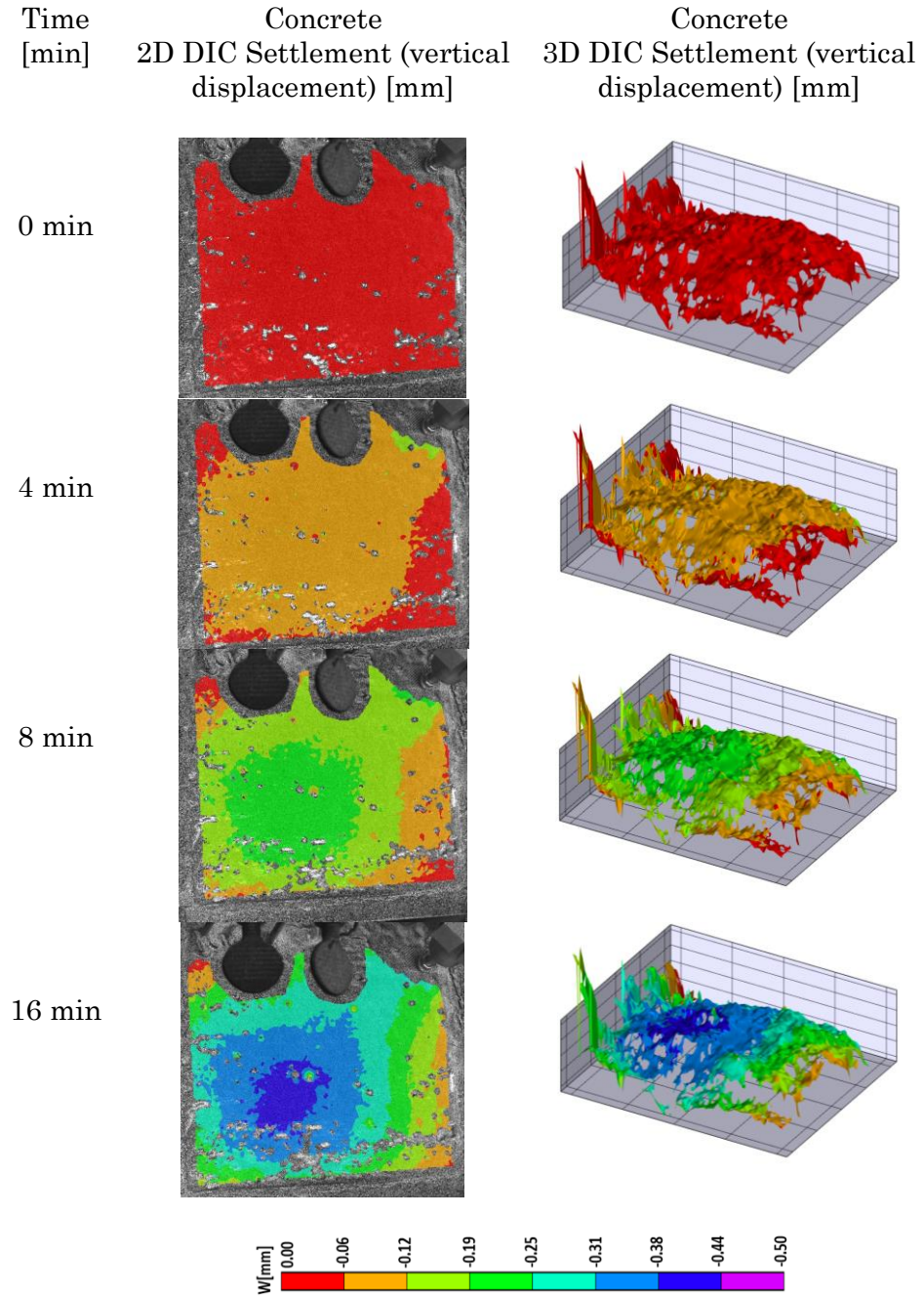
In order to demonstrate this, Fig. 4.17(c) shows an indicative comparison: the shrinkage of a half-filled specimen, with a height of 75 mm and that of a normal specimen of height 150 mm. In both cases, the LVDT was placed 50 mm from the bottom. In the first case, the surface of the specimen was much closer to the LVDT, while the height of the specimen was half. The results confirm that measurement closer to the surface lead to a much stronger shrinkage resulting from the increased water evaporation at the specimen surface. It was not possible to perform DIC on the half-filled mould due to the creation of shadow of the mould walls.

4.4.9 DIC monitoring of concrete

In this section, DIC measurement of concrete is presented by applying the powder speckle pattern, as discussed in the previous section. The DIC strain analysis considers the first image as a reference by controlling the bleed water effect on the specimen surface. Thereafter, an improved DIC strain measurement is introduced for concrete by adding anti-washout admixture (MasterMatrix UW 440) to the concrete.

The concrete specimens were prepared using the same mix design as demonstrated in Section 5.2. The DIC area is equal to 138 x 114 mm^2. DIC analysis has been applied by considering subset of 29 and step size of 7 pixels. A minimum number of 10 specimens were tested and one representative specimen with anti-washout admixture is presented. DIC reference starting point (Time 0) considers the first image for the analysis and the duration of the experiment lasted for approximately 3 days. The mixing and casting of the concrete specimen were done within 15 min. Thereafter, the DIC monitoring started approximately 15 min after casting.

Time [min]	Concrete 2D DIC Settlement (vertical displacement) [mm]	Concrete 3D DIC Settlement (vertical displacement) [mm]
0 min		
4 min		
8 min		
16 min		

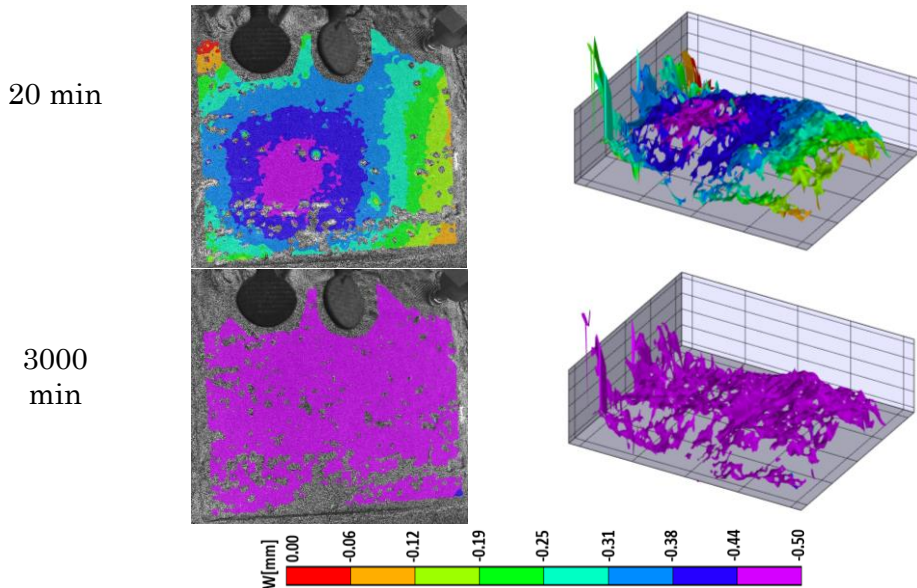W[mm] 0.00 -0.06 -0.12 -0.19 -0.25 -0.31 -0.38 -0.44 -0.50

Fig. 4.18 DIC W displacement maps (vertical displacement) of concrete at discrete stages of curing.

Fig. 4.18 illustrates the DIC 2D and 3D surface settlement (vertical displacement) progression of concrete at different curing stages. As demonstrated, the settlement of concrete is non-uniformly distributed at the surface. In these W displacement maps, as shown figuratively the settlement highest values standing at the middle zone (closer to the bottom edge) of the sample. The edges have lower settlement progression compared to the middle zone. The inhomogeneous settlement progression occurs intensively at the middle zone. The specimen edges are attached to the mould side and cannot move freely during curing leading to lower settlement progression.

Fig. 4.19 demonstrates the settlement caused by gravitational settlement of the solid particles in the fresh concrete. In this figure, the conventional LVDT and average DIC measurement are presented. DIC value of vertical displacement considers the full-field surface for concrete after casting, as average value for the whole monitored area (roughly accounting for 80% the specimen surface). A large amount of vertical displacement was recorded at very early age since the plastic concrete settles. The LVDT curve achieves its maximum settlement with -3 mm/m after 322 min and beyond this moment concrete reveals a steady settlement evolution. The average-DIC increases at early stage for the

124

concrete reaches its maximum value of -6.9 mm/m 368 min after casting, see Fig. 4.19. It is evident that the settlement development follows similar trends in both cases due to common cement material nature.
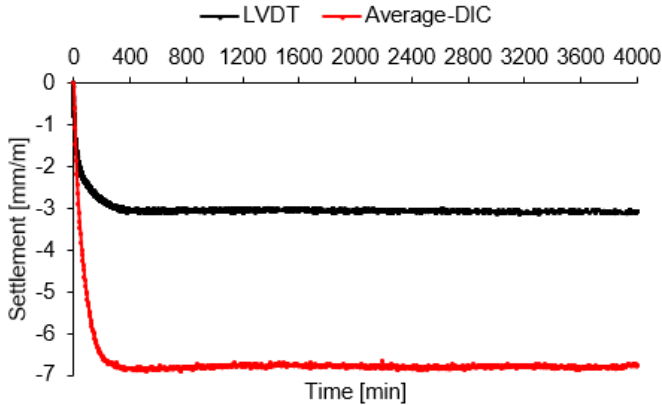

Fig. 4.19 DIC average settlement measurement and LVDT of concrete.

Fig. 4.20 illustrates the horizontal (shrinkage) strains Exx, Eyy, and horizontal LVDT evolution during curing. Exx and Eyy distributions of concrete are very similar at the early curing stage. The bleed water effect on the specimen top surface is almost negligible in the case of concrete. Thus, the anti-washout admixture helps to control the bleed water effect on the DIC speckle pattern. Both strains Exx and Eyy consider the reference image 1 for the DIC analysis. The evolution of Exx and Eyy appear almost identical, while LVDT measurement presents a lower absolute value due to the effect of the specimen height, as previously discussed. DIC measurement of Exx and Eyy illustrate that the shrinkage measurement closer to the surface is much greater than the specimen bottom, as discussed before. It would be interesting to design a mould with a small height to allow DIC monitoring and to eliminate the effect of the height on the shrinkage evolution. Furthermore, Exx and Eyy strains in the top surface are quantified considering the average values of strains measured at the whole gauge surface. The point LVDT strain measurement illustrated -0.17 mm/m after 450 min, followed by the Exx with -2.44 mm/m after 412 min and lastly by Eyy with 2.48 mm/m after 432 min, as shown in Fig. 4.20.
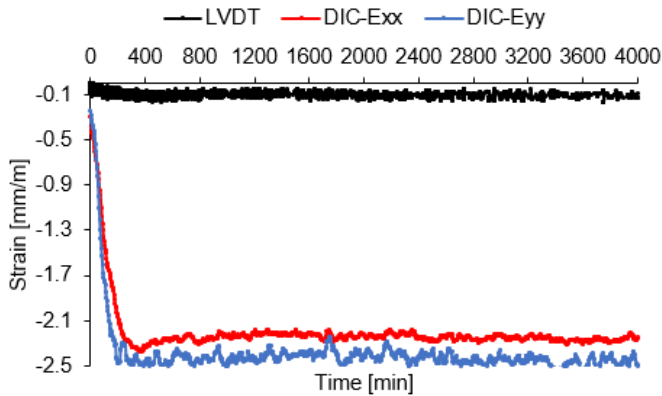
Fig. 4.20 DIC Exx and Eyy strain and LVDT measurement of concrete.

4.5 Discussion

Since the DIC speckle pattern is painted on the surface, its influence on the evaporation process was investigated. The impact of the paint on mortar mass loss is shown in Fig. 4.21. It is observed that the paint layer slows down the evaporation process. The mass loss for mortar with the painted surface is 2% while mortar unpainted surface presents 3.3% mass loss after 5000 min. Although the reason for applying the speckle pattern was measuring of strains, it seems that the paint has a delaying effect on the water evaporation. This may be regarded as a deviation from the normal evaporation rate, see (Fig. 4.21).

Fig. 4.21 Impact of painted mortar surface on mass loss.

Furthermore, concerning the specimen size, concrete in this study is cast in standard specimens of 150mm x 150mm x 150mm used also for the widely accepted compression tests. The sample size is selected to be in scale agreement with the ASTM C1581 shrinkage ring measurement protocol (height 150mm, ring thickness 76mm (ASTM Standard C 1581-04 2004) and the Schleibinger shrinkage-cone that effectively tracks weight loss and settlement using LASER triangulation sensor (cone of 100 mm he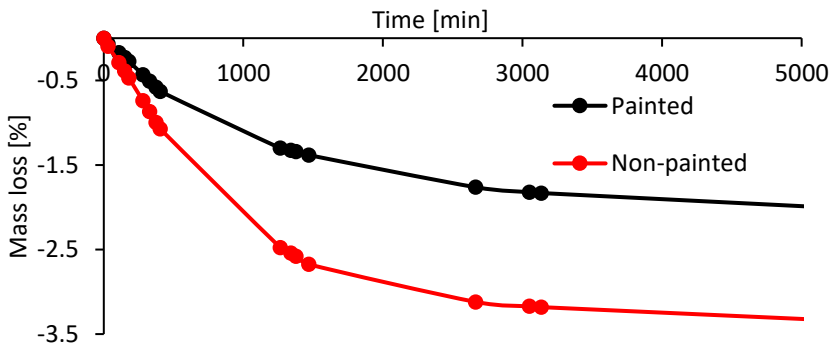ight and volume 349 cm^3 (Mishra et al. 2016)). In literature, measurements of shrinkage have been casually conducted on specimens with lengths from 90 mm to 300 mm (Bhalla et al. 2018; Slowik et al. 2004, 2008). While the outcome of the shrinkage monitoring in laboratory samples cannot be directly extended to bulky concrete elements, it is sufficient to monitor the mobility of the fresh material and compare the trends.

The last point worth to be discussed herein is related to the onset of the DIC monitoring. Starting the DIC measurements at 15 min after casting, may lead to a loss of some early information mainly in terms of the settlement, as horizontal shrinkage starts later. However, the settlement is a process that lasts for hours after casting and therefore, the amount not accounted for during the first minutes, although real, is kept at a minimum. Nevertheless, the time of DIC monitoring onset is similar for all specimens allowing comparisons.

4.6 Conclusions

Drying of fresh cementitious materials is accompanied by volume changes due to water evaporation and the cement hydration process. This study proposes a simple and effective optical technique of 3D-DIC to assess the displacement and strain distribution of fresh cement-based materials 15 min after casting. Following, the main conclusions are obtained:

For the first time in literature, DIC technique has been applied on fresh cementitious material 15 min after casting, providing a global view of the early age deformations.

The classical LVDT measurement and DIC measurement followed the same trend indicating that after proper study that DIC could be used to monitor displacement and strain evolution during the early drying process and hydration process in a non-contact manner. There is a qualitative agreement between the both methods, while an absolute reference provided possibly by laser method would be desirable.

Three-dimensional DIC technique allows an improved assessment of the non-uniform deformation distribution on the specimen surface when concrete shrinks and settles, which is not possible with classical point LVDT measurements.

Despite the overall shrinkage, some regions presented expansive strain, that cannot be measured by conventional LVDTs.

In this study, it has been shown that three-dimensional DIC can measure shrinkage strain and settlement. This approach allows a deeper understanding of fresh cementitious materials early age processes and upgrades the monitoring of concrete to global measurements offering data for the whole surface as compared to the point data of conventional LVDTs. Further research on the accuracy of the technique should be carried out, especially related to the effect of bleed water on the measurements for the first hour after casting.

Chapter 5: **Acoustic emission of concrete with admixtures**

Most concrete produced includes chemical admixtures to improve workability without an effect on hydration behaviour of concrete. The concrete admixtures can contain setting accelerating or setting retarding chemicals that directly can influence the hydration behaviour and affect several properties of the cementitious system. In this chapter, the impact of different chemicals on hydration is studied with an emphasis on the understanding of correlations with acoustic emission activity. It is seen that the acoustic emission resulting from processes on the microstructural level differs from that in the plain concrete, allowing a new perspective to study the hydration of concrete with admixtures.

5.1 Introduction

The hydration reactions are substantial for concrete and known to affect the propagation of elastic waves. It is still not clear how or to what extent the hydration reactions impact the evolution of AE activity. The influence of accelerated and retarded hydration reaction on AE activity still needs to be studied to improve quality control.

The application of accelerators increases the rate of cement hydration and the early strength development caused by the formation of calcium sulfoaluminate hydrates that leads to a rapid rise in stiffness of the specimen (Maltese et al. 2007; Salvador et al. 2014). Higher temperature causes initially rapid hydration process that leads to high early compressive strength development (Escalante-Garcia and Sharp 1998; Lothenbach et al. 2007). Accelerators based on sodium aluminate deplete the amount of sulfate ions from the liquid phase that lead to rapid C_3A reactions (Salvador et al. 2016). At early age, the increase in temperature influences the morphology of hydrates by inhomogeneous distribution of the hydrates, higher porosity (Kjellsen et al. 1991) that leads to the formation of denser C-S-H, smaller ettringite crystals and larger amount of monosulfoaluminate (Lothenbach et al. 2008). However, the strength at 28 and 91 days of concrete and mortar are lower at higher temperature due to accelerating effect of the hydration process (Lothenbach et al. 2008). The pore solution is also influenced by the temperature. At higher temperatures, ion concentrations remain little changed but aluminum concentration decreases and sulphate concentration increases (Thomas et al. 2003).

At low temperature, the process of hydration begins slowly, that gives the dissolved ions enough time for diffusion before the hydrates precipitate. Thereby, a less dense C–S–H formation leads to a more uniform distribution of hydration products as well as lowers the coarse porosity (Kjellsen 1992; Komonen and Penttala 2003). Retardation of cementitious systems consists mainly of two effects. The effects are the increase in the induction period and the decrease (in some cases increase) in the hydration rate after hydration process accelerates (Peschard et al. 2006). Further, some researchers have concluded that the admixtures retard the rate of heat evolution after the induction period and also

reduce the energy of these transient reactions. In another approach, Khan et al. indicated four mechanisms of cement retardation. The first mechanism is called adsorption which forms a protective skin around the surface of cement particles and acts as a diffusion barrier. This layer around the cement particles slows down hydration. The second mechanism is the nuclei of calcium hydroxide. By adding water to cement grains calcium ions are rapidly released from cement grain surface leading to crystallization from the solution and then the hydration proceeds. The retarding admixture incorporates itself into the cement paste and prevents the growth of CSH formation before the crystallization begins. Thereafter the induction period will be lengthened due to the reduction of crystal growth of calcium hydroxide. The third mechanism is the formation of complexes with calcium ions to discourage the nuclei formation. The last mechanism is similar to the first one by forming a protective skin around cement particles. The derivatives of admixtures act as a diffusion barrier and prevent them from reacting with water (Khan and Muhammad 2004).

Retarder based on phosphonate increases the induction period from around 3 h up to 72 h compared to the reference cement (Ramachandran et al. 1993). Cheung et al. indicated that in case of retarder based on sucrose if it is applied above optimal dosage, a rapid stiffening behaviour could result due to the accelerated reactions of aluminate containing phases (Cheung et al. 2011).

The compressive strength development is primarily dictated by Tricalcium silicate (C_3S) and Dicalcium silicate (C_2S). C_3S is primarily responsible for early compressive strength development (1 to 28 days) while C_2S is responsible for later compressive strength (after 28 days). Retarders do not decrease the ultimate compressive strength of cement (Ogbonna 2009).

The effect of the accelerating admixture on concrete hydration process, is investigated in the present chapter. Admixture that contains calcium silicate hydrate (C-S-H) nanoparticles are added to the specimen to accelerate the very early age cement hydration (Hesse et al. 2011). This C-S-H seeding stimulates the formation of C-S-H nuclei during the continuing cement hydration (Land and Stephan 2018). The addition of the accelerator leads to an increase of the very early cement hydration

rate as well as the total hydration at the early nucleation (the first 24 h). The C-S-H seeding effect offers new nucleation within the pore space which is away from the surface of the particle.

The nanoparticulate nature of the C-S-H gel stimulates the creation of new particles caused by the nucleation process. This nucleation process is built on the stimulation of new C-S-H particles by existing particles and thereby development of new regions of hydration product. The three main effects of C-S-H seeding are the following: 1) the induction period is shortened in C_3S due to a high number of nuclei that are existing for development starting already from time zero, 2) the early acceleration rate and the peak rate should be higher due to the simultaneous development of more regions of hydration product (Fig. 5.1), 3) the total hydration amount should be greater during the very early nucleation and evolution stage. The reason behind it is the nucleation of regions of hydration products in the pore space between the particles allowed by the seed effect. Therefore, the growth of the nucleation in the pore space would not cover the C_3S particles with a diffusion barrier built by a layer of hydration product.
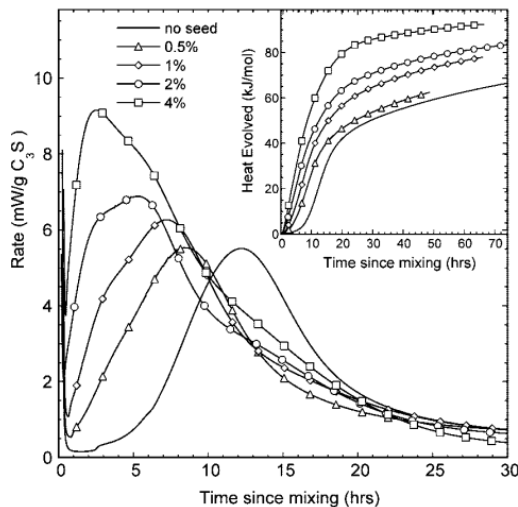

Fig. 5.1 C_3S hydration by addition of S-C-H seed. The addition of the seed refer to the mass of solid C-S-H per mass of C_3S (Thomas et al. 2009).

The C-S-H hydration product is more uniformly distributed throughout the pore space and the capillary porosity is much less in the seeded paste. The two separate nucleation and growth of early hydration is presented in Fig. 5.2, the normal process at the unseeded particle surfaces Fig. 5.2(a-b) and the seeded process in the pore space Fig. 5.2(c-d). Few minutes after mixing, the hydration product (mainly the C-S-H gel) initiated at the particle surfaces and starts to spread out into the pore space Fig. 5.2(a). Several hours later, the thickness of the hydration product layer, which acts as a diffusion barrier, limits further nucleation and growth of hydration process producing substantial capillary porosity Fig. 5.2(b). Few minutes after mixing, C-S-H seeded paste presents hydration products that nucleates on the particle surfaces as well as within C-S-H seed regions, resulting in the higher rate of early hydration Fig. 5.2(c). Several hours later, the amount of early hydration is greater with lower capillary porosity Fig. 5.2(d).
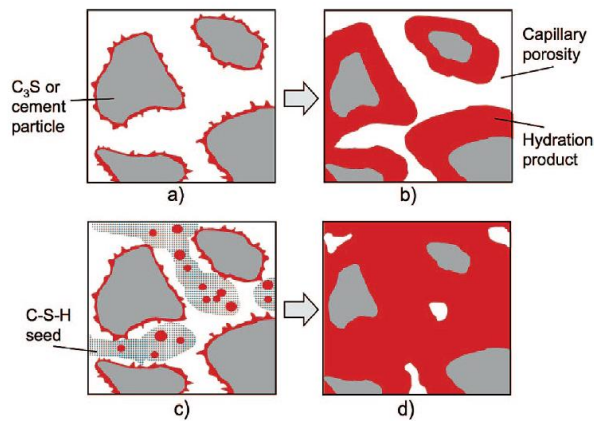
Fig. 5.2 The hydration process of reference and seeded specimens (Thomas et al. 2009).

Beside the effect of the accelerating admixture on concrete hydration process, the influence of the retarding admixture is also investigated in the present chapter. Retarder based on phosphonic acid that affects the hydration process and acts chemically was applied in this research. The addition of retarder to the specimen led possibly to the formation of sparingly soluble surface coatings that delay further progress of hydration (Rickert 1999). The retarder forms a thin layer of sparingly

soluble calcium phosphonate on the cement particle surface that acts as a protective layer. This surface coatings strengthen the retarding action of the ettringite. Calcium ions that are combined by retarder blocks the water access to the clinker surface, leading to delayed effect of the hydration reactions of the silicate phase and lengthening the induction period. The negative acid residue attaches itself to the cement particles within a few minutes. During the retardation period, calcium and sulfate concentration remain at high level in the pore solutions. After the retarding period has completed, the cement and clinker continue to hydrate normally and there are no changes in the hydrate phases comparing to the reference sample.

The objective of this chapter is to evaluate the correlation between the hydration process and the corresponding AE development in the presence of admixtures in concrete. Hydration kinetics were analyzed by isothermal calorimetry and thermocouple measurement, while mechanical measurement was investigated by LVDT sensors and DIC, pressure transducer, AE parameters and Vicat needle. The accelerated and retarded hydration exhibit noticeable difference in the acoustic behaviour relatively to the reference concrete. In the following section, the materials applied to perform the concrete specimens are presented.

5.2 Materials and methods

Experiments were carried out using portland cement (CEM I 52.5N). The concrete composition is given in Table 5.1. The experiments were performed in a metallic mould, as presented in Chapter 4, see Fig 4.2. Every test was performed with the same mixing procedure as explained in Chapter 4. Throughout the study, three specimens per series were investigated and the most representative tests are presented. The effect of two accelerators and two retarders for concrete that are commercially available were studied, labelled as type I and II. The first accelerator is Sika Rapid C-100 and is based on Nitrate-containing calcium silicate compounds while the second accelerator is BASF Master X-Seed 100 and is based on calcium silicate hydrate (CSH) crystallites seeding. The first retarder is Sika VZ 10 con.13% BT and is based on phosphate-containing

phosphonates compounds, whereas the second retarder is BASF MasterSet R 436 and is based on phosphate compounds.

An integrated system has been developed to simultaneously monitor several activities occurring in fresh concrete, as discussed in Chapter 4. Moreover, the DIC measurement with spray speckles has been simultaneously performed and the setup has been discussed in Chapter 4. The ultrasonic measurement was conducted in U-shaped plexiglass, as presented in Chapter 2. The monitoring measurements were performed in a temperature-controlled room at 20 °C with a relative humidity 50 ± 5%. Several specimens of concrete with admixtures were cast and monitored. ACC signifies the addition of accelerator to concrete, RET represents the addition of retarder to concrete and REF represents the reference concrete without the addition of admixtures. ACC-I, ACC-II corresponds to the addition of accelerators of type I and II in concrete and RET-I, RET-II corresponds to the addition of retarders of type I and II in concrete respectively. Throughout the study, a minimum number of 3 specimens for each type of admixture were monitored.

Table 5.1 Composition of the concrete specimens (all units are in kg/m^3, except when mentioned otherwise).

	REF	ACC	RET
Sand (0/2)	482	482	482
Coarse aggregate (2/4)	896	896	896
Coarse aggregate (4/16)	482	482	482
Cement	380	380	380
w/c ratio	0.5	0.5	0.5
Accelerator (m% by cement)	-	5	-
Retarder (m% by cement)	-	-	2

After premixing cement with all dry aggregates for 1 min, the mixing water was added together with the admixture to the mixer. The concrete was mixed for 3 min in a laboratory mixer, as explained in Chapter 4. For the isothermal calorimetry measurements, cement paste with w/c ratio of 0.4 and with identical admixture addition as it is mentioned before (accelerator 5m% by cement and retarder 2m% by cement) were

prepared. Furthermore, for the Vicat needle test and UVP cement paste, the same mixing proportions were applied as the ones used for isothermal calorimetry.

5.3 Results

5.3.1 Impact of admixtures on heat evolution

The mechanisms behind the correlation between AE and physical measurements is not always absolutely clear and straightforward, but there are experimental correlations that are worthy to be discussed. Data for temperature evolution of concrete (REF), retarders (RET) and accelerators (ACC) both types I and II are shown in Fig. 5.3. ACC showed a rapid increase in temperature probably due to a rapid initial reaction, while RET presented excessive slow rate of temperature evolution. ACC-I presented an initial temperature of 23 °C followed by the REF with 21 °C and lastly by RET-I with 20.7 °C as shown in Fig. 5.3. The dormant period or the induction period with a very slow reaction has been extended by RET. ACC-I demonstrated a temperature peak with 22.8 °C after 530 min followed by REF with 21.3 °C after 820 min and lastly by RET-I with 21.2 °C after 2030 min, see Fig. 5.3. First, we examined the pair of ACC-I and RET-I and later the pair of ACC-II and RET-II.

The accelerator contains calcium silicate hydrate (C-S-H) nanoparticles that causes a substantial acceleration of the early hydration kinetics (Thomas et al. 2009). The C-S-H seed causes the formation of hydration in the pore space between the cement particles, while during normal hydration nucleation arises only on or near the particle surface. The presence of two separate hydration processes simultaneously (one at the particle surface and one initiated in the pore space between the particles) leads to higher early hydration rate. Thereafter, the C-S-H gel leads to a shortening of the induction period in C_3S. The maximum hydration rate is raised by C-S-H seed while the time needed to reach the rate peak is reduced and thereby the total heat developed at the end of the main hydration period is increased. The S-C-H effect results in more uniform distribution of hydration products as well as lower capillary porosity.

Similar observations have been illustrated for ACC-II and RET-II. ACC-II illustrated a temperature peak with 21.8 °C after 454 min, followed by REF and lastly by RET-II with 20.9 °C after 1737 min as presented in Fig. 5.3. Like type I, ACC-II presented an initial temperature of 22.5 °C, whereas RET-II demonstrated an initial temperature of 20.9 °C. Thereafter, the accelerator generates a higher initial temperature compared to the reference and retarder. The main temperature development of REF is between 400 min and 1500 min indicating the main hydration process, see Fig. 5.3.

In addition, the retarder delays the hydration process by an extended dormant or induction phase compared to the REF and ACC. This observation could be related to the creation of a barrier around the cement particles that slowly dissolve, thus the hydration process is delayed (Khan and Muhammad 2004). The retarding action is ascribed to the formation of sparingly soluble layer on the particle surface that blocks the access of water to the cement surface and leads to the retardation action (Rickert 1999). This thin layer on the particle surface reinforces the retarding process of ettringite. Thereafter, the induction period is lengthened by the addition of retarder. After the retarding action is completed, the cement hydration continues normally.
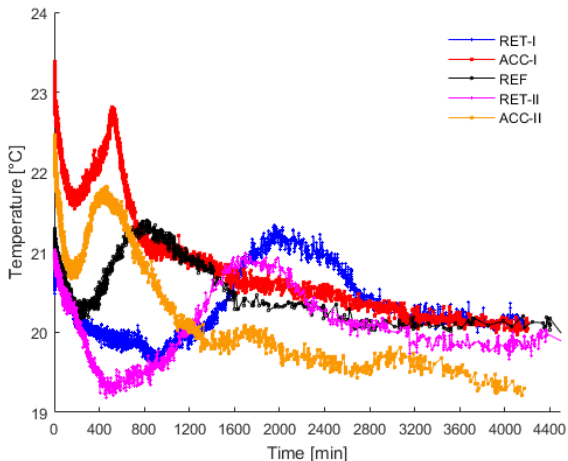

Fig. 5.3 The temperature evolution of concrete as a function of time for reference, accelerator and retarder.

Furthermore, the isothermal calorimeter was applied to determine the heat evolved during the hydration process of cement as a function of time. In Fig. 5.4(a-b) the experimentally obtained heat evolution curves for RET-I and II, ACC-I and II as well as REF are presented. Greatest amount of the heat was released during the first 3000 min of hydration as shown in Fig. 5.4(a-b). Fig. 5.4(b) presents a zoomed-in heat evolution for all specimens up to 3000 min. All the specimens show an initial exotherm within the first 20 min of hydration which is attributed to a combination of reactions such as heat of wetting, hydration of free lime and the formation of ettringite. This effect is followed by an induction or dormant period where the chemical reactivity is relatively low. At the end of this period, heat evolution presents an increase with a peak and this is attributed to the hydration of tricalcium silicate that generates calcium silicate hydrates and calcium hydroxide.

The heat evolutions of both RET present a peak at around 160 min before the onset of the main heat evolution that could be related to mechanism of RET. Both types of ACC exhibit an earlier and intense thermal peak compared to the REF with 4.2 mW/g cement at 480 min for ACC-II and 3.3 mW/g cement at 630 min for ACC-I. REF demonstrated a heat evolution peak with 3.2 mW/g cement at 870 min, followed by RETT-II with 3 mW/g cement at 1140 min and lastly by RET-I with 2.6 mW/g cement at 1430 min. Similarly, both types of RET extend the induction period and demonstrate a delayed heat evolution peak due to delayed reactions compared to REF. From around 3000 min, a steady state occurs and it continues.

The degree of hydration presents the fraction of cement that has fully reacted with water relative to the total amount of the sample. Fig. 5.4(c) illustrates the degree of hydration for RET-I and II, ACC-I and II as well as REF. The increased heat evolution of both types of ACC led to an increased degree of hydration as well, since the heat production rate is strongly temperature-dependent, while RET presented a lower rate of heat of hydration. After 6 days, ACC-I illustrated the greatest degree of hydration with 0.78, followed by ACC-II with 0.76. REF and RET-II presented a degree of hydration of 0.73 and lastly by RET-I with 0.72.

Heat evolution (a)
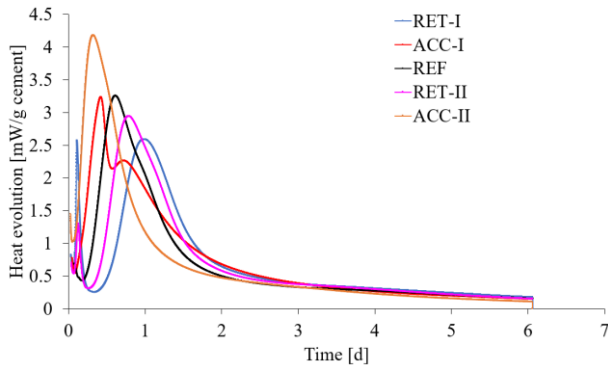
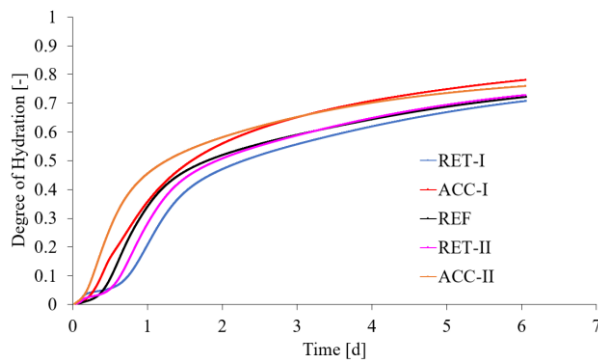
(b)
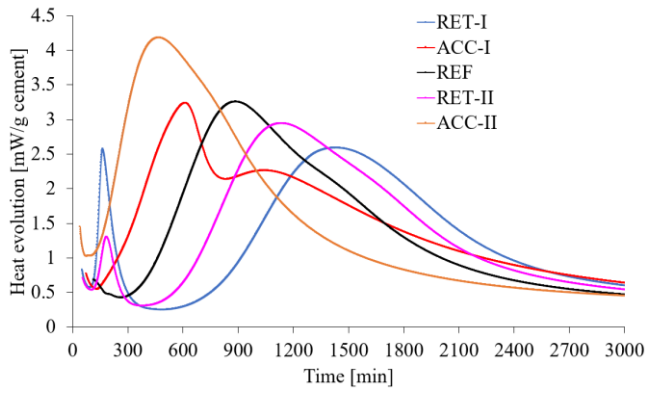
Degree of hydration (c)

Fig. 5.4(a) Heat evolution as a function of time; (b) zoomed-in heat of evolution up to 3000 min; (c) degree of hydration.

5.3.2 Influence of admixtures on setting time

The observation shows that the chemical admixtures significantly impact the setting behaviour. REF illustrated an increase in pulse velocity after 200 min of curing while ACC and RET demonstrated an immediate increase in pulse velocity as shown in Fig. 5.5. Although this would be expected for accelerator addition, it was not expected for retarder. However, this result was repeatably showing very rapid increase of UPV in the case of retarder. Similar behaviour of Vicat needle measurement in cementitious systems containing accelerator and retarder at very early age was noticed, as will be seen later in the chapter. It was observed that immediately after including retarder in the mix, it become seemingly stiffer in mixing. Possibly, the real increase in pulse velocity of ACC-I started after 220 min with 1770 m/s and for RET after 860 min with 1678 m/s, as shown in Fig. 5.5. There, a long plateau is noticed for the RET, after the initial rapid increase of UPV and up to about 800 min. An increasing tendency of velocity is exhibited later, and this should be linked to the actual hydration which comes much later than the reference.
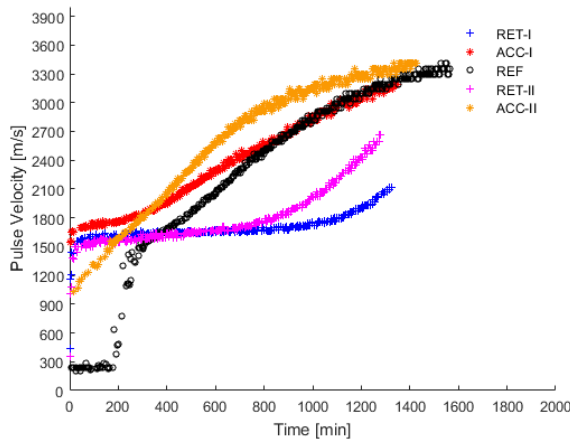

Fig. 5.5 Ultrasonic pulse velocity measurement.

Similar pattern has been observed in type II measurements in Fig. 5.5. This observation indicates that a rapid reaction occurred between cement and accelerator as well as between cement and retarder right after the addition of the admixture. RET presents false set that leads to the rapid

stiffening caused by a secondary gypsum in pores with interlocking needle-like crystals, as will be discussed in detail in the following sections. Further, ACC pulse velocity increase is affected by the accelerated C-S-H seeded action. Beside the nucleation and growth of early hydration at the particle surface, the hydration products are formed in the pore space as well to accelerate the hydration process which increase the pulse velocity.

This behaviour for ACC and RET may be related to rapid setting after applying the maximum dosage of accelerator or retarder. Specifically this observation could be due to rapid stiffening as a consequence of accelerated reactions of aluminate containing phases (Cheung et al. 2011). The interaction between admixture and cement causes a rapid stiffening of the fresh material. The combination of the interstitial phase hydration including C_3A and C_4AF, and alite hydration possibly causes the setting of cement paste (Hanehara and Yamada 1999). The largest amount of the hydration occurs in the first hour after mixing. Large amounts of ettringite are formed in the shape of large needles in low ion concentrations. Under these circumstances, stiffness and pseudo-setting are caused by the large amount of ettringite produced by the continuous hydration of the interstitial phase, see Fig. 5.6. Rapid stiffness or false set of concrete begins within one hour after mixing which is related to the production of a large amount of ettringite from the interstitial phase, as shown in Fig. 5.7.

Further, the addition of retarders can invert their effect and act like accelerator in view of setting at a certain addition level (Winnefeld et al. 2005). This effect leads to an early or shortened setting but not to earlier strength development. The samples containing higher levels of calcium and sulphate present an inversion reaction (Rickert 1999) . This inversion reaction causing false setting depends on the clinker reactivity, calcium and aluminate reactivity, the quantity of retarder and the time at which it is added. Further, the presence of low quantities of hemihydrate gypsum influences the rate of ettringite formation and causes false set (Kurdowski 2014b). Case II presents the false set (Fig. 5.6) by the ettringite layer and the secondary gypsum in pores leading to rapid stiffening. By mixing process of paste a quick dissolution of crystallized gypsum occurs. Therefore, RET presents false set that leads to the rapid

stiffening caused by a secondary gypsum in pores with interlocking needle-like crystals.
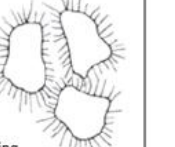
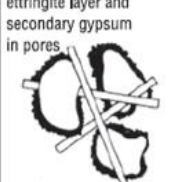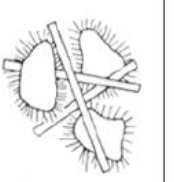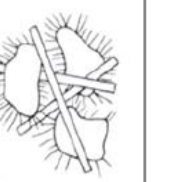Fig. 5.6 Different setting phenomena: I ettringite recrystallization; II secondary gypsum in the pores causing false set (Kurdowski 2014b).
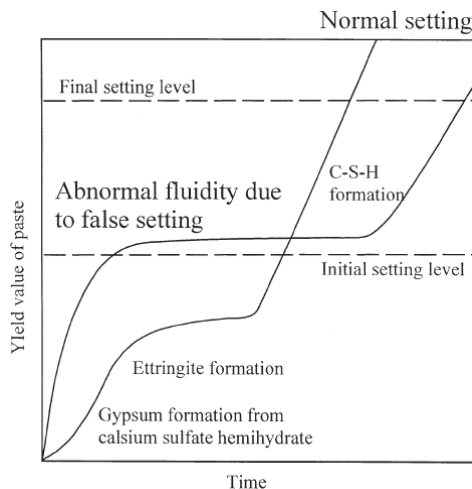
Fig. 5.7 Normal and abnormal setting processes (Hanehara and Yamada 1999).

The Vicat measurements for all the specimens have been performed according to EN 196–3. The initial set point for REF is after 350 min of curing, while for ACC-I and RET-I the initial set point started immediately after curing, see Fig. 5.8. ACC-II illustrated an initial set point after 192 min whereas RET-II demonstrated an immediate increase, see Fig. 5.8, as demonstrated by the Vicat needle test. The obtained results for RET-I and RET-II are unusual because of the rapid setting as mentioned before. This rapid stiffening of RET is due to the false setting as aforementioned. Furthermore, the consistency of the mixtures is probably different by adding the admixtures, which is affecting the needle penetration. The paste consistency is having a significant influence on the needle penetration.
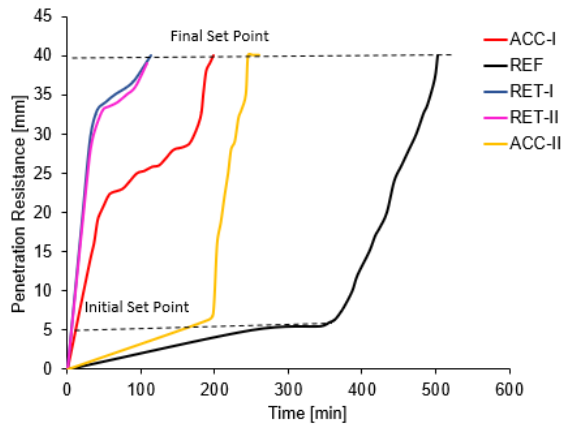
Fig. 5.8 Vicat needle test for REF, ACC and RET.

5.3.3   Impact of admixtures on concrete volume deformation

The settlement progression was also dependent upon hydration process as can be seen from Fig. 5.9. The settlement progression was determined by means of LVDT. ACC illustrated a steep settlement evolution compared to the other curves.
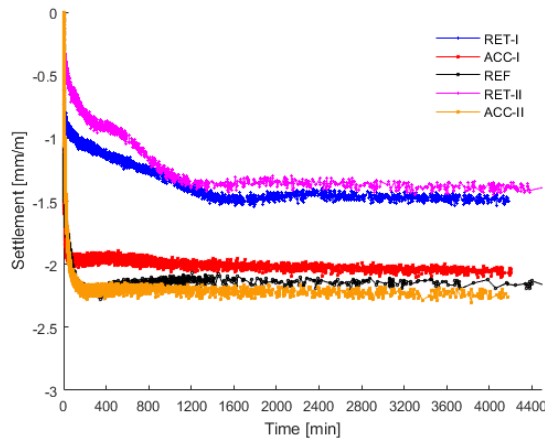
Fig. 5.9 Settlement evolution for REF, ACC and RET type I and II.

RET-I illustrated a slow and extended settlement evolution till 1358 min with -1.5 mm/m, while ACC-I presents a steep settlement curve with -2.2 mm/m at 72 min, see Fig. 5.9. The settlement curves present -1.3 mm/m at 980 min for RET-II, -2.2 mm/m at approximately 147 min for ACC-II and -2.1 mm/m at around 142 min for REF as can be seen from Fig. 5.9. The obtained results demonstrated a delayed settlement curve for both types of RET.

RET leads to a longer plastic state, and so there is a higher risk of plastic settlement, and a longer evolution of plastic settlement. The settlement values of RET are lower compared to REF and ACC and this is possibly attributed to false setting. RET presents false set due to the presence of gypsum hemihydrate that leads to the rapid stiffening caused by a secondary gypsum in pores with interlocking needle-like crystals.

ACC specimens show a shorter evolution of settlement but with higher settlement values, possibly caused by the initial increase of the workability by the S-C-H seed. The C-S-H nanoparticles result in the nucleation of hydration products in the pore space between the cement particles, apart from the hydration process at the particle surface.

Furthermore, the non-contact optical technique of DIC has been compared to the classical point measurement of LVDT to measure not only a point at the specimen surface, but also the global settlement

evolution of the total surface as shown in Fig. 5.10. A point measurement at the surface is not sufficient to describe the settlement evolution since the settlement is not uniformly distributed, as discussed in Chapter 4. Additionally, DIC average considering the total surface average area is presented in this section to investigate the impact of admixtures on the vertical displacement. The spray speckle pattern was applied on the sample surface to allow DIC monitoring.

"Settlement-DIC-average" considers the total settlement area at the surface as aforementioned. "Settlement-DIC-point" represents a point measurement of DIC at the surface. This DIC point is placed close to the LVDT point measurement. The curves of the global DIC measurement and the DIC point measurement are compared to the LVDT surface measurement in Fig. 5.10. The LVDT point measurement follows the same trend as the DIC measurement but with differences in the absolute value due to the no uniform settlement distribution. REF presents the greatest DIC global measurement with approximately 7 mm/m (Fig. 5.10(e)) after 400 min. After 4000 min, ACC-I is around -1.9 mm/m (Fig. 5.10(a)) and RET-I is around -2.2 mm/m (Fig. 5.10(c)). The same observation is demonstrated for ACC-II and RET-II. DIC and LVDT measurement of ACC illustrated a steep settlement evolution compared to RET due to intensive hydration process at very early age. It can be concluded that the settlement progression of RET and ACC are diminished compared to REF.

The impact of admixtures is also presented in the horizontal displacement (shrinkage) of concrete, as shown in Fig. 5.11. The results of shrinkage evolution are presented in the form of "moving average" trend line (sliding window of 40 successive points) to present their evolution during the hardening process. After the hydration rate of ACC is accelerated, the shrinkage evolution illustrated a fast progression compared to REF and RET.
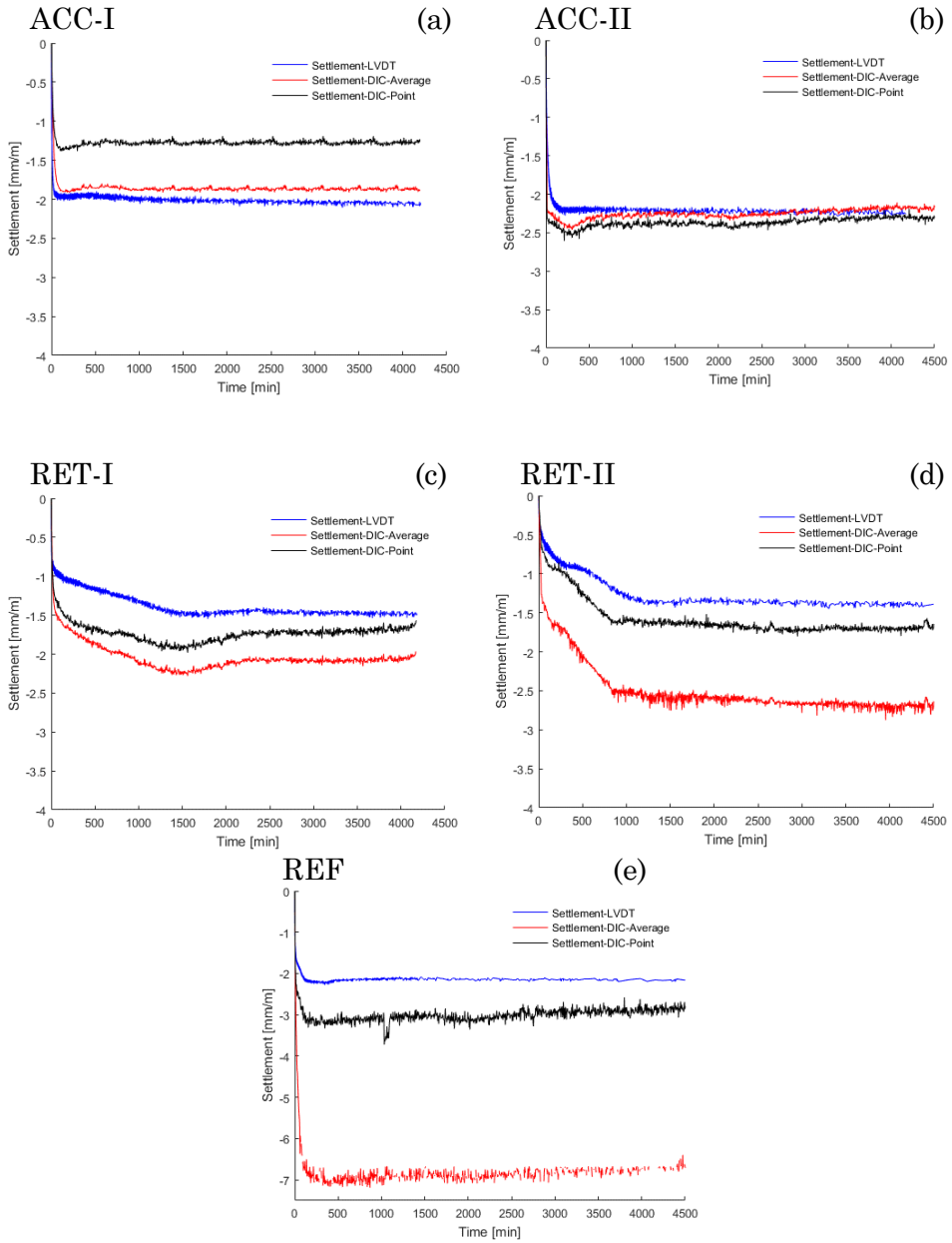
Fig. 5.10 DIC measurement compared to classical LVDT measurement for (a-b) ACC type I and II; (c-d) RET type I and II; (e) REF.

RET-I demonstrated a shrinkage progression of -0.14 mm/m after 1600 min, while ACC-I presented -0.1 mm/m after 1600 min as shown in Fig. 5.11. Similar trend is presented by type II but with a greater absolute value of shrinkage. RET-II presented the greatest shrinkage development with -0.4 mm/m after 1250 min, followed by ACC-II with -0.21 mm/m at approximately 280 min and lastly by REF with -0.06 mm/m at around 260 min, see Fig. 5.11. The obtained results show that the addition of accelerator and retarder increased the shrinkage evolution for type II. Additionally, ACC-II illustrated a steep shrinkage evolution but with a smaller absolute value compared to RET-II. ACC II shows a shorter evolution of shrinkage with lower shrinkage values compared to RET II, possibly caused by the S-C-H action. The C-S-H nanoparticles result in the nucleation of hydration products in the pore space between the cement particles in addition to the hydration process at the particle surface to accelerate the early hydration. RET II leads to a longer plastic state, and a longer evolution of plastic shrinkage due to the extended induction period. Thereafter, the settlement values of RET II is higher compared to REF and ACC II and this is possibly attributed to the formation of a protective layer at the particle surface to attain sharp retardation of all hydration reactions.

Fig. 5.11 Shrinkage evolution for REF, ACC and RET.

Besides the effect of the hydration process on the AE activity, the settlement and shrinkage evolution affect the cumulative hits as aforementioned in Chapter 3. This effect is demonstrated in the

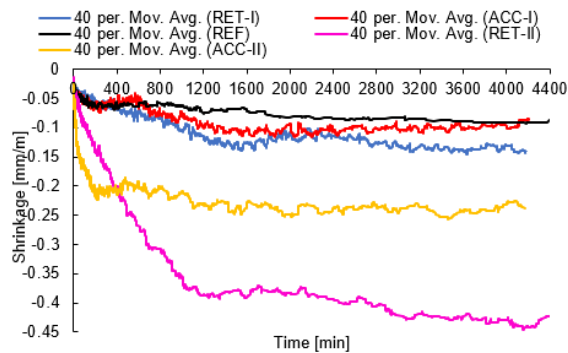cumulative hits curve (Fig. 5.12). As for the cumulative hits curve, there are differences in the evolution of ACC, RET and REF. The retarding and accelerating ability increased the cumulative hits for both types, indicating the impact of hydration on AE hits. Particularly in the case of ACC, a steep increase of cumulative hits is observed.
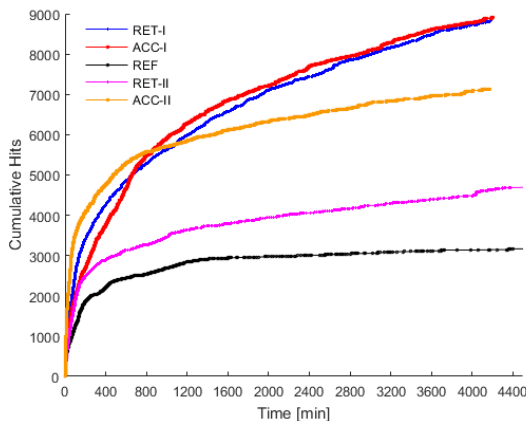
Fig. 5.12 Cumulative hits evolution for REF, ACC and RET.

ACC-I and RET-I demonstrated a sharp curve of cumulative hits evolution with 8785 hits and 8722 hits respectively after 4000 min, as shown in Fig. 5.12. The cumulative hits for ACC-II is 7098 hits followed by RET-II with 4500 hits and lastly by REF with 3130 hits after 4000 min in Fig. 5.12. It can be seen that the addition of accelerator or retarder to concrete affects the mechanisms of the hydration process (Khan and Muhammad 2004). This addition of admixtures leads to additional reactions and processes apart from the regular hydration occurring in concrete, as aforementioned. Thereafter, the formation of concrete microstructure is influenced resulting in additional release of energy as well as additional AE hits. The additional hydration process by ACC generated by the C-S-H nanoparticles during the very early hydration causes an increased AE activity due to the nucleation and growth of early hydration products at the particle surface and in the pore space which affects the microstructure of the paste. The retarding action of the retarder also increased the AE signals due to the formation of sparingly soluble surface film which severely delays the hydration process at the early age. The accelerated and retarded effect of admixtures is also

148

presented in the capillary pressure development, as will be discussed in the following section.

5.3.4 Impact of admixtures on capillary pressure development

The chemical admixtures have a primary impact on hydration related kinetics as well as a secondary effect on the capillary pressure development. The capillary pressure development is observed to be very similar to the temperature evolution, in addition of the chemical admixtures. The set of retarding ability leads to an extended delay of capillary pressure development with a higher absolute value compared to the reference and accelerator effect.
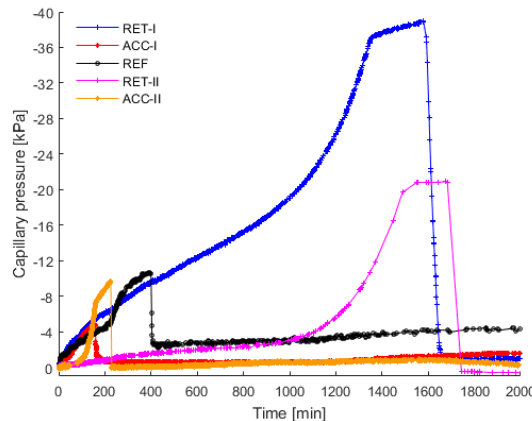
Fig. 5.13 The capillary pressure evolution as a function of time for reference, accelerator and retarder.

The capillary pressure evolution of RET-I is extended for a long period of time with a peak of -39 kPa after 1580 min, whereas accelerator showed an immediate increase with a peak of -4.8 kPa after 160 min, see Fig. 5.13. REF illustrated a behaviour in between the other two extreme cases with a peak of -11 kPa after 400 min. A similar trend is observed for type II, ACC-II demonstrated a capillary pressure peak of -10 kPa after 225 min, followed by REF with -11 kPa after 400 min and lastly by RET-II with -21 kPa after 1680 min as presented in Fig. 5.13. Thereafter, ACC decreases the setting time and leads to an accelerated capillary pressure

build up, while retarder delays the setting time that is extending the period of capillary pressure development. Possibly the accelerated hydration process by the C-S-H seed of ACC at very early age resulted in the formation of water menisci that led to a rapid capillary pressure build up in a short period of time compared to REF and RET.

It is interesting to discuss the behaviour of the absolute energy of AE activity coupled with the capillary pressure as illustrated in Fig. 5.14. In this Fig. the AE of each bar corresponds to the average absolute energy of 24 min. Both types of ACC in Fig. 5.14 (a-b) and RET in Fig. 5.14(c-d) are illustrating increased average absolute energy in the order of 10^4 or even 10^5 aJ compared to REF (10^3 aJ as seen in Fig. 5.14(e)). The addition of accelerator or retarder causes additional reactions as aforementioned apart from the regular hydration occuring in concrete. The addition of the chemical admixture contributes to an increased absolute energy. Beside the impact of hydration, the initial average absolute energy activity is also related to the settlement progression, when concrete is in plastic state, as shown in Fig. 3.8.

Further, ACC and RET present several peaks of the absolute energy with higher values compared to REF. The pore strucure is not uniformly distributed at concrete surface that may lead to local air penetration at different time stages. The several fluctuations of the absolute energy indicated the release of energy due to different processes occuring in concrete. A quite consistent detail concerns the capillary pressure breaking-through when all concrete mixes present an increased average absolute energy.
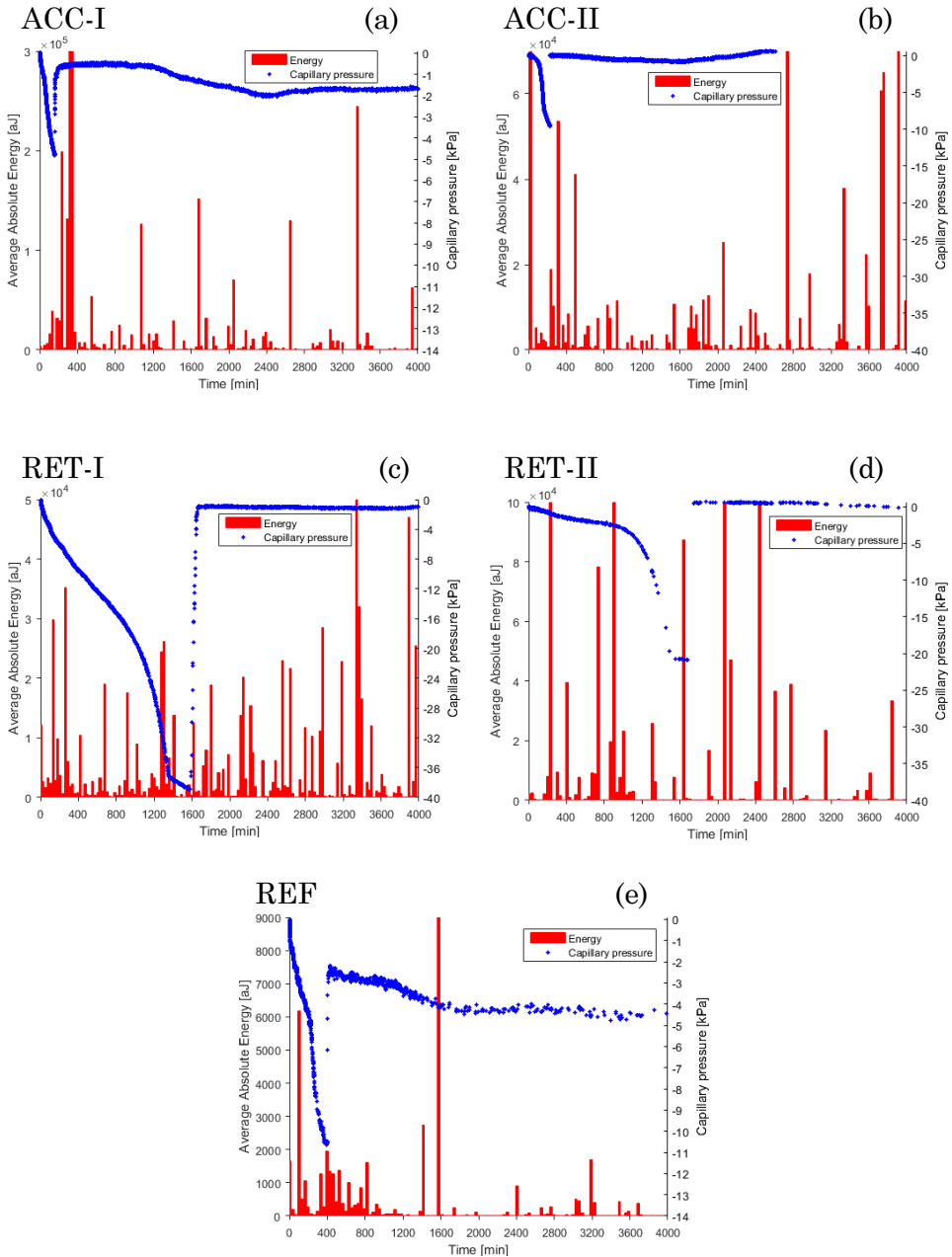
Fig. 5.14 Average absolute energy and capillary pressure development (a-b) ACC both types; (c-d) RET both types; (e) REF.

5.3.5 Impact of admixtures on rise time, amplitude and energy evolution

The results of average frequency, absolute energy, rise time and amplitude are presented in the form of "moving average" (sliding window of 200 successive points), as shown in Fig. 5.15, Fig. 5.16, Fig. 5.17 and Fig. 5.18). ACC illustrated higher initial values of average frequency compared to REF and RET. Particularly, in the fresh state of concrete, the average frequency of ACC-I started at 125 kHz, whereas RET-I presented approximately 100 kHz and lastly REF illustrated approximately 95 kHz in Fig. 5.15 (b). Similar pattern has been observed for type II. The average frequency content of ACC-II started at an average of 117 kHz, while RET-II started at an average frequency at approximately 102 kHz, see Fig. 5.15(b). For all concrete mixes, the fresh state illustrates a higher average frequency compared to the hardened state. However, in the hardened state, REF illustrated higher values of average frequency content compared to ACC and RET.

The moving average of absolute energy is plotted in logarithmic scale, as shown in Fig. 5.16. REF illustrates an absolute energy of around 1000 aJ, followed by RET-I with approximately 5000 aJ and lastly by ACC-I with around 10000 aJ after 2000 min Fig. 5.16. Similar pattern has been observed for admixture type II, ACC-II illustrated 2700 aJ while RET-II presented 13800 aJ after 2000 min Fig. 5.16. The obtained results shows the additional activities by the admixtures resulting in higher average absolute energy like for ACC both types and for RET both types.

(a)

(b)
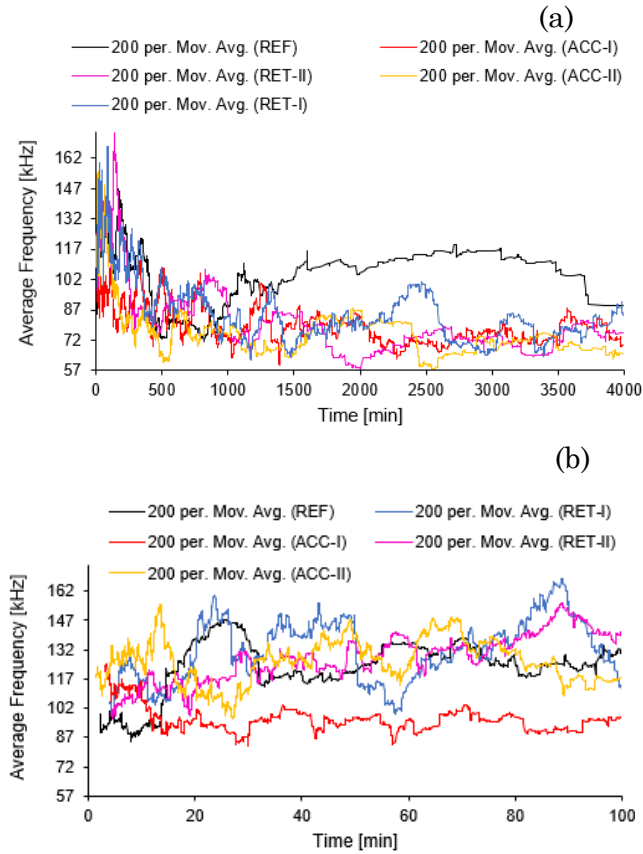
Fig. 5.15 Average frequency evolution for REF, RET and ACC type I and II (a) up to 4000 min; (b) up to 100 min.

Furthermore, the AE parameters of rise time and amplitude evolution are presented in Fig. 5.17 and Fig. 5.18. REF illustrates a rise time progression between 400 min and 1000 min (Fig. 5.17), while the amplitude progresses between 100 min and 1400 min (Fig. 5.18). The rise time and amplitude curve of REF follow the same trend as the temperature curve.
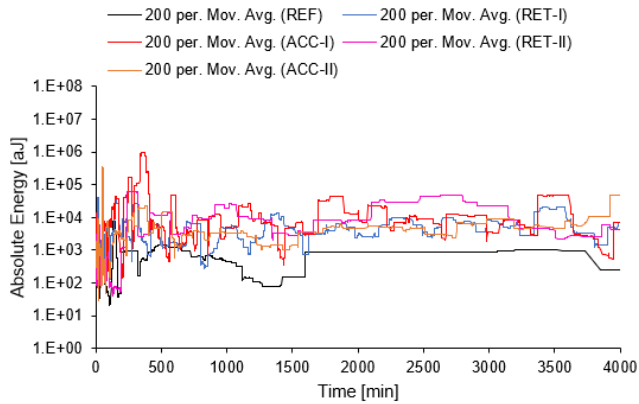
Fig. 5.16 Absolute energy evolution of REF, RET and ACC type I and II.

The rise time and amplitude of ACC and RET exhibited higher maximum values and higher fluctuations for the whole duration of the test compared to REF. Initially, ACC and RET present high fluctuations particularly when concrete is in plastic state. The rise time and amplitude lines are increasing with time during the hardening process. ACC-II presents a rise time peak at around 500 min (Fig. 5.17) where the temperature of ACC-II also presents its peak, see Fig. 5.3.
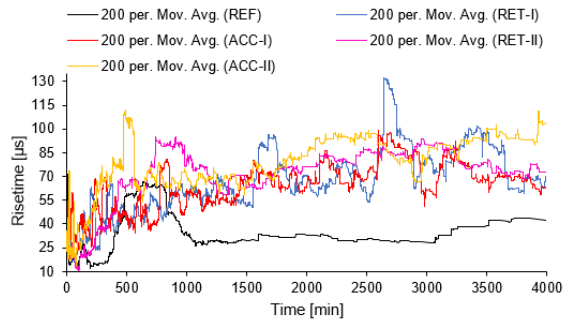
Fig. 5.17 Rise time evolution for REF, RET and ACC type I and II.

From the AE point of view, the rise time and amplitude evolution of REF shows similar trends as the temperature evolution. REF presents an increase of rise time and amplitude around the setting time, see Fig. 5.8.
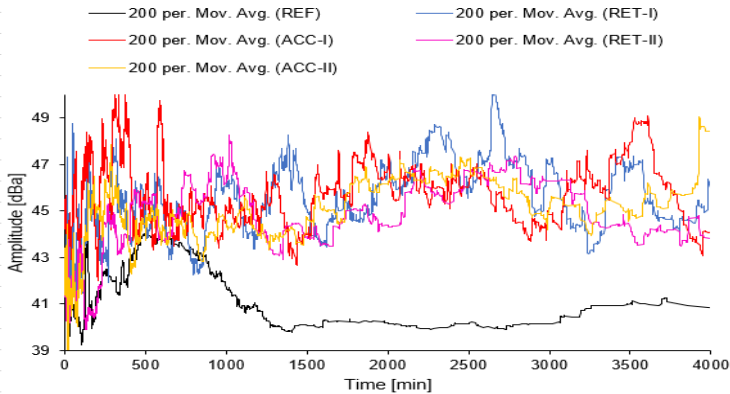
Fig. 5.18 Amplitude evolution for REF, ACC and RET type I and II.

5.3.6 Acoustic emission waveforms

Fig. 5.19 illustrates AE waveforms of the hardening process at different phases of REF. The discrete stages are the settlement, capillary pressure peak, temperature peak and hardened state. Each stage has been discussed before in this section. For each stage two representative waveforms are selected. The representative waveforms are based on the moving average values of the average frequency and the amplitude at discrete curing stages.

The waveforms during the settlement demonstrate small amplitude with a large AF and shorter duration, while the concrete is in fresh state in Fig. 5.19(a). This may be attributed to the high damping but also in the nature of the sources which comprises by micro-particle movement during settlement, as already discussed.

Settlement (a)
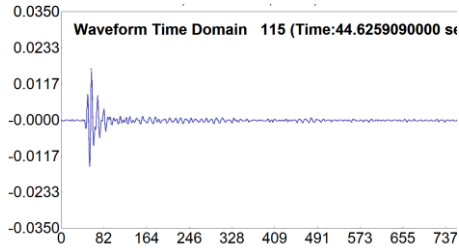
Amplitude= 44 dB; AF= 150 kHz
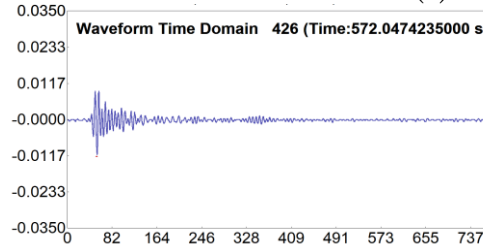
Amplitude= 40dB; AF= 105 kHz

Capillary pressure peak (b)
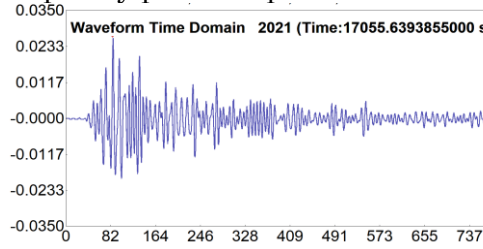
Amplitude= 48 dB; AF= 52 kHz
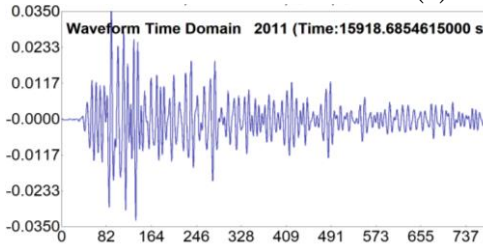
Amplitude= 51 dB; AF= 65 kHz

Temperature peak (c)
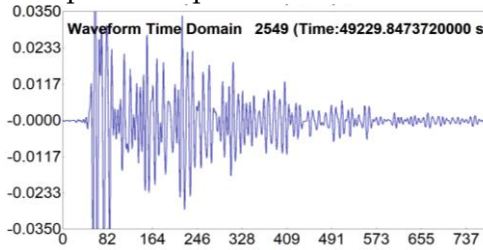
Amplitude= 59 dB; AF= 81 kHz
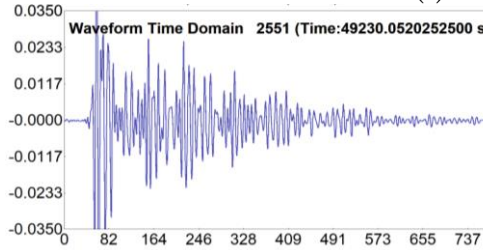
Amplitude= 58 dB; AF= 88 kHz

Hardened state (d)
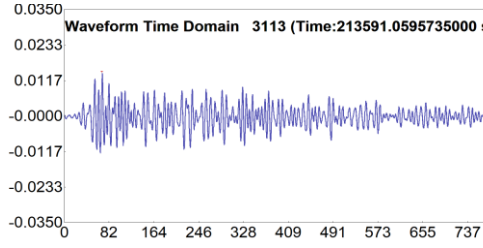
Amplitude= 42 dB; AF= 66 kHz
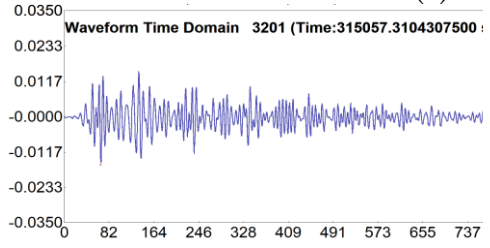
Amplitude= 43 dB; AF= 60 kHz

Fig. 5.19 Voltage versus time (µs) of AE waveforms evolution during (a) settlement; (b) capillary pressure peak; (c) temperature peak; (d) hardened state.

During the capillary pressure progression, the hardening is increasing while the attenuation is decreasing leading to a larger amplitude of the waveforms between 48 dB and 51 dB, see Fig. 5.19(b).

The largest amplitude of 59 dB is recorded during the temperature peak caused due to the high rate of hydration. The increased waveform amplitude should be connected to the formation of hydrates which is mentioned as a strong source of AE in the hydration phase (Fig. 5.19(c)).

In the hardened state, the duration of the waveforms is longer but with smaller amplitude of 42 dB and AF of 66 kHz in average, as shown in Fig. 5.19(d). It would be reasonable to link these waveforms to shrinkage cracking as at that time, the rate of hydration reaction has slowed down. Obviously, the exact origin of each signal cannot be verified; however, it is important that the trends shift throughout the hydration time, which indicates that different sources are active always combined with the propagation properties of the hardening medium.

Moreover, in Fig. 5.20 and Fig. 5. 21 the average rise time during the first 60 min of curing is related to the initial compressive strength development after 72 h of curing. The results obtained from 6 different specimens of ACC showed a correlation between the rise time and the compressive strength. Specifically, higher average RT values within 60 min after mixing, are accompanied by higher compressive strengths. As seen in Fig. 5. 21, rise time lower than 25 μs during the first hour after mixing results in compressive strength lower than 35 N/mm², while higher rise time is connected to higher compressive strength at 72 h. This way, although the correlation is not monotonic the measurement of the rise time during the first 60 min could provide information relating the hardened state of concrete. Therefore, further research and standardization are proposed. More tests are required to provide detailed information on the long-term concrete performance.
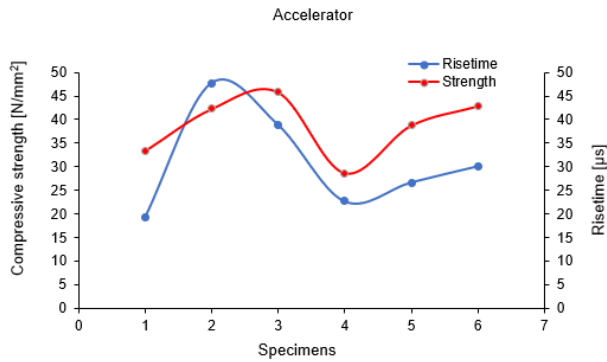
Fig. 5.20 Correlation between rise time and compressive strength.
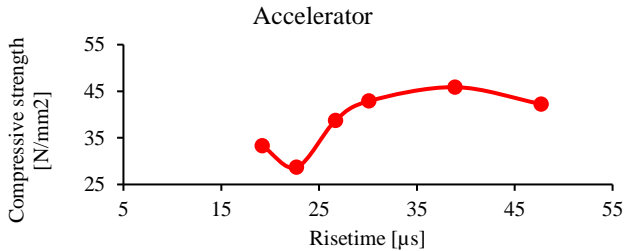
Fig. 5. 21 Compressive strength versus rise time for different specimens.

5.4 Conclusion

This chapter focuses on how the hydration of concrete with admixtures influences the received acoustic activity. Therefore, the early-age behaviour of AE allows monitoring the effect of admixtures in fresh concrete before these differences influence the mechanical properties. Following conclusions have been found:

- The absolute energy and cumulative hits of RET and ACC were increased compared to REF. The addition of the chemical admixture contributes to an increased AE activity due to additional energy release in concrete.
- AF evolution was decreased by ACC and RET compared to REF.

- Correlation between compressive strength and rise time evolution was found. Specimens with higher initial rise time during the first hour, exhibited in principal higher compressive strength after 3 days.
- During the setting time, when the fluid-solid transition appears in concrete the rate of rise time and amplitude signals increases.
- The addition of retarder and accelerator to concrete influenced the setting time leading to a rapid setting (false setting) after casting that was observed by the Vicat test and UPV measurement.

Chapter 6: **Acoustic emission in cement-based materials at different scale**

In this chapter, the AE signals of multiscale cementitious materials are analyzed from the hydration state till 66 h. Three different scales of cement based-materials, namely, cement paste, cement mortar and concrete are studied. The AE signals at different hydration stages are analyzed, and correlations associated with hydration process are emphasized.

6.1 Introduction

The objective of this chapter is to study the AE activity in cement paste, cement mortar and concrete. Concrete is considered to have a range of scale sizes, from the atomic scale (10^{-10}m), which is defined by the crystalline particles of the hydrates, to the macroscopic scale (cm). The heterogenous material of concrete with the constituent of different properties (mortar, aggregate and interface material) has been studied by different researchers for the early hydration period, without however, considering acoustic effects. Xiao et al. investigated the hydration process of paste, mortar and concrete by means of electrical resistivity during the hardening process. The addition of fine aggregate (sand) led to higher specific surface area as well as tortuosity that caused a higher electrical resistivity. This effect led to a faster rate of densification of mortar sample compared to paste and concrete (Xiao and Wei 2017). Vilane et al. studied the effect of coarse aggregate size on concrete slump and compressive strength. The workability of concrete (slump) increased with increasing the size of aggregate. The mean compressive strength also increased with increasing aggregate size (Vilane and Sabelo 2016).

On the other hand, concerning the propagation of elastic waves, it is clear that the scale of the material, influences the conditions. Besides the effect of the different aggregate sizes on the elastic waves, the hydration process and corresponding microstructure formation also affects the AE activity. At different hydration stages different cement microstructures evolve, and different chemical reactions occur in the composition. There might be an overlapping of some of the different processes (settlement, capillary pressure increase, thermal evolution, shrinkage evolution) caused by the cement hydration at discrete stages. Thirumalaiselvi et al. studied AE on different cementitious materials and their impact on AE parameters (Thirumalaiselvi and Sasmal 2019). Sherzer et al. investigated a multiscale analysis to obtain fracture, shear and elastic concrete mechanical parameters (Sherzer et al. 2017). In another approach, Pitangueira et al. studied concrete heterogeneity and particle size effect by finite element model (Pitangueira and Silva 2005). The heterogenous material of concrete has been examined by a meso-scale model to obtain mechanical parameters (Häfner et al. 2006; Roubin 2013).

The evolution of the elastic wave alters from the fresh state towards the hardened state. Several researchers investigated the elastic wave propagation and attenuation in cement-based materials and their impact on aggregate size. In literature, sand and fine aggregates were shown to act as carriers of wave energy without crucially affecting the scattering attenuation. Kim et al. studied the elastic waves attenuation and dispersion in multi-phase materials (cement, mortar and concrete) by ultrasonic technique. The attenuation of elastic waves was attributed to the scattering of the elastic waves. The sequence of dispersion was cement, mortar and concrete; however, that for attenuation was mortar, cement and concrete in increasing order (Kim et al. 1991). Gaydecki et al. determined that concrete specimens demonstrated less attenuation than the paste. This is attributed to the larger homogenous structure which facilitates the propagation of the frequency (Gaydecki et al. 1992). Jacobs et al. demonstrated experimentally by laser ultrasonic technique that absorption from the aggregate is the main attenuation mechanism in cement-based materials (Jacobs and Owino 2000). In another approach, Aggelis et al. investigated the impact of aggregate size on the wave attenuation of cement-based materials by measuring different aggregate to cement ratio. Mortar with higher aggregate to cement ratio presented higher attenuation with respect to frequency by a w/c of 0.5. One explanation could be related to scattering. Another reason could be the loss of adsorption in the interfacial zone which is between the aggregate and the mix (Philippidis and Aggelis 2005).

In this chapter, cementitious media with different scales are tested, namely paste, mortar and concrete aiming at examining the influence of the presence as well as the different size of the aggregates in the AE behaviour always in relation to mechanical and physical measurements like volume deformation and heat of hydration.

6.2 Materials and methods

Cube specimens of the dimension (150 mm x 150 mm x 150 mm) were prepared for each cementitious mixture. Portland cement CEM I 52.5 N was applied in all the mixtures to prepare the specimens. The composition of each mix is presented in Table 4.1, see Chapter 4. To

ensure the repeatability, more than 10 specimens were cast for each mixture (cement paste, cement mortar and concrete) and the representative curves are presented in this chapter. The complicated setup including several measuring methods did not allow the successful monitoring of all the specimens with all techniques. The presented specimens were successfully monitored with all the different techniques. AE technique was continuously monitoring the cement mixture till 66 h. Beside the AE monitoring, an integrated setup of different techniques (DIC, LVDT, pressure sensor, thermocouple) was simultaneously monitoring the cement system, as already discussed in Section 4. This mixture was cast in a metallic mould and the installation of the sensors required approximately 15–20 min, after which the recording started. The test was conducted in a temperature-controlled laboratory room at 20 ± 1 °C so that uniform measurement can be performed on all the mixtures during the hydration. These specimens are prepared under the same condition as performed in Chapter 4.

6.3 Results

6.3.1 Cumulative hits and settlement evolution

Experimental results obtained on cement systems at different scales (cement paste, cement mortar and concrete) are studied and discussed. These experimental observations are not always straightforward and easy to interpret. Mechanical measurements are easier to understand (e.g. paste has higher settlement and shrinkage etc.). Having these as benchmark (e.g. higher AE activity due to settlement evolution, higher average absolute energy by larger particle size), as the first effort in literature to correlate these different measurements.

From the observations made by the experimental measurements, cement paste illustrated the largest settlement with -10.4 mm/m after 125 min, followed by mortar with -4.6 mm/m after 140 min and lastly by concrete with -1 mm/m after 100 min, see Fig. 6.1. The settlement curve of cement paste presents a steep increase compared to mortar and concrete. The settlement evolution is therefore, affected by the amount of aggregate as well as the particle size. Concrete with the largest particle size and

highest total amount of aggregates, presented the smallest settlement, as the stiff aggregates limit the particles' mobility. Thereafter, the gravitational forces of coarse aggregates are larger comparing to the interparticle forces. In this way, the particles rest on each other and remain almost unmoved. Further, the settlement evolution might be influenced by the fresh density of the material. Cement paste with the lowest fresh density presented the largest settlement, while concrete with the largest density illustrated the smallest settlement progression.
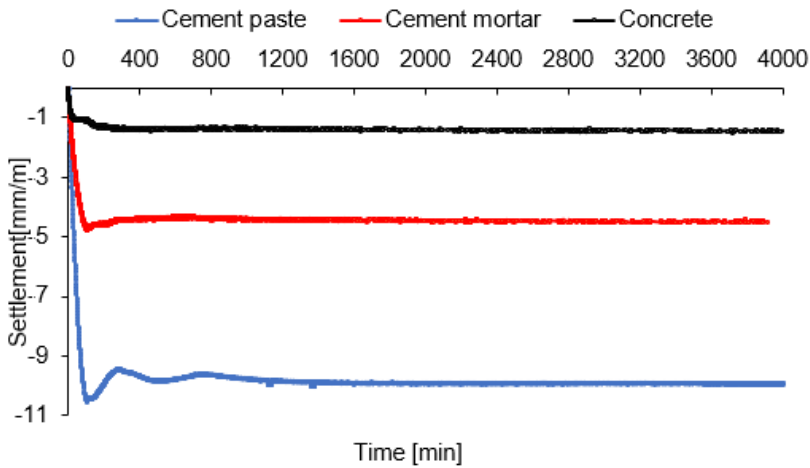
Fig. 6.1 Settlement evolution in cementitious materials.

The same pattern is observed for the cumulative hit evolution with the largest activity of 5780 for cement paste after 870 min. The curve of cement paste is followed by mortar with 3087 hits and lastly by concrete with 2580 hits after 870 min, as shown in Fig. 6.2. The experimental measurements confirmed, that the cumulative hits of all three mixes are accompanied by a rapid increase of settlement during the first few hours after mixing. As shown previously, it is once again observed that the AE at early ages is strongly connected to the amount of settlement, with the specimen exhibiting the highest settlement emitting also the highest number of acoustic signals at the first hours after mixing. However, it can be seen that after approximately 700 min, the AE slope of the mortar and concrete is higher than paste, indicating later hydration or possible shrinkage cracking due to the aggregates constrain.
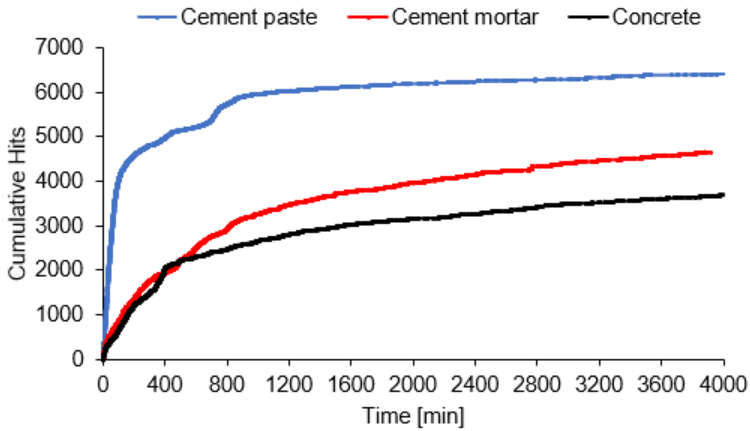
Fig. 6.2 Cumulative hits development for 66 h.

6.3.2 Absolute energy and capillary pressure development

Fig. 6.3 illustrates the capillary pressure development versus time. Firstly, concrete illustrates a capillary pressure increase in the pore system after 100 min, and then followed by paste after 130 min and lastly by mortar after 150 min. The capillary pressure increase depends mainly on the pore structure at the material surface and the rate of water loss due to evaporation. The continuous evaporation of the bleed water at the surface led to the formation of menisci between the solid particles. Consequently, the negative capillary pressure increases till a certain value and breaks-through since the water menisci at the surface are not able to bridge the spaces between the solid particles. The largest capillary pressure peak is demonstrated by paste with -16.6 kPa at 304 min, while mortar presented the lowest capillary pressure peak with -8 kPa at 243 min. Concrete capillary pressure peak was in between the paste and mortar with -12.8 kPa at 243 min. The capillary pressure growth of concrete starts earlier due to different pore structure and possibly additional pore water loss caused by cement hydration (Slowik et al. 2008). After the peak, the pores at the material surface are no longer fully filled with water. At this point, air might penetrate into the pore system, starting from the largest pores, and the risk of crack formation achieves its maximum (Slowik et al. 2009).
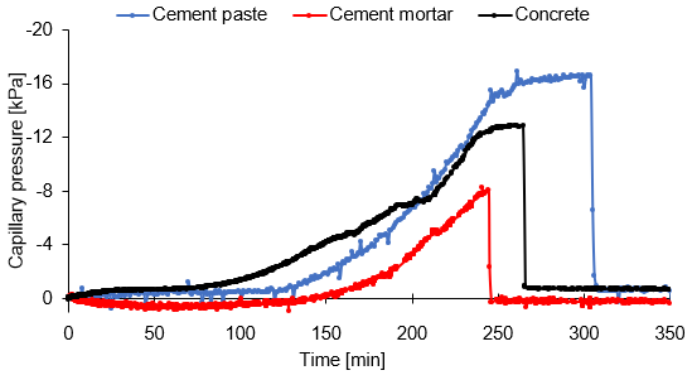
Fig. 6.3 Capillary pressure development.

During the capillary pressure drop, increased average absolute energy is recorded. The air entry into the system occurs locally due to the non-uniform pore structure distribution at the surface. In Fig. 6.4 the average absolute energy of each bar corresponds to the average absolute energy of 24 min. The smallest average absolute energy around the capillary pressure break-through was observed by cement paste with 2000 aJ (Fig. 6.4(a)), followed by mortar with 3000 aJ (Fig. 6.4(b)) and finally by concrete with 6500 aJ, see Fig. 6.4(c).

Over the hydration process, several absolute energy fluctuations are registered. Concrete illustrated the highest number of fluctuations, while paste presented the lowest energy fluctuations. For paste and concrete, the average absolute energy increases around the capillary pressure drop compared to the initial absolute energy. Thereafter, the attenuation effect is decreasing as the material stiffens. Furthermore, the presence of sand in mortar mixture led to a higher initial absolute energy from the beginning of the test.
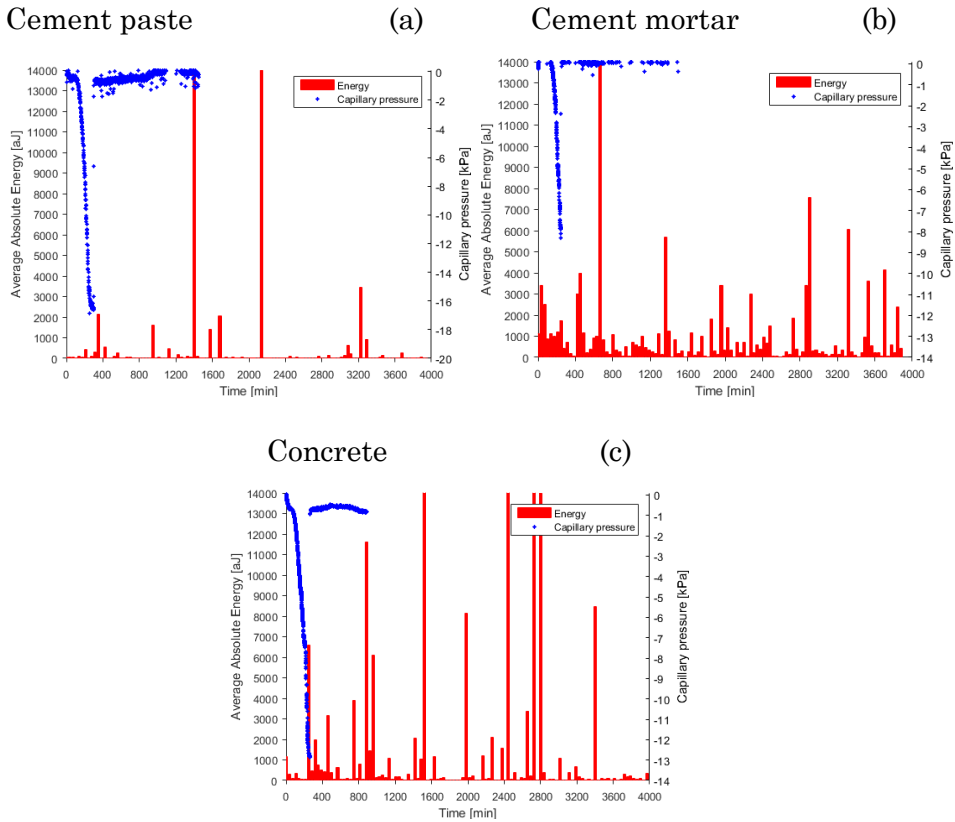
Fig. 6.4 Absolute energy and capillary pressure evolution (a) cement paste; (b) cement mortar; (c) concrete.

In Fig. 6.5 the cumulative absolute energy curve of concrete illustrates several large increases in form of steps at 1500 min, 2400 min and 2670 min, which might be caused by internal damage due to self-desiccation or shrinkage crack evolution. This step-like increase is also observed in mortar and paste but to a smaller extent. Concrete containing the largest particle size (coarse aggregate) illustrated higher cumulative absolute energy compared to mortar and paste starting from approximately 1400 min. Following the rise time and amplitude evolution for all mixtures is presented.
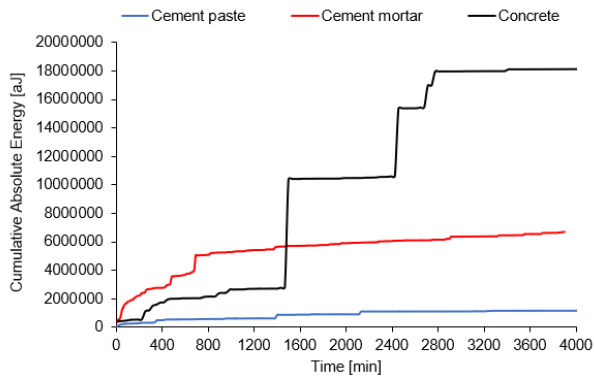
Fig. 6.5 Cumulative absolute energy during the hardening process.

6.3.3 Rise time and amplitude evolution

Cement paste illustrates an increased initial temperature compared to mortar and concrete. This could be related to the high content of cement in cement paste. This effect led also to a higher temperature peak due to the generated thermal energy. Cement paste demonstrates a steep temperature evolution between 350 min and 1300 min with a temperature peak of 38 °C after 800 min, as illustrated in Fig. 6.6.

Similar observation was found for rise time with an increase between 450 min and 700 min and a rise time peak of 55 µs at 550 min, see Fig. 6.7. Initially, rise time presents high fluctuations particularly in plastic state. The moving average of AE parameters (sliding window of 200 successive points) is plotted in Fig. 6.7 (rise time); Fig. 6.8 (amplitude) and Fig. 6.12 (average frequency).

Mortar presents a smaller temperature peak with 32 °C after 670 min compared to paste, and a temperature progression between 150 min and 1100 min but the progression is not as intensive as paste. Cement hydration undergoes an exothermic reaction which releases energy and thereafter causes shrinkage and crack evolution. In cement mortar, sand is included that decreases the heat of hydration and corresponding temperature development. Also, rise time presented an increase between 130 min and 800 min but with fluctuations and a peak of 101 µs at 150 min, as illustrated in Fig. 6.7.
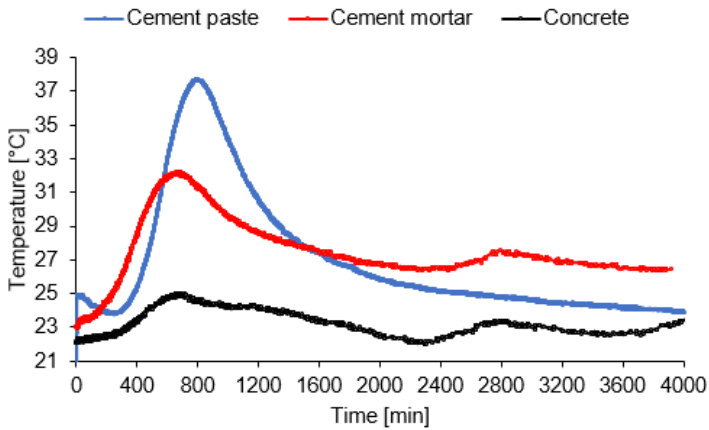
Fig. 6.6 Temperature development during the hydration process.

The temperature development of concrete occurs between 300 min and 1200 min with a peak of 25 °C at 670 min (Fig. 6.6). The rise time increases between 250 min and 700 min with a peak of 100 µs at 330 min, see Fig. 6.7. The development of RT seems to precede the one of temperature in all specimens. However, it is not straightforward to interpret the source of rise time increase. The rise time of concrete, mortar and paste increase with time possibly due to the hardening process. The obtained results exhibit, that cement mortar presented the largest initial rise time and amplitude as it dried. This behaviour can be explained by the faster densification of mortar due to higher specific surface area by the addition of sand according to Xiao et al. (Xiao and Wei 2017).
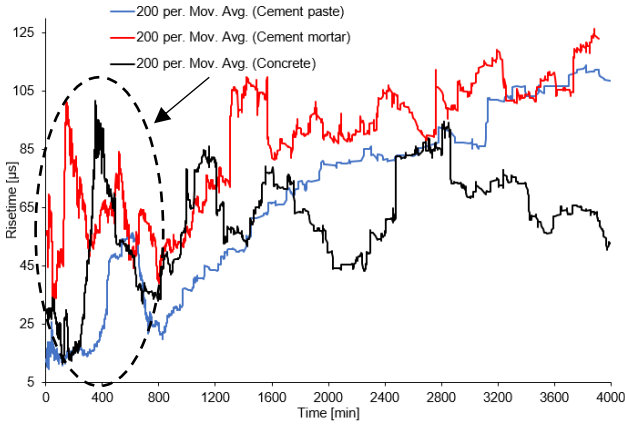
Fig. 6.7 Rise time evolution during the first 66 h of curing.

The amplitude evolution of concrete, mortar and paste illustrates several large fluctuations over the first 500 min of the hydration period (Fig. 6.8). Later, smaller fluctuations are observed while the material gains strength. Mortar illustrated the highest amplitude evolution over the hydration period, followed by concrete and lastly by paste. The largest amplitude peak is demonstrated by mortar with 46 dB after 500 min, while concrete presented a peak of 44 dB after 350 min and paste demonstrated a peak of 42 dB at 400 min. Mortar demonstrates the highest amplitude curve that appears to be connected to the inclusion of sand. A global trend is that cement paste exhibits the lowest level of amplitude during the whole monitoring period, although it showed the highest cumulative activity. This means that in paste the activity occurs in more, but smaller events compared to the other mixes. The fact that mortar presents the highest amplitude curve seems to be connected to the addition of sand, which certainly reinforces the material in terms of stiffness, but at the same time it does not impose serious scattering attenuation to the stress waves due to small size. Indeed, considering a propagation velocity of 2000 m/s and a frequency of 100 kHz, which is typical of recorded signals, indicative wavelengths can be calculated to approximately 20 mm much larger than the sand grain size. In literature sand and small aggregates were shown to act as carriers of wave energy

without crucially affecting the scattering attenuation (Gaydecki et al. 1992; Jacobs and Owino 2000; Philippidis and Aggelis 2005).
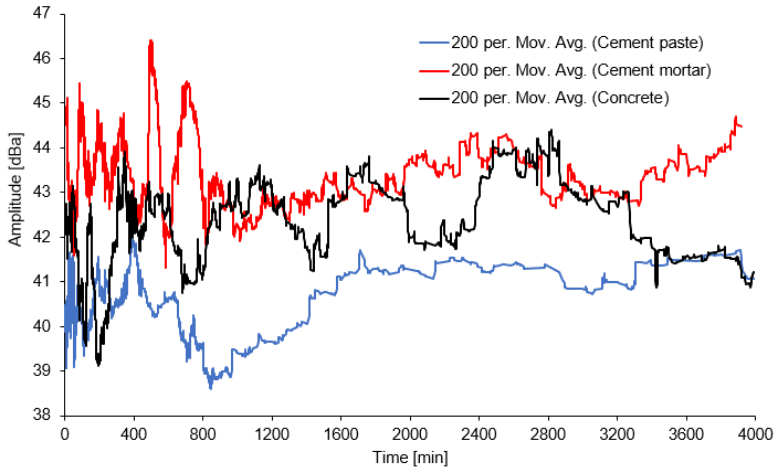
Fig. 6.8 Amplitude progression during hydration process.

6.3.4 Average frequency and shrinkage development

The shrinkage evolution of the paste presents the highest expansion period between 500 min and 800 min compared to mortar and concrete, with the highest temperature peak of 38 °C. Further, the shrinkage evolution presented the highest value with 0.26 mm/m after 4000 min, in Fig. 6.9. The curves of mortar and concrete presents similar trend with an expansion period due to the thermal effect. Mortar presented temperature peak of 32 °C and corresponding lower shrinkage of 0.2 mm/m after 4000 min. Concrete shrinkage evolution began immediately to increase and presents a small expansion period due to the lower temperature peak of 25 °C. In addition, concrete demonstrated the smallest shrinkage evolution with 0.16 mm/m after 4000 min. It is shown that the existence of stiff aggregates (coarse aggregate) which do not deform, reduce the shrinkage and settlement evolution.
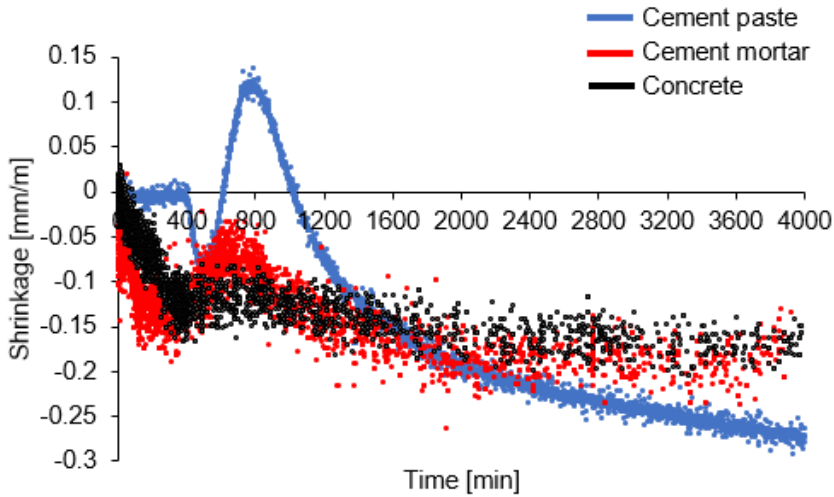
Fig. 6.9 Shrinkage evolution during the first 66 h.

The plastic shrinkage is found to be greater, for higher cement content due to the loss of water from the paste. The grading and the max size of aggregate influences the shrinkage evolution (Liu and Hansen 2016). Thus, the application of larger aggregate results in the reduction in shrinkage. The reduction in shrinkage by the increase of aggregate size and aggregate content is attributed to the uniform shrinkage and a decrease in the internal cracking of the paste. The influence of paste volume is relatively strong on the concrete drying shrinkage (Bissonnette et al. 1999; Brooks 2015; Leemann et al. 2011; Piasta and Zarzycki 2017; Rozière et al. 2007).

The shrinkage evolution is considerably restrained by the increase in aggregate volume. Therefore, the shrinkage is affected by the volumetric proportions of aggregate as well as cement paste. Aggregates with cubic shape and rough texture of the surface and with higher modulus of elasticity offer higher restraint to shrinkage. Furthermore, the quality of cement paste has an effect on the shrinkage growth, which depends on the water cement ratio. Higher w/c ratio results in greater shrinkage as shown in Fig. 6.10. The relationship between aggregate volume, w/c ratio and shrinkage of concrete after 7 days is presented in Fig. 6.10. the estimated shrinkage for concrete with a w/c ratio of 0.5 and a 77% volume

content of aggregate is 0.35 mm/m after 7 days according to (Brooks 2015). In the case of mortar, the shrinkage is estimated to be 0.8 mm/m, with a w/c ratio of 0.45 and a 65% volume content of aggregate after 7 days.
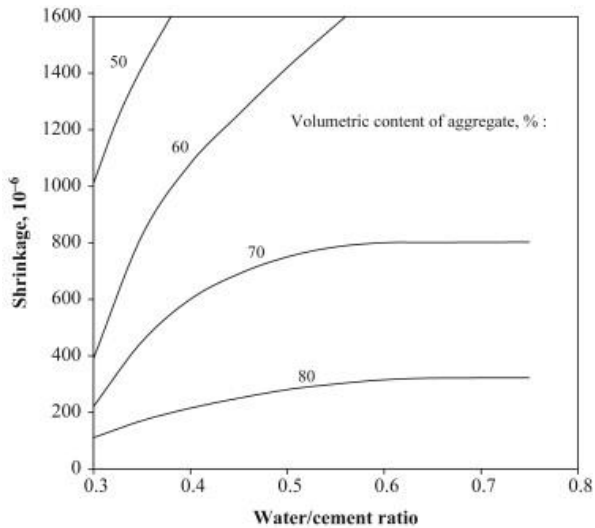
Fig. 6.10 The impact of w/c ratio and aggregate content on the evolution of concrete shrinkage (Brooks 2015).

Following, the temperature and shrinkage developments are presented to investigate their correlation (Fig. 6.11). It is clear to see, that the cement paste and mortar shrinkage curve follow the temperature curve. It seems that the temperature peak induces a reverse temporary peak to the shrinkage curve due to thermal expansion of the material. After the temperature peak, the shrinkage evolution starts to increase as the temperature drops in Fig. 6.11(a-b). However, concrete shrinkage curve increases immediately and stabilizes with 0.16 mm/m after approximately 400 min, while the temperature is still increasing, see Fig. 6.11(c). The temperature increase for mortar and concrete is due to the environmental temperature after 3000 min. The shrinkage evolution of concrete with a w/c of 0.5 and a 77% volume content of aggregate is estimated to be 0.35 mm/m after 7 days according to (Brooks 2015). In the case of mortar with a w/c of 0.45 and a 65% volume content of aggregate, the estimated shrinkage is 0.8 mm/m after 7 days.

174
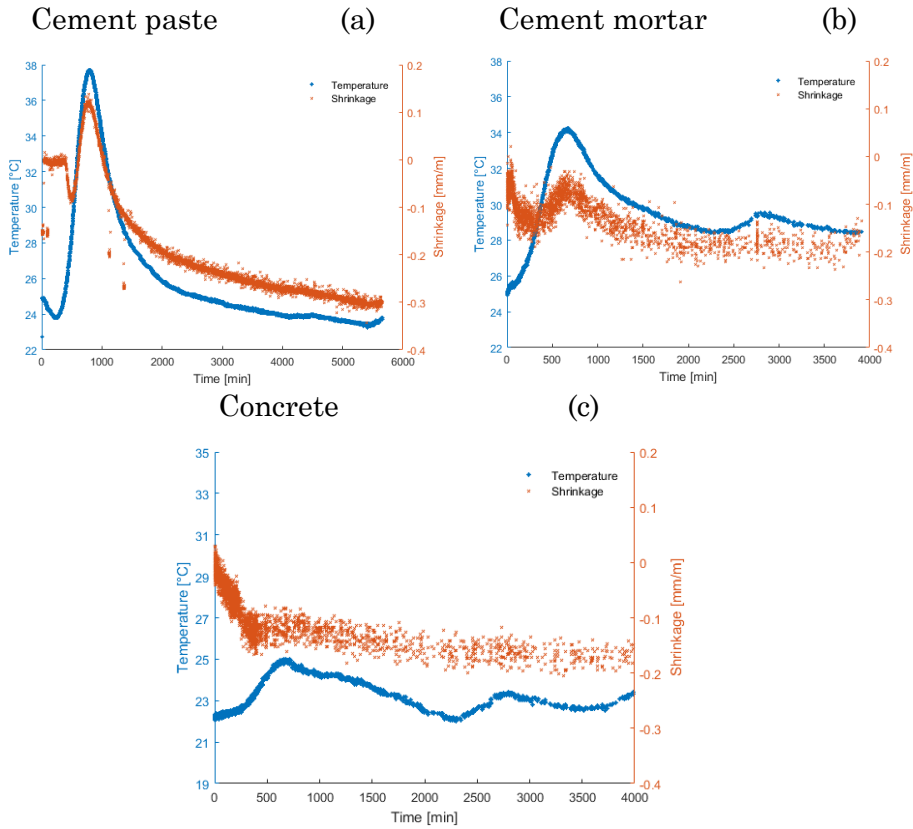
Fig. 6.11 Temperature and shrinkage evolution during different hydration stages (a) cement paste; (b) cement mortar; (c) concrete.

The average frequency progression presents large fluctuations initially, when the material is in plastic state. Furthermore, the plastic state illustrates higher average frequency compared to the hardened state. Cement paste presents the highest average frequency which is followed by concrete and lastly by mortar. During the intensive temperature evolution, cement paste illustrated a peak with 200 kHz after 700 min, mortar presented a peak with 120 kHz at 770 min while concrete demonstrated a peak with 115 kHz at 750 min, as illustrated in Fig. 6.12. It can be observed, that the average frequency presents higher value as the temperature increases. The maximum temperature increase is diminished with the increase in aggregate content. The addition of fine and coarse aggregates to the mixture reduces the average frequency

content as is the case for the total AE activity. This trend is the inverse of rise time that was presented earlier, confirming the global trend in AE that when signals are longer in time (rise time, duration, they exhibit lower frequency). The reasons should be sought in the combined action of the settlement mobility of small cement particles compared to larger sand and aggregate grains, as well as wave propagation effects (stiffening but at the same time higher scattering attenuation for sand and aggregates).
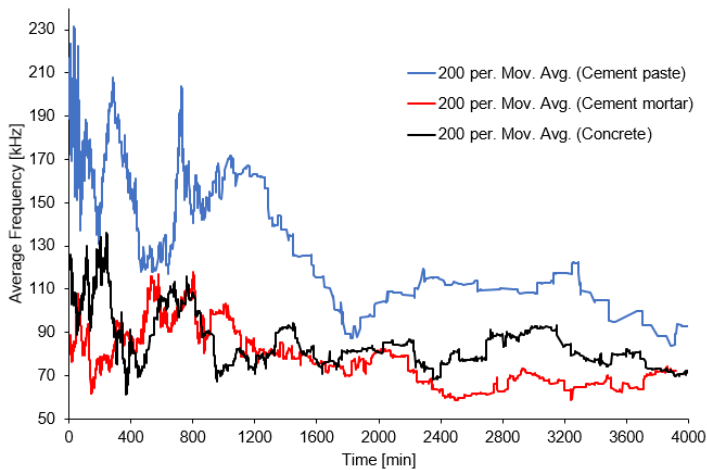
Fig. 6.12 Average frequency progression in cement-based materials.

6.4 Discussion

In the chapter, trends from typical specimens of several mixes are presented. This section contains data from five specimens of each mix (cement paste, cement mortar and concrete) to discuss the representativity of the results. Furthermore, the results are presented in the form of "moving average" trend line (sliding window of 200 successive points).
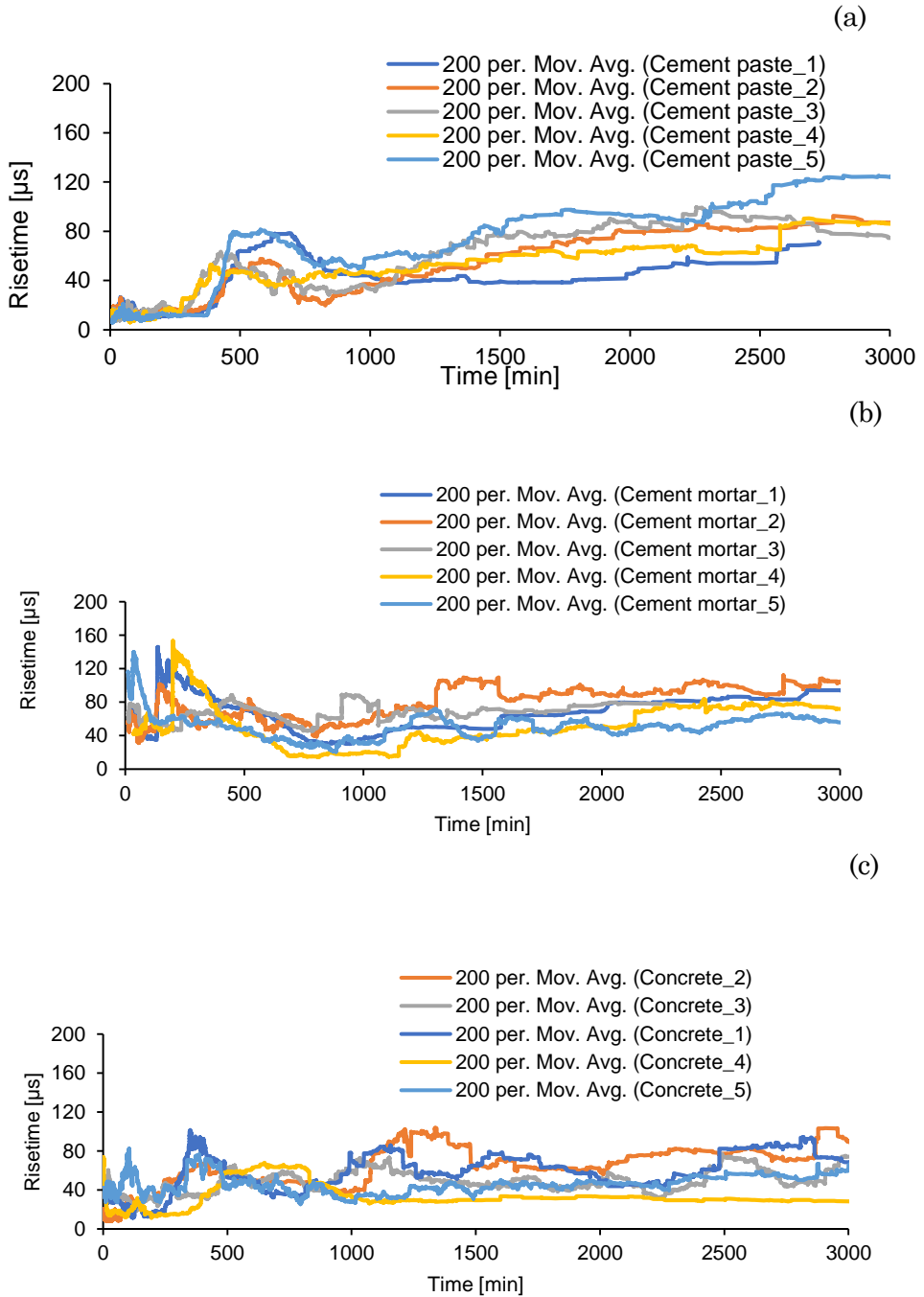
Fig. 6.13 Rise time evolution for (a) cement paste; (b) cement mortar and (c) concrete.

Interpretation is not always straightforward and comes mainly through the comparison between the behaviour of the specimens. However, specific trends can be distinguished. Specifically, the rise time of CP starts at lower value compared to mortar and concrete following the particle size, similarly to what was already shown in chapter 3 for cement paste and fly ash. In addition, due to the highest hydration of CP the rise time presents a local peak around 500 min which is not as strong in mortar and concrete.

Fig. 6.13 (a-c) shows the rise time evolution of the AE signals of 5 different specimens. Initially, the cement paste specimens exhibited the lowest values compared to cement mortar and concrete. It is notable that all cement pastes specimens exhibit a low start in their curve at the level of 20 µs, much lower than the cement mortar ones which lie at approximately 80 µs. This can be connected to the particle size difference, which plays an important role in the settlement period. After setting, the rise time illustrated a significant increase for all five cement paste specimens at around 350 min, see Fig. 6.13(a).Later, at around 900 min, the rise time curves of all cement pastes decrease, while cement mortar and concrete presented higher fluctuations, as revealed in Fig. 6.13(b-c). Furthermore, the CP specimens presented a much smoother rise time evolution in the first 400 min after mixing compared to mortar and concrete. At later stage, as the CP hardens the rise time curves increases, while cement mortar and concrete presented higher fluctuations without systematic increase.

In addition, the experimental results confirm that for the whole duration of the test, CP demonstrated lower values of amplitude as well as lower fluctuations, as shown in Fig. 6.14(a-c). The curves of cement paste demonstrated amplitude values below 44 dB, throughout the experiment, while the cement mortar presented higher peaks with more than 45 dB as presented in Fig. 6.14(a-b). The amplitude value of cement mortar specimens illustrated the highest fluctuations particularly in the fresh state. CP and mortar highlight the extreme cases of amplitude values, but the average amplitude of concrete stands in between.
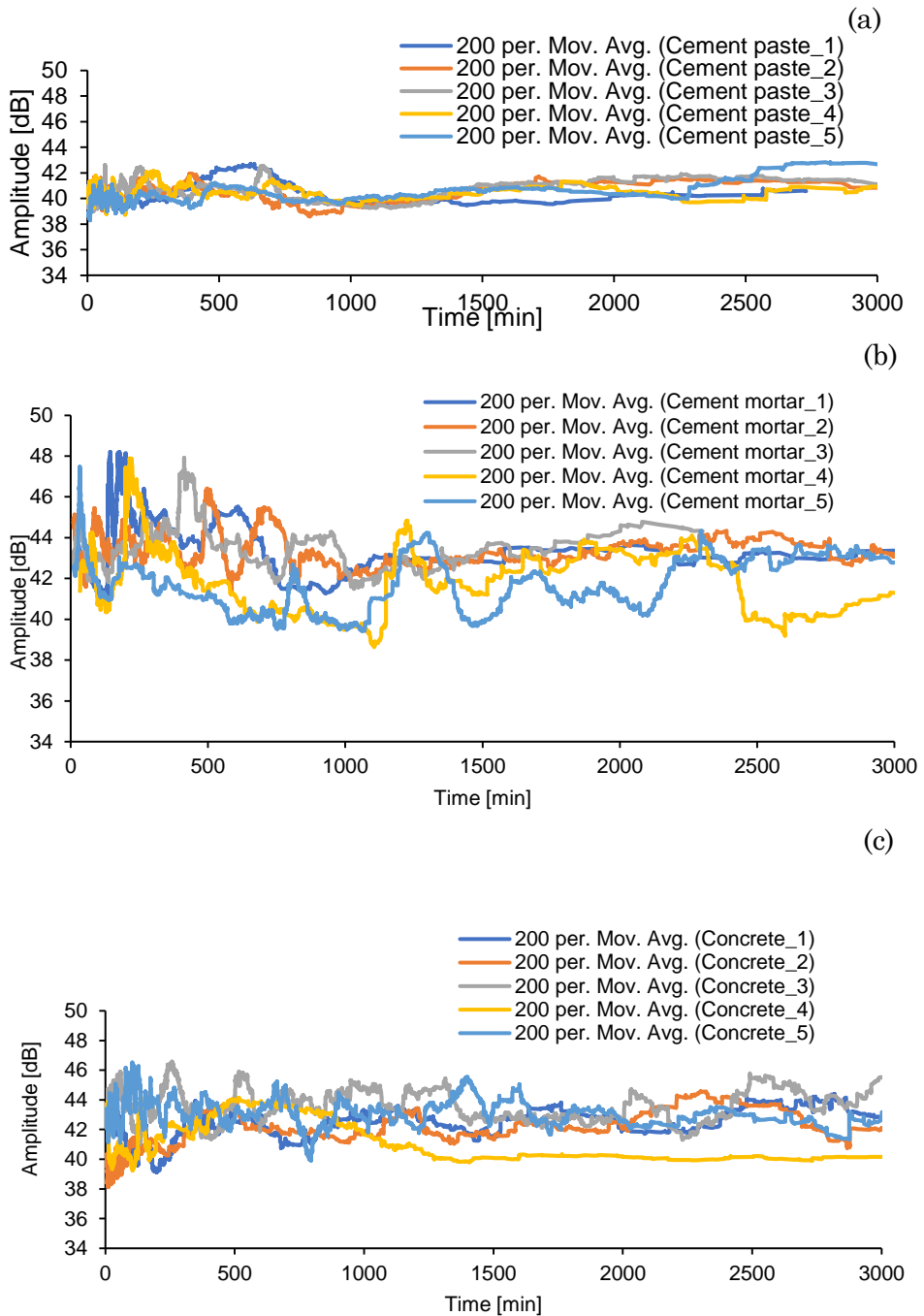
Fig. 6.14 Amplitude development for (a) cement paste; (b) cement mortar and (c) concrete.
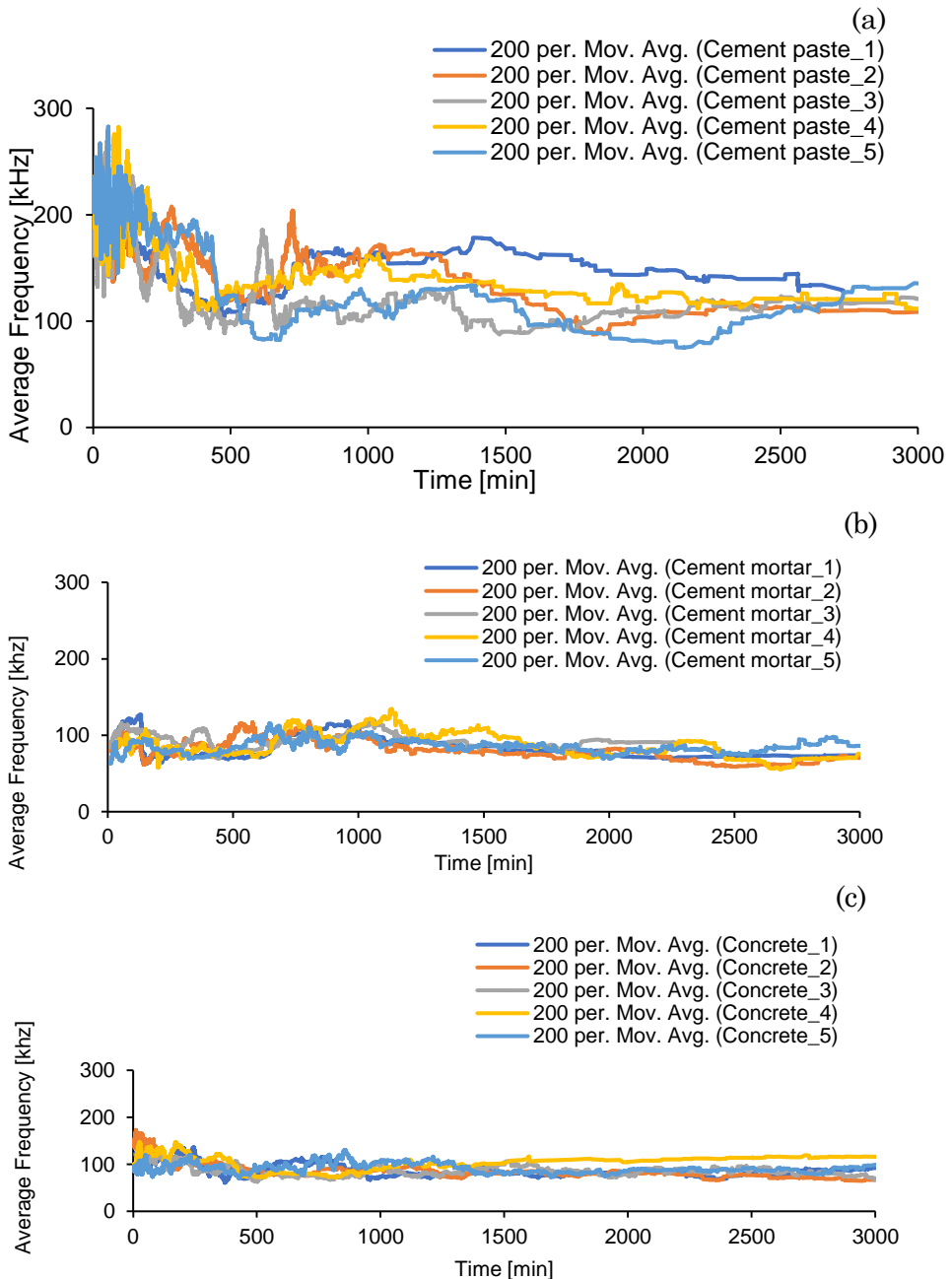
Fig. 6.15 Average frequency development for (a) cement paste; (b) cement mortar and (c) concrete.

Based on the obtained experimental results, cement paste curves illustrated higher values of AF as well as higher fluctuations compared to the mortar and concrete, as presented in Fig. 6.15(a-c). In the fresh state, the AF content of the cement paste started at an average frequency of about 250 kHz, while the concrete demonstrated a lower value with approximately 150 kHz, followed by mortar with approximately 100 kHz as revealed in Fig. 6.15. Additionally, the AF curves of all concrete specimens are steady with smaller fluctuations compared to the cement pastes, since concrete contains the smallest amount of paste.

6.5 Conclusion

In this chapter different scales of cement system, namely, concrete, mortar and cement paste have been studied. Characterizing the origin of AE activity is a challenging task since an overlapping of different processes occur during the hydration process. The elastic wave propagation is evolving differently in different materials as well as in different scale systems. Furthermore, the wave scattering is behaving differently in different material scales. The experimental observations showed the following:

- cement paste exhibits the lowest level of amplitude during the whole monitoring period, although it showed the highest cumulative activity. This means that in paste the activity occurs in more, but smaller events compared to the other mixtures.
- The fact that mortar presents the highest amplitude curve seems to be connected to the inclusion of sand, which certainly reinforces the material in terms of stiffness, but at the same time it does not impose serious scattering attenuation to the stress waves due to the small size of the sand.
- The development of RT seems to precede the one of temperature in cement paste, mortar and concrete.
- The absolute energy of cement paste presented the lowest value compared to mortar and concrete. This could be attributed to the presence of smallest particle size.

- During the entire hydration period, the highest frequency content was observed in cement paste in agreement with the particle size, while the frequency dropped during the hardening state.

Chapter 7: **Conclusions**

This chapter summarizes the general findings of the research that was performed in the framework of this doctoral thesis. At the end of this chapter, suggestions for the future work are pronounced.

7.1 Conclusions

In this section, the main research findings and conclusions are presented. The innovation of the present work concerns the application of digital image correlation (DIC) on fresh cement-based material and investigating the 3D-Full field optical measurement of material deformations and strain distributions. Further, the impact of physical mechanisms on acoustic emission (AE) activity was investigated. The integrated experimental setup of advanced full-field optical and acoustic techniques builds a continuous monitoring system that allows the detection of early age processes in fresh cementitious materials. Further, the technique of AE can be applied to determine the time, when the risk of plastic cracking achieves its maximum allowing specific action to mitigate cracking with suitable curing treatment (spraying water or curing admixture on concrete surface). In addition, AE technique can determine the fluid-solid transition of concrete without facing the attenuation problems that hinders the application of ultrasound in large scale. Furthermore, AE could assist cementitious materials and admixtures development in the laboratory due to its sensitivity in the nanoscale. Specifically, the innovative points are summarized below:

7.1.1 3D-DIC Full-field measurement of cementitious material

The investigation of the 3D-full field optical DIC technique on fresh cementitious materials was characterized within this thesis (chapter 4).

Fresh cementitious materials experience drying process that is resulting in volume changes caused by water evaporation and the cement hydration process. This research work proposes an optical technique of 3D-DIC to evaluate the surface displacement and strain distribution of fresh cementitious materials. The obtained results revealed that three-dimensional DIC can measure the non-uniform shrinkage strain and settlement evolution. Thereby, this research upgrades the monitoring of concrete to global measurements offering data for the whole surface as compared to the point data of classical LVDTs. It has to be emphasized, that for the first time in literature, DIC technique has been applied on fresh cementitious material 15 min after casting, allowing a global view

of the early age deformations. In addition, the spray speckle pattern on the sample surface has an positive effect on the evaporation process leading to a lower drying rate. The 3D-DIC detected in some regions expansive strain, that cannot be measured by conventional LVDTs. DIC technique provides an enhanced assessment of the non-uniform deformation distribution on the specimen surface when concrete shrinks and settles, that is not possible with conventional point LVDT measurements.

7.1.2   Impact of aggregates and the effect of bubble release on AE

The physical processes in fresh cementitious materials are studied to evaluate their potential of creating AE activity (Chapter 2).

AE setup shows sensitivity to capture thousands of signals from the first moments after mixing, enabling monitoring even during the settlement period, while in most cases in literature significant AE comes much later. The aggregate movement and air bubbles produce measurable AE. The obtained results illustrated mainly two physical processes. The two mechanisms are the aggregate and the bubble movement through cement paste. Good correlation between AE and settlement during the first two hours was observed, that indicates that the combined phenomena during this period (cement grain movement, water transport) can be monitored. The AE sensors received the processes that occurred close to the mould wall with higher amplitude indicating the ability of the sensors to detect the activity as well as the suitability of the experimental strategy. Further, the numerical simulations confirmed that most of the acoustic energy propagates through the mould wall that acts as a waveguide. The liquid matrix exercises indirectly a certain influence on the received wave and controls the mobility (e.g. physical speed) of the constituents (e.g. aggregate and bubbles).

7.1.3   Isolating AE mechanical and chemical sources

The evolution of the acoustic emission sources in cement paste during early-age hydration is examined in Chapter 3.

In the first hours, the significant acoustic activity of cement paste is ascribed to the settlement process. The specimens of fly ash were compared to cement paste to isolate the chemical sources from the mechanical sources. The fly ash suspension decreased the rate of cumulative AE activity. Around the capillary pressure drop the average absolute energy of AE illustrated an increase demonstrating the air entry point. The AE experimental results obtained, showed sensitivity to the size of the particles. Fresh cement paste with smaller particles emits higher frequency, lower energy and shorter signals compared to FA, of which the FA particles are 5 times larger in average.

7.1.4 Effect of hydration on AE evolution

Similarly, to Chapter 3, Chapter 5 demonstrates the impact of the hydration of concrete with admixtures on the elastic wave of AE activity.

The addition of admixtures (accelerator and retarder) exhibited noticeable difference in the acoustic behaviour relatively to the reference concrete. The chemical admixtures contribute to an increased AE activity due to additional energy release in concrete. The addition of accelerator to concrete led to the nucleation and growth of early hydration at the particle surface as well as to the formation of hydration products in the pore space. Further, the addition of retarder to concrete led possibly to the formation of sparingly soluble surface coatings that acts as a protective layer and delays further progress of hydration. The temperature development of concrete including retarder (RET) was detected to be slower than the reference sample (REF) without the addition of admixture and concrete including accelerator (ACC). The lower rate of heat evolution extends the induction period on concrete with retarder. The obtained results showed correlation between compressive strength and rise time evolution. Specimens with higher initial rise time during the first hour, exhibited higher compressive strength after 3 days. The UPV and Vicat test exhibited a rapid increase of values, not necessarily connected to the hydration itself but due to false setting.

7.1.5 Impact of different aggregate scales on acoustic emission

In Chapter 6 different scales of cementitious materials such as cement paste, cement mortar and concrete are examined. The obtained results demonstrated that characterizing the AE source is not straightforward due to overlapping of different processes. The propagation of AE elastic waves is different in different cement scales.

Cement paste illustrated the highest cumulative hits with the lowest level of amplitude during the entire hydration process compared to mortar and concrete. It can be concluded that in cement paste a high number of AE activity took place but with smaller events compared to the other mixtures. Monitoring of cement paste led to the lowest absolute energy evolution. Mortar specimens exhibited the highest amplitude during the whole monitoring period. This implies that the sand in mortar increases the material stiffness but does not seriously increase the scattering attenuation of the stress waves due to its small size.

7.2 Future work

The present research studied the deformation and strain distribution of fresh cementitious materials. Furthermore, the impact of the drying and hydration process of fresh cement-based materials on AE activity was extensively studied. However, various subjects need to be further investigated to develop improved methodology. Within this section, some of the main subjects are addressed.

DIC speckle pattern on fresh cementitious materials: DIC is a full-field monitoring tool that provides surface measurement of deformation and detects the strain distribution. The accuracy of this analysis depends on the speckle pattern creation. Due to several factors, small displacement errors arise during the measurement of the specimen. These errors can be caused by the application of the speckle pattern, since the application of the speckle pattern on fresh cement-based materials is challenging. The speckles might move due to bleed water at the surface or get absorbed on the wet surface. Thereafter, it would be of utmost

importance to propose an improved methodology for the creation of the speckles on the wet surface.

Localization of signals: An important addition would be the localization of different AE signals in a next stage. In the fresh state and later in the hardened state, it would be of significance to detect the location of the AE events in the specimen in order to evaluate the AE source.

Concrete with different admixtures: It would be desirable to examine further concrete admixtures such as, shrinkage reducing admixture, air entraining-agent, superplasticizer to determine their impact on AE signals in the fresh state as well as in the hardened state.

Concrete initial strength evolution: Concrete including accelerator presented a relation between the average rise time of the first 60 min and the initial strength development after 72 h. To establish an exact relationship between those parameters, it is essential to perform a number of tests to investigate in detail the possible relation between strength and initial rise time evolution or other AE parameter.

Agreement between DIC and LVDT measurement: To compare the two different techniques, measurement can be simultaneously applied on a solid surface (hardened concrete) to demonstrate the agreement between DIC and LVDT.

Monitoring of fresh concrete immediately after casting is a very complicated and delicate procedure. The fresh state of concrete affects the hardened state as well as the durability of concrete. However, it is demonstrated that the potential is great in terms of non-contact and global monitoring of displacements as well as the passive monitoring of acoustic emission which enables recording sources that cannot be detected in any other way. With the advancement and availability in acoustic technology, the present study shows the capability to contribute not only to basic material studies, but also on the site.

Appendix

Sensors

CALIBRATION CERTIFICATE

Model No: XTL-123C-190M-1.7BARA   Serial No: 7971-4-160
                                         ALPHA CODE: JJ6-26
Customer: K.F./VRIJE UNIVERSIT   P.O.: CD04409

STANDARD ELECTRICAL CONNECTIONS: X | SPECIAL CONNECTIONS:

RED   +Input   GREEN   +Output
BLACK   -Input   WHITE   -Output

TEST CONDITIONS:

Rated pressure: 1.70 BAR A   Operational Mode: ABSOLUTE
Maximum Pressure: 3.40 BAR A
Maximum Reference Pressure: N.A.
Tested At: 10.00 VDC Excitation   Maximum Excitation: 15.00 VDC

                    CALIBRATION

Sensitivity: 58.906mV/BAR A
Zero Balance Output: ±5mV(TYP)
Compensated Temperature Range: -40 DEG.C to 177 DEG.C
Output Impedance: 1277 Ohms   Input Impedance: 2040 Ohms
        NO SCREEN / 'O' RING SUPPLIED
        TESTED IN WATER

REMARKS:

QUALITY ASSURANCE: calibration traceable to NIST

Pressure Source Id#: PG208   Model#: CPC 6000

        Tested by: S. RANA   Inspected by:
        Date: 02/27/2013   Date: FEB 27 2013

        The calibration of Kulite Semiconductor Products, Inc.
        Instrumentation is in conformance with MIL-STD-45662A

<< RDP CALIBRATION CERTIFICATE >>

Type ACT500C

Linear Range ±12.5mm(0.492125")

Sensitivity 53.04mV/V/mm(1.347mV/V/.001")

Linearity 0.07%

Serial N° 192483

Cal Temp 20 °C

with 5V(RMS) 5kHz

Calibrated by

Cal Load 100k

Energising Supply

UNCERTAINTY OF CALIBRATION: 6.2 microns.
This expanded uncertainty is with a level of confidence of approximately 95%

AKRON N.V.-S.A.
Nieuw adres vanaf 01.01.2016
J. Vandenbemptlaan 71   Tel: 016 23 01 0:
BE-3001 Leuven   Fax: 016 23 26 9
www.akron.be   E-mail: info@akron.b

<< RDP CALIBRATION CERTIFICATE

AKRON N.V.-S.A.
Nieuw adres vanaf 01.01.2016
J. Vandenbemptlaan 71   Tel: 016 23 01 03
BE-3001 Leuven   Fax: 016 23 26 96
www.akron.be   E-mail: info@akron.be

Type D6/02500URA

Linear Range ±2.5mm(0.098425")

Sensitivity 155.68mV/V/mm(3.954mV/V/.001")

Linearity 0.06%

Serial N° 189847

Cal Temp 21 °C

with 5V(RMS) 5kHz

Calibrated by

Cal Load 100k

Energising Supply

UNCERTAINTY OF CALIBRATION: 1.6 microns.
This expanded uncertainty is with a level of confidence of approximately 95%

Bibliography

Aggelis, D. G. and T. P. Philippidis. 2004. "Ultrasonic Wave Dispersion and Attenuation in Fresh Mortar." *NDT and E International* 37(8):617–31.

Aïtcin, P. C. 2008. *Binders for Durable and Sustainable Concrete*. Taylor & Francis Group.

Amziane, S. 2006. "Setting Time Determination of Cementitious Materials Based on Measurements of the Hydraulic Pressure Variations." *Cement and Concrete Research* 36(2):295–304.

Arrington, M. and B. M. Evans. 1977. "Acoustic Emission Testing of High Alumina Cement Concrete." *NDT International* (April):81–87.

Ashrafian, A., Taheri Amiri M.J., Rezaie-Balf M., Ozbakkaloglu T., and Lotfi-Omran O. 2018. "Prediction of Compressive Strength and Ultrasonic Pulse Velocity of Fiber Reinforced Concrete Incorporating Nano Silica Using Heuristic Regression Methods." *Construction and Building Materials* 190:479–94.

Assi, L., Soltangharaei V., Anay R., Ziehl P., and Matta F. 2018. "Unsupervised and Supervised Pattern Recognition of Acoustic Emission Signals during Early Hydration of Portland Cement Paste." *Cement and Concrete Research* 103(September 2017):216–25.

ASTM C1679. 2014. "Standard Practice for Measuring Hydration Kinetics of Hydraulic Cementitious Mixtures Using Isothermal Calorimetry." *American Society for Testing and Materials, West Conshohocken, PA, USA*. 1–15.

ASTM Standard C 1581- 04. 2004. "Standard Test Method for Determining Age at Cracking and Induced Tensile Stress Characteristics of Mortar and Concrete under Restrained Shrinkage." *American Society for Testing and Materials, West Conshohocken, PA, USA*. 1–6.

Azenha, M., Faria R., and Ferreira D. 2009. "Identification of Early-Age Concrete Temperatures and Strains : Monitoring and Numerical Simulation." *Cement and Concrete Composites* 31(6):369–78.

Banthia, N. and R. Gupta. 2009. "Plastic Shrinkage Cracking in Cementitious Repairs and Overlays." *Materials and Structures* 42(5):567–79.

Barcelo, L., Boivin S., Acker P., Toupin J., and Clavaud B. 2011. "Early Age Shrinkage of Concrete Back to Physical Mechanisms." *Concrete Science and Engineering* 3(June):85–91.

Bardakov, V. and A. Sagaidak. 2016. "Forecasting of Concrete Strength during the Hardening Process by Means of Acoustic Emission Method, PROGRESS in ACOUSTIC EMISSION XVIII." in *Proceedings of the 23rd International Acoustic Emission Symposium, the Inauguration Conference of International Institute of Innovative Acoustic Emission & the 8th International Conference on Acoustic Emission JSNDI & IIIAE (2016).*

Barranger, Y., Doumalin P., Dupré J.C., and Germaneau A. 2010. "Digital Image Correlation Accuracy : Influence of Kind of Speckle and Recording Setup." *EPJ Web of Conferences* 31002.

Ben-Zeitun, A. E. 1986. "Use of Pulse Velocity to Predict Compressive Strength of Concrete." *International Journal of Cement Composites and Lightweight Concrete* 8(1):51–59.

Bentz, D. P., Ferraris C.F., Galler M.A., Hansen A.S., and Guynn J.M. 2012. "Influence of Particle Size Distributions on Yield Stress and Viscosity of Cement-Fly Ash Pastes." *Cement and Concrete Research* 42(2):404–9.

Bertil, P. and F. Göran. 2002. *Self-Desiccation and Its Importance in Concrete Technology*. Division o. Lund: proceedings of the third international research seminar in Lund.

Bhalla, N., Sharma S., Sharma S., and Siddique R. 2018. "Monitoring Early-Age Setting of Silica Fume Concrete Using Wave Propagation Techniques." *Construction and Building Materials* 162:802–15.

Bissonnette, B., Pascale P., and Michel P. 1999. "Influence of Key Parameters on Drying Shrinkage of Cementitious Materials." *Cement and Concrete Research* 29(10):1655–62.

Brooks, J. J. 2015. *Shrinkage of Concrete, Chapter 6*. Concrete and masonry movements.

Caduff, D. and J. G. M. Van Mier. 2010. "Analysis of Compressive Fracture of Three Different Concretes by Means of 3D-Digital Image Correlation and Vacuum Impregnation." *Cement and Concrete Composites* 32(4):281–90.

Carlson, J., Nilsson M., Fernández E., and Planell J.A. 2003. "An Ultrasonic Pulse-Echo Technique for Monitoring the Setting of CaSO4-Based Bone Cement." *Biomaterials* 24(1):71–77.

Carrillo, J., Ramirez J., and Lizarazo-Marriaga J. 2019. "Modulus of Elasticity and Poisson's Ratio of Fiber-Reinforced Concrete in Colombia from Ultrasonic Pulse Velocities." *Journal of Building Engineering* 23(January):18–26.

Chen, T. C., Ferraro C.C., Yin W.Q., Ishee C.A., and Ifju P.G. 2010. "A Novel Two-Dimensional Method to Measure Surface Shrinkage in Cementitious Materials." *Cement and Concrete Research* 40(5):687–98.

Chen, Y., Wei J., Huang H., Jin W., and Yu Q. 2018. "Application of 3D-DIC to Characterize the Effect of Aggregate Size and Volume on Non-Uniform Shrinkage Strain Distribution in Concrete." *Cement and Concrete Composites* 86:178–89.

Cheung, J., Jeknavorian A., Roberts L., and Silva D. 2011. "Impact of Admixtures on the Hydration Kinetics of Portland Cement." *Cement and Concrete Research* 41(12):1289–1309.

Choi, S. and S. P. Shah. 1997. "Measurement of Deformations on Concrete Subjected to Compression Using Image Correlation." *Experimental Mechanics* 37(3):307–13.

Chotard, T., Rotureau D., and Smith A. 2005. "Analysis of Acoustic Emission Signature during Aluminous Cement Setting to Characterise the Mechanical Behaviour of the Hard Material." *Journal of the European Ceramic Society* 25:3523–31.

Chotard, T. J., Smith A., Boncoeur M. P., Fargeot D., and Gault C. 2003. "Characterisation of Early Stage Calcium Aluminate Cement Hydration by Combination of Non-Destructive Techniques : Acoustic Emission and X-Ray Tomography." *Journal of the European Ceramic Society* 23:2211–23.

Chotard, T. J., Smith A., Codet N., De Baillencourt M., Fargeot D., and Gault C. 2002. "New Applications of Acoustic Emission Technique for Real-Time." *Journal of Materials Science Letters* (iii):1261–66.

Chotard, T. J., Barthelemy J., Smith A., Gimet-Breat N., Huger M., Fargeot D., and Gault C. 2001. "Acoustic Emission Monitoring of Calcium Aluminate Cement Setting at the Early Age." *Journal of Materials Science Letters* 20(7):667–69.

Chung, C. W., Suraneni P., Popovics J.S., and Struble L.J. 2017. "Using Ultrasonic Wave Reflection to Monitor False Set of Cement Paste." *Cement and Concrete Composites* 84:10–18.

Cohen, M. D., Olek J., and Dolch W.L. 1990. "Mechanism of Plastic Shrinkage Cracking in Portland Cement and Portland Cement-Silica Fume Paste and Mortar." *Cement and Concrete Research* 20(c).

Colbeck, I. and M. Lazaridis. 2014. *Aerosol Science: Technology and Application*. John Wiley & Sons Ltd Registered.

Combrinck, R., Steyl L., and Boshoff W. P. 2018a. "Interaction between Settlement and Shrinkage Cracking in Plastic Concrete." *Construction and Building Materials* 185:1–11.

Combrinck, R., Steyl L., and Boshoff W. P. 2018b. "Interaction between Settlement and Shrinkage Cracking in Plastic Concrete." *Construction and Building Materials* 185:1–11.

Copeland, L. E., Kantro D. L., and Verbeck G. 1960. "Chemistry of Hydration of Portland Cement." *Research Department Bulletin 153, Portland Cement Association* I:429–65.

Corr, D., Accardi M., Graham-Brady L., and Shah S. 2007. "Digital Image Correlation Analysis of Interfacial Debonding Properties and Fracture Behavior in Concrete." *Engineering Fracture Mechanics* 74(1–2):109–21.

Correlated solutions. n.d. "Optical Measurement Solutions." *Http://Www.Isi-Sys.Com/3d-Micro-Dic/*.

CyberLogoc, Inc. 2017. "Http://Www.Cyberlogic.Org/Wave2000.Html." *CyberLogic, Inc.*

D'Angelo, R., Plona T.J., Schwartz L.M., and Coveney P. 1995. "Ultrasonic Measurements on Hydrating Cement Slurries." *Advanced Cement Based Materials* 2(1):8–14.

Dzaye, E., De Schutter G., and Aggelis D.G. 2017. "Acoustic Emission Monitoring of Fresh Cementitious Material." Pp. 243–44 in *XIV DBMC,14th International Conference on Durability of Building Materials and Components*. Ghent, Belgium.

Escalante-Garcia, J. I. and J. H. Sharp. 1998. "Effect of Temperature on the Hydration of the Main Clinker." *Cement and Concrete Research* 28(9):1259–74.

Farin, Maxime, Anne Mangeney, Renaud Toussaint, Julien De Rosny, Nikolai Shapiro, Thomas Dewez, Clément Hibert, Christian Mathon, Olivier Sedan, and Frédéric Berger. 2015. "Characterization of Rockfalls from Seismic Signal: Insights from Laboratory Experiments." *Journal of Geophysical Research: Solid Earth* 120(10):7102–37.

Feng, X., Garboczi E.J., Bentz D.P., Stutzman P.E., and Mason T.O. 2004. "Estimation of the Degree of Hydration of Blended Cement Pastes by a Scanning Electron Microscope Point-Counting Procedure." *Cement and Concrete Research* 34:1787–93.

Frølich, L., Wadsö L., and Sandberg P. 2016. "Using Isothermal Calorimetry to Predict One Day Mortar Strengths." *Cement and Concrete Research* 88:108–13.

Gajewski, T. and T. Garbowski. 2014. "Calibration of Concrete Parameters Based on Digital Image Correlation and Inverse Analysis." *Archives of Civil and Mechanical Engineering* 14(1):170–80.

Gaydecki, P. A., F. M. Burdekin, W. Damaj, DG John, and Payne P. A. 1992. "The Propagation and Attenuation of Medium-Frequency Ultrasonic Waves in Concrete: A Signal Analytical Approach." *Measurement Science and Technology* 3(1):126–34.

Gencturk, B., Hossain K., Kapadia A., Labib E., and Mo Y.L. 2014. "Use of Digital Image Correlation Technique in Full-Scale Testing of Prestressed Concrete Structures." *Measurement: Journal of the International Measurement Confederation* 47(1):505–15.

Ghourchian, S., Wyrzykowski M., Baquerizo L., and Lura P. 2018. "Performance of Passive Methods in Plastic Shrinkage Cracking Mitigation." *Cement and Concrete Composites* 91(February):148–55.

Ghourchian, S., Wyrzykowski M., and Lura P. 2016. "The Bleeding Test : A Simple Method for Obtaining the Permeability and Bulk Modulus of Fresh Concrete." *Cement and Concrete Research* 89:249–56.

Glisic, B. and N. Simon. 2000. "Monitoring of Concrete at Very Early Age Using Stiff SOFO Sensor." *Cement and Concrete Composites* 22:115–19.

Goszczyńska, B., Świt G., Trampczyński W., Krampikowska A., Tworzewska J., and Tworzewski P. 2012. "Experimental Validation of Concrete Crack Identification and Location with Acoustic Emission Method." *Archives of Civil and Mechanical Engineering* 12(1):23–28.

Grosse, C. U., Aggelis D.G., and Shiotani T. 2016. "Innovative AE and NDT Techniques for On-Site Measurement of Concrete and Masonry Structures." *RILEM State-of-the-Art Reports, Springer* 20:5–25.

Grosse, C.U. and M. Ohtsu. 2008. *AE in Concrete. In Acoustic Emission Testing: Basics for Research Application in Civil Engineering*. edited by Christian U. Grosse and Masayasu Ohtsu. Berlin: Springer.

Gruyaert, Elke. 2011. "Effect of Blast-Furance Slag as Cement Replacement on Hydration, Microstructure, Strength and Durability of Concrete." Ghent University.

Häfner, Stefan, Stefan Eckardt, Torsten Luther, and Carsten Knöke. 2006. "Mesoscale Modeling of Concrete : Geometry and Numerics Stefan Ha." *Computers and Structures* 84:450–61.

Hanehara, S. and K. Yamada. 1999. "Interaction between Cement and Chemical Admixture from the Point of Cement Hydration, Absorption Behaviour of Admixture, and Paste Rheology." *Cement and Concrete Research* 29(8):1159–65.

Helm, J. D. 2008. "Digital Image Correlation for Specimens with Multiple Growing Cracks." *Experimental Mechanics* 48(6):753–62.

Hesse, C., Goetz-Neunhoeffer F., and Neubauer J. 2011. "A New Approach in Quantitative In-Situ XRD of Cement Pastes: Correlation of Heat Flow Curves with Early Hydration Reactions." *Cement and Concrete Research* 41(1):123–28.

Holt, E. E. 2001. *Early Age Autogenous Shrinkage of Concrete*. VTT Publications 446, Technical Research Center of Finland, Espoo.

Holt, E. and M. Leivo. 2004. "Cracking Risks Associated with Early Age Shrinkage." *Cement & Concrete Composites* 26:521–30.

Hwang, E., Kim G., Choe G., Yoon M., Gucunski N., and Nam J. 2018. "Evaluation of Concrete Degradation Depending on Heating Conditions by Ultrasonic Pulse Velocity." *Construction and Building Materials* 171:511–20.

Iliopoulos, S., El Khattabi Y., and Aggelis D. G. 2016. "Towards the Establishment of a Continuous Nondestructive Monitoring Technique for Fresh Concrete." *Journal of Nondestructive Evaluation* 35(3):1–11.

Ismail, K. N., Kamarudin H., and Idris M.S. 2007. "Physical , Chemical & Mineralogical Properties of Fly-Ash." *Journal of Nuclear and Related Technology* (March 2015).

Jacobs, Laurence J. and Joseph O. Owino. 2000. "Effect of Aggregate Size on Attenuation of Rayleigh Surface Waves in Cement-Based Materials." *JOURNAL OF ENGINEERING MECHANICS* (November):1124–30.

Kaplan, M. F. and T. N. W. Akroyd. 1959. "The Effects of Age and Water/Cement Ratio upon the Relation between Ultrasonic Pulse Velocity and Compressive Strength of Concrete." *Magazine of Concrete Research* 11(32):85–92.

Kaufmann, J. P. 2004. "Experimental Identification of Ice Formation in Small Concrete Pores." *Cement and Concrete Research* 34:1421–27.

Khan, B. and U. Muhammad. 2004. "Effect of a Retarding Admixture on the Setting Time.of Cement Pastes in Hot Weather." *Journal of King Abdulaziz University-Engineering Sciences* 15(1):63–79.

Kim, B. and W. J. Weiss. 2003. "Using Acoustic Emission to Quantify Damage in Restrained Fiber-Reinforced Cement Mortars." *Cement and Concrete Research* 33:207–14.

Kim, Young H., Sekyung Lee, and HC Kim. 1991. "Attenuation and Dispersion of Elastic Waves in Multi-Phase Materials." *Journal of Physics D: Applied Physics* 1–4.

Kjellsen, K. O. 1992. "Reaction Kinetics of Portland Cement Mortars Hydrated at Different Temperatures." *Cement and Concrete Research* 22(1):112–20.

Kjellsen, K. O., Detwiler R.J., and Gjorv O.E. 1991. "Development of Microstructures in Plain Cement Pastes." *Cement and Concrete Research* 21(c):179–89.

Komlos, K., Popovics S., Niirnbergeroh T., Babd B., and Popovics J.S. 1996. "Ultrasonic Pulse Velocity Test of Concrete Properties as Specified in Various Standards." *Cement & Concrete Composites* 18:357–64.

Komonen, J. and V. Penttala. 2003. "Effects of High Temperature on the Pore Structure and Strength of Plain and Polypropylene Fiber Reinforced Cement Pastes." *Fire Technology* 39(1):23–34.

Konsta-Gdoutos, M. S., Metaxa Z.S., and Shah S.P. 2010. "Highly Dispersed Carbon Nanotube Reinforced Cement Based Materials." *Cement and Concrete Research* 40(7):1052–59.

Kosmatka, S. H., Kerkhoff B., and Panarese W. C. 2002. *Design and Control of Concrete Mixtures*. Portland Cement Association.

Kozikowski, Ronald L. and Jerzy Z. Zemajtis. 2006. "Identifying Incompatible Combinations of Concrete Materials : - Volume II – Test Protocol." II(August).

Kurdowski, W. 2014a. *Cement and Concrete Chemistry*. 1st ed. Krakow: Springer.

Kurdowski, W. 2014b. *Cement and Concrete Chemistry*. Springer.

Kwak, H. G., Ha S., Weiss W.J., and Asce M. 2010. "Experimental and Numerical Quantification of Plastic Settlement in Fresh Cementitious Systems." *Journal of Materials in Civil Engineering* 22(10):951–66.

Kwasny, J., Sonebi M., and Basheer P. A.M. 2009. "Optimization of Self-Consolidating Pastes Containing Limestone Powder and Chemical Admixtures." *American Concrete Institute, ACI Special Publication* c(261 SP):115–32.

Lagier, F., Jourdain X., De Sa C., Benboudjema F., and Colliat J. B. 2011. "Numerical Strategies for Prediction of Drying Cracks in Heterogeneous Materials : Comparison upon Experimental Results." *Engineering Structures 33* 33:920–31.

Land, G. and D. Stephan. 2018. "The Effect of Synthesis Conditions on the Efficiency of C-S-H Seeds to Accelerate Cement Hydration." *Cement and Concrete Composites* 87:73–78.

Lecompte, D., Smits A., Bossuyt S., Sol H., Vantomme J., Van Hemelrijck S., and Habraken A.M. 2006. "Quality Assessment of Speckle Patterns for Digital Image Correlation." *Optics and Lasers in Engineering* 44:1132–45.

Leemann, A., Lura P., and Loser R. 2011. "Shrinkage and Creep of SCC - The Influence of Paste Volume and Binder Composition." *Construction and Building Materials* 25(5):2283–89.

Leemann, A., Nygaard P., and Lura P. 2014. "Impact of Admixtures on the Plastic Shrinkage Cracking of Self-Compacting Concrete." *Cement and Concrete Composites* 46:1–7.

Leighton, T. G. 1995. "Bubble Population Phenomena in Acoustic Cavitation." *Ultrasonic Sonochemistry* 2(2):123–36.

Lionello, G. and L. Cristofolini. 2014. "A Practical Approach to Optimizing the Preparation of Speckle Patterns for Digital-Image Correlation." *Measurement Science and Technology* 107001.

Lionello, G., Sirieix S., and Baleani M. 2014. "An Effective Procedure to Create a Speckle Pattern on Biological Soft Tissue for Digital Image Correlation Measurements." *Journal of the Mechanical Behavior of Biomedical Materials* 39:1–8.

Liu, Zhichao and Will Hansen. 2016. "Aggregate and Slag Cement Effects on Autogenous Shrinkage in Cementitious Materials." *Construction and Building Materials* 121:429–36.

Lomov, S. V., Ivanov D. S., Verpoest I., Zako M., Kurashiki T., Nakai H., Molimard J., and Vautrin A. 2008. "Full-Field Strain Measurements for Validation of Meso-FE Analysis of Textile Composites." *Composites Part A: Applied Science and Manufacturing* 39(8):1218–31.

Lothenbach, B., Winnefeld F., Alder C., Wieland E., and Lunk P. 2007. "Effect of Temperature on the Pore Solution, Microstructure and Hydration Products of Portland Cement Pastes." *Cement and Concrete Research* 37(4):483–91.

Lothenbach, B., Matschei T., Möschner G., and Glasser F.P. 2008. "Thermodynamic Modelling of the Effect of Temperature on the Hydration and Porosity of Portland Cement." *Cement and Concrete Research* 38(1):1–18.

Lourenco, S. D. N., Gallipoli D., Augarde C.E., Toll D.G., Fischer P.C., and Congreve A. 2011. "Formation and Evolution of Water Menisci in Unsaturated Granular Media." *Géotechnique* 62(3):193–99.

Lu, Y., Zhang J., and Li Z. 2013. "Study on Hydration Process of Early-Age Concrete Using Embedded Active Acoustic and Non-Contact Complex Resistivity Methods." *Construction and Building Materials* 46:183–92.

Luo, P. F., Chao Y. J., Sutton M. A., and Peters W. H. 1993. "Accurate Measurement of Three-Dimensional Deformations in Deformable and Rigid Bodies Using Computer Vision." *Experimental Mechanics* 33(2):123–32.

Lura, P., Pease B., Mazzotta G., Rajabipour F., and Weiss J. 2007. "Influence of Shrinkage-Reducing Admixtures on Development of Plastic Shrinkage Cracks." *ACI Materials Journal* (January).

Lura, P., Mazzotta G.B., Rajabipour F., and Weiss J. 2006. "Evaporation, Settlement, Temperature Evolution, and Development of Plastic Shrinkage Cracks in Mortars with Shrinkage-Reducing Admixtures." *RILEM-JCI Seminar on Concrete Durability and Service Life Planning* (1):1–11.

Lura, P., Couch J., Jensen O. M., and Weiss J. 2009. "Early-Age Acoustic Emission Measurements in Hydrating Cement Paste: Evidence for Cavitation during Solidification Due to Self-Desiccation." *Cement and Concrete Research* 39(10):861–67.

Maltese, C., Pistolesi C., Bravo A., Cella F., Cerulli T., and Salvioni D. 2007. "Effects of Setting Regulators on the Efficiency of an Inorganic Acid Based Alkali-Free Accelerator Reacting with a Portland Cement." *Cement and Concrete Research* 37(4):528–36.

Maruyama, I. and H. Sasano. 2013. "Strain and Crack Distribution in Concrete during Drying." *Materials and Structures* (546).

Mauroux, T., Benboudjema F., Turcry P., Aït-mokhtar A., and Deves O. 2012. "Study of Cracking Due to Drying in Coating Mortars by Digital Image Correlation." *Cement and Concrete Research* 42(7):1014–23.

McCrory, J. P., Al-Jumaili S.K., Crivelli D., Pearson M.R., Eaton M.J., Featherston C.A., Guagliano M., Holford K.M., and Pullin R. 2015. "Damage Classification in Carbon Fibre Composites Using Acoustic Emission: A Comparison of Three Techniques." *Composites Part B: Engineering* 68:424–30.

McGinley, T. J. and B. S. Choo. 1990. *Reinforced Concrete: Design Theory and Examples*. Second edi.

McLaskey, G. C., Glaser S.D., and Grosse C.U. 2007. "Integrating Broad-Band High-Fidelity Acoustic Emission Sensors and Array Processing to Study Drying Shrinkage Cracking in Concrete." P. 65290C in *Sensors and Smart Structures Technologies for Civil, Mechanical, and Aerospace Systems*. Vol. 6529.

McLaskey, Gregory C. and Steven D. Glaser. 2010. "Hertzian Impact: Experimental Study of the Force Pulse and Resulting Stress Waves." *The Journal of the Acoustical Society of America* 128(3):1087.

McNeill, S. R., Sutton M. A., Miao Z., and Ma J. 1997. "Measurement of Surface Profile Using Digital Image Correlation." *Experimental Mechanics* 37(1):13–20.

Mette Geike and Torben Knudsen. 1982. "CHEMICAL SHRINKAGE OF PORTLAND CEMENT PASTES." *Cement and Concrete Research* 1(12):603–61.

Michlmayr, G. and D. Or. 2014. "Mechanisms for Acoustic Emissions Generation during Granular Shearing." *Granular Matter* 16(5):627–40.

Mishra, R. K., Tripathi R.K., and Dubey V. 2016. "Early Age Shrinkage Pattern of Concrete on Replacement of Fine Aggregate with Industrial By-Product." *Journal of Radiation Research and Applied Sciences* 9(4):386–91.

Mix, P. E. 2003. *Introduction to Nondestructive Testing: A Training Guide,*. Vol. 21. New Jersey.

Mora-Ruacho, J., Gettu R., and Aguado A. 2009. "Influence of Shrinkage-Reducing Admixtures on the Reduction of Plastic Shrinkage Cracking in Concrete." *Cement and Concrete Research* 39(3):141–46.

Mostafa, N. Y. and P. W. Brown. 2005. "Heat of Hydration of High Reactive Pozzolans in Blended Cements: Isothermal Conduction Calorimetry." *Thermochimica Acta* 435(2):162–67.

Mpalaskas, A. C., Vasilakos I., Matikas T.E., Chai H.K., and Aggelis D. G. 2014. "Monitoring of the Fracture Mechanisms Induced by Pull-out and Compression in Concrete." *Engineering Fracture Mechanics* 128(C):219–30.

Mpalaskas, A. C., Matikas T.E., Van Hemelrijck D., Papakitsos G.S., and Aggelis D.G. 2016. "Acoustic Emission Monitoring of Granite under Bending and Shear Loading." *Archives of Civil and Mechanical Engineering* 16(3):313–24.

Muller, M., Toussaint E., Destrebecq J.F., and Grédiac M. 2004. "Experimental and Numerical Study of Reinforced Concrete Specimens Strengthened with Composite Plates." *Composites Part A: Applied Science and Manufacturing* 35(7–8):885–93.

Naik, T. R., Malhortra V.M., and Popovics J.S. 2004. "The Ultrasonic Pulse Velocity Method, 2nd Edition, Eds. V.M. Malhotra, Nicholas J. Carino (Ch.8)." *Handbook on Nondestructive Testing of Concrete* 169–88.

Nair, A. and C. S. Cai. 2010. "Acoustic Emission Monitoring of Bridges : Review and Case Studies." *Engineering Structures* 32(6):1704–14.

Nguyen-Tat, T., Ranaivomanana N., and Balayssac J.P. 2018. "Characterization of Damage in Concrete Beams under Bending with Acoustic Emission Technique (AET)." *Construction and Building Materials* 187:487–500.

Nichols, G. 2009. *Sedimentology and Stratigraphy*. 2nd ed. A John Wiley & Sons, Ltd.

Nilsen, V., Pham L.T., Hibbard M., Klager A., Cramer S.M., and Morgan D. 2019. "Prediction of Concrete Coefficient of Thermal Expansion and Other Properties Using Machine Learning." *Construction and Building Materials* 220:587–95.

Ogbonna, J. F. 2009. "The Secondary Effects of Lignosulfonate Cement Retarder on Cement Slurry Properties." *Journal of Engineering and Applied Sciences* 4(9):1–7.

Ohtsu, M. 2010. "RILEM Technical Committee (Masayasu Ohtsu), Recommendations of RILEM Technical Committee 212-ACD: Acoustic Emission and Related NDE Techniques for Crack Detection and Damage Evaluation in Concrete: Test Method for Damage Qualification of Reinforced Concre." Pp. 1183–86 in *Materials and Structures 43 (9)*.

Ohtsu, M. 2018. "Acoustic Emission Energy b -Value for Local Damage Evaluation in Reinforced Concrete Structures Subjected to Seismic Loadings." *Mechanical Systems and Signal Processing* 102:262–77.

Ohtsu, M., Ohno K., and Hamstad M.A. 2005. "Moment Tensors of In-Plane Waves Analyzed by Sigma-2D." *J. Acoustic Emission* 23.

Ohtsu, M., Yamada M., and Sonoda T. 2013. "Quantitative Evaluation of SIBIE Procedure and Case Studies." *Construction and Building Materials* 48:1248–54.

Ohtsu, M., Isoda T., and Tomoda Y. 2007. "Acoustic Emission Techniques Standardized for Concrete Structures." *J. Acoustic Emission* 25:21–32.

Ohtsu, M. and H. Watanabe. 2001. "Quantitative Damage Estimation of Concrete by Acoustic Emission." *Construction and Building Materials* 15:217–24.

Ohtsu, M. and T. Watanabe. 2002. "Stack Imaging of Spectral Amplitudes Based on Impact-Echo for Flaw Detection." *NDT and E International* 35(3):189–96.

Olivier, G., Combrinck R., Kayondo M., and Boshoff W.P. 2018. "Combined Effect of Nano-Silica, Super Absorbent Polymers, and Synthetic Fibres on Plastic Shrinkage Cracking in Concrete." *Construction and Building Materials* 192:85–98.

Omondi, B., Aggelis D.G., Sol H., and Sitters C. 2016. "Improved Crack Monitoring in Structural Concrete by Combined Acoustic Emission and Digital Image Correlation Techniques." *Structural Health Monitoring* 15(3):359–78.

Pal Kaur, N., Kumar Shah J., Majhi S., and Mukherjee A. 2019. "Healing and Simultaneous Ultrasonic Monitoring of Cracks in Concrete." *Materials Today Communications* 18(October 2018):87–99.

Pan, B., Qian K., Xie H., and Asundi A. 2009. "Two-Dimensional Digital Image Correlation for in-Plane Displacement and Strain Measurement: A Review." *Measurement Science and Technology* 20(6).

Pan, B., Tian L., and Song X. 2016. "Real-Time , Non-Contact and Targetless Measurement of Vertical Deflection of Bridges Using off-Axis Digital Image Correlation." *NDT and E International* 79:73–80.

Pane, Ivindra and Will Hansen. 2005. "Investigation of Blended Cement Hydration by Isothermal Calorimetry and Thermal Analysis." *Cement and Concrete Research* 35:1155–64.

Pane, Ivindra and Will Hansen. 2008. "Predictions and Verifications of Early-Age Stress Development in Hydrating Blended Cement Concrete." *Cement and Concrete Research* 38:1315–24.

Papo, A. and L. Piani. 2004. "Effect of Various Superplasticizers on the Rheological Properties of Portland Cement Pastes." *Cement and Concrete Research* 34(11):2097–2101.

Pazdera, L., Topolar L., Korenska M., Smutny J., and Bilek V. 2014. "Advanced Analysis of Acoustic Emission Parameters during the Concrete Hardening for Long Time." Pp. 1–8 in *11th European Conference on Non-Destructive Testing*. Prague, Czech republic.

Pazdera, L., Topolar L., Korenska M., Vymazal T., Smutny J., and Bilek V. 2015. "Monitoring Early-Age Concrete with the Acoustic-Emission Method and Determining the Change in the Electrical Properties." *Materials and Technology* 49(5):703–7.

Pease, B., Hossain A.B., and Weiss J. 2004. "Quantifying Volume Change, Stress Development, and Cracking Due to Early-Age Autogenous Shrinkage." *Aci Special Publications* C(March 2015):23–38.

Peschard, A., Govin A., Pourchez J., Fredon E., Bertrand L., Maximilien S., and Guilhot B. 2006. "Effect of Polysaccharides on the Hydration of Cement Suspension." *Journal of the European Ceramic Society* 26(8):1439–45.

Petro, J. T. and Kim J. 2012. "Detection of Delamination in Concrete Using Ultrasonic Pulse Velocity Test." *Construction and Building Materials* 26(1):574–82.

Philippidis, T. P. and D. G. Aggelis. 2005. "Experimental Study of Wave Dispersion and Attenuation in Concrete." *Ultrasonics* 43(7):584–95.

Piasta, Wojciech and Bartlomiej Zarzycki. 2017. "The Effect of Cement Paste Volume and w/c Ratio on Shrinkage Strain, Water Absorption and Compressive Strength of High Performance Concrete." *Construction and Building Materials* 140:395–402.

Pitangueira, Roque Luiz and Raul Rosas e Silva. 2005. "Numerical Characterization of Concrete Heterogeneity." *Materials Research* 5(3):309–14.

Poppe, A. M. and Geert De Schutter. 2005. "Cement Hydration in the Presence of High Filler Contents." *Cement and Concrete Research* 35(12):2290–99.

Qi, C., Weiss J., and Olek J. 2003. "Characterization of Plastic Shrinkage Cracking in Fiber Reinforced Concrete Using Image Analysis and a Modified Weibull Function." *Materials and Structures* 36(July):386–95.

Qin, L., Ren H. W., Dong B. Q., and Xing F. 2014. "Acoustic Emission Behavior of Early Age Concrete Monitored by Embedded Sensors." *Materials* 7:6908–18.

Ramachandran, V. S., Lowery M.S., Wise T., and Polomark G.M. 1993. "The Role of Phosphonates on the Hydration of Portland Cement." *Materials and Structures* 26(161):425–32.

Rickert, J. 1999. "Influence of Retarders on the Hydration of Clinker and Cement." *Concrete Technology* 71–86.

Robeyst, N., Grosse C.U., and De Belie N. 2009. "Measuring the Change in Ultrasonic P-Wave Energy Transmitted in Fresh Mortar with Additives to Monitor the Setting." *Cement and Concrete Research* 39(10):868–75.

Roubin, Emmanuel. 2013. "Multi-Scale Simulation of Quasi-Brittle Heterogeneous Materials : Application to Concrete like Materials To Cite This Version : HAL Id : Hal-02023895." in *31èmes Rencontres de l'AUGC,*. Cachan.

Rouchier, S., Foray G., Godin N., Woloszyn M., and Roux J.J. 2013. "Damage Monitoring in Fibre Reinforced Mortar by Combined Digital Image Correlation and Acoustic Emission." *Construction and Building Materials* 38:371–80.

Rozière, E., Granger S., Turcry Ph., and Loukili A. 2007. "Influence of Paste Volume on Shrinkage Cracking and Fracture Properties of Self-Compacting Concrete." *Cement and Concrete Composites* 29(8):626–36.

Sadowski, Ł., Popek M., Czarnecki S., and Mathia T.G. 2017. "Morphogenesis in Solidification Phases of Lightweight Concrete Surface at Early Ages." *Construction and Building Materials* 148:96–103.

Sadowski, Łukasz and Thomas G. Mathia. 2016. "Multi-Scale Metrology of Concrete Surface Morphology : Fundamentals and Specificity." *Construction and Building Materials* 113:613–21.

Safiuddin, M., Kaish A.B.M., Woon C.O., and Raman S.N. 2018. "Early-Age Cracking in Concrete: Causes, Consequences, Remedial Measures, and Recommendations." *Applied Sciences*.

Saint-Pierre, F., Philibert A., Giroux B., and Rivard P. 2016. "Concrete Quality Designation Based on Ultrasonic Pulse Velocity." *Construction and Building Materials* 125:1022–27.

Sakai, E., Miyahara S., Ohsawa S., Lee S.H., and Daimon M. 2005. "Hydration of Fly Ash Cement." *Cement and Concrete Research* 35:1135–40.

Salvador, R. P., Cavalaro S.H.P., Rueda A., and Figueiredo A.D. 2014. "Effect of Cement Composition on the Reactivity of Alkali-Free Accelerating Admixtures for Shotcrete." *7th International Symposium on Sprayed Concrete* (November 2015):350–60.

Salvador, R. P., Cavalaro S.H.P., Segura I., Figueiredo A.D., and Perez J. 2016. "Early Age Hydration of Cement Pastes with Alkaline and Alkali-Free Accelerators for Sprayed Concrete." *Construction and Building Materials* 111:386–98.

Sansalone, M. J. and W. .. B. Streett. 1997. "Impact-Echo. Nondestructive Evaluation of Concrete and Masonry." *Bullbrier Press*.

Sant, G., Dehadrai M., Bentz D., Lura P., Ferraris C.F., Bullard J.W., and Weiss J. 2009. "Detecting the Fluid-to-Solid Transition in Cement Pastes: Part II -Comparison of Experimental and Numerical Techniques." *Concr. Intl.* (May 2014):53–58.

Schmidt, T., Tyson J., and Galanulis K. 2003. "Full-Field Dynamic Displacement and Strain Measurement Using Advanced 3D Image Correlation Photogrammetry: Part II." *Experimental Techniques* 27(3):47–50.

De Schutter, G. 1995. "General Hydration Model for Portland Cement and Blast Furance Slag Cement." *Cement and Concrete Research* 25(3):593–604.

De Schutter, G., Yuan Y., Liu X., and Jiang W. 2014. "Degree of Hydration-Based Creep Modeling of Concrete with Blended Binders: From Concept to Real Applications." *Journal of Sustainable Cement-Based Materials* 4(1):1–14.

Selly, R. C. 2000. *Applied Sedimentology*. Vol. 7.

Serra, J., Pierré J.E., Passieux J.C., Périé J.N., Bouvet C., and Castanié B. 2017. "Validation and Modeling of Aeronautical Composite Structures Subjected to Combined Loadings : The VERTEX Project . Part 1 : Experimental Setup , FE-DIC Instrumentation and Procedures." *Composite Structures* 179:224–44.

Sherzer, Gili, Peng Gao, Erik Schlangen, Guang Ye, and Erez Gal. 2017. "Upscaling Cement Paste Microstructure to Obtain the Fracture, Shear, and Elastic Concrete Mechanical LDPM Parameters." *Materials* 10(3).

Shiotani, T. 2008. *Chapter 4 Parameter Analysis, in: C.U. Grosse, M. Ohtsu (Eds.), Acoustic Emission Testing, Springer*. Berlin.

Shiotani, T., Bisschop J., and Van Mier J.G.M. 2003. "Temporal and Spatial Development of Drying Shrinkage Cracking in Cement-Based Materials." *Engineering Fracture Mechanics* 70(12):1509–25.

Skal's'kyi, V. R., Koval' P.M., Serhienko O.M., and Lotots'kyi Yu.L. 2004. "Investigation of the Solidification of Concrete According to the Signals of Acoustic Emission." *Materials Science* 40(5):698–701.

Slowik, V., Schlattner E., and Klink T. 2004. "Experimental Investigation into Early Age Shrinkage of Cement Paste by Using Fibre Bragg Gratings." *Cement and Concrete Composites* 26:473–79.

Slowik, V., Schmidt M., Kässler D., and Eiserbeck M. 2014. "Capillary Pressure Monitoring in Plastic Concrete for Controlling Early-Age Shrinkage Cracking." (2441):1–5.

Slowik, V., Schmidt M., and Fritzsch R. 2008. "Capillary Pressure in Fresh Cement-Based Materials and Identification of the Air Entry Value." *Cement and Concrete Composites* 30(7):557–65.

Slowik, V., Hübner T., Schmidt M., and Villmann B. 2009. "Simulation of Capillary Shrinkage Cracking in Cement-like Materials." *Cement and Concrete Composites* 31(7):461–69.

Sonebi, M. and Peter J. M. Bartos. 2002. "Filling Ability and Plastic Settlement of Self-Compacting Concrete." *Materials and Structures / Materiaux et Constructions* 35(252 SPEC.):462–69.

Van Steen, C., Pahlavan L., Wevers M., and Verstrynge E. 2019. "Localisation and Characterisation of Corrosion Damage in Reinforced Concrete by Means of Acoustic Emission and X-Ray Computed Tomography." *Construction and Building Materials* 197:21–29.

Struble, L. and Sun Guo Kuang. 1995. "Viscosity of Portland Cement Paste as a Function of Concentration." *Advanced Cement Based Materials* 2(2):62–69.

Suryanto, B., Buckman J.O., Mccarter W.J., and Taha H. 2018. "In-Situ Dynamic WetSEM Imaging and Electrical Impedance Measurements on Portland Cement during Early Hydration." *Materials Characterization* 142(May):86–100.

Sutton, M. A., Orteu J.J., and Schreier H.W. 2009. *Image Correlation for Shape, Motion and Deformation Measurements, Basic Concepts, Theory and Applications*. New York: Springer.

Suzuki, T. and Ohtsu M. 2004. "Quantitative Damage Evaluation of Structural Concrete by a Compression Test Based on AE Rate Process Analysis." *Construction and Building Materials* 18(3):197–202.

Tao, G. and Z. Xia. 2005. "A Non-Contact Real-Time Strain Measurement and Control System for Multiaxial Cyclic/Fatigue Tests of Polymer Materials by Digital Image Correlation Method." *Polymer Testing* 24(7):844–55.

Taylor, H. F. W. 1997. *Cement Chemistry*. 2nd ed. London: Thomas Telford.

Thirumalaiselvi, A. and Saptarshi Sasmal. 2019. "Acoustic Emission Monitoring and Classification of Signals in Cement Composites during Early-Age Hydration." *Construction and Building Materials* 196:411–27.

Thomas, J. J., Rothstein D., Jennings H.M., and Christensen B.J. 2003. "Effect of Hydration Temperature on the Solubility Behavior of Ca-, S-, Al-, and Si-Bearing Solid Phases in Portland Cement Pastes." *Cement and Concrete Research* 33(12):2037–47.

Thomas, J. J., Jennings H. M., and Chen J.J. 2009. "Influence of Nucleation Seeding on the Hydration Mechanisms of Tricalcium Silicate and Cement." *Journal of Physical Chemistry C* 113(11):4327–34.

Topolár, L., Pazdera L., Kucharczyková B., Smutný J., and Mikulášek K. 2017. "Using Acoustic Emission Methods to Monitor Cement Composites during Setting and Hardening." *Applied Sciences* 7(5):451.

Topu, I. B., Uygunolu T., and Hocaolu I. 2012. "Electrical Conductivity of Setting Cement Paste with Different Mineral Admixtures." *Construction and Building Materials* 28(1):414–20.

Triconnet, K., Derrien K., Hild F., and Baptiste D. 2009. "Parameter Choice for Optimized Digital Image Correlation." *Optics and Lasers in Engineering* 47:728–37.

Troccaz, Philippe, Roland Woodcock, and Frédéric Laville. 2000. "Acoustic Radiation Due to the Inelastic Impact of a Sphere on a Rectangular Plate." *The Journal of the Acoustical Society of America* 108(5):2197–2202.

Trtnik, G. and M. Gams. 2014. "Recent Advances of Ultrasonic Testing of Cement Based Materials at Early Ages." *Ultrasonics* 54(1):66–75.

Tung, S. H., Shih M.H., and Sung W.p. 2008. "Development of Digital Image Correlation Method to Analyse Crack Variations of Masonry Wall." *Sadhana - Academy Proceedings in Engineering Sciences* 33(6):767–79.

Van den Abeele, K., Desadeleer W., De Schutter G., and Wevers M. 2006. "Acoustic Emission (AE) and Nonlinear Elastic Wave Spectroscopy (NEWS) for Online Monitoring of Concrete Curing." *Advanced Materials Research* 13–14(January).

Van den Abeele, K., Desadeleer W., De Schutter G., and Wevers M. 2009. "Active and Passive Monitoring of the Early Hydration Process in Concrete Using Linear and Nonlinear Acoustics." *Cement and Concrete Research* 39(5):426–32.

Verbruggen, S., De Sutter S., Iliopoulos S., Aggelis D.G., and Tysmans T. 2016. "Experimental Structural Analysis of Hybrid Composite-Concrete Beams by Digital Image Correlation (DIC) and Acoustic Emission (AE)." *Journal of Nondestructive Evaluation* 35(1):1–10.

Vidya Sagar, R. and Raghu Prasad B. K. 2012. "A Review of Recent Developments in Parametric Based Acoustic Emission Techniques Applied to Concrete Structures." *Nondestruct. Test. Eval.* 27 (1):47–68.

Vilane, Roy Bruce Thulane and Ndlangamandla Sabelo. 2016. "The Effect of Aggregate Size on the Compressive Strength of Concrete." *Journal of Agricultural Science and Engineering* 2(6):66–69.

Weyers, R. E., Conway J.C., and Cady P.D. 1982. "Photoelastic Analysis of Rigid Inclusions in Fresh Concrete." *Cement and Concrete Research* 12(c):475–84.

Wierig, H. J. 1990. "Properties of Fresh Concrete." *Proceedings of the RILEM Colloquium*.

Winnefeld, F., Lothenbach B., Figi R., Rytz G., and Plötze M. 2005. "The Influence of Different Calcium Sulfates on the Hydration of Portland Cement - A Practical Study | Einflüsse Verschiedener Sulfatträger Auf Die Hydratation von Portlandzement - Eine Praxisnahe Studie." *ZKG International* 58(3).

Wittmann, F. H. 1976. "On the Action of Capillary Pressure in Fresh Concrete." *Cement and Concrete Research* 6:49–56.

Wu, B. and Wu D. 2017. "Test Study on Hydration Temperature of Compound Concrete Made of Demolished Concrete Lumps and Fresh Concrete." *Procedia Engineering* 210:120–25.

Wu, K., Chen B., and Yao W. 2000. "Study on the AE Characteristics of Fracture Process of Mortar , Concrete and Steel-Fiber-Reinforced Concrete Beams." *Cement and Concrete Research* 30:0–5.

Xiao, L. and X. Wei. 2017. "Study on the Hydration Parameters in Hardening Paste , Mortar and Concrete Based on Electrical Resistivity Measurement." *Materials and Structures* 50(1):1–11.

Yamaguchi, I. 1981. "A Laser-Speckle Strain Gauge." *Journal of Physics E: Scientific Instruments* 14:1270–73.

Yamakawa, M., Hashimoto C., and Watanabe T. 2003. "Study on Settlement Crack for Reinforced Concrete Structures Using the Concrete with Type IV Fly Ash." *International Journal of Modern Physics* 17:1470–75.

Ye, G., Lura P., Van Breugel K., and Fraaij A.L.A. 2004. "Study on the Development of the Microstructure in Cement-Based Materials by Means of Numerical Simulation and Ultrasonic Pulse Velocity Measurement." *Cement and Concrete Composites* 26(5):491–97.

Zhou, C., Shu X., and Huang B. 2014. "Predicting Concrete Coefficient of Thermal Expansion with an Improved Micromechanical Model." *Construction and Building Materials* 68:10–16.

Zongjin, L. 2011. *Advanced Concrete Technology*. New Jersey: John Wiley & Sons, INC.

Publications

Journal papers (published)

Dzaye, E., Tsangouri E., De Schutter G., and Aggelis D.G. 2019. "Full-Field Settlement Measurement at Fresh Cementitious Material by Digital Image Correlation." Journal of Advanced Concrete Technology 17(April):168–76.

Dzaye, E., Tsangouri E., Spiessens K., De Schutter G., and Aggelis D.G. 2019. "Digital Image Correlation (DIC) on Fresh Cement Mortar to Quantify Settlement and Shrinkage." Archives of Civil and Mechanical Engineering 19(1):205–14.

Dzaye, E., De Schutter G., and Aggelis D.G. 2017. "Study on Mechanical Acoustic Emission Sources in Fresh Concrete." Archives of Civil and Mechanical Engineering 18(3):742–54.

Dzaye, E., De Schutter G., and Aggelis D.G. 2020. "Monitoring early-age acoustic emission of cement paste and fly ash." Cement and concrete Research 129(105964).

Conference papers (published)

Dzaye, E., De Schutter G., and Aggelis D. 2018. "Application of Digital Image Correlation to Cement Paste." Pp. 2–7 in *18th International Conference on Experimental Mechanics (ICEM 2018)*. Brussel, Belgium.

Dzaye, E., De Schutter G., and Aggelis D.G. 2017. "Acoustic Emission Monitoring of Fresh Cementitious Material." Pp. 243–44 in *XIV DBMC,14th International Conference on Durability of Building Materials and Components*. Ghent, Belgium.

Dzaye, Evin Dildar, Geert De Schutter, and Dimitrios Aggelis. 2018. "Monitoring Fresh Cementitious Material By Digital Image Correlation (Dic)." Pp. 267–72 in *SynerCrete'18 International*

215

Conference on Interdisciplinary Approaches for Cement-based Materials and Structural Concrete. Funchal, Portugal.

Dzaye, Evin, G. DE Schutter, and Aggelis Dimitrios. 2017. "Early-Age Monitoring of Fresh Cementitious Material by Acoustic Emission." Pp. 417–22 in *Second International RILEM/ COST Conference on Early Age Cracking and Serviceability in Cement-based Materials and Structures (EAC02)*. Brussel, Belgium.

Dzaye, Evin, G. DE Schutter, and Aggelis Dimitrios. 2018. "Fresh Concrete Monitoring by NDT Techniques." Pp. 1–9 in *17th European Bridge Conference, Structural Faults + Repair-2018 University of Edinburgh School of Engineering*. Edingburgh, Schotland.

Dzaye, Evin, Geert De Schutter, and Dimitrios Aggelis. n.d. "Early-Age Monitoring of Fresh Cementitious Material by Acoustic Emission,." Pp. 417–22 in *Proceedings of the 2nd International RILEM/COST Conference on Early Age Cracking and Serviceability in Cement-based Materials and Structures, PRO 120*. Delft, Netherland: RILEM Publications S.A.R.

Dzaye, Evin, Geert De Schutter, and Aggelis Dimitrios. 2016. "Acoustic Emission Monitoring of Fresh Cementitious Material." Pp. 105–13 in *International RILEM Conference on Materials, Technical University of Denmark*. Lyngby, Denmark.

Dzaye, Evin, Geert De Schutter, and Aggelis Dimitrios. 2017. "Monitoring Acoustic Emission of Fresh Cement Paste." Pp. 507–15 in *71st RILEM Annual Week & ICACMS 2017, International Conference on Advanceds in Construction Materials and Systems', IIT Madras*. Chennai, India.

Dzaye, Evin, Geert De Schutter, and Aggelis Dimitrios. 2018. "Assessment of Fresh Cement- Based Materials by Acoustic Emission." Pp. 179–83 in *PROGRESS in ACOUSTIC EMISSION XIX, Proceedings of the 24th International Acoustic Emission Symposium (IAES-24 SAPPORO)*, edited by T. Shiotani, T. Mizutani, and H. Yuki. Sapporo, Japan.

Dzaye, Evin, Geert De Schutter, and Aggelis Dimitrios. n.d. "Monitoring The Hydration Of Cementitious Material By Acoustic Emission." Pp. 28.1-28.10 in *10th ACI/RILEM International Conference on Cementitious Materials and Alternative Binders for Sustainable Concrete*. Vol. 10, edited by Arezki Tagnit-Hamou. Montreal,

Canada: American Concrete Institute.

Dzaye, Evin, Eleni Tsangouri, Geert De Schutter, and Aggelis Dimitrios. 2019. "Characterization of Curing of Concrete Based on Combination of NDT Techniques." Pp. 185–90 in *International Conference on Sustainable Materials, Systems and Structures (SMSS2019), Novel Methods for Characterization of Materials and Structures*. Rovinj, Croatia.

Iliopoulos, Sokratis N., Evin Dzaye, Yassir El Khattabi, Geert De Schutter, and Dimitrios G. Aggelis. 2016. "Continuous AE Monitoring of Fresh Concrete." Pp. 6–11 in *Progress in Acoustic Emission XVIII, JSNDI & IIIAE*. Kyoto, Japan.